ATHEROSCLEROTIC CAROTID PLAQUE ASSESSMENT WITH MULTIDETECTOR COMPUTED TOMOGRAPHY ANGIOGRAPHY

Thomas T. de Weert

Cover design : Ton Everaers and Thomas de Weert
Layout : Ton Everaers
Printed by : PrintPartners Ipskamp, Enschede, The Netherlands
ISBN : 978-90-9023871-5

The printing of this thesis was financially supported by the department of Radiology of the Erasmus MC, University Medical Center Rotterdam, The Netherlands.

Copyright © 2008 Thomas de Weert, Rotterdam, The Netherlands
All rights reserved. No part of this thesis may be reproduced, stored in a retrieval system or transmitted in any form or by any means, without written permission of the author, or, when appropriate, of the scientific journal in which parts of this thesis may have been published.

Atherosclerotic Carotid Plaque Assessment with Multidetector Computed Tomography Angiography

Atherosclerotische Carotis Plaque Evaluatie middels Multidetector Computer Tomografie Angiografie

PROEFSCHRIFT

ter verkrijging van de graad van doctor aan de
Erasmus Universiteit Rotterdam
op gezag van de
rector magnificus

Prof.dr. S.W.J. Lamberts

en volgens besluit van het College voor Promoties.

De openbare verdediging zal plaatsvinden op
vrijdag 06-02-2009 om 11:00 uur

door

THOMAS THIJS DE WEERT
Geboren te Nijmegen

Promotiecommissie:

Promotor	Prof.dr. P.M.T. Pattynama
Overige leden:	Prof.dr. H. van Urk Prof.dr. P.W.J.C. Serruys Prof.dr. J.C.M. Witteman
Copromotoren:	Dr. A. van der Lugt Dr. D.W.J. Dippel

Table of contents

INTRODUCTION

Stroke is the third cause of death worldwide, after coronary heart disease and all types of cancer combined. In addition, because stroke more often leads to disability than to death, it represents an enormous burden on health care funding.[1] As an inevitable consequence of the aging of the Dutch population, by the year 2020 the incidence of stroke in the Netherlands is expected to have increased by 15% (to 2.5 per 1000 for the whole population) and the prevalence by 16% (to 8.7 per 1000 for the whole population).[2]

Stroke can be defined as the clinical syndrome of a sudden, focal or global neurological deficit that is presumed to be of vascular origin and that is caused by different pathological mechanisms: cerebral ischemia (≈80%), primary intracerebral hemorrhage (≈15%), and subarachnoid hemorrhage (≈5%).[1] Ischemic stroke is confined to an area of the brain perfused by a specific artery, and lasts longer than 24 hours or has led to death. Transient-ischemic attack (TIA) differs from ischemic stroke in its duration, in that it lasts less than 24 hours.[1]

Characteristic for cerebral ischemia is the presence of obstructed blood flow to (some part of) the brain. The causes are multiple, but can be grouped under three main pathophysiological mechanisms.

Firstly, the most common mechanism is large vessel disease (≈50%).[1] Large vessel disease is characterized by atherosclerosis of the greater vessels that supply the brain with blood, such as the aortic arch, the carotid arteries including the carotid siphon, the vertebral arteries, and the basilar artery. In case of large vessel disease cerebral ischemia can occur when an atherosclerotic lesion significantly obstructs the blood flow to the brain (near occlusion), or when an atherosclerotic lesion ruptures and, due to thrombus formation and subsequent thrombus and/or plaque material embolization, obstructs a smaller distal vessel in the brain. The latter mechanism is by far the most common.

Secondly, small vessel disease (≈25%)[1]; this is characterized by occlusion of small arteries perforating the brain and leads to lacunar infarcts and leucoariosis[3]. Thirdly, cardiac embolism (≈20%). This can be caused by a variety of cardiac conditions, but the most common is atrial fibrillation with presumed (but seldom proven) thrombus in the left atrium.[4] Other possible conditions include recent myocardial infarction, prosthetic valves, dilated cardiomyopathy, and infectious endocarditis. In addition, cerebral ischemia can originate infrequently (≈5%) from some rare causes like vasculitis and dissection.

After onset of ischemic stroke there is only a small time frame in which thrombolytic therapy can be used to achieve primary reduction of death and disability. After this acute phase has passed, an additional reduction in death and disability can be obtained from surveillance on a stroke unit, optimization of vital functions and prescription of acetylsalicylic acid.

Because the risk of recurrent ischemic events is significantly increased (11-15%)[5], prevention is of utmost importance. Secondary prevention consists of multiple strategies. Firstly,

medical treatment, which mainly covers platelet aggregation inhibitors (e.g. acetylsalicylic acid[6] and dipyridamole[7]), and in case of cardiac conditions associated with cardiac embolism coumarin derivatives. Secondly, treatment of the most important cardiovascular risk factors. It has been shown that nine easily detectable and potentially modifiable cardiovascular risk factors (smoking, abnormal blood lipid levels, hypertension, diabetes, abdominal obesity, psychosocial factors, low daily fruit and vegetable consumption, high regular alcohol consumption, low regular physical activity) account for an overwhelmingly large (over 90%) proportion of the worldwide risk of myocardial infarction[8]. Furthermore, the combination of smoking and abnormal blood lipid levels accounted for two-thirds of the worldwide risk. The third and final focus of secondary prevention is evaluation of the underlying cause of the event, because determining a specific cause enables specific therapy. During such evaluation special attention is paid to the carotid artery, because large randomized trials have shown that, in patients with a severe carotid stenosis (>70%) on digital subtraction angiography (DSA), the risk of recurrent stroke can be reduced with carotid endarterectomy (surgical removal of an atherosclerotic carotid lesion).[9,10] This is probably true for patients with both large vessel disease and small vessel disease.[11,12] This benefit of endarterectomy exists because the risk of a recurrent event during best medical treatment (≈25% in 2 years) in patients with a severe stenosis is larger than the peri-operative risk and recurrent event risk after operation together (≈9% in 2 years).[11] This risk difference of 16% means that 6 severely stenotic patients have to be treated to prevent one recurrent stroke in the next 2 years following treatment. However, the number to treat (NTT) is considerably higher (NTT=12)[13] in patients with less severe stenosis (50-70%), and in asymptomatic patients (NTT=50, for stenosis >50%).[14] As a result, patients with a moderate stenosis and asymptomatic patients are regularly not operated. Therefore, it is important to be able to select patients within these categories who may benefit more from intervention. For this purpose, the assessment and evaluation of additional risk parameters has started. Clinical parameters (such as age, gender, type of event, and vascular risk factors) are major determinants of subsequent stroke risk and, therefore, of the potential benefit of endovascular or surgical treatment.[15]

Furthermore, it is currently considered that assessment of plaque vulnerability with imaging modalities might play an essential role in risk prediction.

Plaque vulnerability

Morphology studies on carotid and coronary atherosclerotic plaque have stressed the importance of plaque vulnerability in the occurrence of clinical events.[16] Plaque vulnerability is the chance of initiating the cascade of plaque rupture, thrombus formation, and thrombomaterial and/or plaque-material embolization (Fig. 1). A wide range of atherosclerotic plaque features has been related to plaque vulnerability[16-20]: stenosis degree, plaque morphology, plaque volume and plaque component volumes, luminal plaque surface, degree of inflammation, neovascularization, arterial stiffness, and shear stress. Imaging of

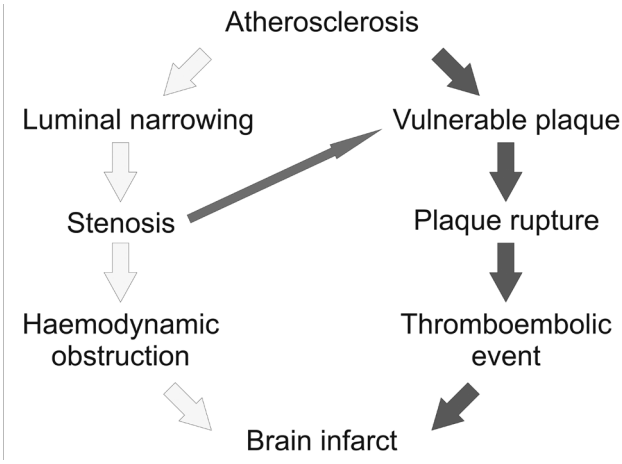

Figure 1. The two major pathways through which atherosclerotic disease can lead to brain infarction. Ideal, both pathways are covered when assessing stroke risk. However, stroke risk is now almost entirely based on measurement of stenosis degree, which covers only partly the vulnerability pathway.

these features might eventually improve risk prediction, and the selection of patients who are likely to benefit from intervention (endarterectomy or stent placement).

DSA

DSA, the gold standard imaging technique for degree of stenosis, depicts no more than the contour of the vessel lumen, thus limiting its possibility to determine additional risk parameters besides plaque surface characteristics. Nevertheless, several studies[21,22] have shown that plaque surface irregularity and ulceration are strongly and independently associated with ipsilateral ischemic stroke, making plaque surface eligible as a possible additional parameter to select patients for endarterectomy. However, the reported sensitivity of DSA for the detection of ulcerations was moderate (46-69%)[22,23] which might be due the limited viewing directions (usually two).

EBCT

Agatston and colleagues were the first to show that coronary calcifications could be detected and quantified with electron-beam computed tomography (EBCT).[24] Later, this principle of calcium quantification was also used in the carotid arteries.[25,26] However, the Agatston score for calcifications assessed with EBCT has a substantial measurement variability (up to 30%[27]) making it less attractive for clinical use. Furthermore, similar to DSA, the imaging possibilities of EBCT are restricted because, besides assessment of calcium volume, no other risk parameters can accurately be assessed.

CT

Computed tomography angiography (CTA) is able to accurately grade the severity of carotid luminal stenosis.[28] Therefore, computed tomography (CT) is increasingly used in stroke patients for evaluation of the degree of carotid stenosis. The question then arises as to whether CT can also provide detailed information about possible additional risk parameters.

In 1984 it was demonstrated that single-slice CT was able to detect (besides the degree of stenosis) intimal disease in the carotid bifurcation.[29] However, the results from later studies comparing CT images with histologic sections of endarterectomy specimens were confusing: Estes et al.[30] and Oliver et al.[31] showed that hyperdense structures corresponded with calcifications, hypodense regions with

lipid or hemorrhage, and isodense regions with fibrosis. On the other hand, Walker et al.[32] demonstrated that CT fails to reliably indicate the presence of lipid or fibrous tissue, and that the predictive value of CT for the detection of plaque ulceration was only moderate They concluded that single-slice CT was insufficiently robust to be a useful tool for the characterization of carotid plaque morphology and carotid plaque surface morphology, and expressed the need for multidetector technology.[32]

MDCT

Multidetector CT (MDCT) has recently been introduced and allows full vascular imaging from the aorta to the circle of Willis. By providing this large coverage MDCT angiography (MDCTA) can now evaluate, besides the carotid bifurcation, other important atherosclerotic predilection sites, like the aortic arch, the origin of the supra-aortic vessels, the carotid siphon, and the vertebrobasilar arteries. Another advantage of MDCTA for atherosclerotic plaque evaluation is the increased in-plane resolution, the decreased slice thickness (<0.75 mm), and the subsequent ability to obtain near isotropic voxels. More detailed analysis of atherosclerotic plaque morphology and luminal plaque surface may now be possible.

The work in this thesis evaluates the role of MDCTA in 1) the depiction of atherosclerotic disease and subsequent luminal stenosis in the whole vascular tree that supplies the brain with blood, and 2) the assessment of atherosclerotic plaque features that have been related to plaque vulnerability.

Part 1: Optimization of contrast, scanning and reconstruction protocol

The presence of contrast material in the patent vessel lumen is a prerequisite to differentiate lumen from a normal vessel wall and/or from an atherosclerotic plaque. However, because contrast material is expensive and the volume of contrast material is associated with nephrotoxicity it seems important to reduce the volume of contrast material whilst maintaining adequate depiction of the vessel lumen. Therefore, we evaluated whether the application of a saline bolus chaser after the injection of contrast material improves enhancement, and whether the amount of contrast material can be reduced. In this study 75 patients were allocated to three different contrast material administration protocols: i) 80 ml contrast material, ii) 80 ml contrast material with 40 ml saline bolus chaser, and iii) 60 ml contrast material and 40 ml saline bolus chaser. For each group we assessed the time-attenuation curves by measuring the intraluminal enhancement at multiple specific locations from the ascending aorta to the circle of Willis. In addition, the association between intraluminal enhancement and patient body weight was evaluated (**Chapter 1**).

In many cases intravenous contrast injection has not ended before the start of the CT scan, which was normally performed with a caudal-cranial direction. Undiluted contrast material in the subclavian vein, brachiocephalic vein and/or superior vena cava often produces artifacts (perivenous artifacts), which can obscure adjacent structures and hamper adequate vessel imaging. We hypothesized that a

cranio-caudal scan direction might reduce the number of perivenous artifacts whilst maintaining sufficient arterial enhancement for the depiction of the arterial lumen. Therefore, we explored the effect of a caudo-cranial scan direction versus a cranio-caudal scan direction on perivenous artifacts and arterial enhancement. Forty patients were divided into two groups; the scanning protocols of both groups were the same, except for the scan direction. The two groups were compared with regard to the presence of perivenous artifacts, and the intraluminal enhancement at multiple locations from the ascending aorta to the circle of Willis (**Chapter 2**).

On CT images of the atherosclerotic plaque, calcifications create a so-called blooming artifact which results in a larger appearance of the calcifications. Such a blooming artifact leads to overestimation of the true volume of the calcium, which hampers plaque volume assessment and optimal characterization of the non-calcified part of the plaque. Voltage settings have an effect on the contrast between different structures. CT image reconstruction algorithms differ in the averaging of image data and the subsequent enhancement of contrast differences. These parameters may have an impact on the evaluation of the calcified and non-calcified parts of the atherosclerotic plaque. Therefore, in five endarterectomy specimens we analyzed the effects of different voltage settings (80, 100, 120 and 140 kVp) and different reconstruction algorithms (smooth, medium smooth, medium sharp and sharp) on the depiction of calcifications and image quality, in order to optimize these settings for atherosclerotic plaque analysis (**Chapter 3**).

Part 2: Validation studies

MDCT angiography has the potential to analyze atherosclerotic plaque morphology in more detail than is possible with single-slice CT. However, until now no validation studies have been conducted and it was unknown which Hounsfield unit thresholds had to be applied to characterize specific plaque components. The aim of our in vitro study was to assess the ability of MDCT to characterize and quantify plaque components in carotid endarterectomy specimens, with histology as gold standard. We imaged 21 endarterectomy specimens, and matched MDCT images with corresponding histologic sections. Identification of pure lipid regions and pure fibrous regions in the histologic sections allowed to assess the true Hounsfield unit value (HV) of these components. Based on these measurements an optimal HV cut-off point was established to differentiate between lipid and fibrous tissue. This cut-off point was then used during quantification of plaque area and plaque component area (**Chapter 3**).

Following this in vitro study, we performed an in vivo study to evaluate the ability of MDCTA to characterize and quantify atherosclerotic carotid plaque and plaque component areas, also with histology as gold standard.

Fifteen patients were imaged using an optimized protocol based on the results of our former studies. MDCTA images and corresponding histologic sections were matched, and we assessed the HVs for lipid and fibrous tissue. Based on these measurements an optimal HV cut-off point was assessed to differentiate between lipid and fibrous tissue. Finally, we

investigated the interpretation of hypodense regions, assumed to be lipid, on MDCTA images (**Chapter 4**).

Besides the detection of specific plaque components, quantification of the absolute and relative contribution of specific plaque components to the total plaque volume is important. Freely available software with custom-made plug-ins allowed semi-automatic assessment of plaque and plaque component areas in the MDCT images. The custom-made plug-ins were developed because no tools exist that are able to make such area measurements. After a trained observer had drawn the outer and inner vessel wall contours in the MDCT image, the plaque and plaque component areas were semi-automatically calculated. Area calculations of the plaque components were based on the previously determined plaque component specific HV ranges. We compared the measurements of plaque and plaque component areas in MDCT images of carotid endarterectomy specimens with histologic area measurements (**Chapter 3**). This study was then repeated using the MDCTA data from the in vivo study (**Chapter 4**).

After improvement of our custom-made software tool, we were able to semi-automatically assess plaque volumes and plaque component volumes (instead of areas). However, it remained necessary for an observer to draw the outer and inner wall contours, making the tool susceptible to observer variability. Therefore, in another study we evaluated observer variability of plaque and plaque component area and volume measurements performed with our custom-made software tool.

Firstly, two observers (blinded from each other) in 41 MDCTA images drew the outer and inner vessel wall contour. Then intra- and inter-observer differences in the assessment of plaque areas were assessed (**Chapter 4**). Secondly, three observers evaluated the MDCTA images of 56 patients for the presence of atherosclerosis and, if atherosclerosis was present, they drew the outer and inner vessel wall contours in all the images that showed atherosclerosis. The interobserver variability in the assessment of plaque volume and plaque component volume was assessed (**Chapter 5**).

In our clinical studies (discussed in **Part 3** of this thesis) we used a new measurement tool to assess intracranial calcification volume and a plaque surface morphology scoring system; however, because neither of these have been validated we had to perform two additional validation studies. To validate the quantification tool, two observers assessed independently the volume of intracranial internal carotid artery calcifications in 100 patients. Interobserver differences in volume measurements were assessed and presented with an intraclass correlation coefficient, a coefficient of variation, and a Bland-Altman plot (**Chapter 7**). To validate the plaque surface morphology scoring system, two observers assessed independently the carotid plaque surface of 100 patients. Interobserver differences in type of plaque surface morphology were assessed and presented as a weighted kappa (**Chapter 8**).

Part 3: Clinical studies

Since November 2002 patients with ischemic cerebrovascular symptoms (amaurosis fugax,

TIA, or minor ischemic stroke) are included in an ongoing prospective study. Patients are enrolled from the neurology department's TIA/stroke outpatient clinic or neurology ward. Patients undergo neurological examination on admission, and medical history and information on risk factors are recorded. Furthermore, in all patients MDCT of the brain and MDCTA of the carotid arteries is performed. From all patients, follow-up data after 4 years on recurrent vascular events (MI, stroke, TIA vascular death) and death from other causes are collected. The main purpose of this study is to determine the ability of MDCTA to assess (vulnerable) atherosclerotic plaque features, and to prospectively evaluate if these plaque features have an additional value over degree of carotid stenosis in the prediction of ischemic cerebrovascular events, and/or have a value as a marker of systemic atherosclerotic disease. This thesis contains three cross-sectional studies based on the data of 406 analyzed patients.

In the first of these studies we measured the volume of intracranial internal carotid artery calcifications and assessed the association between these calcifications and cardiovascular risk factors. To evaluate the role of these calcifications in ischemic stroke we evaluated whether calcifications were more extensively present in the symptomatic internal carotid artery than in the contralateral asymptomatic internal carotid artery. In addition we compared the volume of intracranial calcification in symptomatic intracranial internal carotid artery in patients with amaurosis fugax, TIA or minor stroke (**Chapter 7**).

In the second study we assessed the atherosclerotic plaque surface morphology in the carotid artery and assessed the association between plaque surface morphology and 1) the severity of stenosis and 2) cardiovascular risk factors. To establish the role of plaque surface morphology in ischemic stroke we evaluated whether plaque irregularities and ulcerations were more frequently present in the symptomatic internal carotid artery than in the contralateral asymptomatic internal carotid artery. In addition, we compared the frequency of plaque irregularities and ulcerations in symptomatic intracranial internal carotid artery in patients with amaurosis fugax and TIA or minor stroke (**Chapter 8**).

In the third study, with MDCTA we measured the volume of the atherosclerotic plaque and the proportion of the different plaque components in symptomatic carotid arteries. We analysed the relationship of these volumes with 1) severity of stenosis and 2) cardiovascular risk factors. We hypothesized 1) that severity of stenosis was not closely related to plaque volume, and 2) that cardiovascular risk factors are more related to plaque volume than to severity of stenosis. Finally, we evaluated the relationship between plaque volume and the contribution of the different components (**Chapter 9**).

Chapter 6 presents a review of the CT and MDCT validation studies on evaluation of plaque surface, quantification of calcifications, and characterization and quantification of the non-calcified portion of coronary and carotid atherosclerotic plaque. The influence of scanning and reconstruction parameters

on plaque imaging is described. The clinical applications and future direction of CT-based plaque imaging is discussed.

The **final chapter** of this thesis presents a summary and discusses potential clinical applications. In addition, directions for further research are suggested. The focus of further research will be on follow-up studies that explore the association between vulnerable plaque parameters and (recurrent) ischemic cerebrovascular events. The main aim will be to achieve an optimal selection of patients for carotid endarterectomy and stent placement.

References

1. Warlow C, et al. Stroke. Lancet. 2003;362:1211-24.
2. Struijs JN, et al. Modeling the future burden of stroke in The Netherlands: impact of aging, smoking, and hypertension. Stroke. 2005;36:1648-55.
3. Khan U, et al. Risk factor profile of cerebral small vessel disease and its subtypes. J Neurol Neurosurg Psychiatry. 2007;78:702-6.
4. Kittner SJ, et al. Infarcts with a cardiac source of embolism in the NINCDS Stroke Data Bank: historical features. Neurology. 1990;40:281-4.
5. Coull AJ, et al. Population based study of early risk of stroke after transient ischaemic attack or minor stroke: implications for public education and organisation of services. Bmj. 2004;328:326.
6. Collaborative overview of randomised trials of antiplatelet therapy--I: Prevention of death, myocardial infarction, and stroke by prolonged antiplatelet therapy in various categories of patients. Antiplatelet Trialists' Collaboration. Bmj. 1994;308:81-106.
7. Halkes PH, et al. Aspirin plus dipyridamole versus aspirin alone after cerebral ischaemia of arterial origin (ESPRIT): randomised controlled trial. Lancet. 2006;367:1665-73.
8. Yusuf S, et al. Effect of potentially modifiable risk factors associated with myocardial infarction in 52 countries (the INTERHEART study): case-control study. Lancet. 2004;364:937-52.
9. Randomised trial of endarterectomy for recently symptomatic carotid stenosis: final results of the MRC European Carotid Surgery Trial (ECST). Lancet. 1998;351:1379-87.
10. Beneficial effect of carotid endarterectomy in symptomatic patients with high-grade carotid stenosis. North American Symptomatic Carotid Endarterectomy Trial Collaborators. N Engl J Med. 1991;325:445-53.
11. Barnett HJ, et al. The appropriate use of carotid endarterectomy. Cmaj. 2002;166:1169-79.
12. Streifler JY, et al. Prognostic importance of leukoaraiosis in patients with symptomatic internal carotid artery stenosis. Stroke. 2002;33:1651-5.
13. Barnett HJ, et al. Benefit of carotid endarterectomy in patients with symptomatic moderate or severe stenosis. North American Symptomatic Carotid Endarterectomy Trial Collaborators. N Engl J Med. 1998;339:1415-25.

14. Benavente O, et al. Carotid endarterectomy for asymptomatic carotid stenosis: a meta-analysis. Bmj. 1998;317:1477-80.
15. Rothwell PM, et al. Endarterectomy for symptomatic carotid stenosis in relation to clinical subgroups and timing of surgery. Lancet. 2004;363:915-24.
16. Naghavi M, et al. From vulnerable plaque to vulnerable patient: a call for new definitions and risk assessment strategies: Part I. Circulation. 2003;108:1664-72.
17. Lovett JK, et al. Histological correlates of carotid plaque surface morphology on lumen contrast imaging. Circulation. 2004;110:2190-7.
18. Shah PK. Mechanisms of plaque vulnerability and rupture. J Am Coll Cardiol. 2003;41:15S-22S.
19. Slager CJ, et al. The role of shear stress in the destabilization of vulnerable plaques and related therapeutic implications. Nat Clin Pract Cardiovasc Med. 2005;2:456-64.
20. Oliver JJ, et al. Noninvasive assessment of arterial stiffness and risk of atherosclerotic events. Arterioscler Thromb Vasc Biol. 2003;23:554-66.
21. Eliasziw M, et al. Significance of plaque ulceration in symptomatic patients with high-grade carotid stenosis. North American Symptomatic Carotid Endarterectomy Trial. Stroke. 1994;25:304-8.
22. Rothwell PM, et al. Interrelation between plaque surface morphology and degree of stenosis on carotid angiograms and the risk of ischemic stroke in patients with symptomatic carotid stenosis. On behalf of the European Carotid Surgery Trialists' Collaborative Group. Stroke. 2000;31:615-21.
23. Streifler JY, et al. Angiographic detection of carotid plaque ulceration. Comparison with surgical observations in a multicenter study. North American Symptomatic Carotid Endarterectomy Trial. Stroke. 1994;25:1130-2.
24. Agatston AS, et al. Quantification of coronary artery calcium using ultrafast computed tomography. J Am Coll Cardiol. 1990;15:827-32.
25. Arad Y, et al. Correlations between vascular calcification and atherosclerosis: a comparative electron beam CT study of the coronary and carotid arteries. J Comput Assist Tomogr. 1998;22:207-11.
26. Allison MA, et al. Patterns and risk factors for systemic calcified atherosclerosis. Arterioscler Thromb Vasc Biol. 2004;24:331-6.
27. Wang S, et al. Detection of coronary calcification with electron-beam computed tomography: evaluation of interexamination reproducibility and comparison of three image-acquisition protocols. Am Heart J. 1996;132:550-8.
28. Koelemay MJ, et al. Systematic review of computed tomographic angiography for assessment of carotid artery disease. Stroke. 2004;35:2306-12.
29. Heinz ER, et al. Examination of the extracranial carotid bifurcation by thin-section dynamic CT: direct visualization of intimal atheroma in man (Part 1). AJNR Am J Neuroradiol. 1984;5:355-9.

30. Estes JM, et al. Noninvasive characterization of plaque morphology using helical computed tomography. J Cardiovasc Surg (Torino). 1998;39:527-34.
31. Oliver TB, et al. Atherosclerotic plaque at the carotid bifurcation: CT angiographic appearance with histopathologic correlation. AJNR Am J Neuroradiol. 1999;20:897-901.
32. Walker LJ, et al. Computed tomography angiography for the evaluation of carotid atherosclerotic plaque: correlation with histopathology of endarterectomy specimens. Stroke. 2002;33:977-81.

PART 1

Optimization of contrast, scanning and reconstruction protocol

1 SIXTEEN-DETECTOR ROW CT ANGIOGRAPHY OF CAROTID ARTERIES: COMPARISON OF DIFFERENT VOLUMES OF CONTRAST MATERIAL WITH AND WITHOUT A BOLUS CHASER

Cécile de Monyé • Filippo Cademartiri • Thomas T de Weert • Dorine AM Siepman • Diederik WJ Dippel • Aad van der Lugt

Radiology 2005; 237:555-62

Sixteen-detector row CT angiography of carotid arteries: Comparison of different volumes of contrast material with and without a bolus chaser

Abstract

Objective

to prospectively compare different volumes of intravenously administered contrast material with and without a bolus chaser at 16-detector row computed tomographic (CT) angiography of the carotid arteries.

Materials and Methods

Institutional Review Board approval and informed consent were obtained. Seventy-five consecutive patients (44 men and 31 women; mean age, 63 years; range, 22-85 years) were allocated to one of three protocols: group 1, 80 mL of contrast material; group 2, 80 mL contrast material followed by 40 mL of saline; and group 3, 60 mL of contrast material followed by 40 mL of saline. Bolus tracking was used to synchronize contrast material injection with CT scanning. The attenuation in Hounsfield Units was measured from the ascending aorta to the intracranial arteries at 1-second intervals. Differences were tested with the Student t-test.

Results

The maximum attenuation was reached in the proximal internal carotid artery in all groups. The addition of a bolus chaser to 80 mL contrast material resulted in a higher mean attenuation (323 ± 39 HU vs 351 ± 60 HU; $p = 0.06$), higher maximum attenuation (393 ± 53 HU, 425 ± 76 HU; $p = 0.09$) and higher minimum attenuation (240 ± 34 HU vs 264 ± 48 HU; $p < 0.05$). Group 3 had lower mean, maximum and minimum attenuation than did groups 1 and 2 ($p < 0.001$).

Conclusion

The addition of a bolus chaser to 80 mL of contrast material results in a slightly higher attenuation. Decreasing the volume of contrast material from 80 mL to 60 mL results in a significantly lower attenuation.

Introduction

The benefit of carotid endarterectomy in patients with severe symptomatic carotid artery stenosis (> 70%) has been established in large randomized trials[1, 2]. The degree of stenosis in these trials was assessed with digital subtraction angiography. The inherent risk of this invasive procedure has led to a non-invasive diagnostic strategy in which patients are screened with duplex ultrasonography (US) followed by a magnetic resonance angiography (MRA) in case of abnormal US findings[3].

With the introduction of spiral computed tomography (CT), CT angiography entered clinical practice[4, 5]. Evaluation of CT Angiography for the assessment of significant stenosis (> 70%) in the carotid artery has already revealed a high sensitivity and specificity[6-11]. However, single-section CT angiography has not gained much popularity in the diagnostic work-up of patients suspected of having symptomatic carotid artery stenosis. This may have been related to limitations in the required volume of contrast material (> 100 ml), scan range (< 120 mm), section thickness (≥ 2 mm) and available postprocessing techniques.

Multi-detector row CT (MDCT), and in particular, 16-detector row CT, has eliminated several of these limitations[12-15]. It allows CT angiography of the carotid arteries to be performed with an increased coverage from aortic arch to the circle of Willis, an improved spatial resolution of less than 1-mm section thickness, shorter acquisition times of less than 15 seconds, and lower doses of contrast material.

The application of a saline bolus chaser after the injection of contrast material may further reduce the volume of contrast material[16-20], but an optimal contrast material injection protocol has not yet been established for 16-detector row CT angiography of the carotid arteries. Thus, the purpose of our study was to prospectively compare different volumes of intravenously administered contrast material with and without a bolus chaser at 16-detector row CT angiography of the carotid arteries.

Materials and Methods

Study population

From October 2002 to February 2003, 75 consecutive patients (44 men and 31 women; mean age, 63 years; range, 22-85 years) who underwent CT angiography of the carotid arteries were enrolled in the study (62 outpatients, 13 inpatients). Indication for CT angiography was suspected atherosclerotic disease of the carotid or vertebrobasilar vascular system in patients with a transient ischemic attack or minor ischemic stroke. Exclusion criteria were previous allergic reaction to iodinated contrast media, renal insufficiency (serum creatinine level of >100 mmol/L), pregnancy, and age younger than 18 years. Patients with an occlusion of the carotid artery were also excluded. The Institutional Review Board approved the study and patients provided informed consent.

Each patient was allocated to one of three contrast material administration protocols. The first 25 patients (group 1: 14 men and

11 women; mean age, 60 years; range, 36-81 years) received 80 mL of contrast material without bolus chaser, the next 25 patients (group 2: 17 men and 8 women; mean age, 68 years; range, 27-84 years) received 80 mL of contrast material followed by 40 mL of saline bolus chaser, and the last group of 25 patients (group 3: 13 men and 12 women; mean age, 60 years; range: 22-85 years) received 60 mL of contrast material followed by 40 mL of saline bolus chaser. In case of bolus tracking, which allows synchronization of CT scanning with the passage of contrast material, the amount of contrast material should be equal to or more than the scan time times the injection rate as follows: ±15 seconds x 4 mL/sec = 60 mL. As a precaution, we started the study with 80 mL of contrast material and tried to reduce the dose to 60 mL. With an injection rate of 4 mL/sec, 40 mL saline is a reasonable amount of fluid to flush the vein for injection and to push the tail of the contrast material bolus to the superior vena cava. For each patient, age, sex, and weight were recorded.

Scanning protocol

Patients underwent CT angiography of the carotid arteries with a 16-detector row CT scanner (Sensation 16; Siemens Medical Solutions, Forchheim, Germany). Patients were positioned supine on the CT table with the arms along the chest. A lateral scout view that included the thorax, neck and skull was acquired. The scan range reached from the ascending aorta to the intracranial circulation (2 cm above the sella turcica). Scanning parameters were 0.75-mm collimation, 12-mm (pitch of 1) table feed per rotation, 0.5-second rotation time, 120 kV, 180 mAs, caudocranial scanning direction, and 10-14 seconds scan time (depending on individual patient's size and anatomy). The entire examination took 15 minutes.

The contrast material iodixanol (320 mg of iodine per milliliter, Visipaque; Amersham Health, Little Chalfont, UK) was injected intravenously through an 18-20-gauge cannula, depending on the size of the vein, into the antecubital vein by using a power injector (EnVision; MedRAD, Pittsburgh, Pa). The right antecubital vein was preferentially used, because it provides the shortest path of the contrast material through the venous system and therefore the least dilution. When venous access on the right side could not be achieved, the left antecubital vein was used. The saline bolus chaser was injected immediately after the injection of contrast material was completed, using a second power injector (EnVision; MedRAD). Both power injectors were connected to the injection cannula with a T-shaped tube (MedRAD) with an integrated one-way valve attached to the power injector that contained the saline bolus chaser to prevent reflux of the contrast medium. Contrast material and saline bolus chaser injection rate were 4 mL/sec.

Synchronization between the passage of contrast material and data acquisition was achieved by real-time bolus tracking. The arrival of the injected contrast material was monitored in real time by using a series of dynamic transverse low-dose monitoring scans (120 kV, 20-40 mAs) at the level of the ascending aorta at intervals of 1 second. The monitoring sequence started 5 seconds after the initiation of contrast material administra-

tion. CT angiography was triggered automatically on the basis of a threshold measured in a region of interest (ROI) in the ascending aorta. The size of the ROI in the ascending aorta for the bolus triggering was adjusted to the size and composition of the ascending aorta, but was always greater than 5 mm in diameter. The trigger threshold was set at an increase in attenuation of 75 HU over the baseline (approximately 150 HU in absolute value). When the threshold was reached, the table was moved to the caudal start position while the patient was instructed not to swallow. Four seconds after the trigger threshold was reached, CT angiographic data acquisition was started automatically. All bolus timing procedures and CT angiographic scans were successfully completed. No adverse reactions to contrast material were observed.

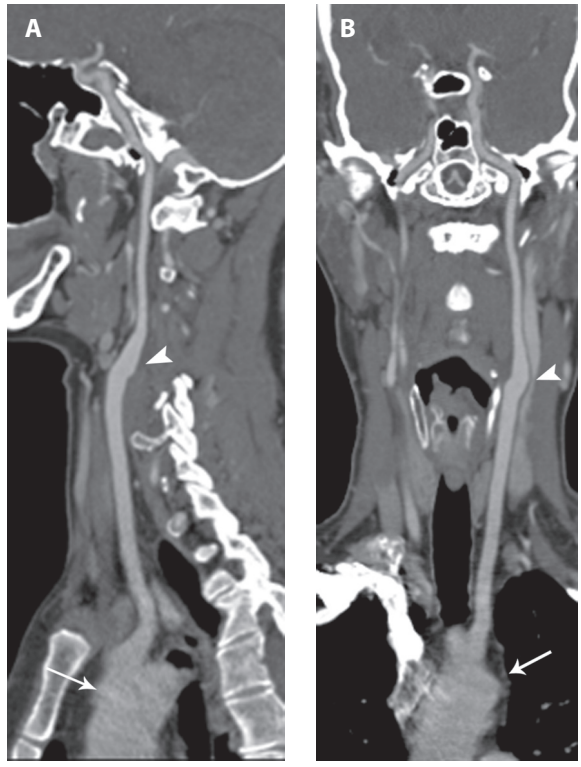

Figure 1. CT angiograms of the left carotid artery. (a) Sagittal and (b) coronal curved planar reformations from the aortic arch to the carotid siphon. The curved planar reformations demonstrate an homogeneous attenuation in the artery from the aortic arch (arrow) through the carotid bifurcation (arrowhead) to the intracranial circulation.

Data collection and analysis

Images were reconstructed with an effective section width of 1 mm, reconstruction interval of 0.6 mm, field of view of 100 mm, and a medium-smooth convolution kernel (B30f; Siemens Medical Solutions). The images were transferred to a stand-alone workstation and evaluated using dedicated analysis software (Leonardo; Siemens Medical Solutions). For clinical analysis, two curved planar reformations of each carotid artery from the aortic arch to the carotid siphon were created in perpendicular planes (Fig. 1).

In each patient, the site of injection, scan coverage (in millimeters), number of transverse sections, scan delay (in seconds), and scan time (in seconds) were recorded.

Transverse images were used for attenuation measurements. The Digital Imaging and Communications in Medicine layout of the images showed the time at which the scanning was performed. At intervals of 1 second (each 40th section), an ROI was drawn throughout the data sets in two regions: (a) the ascending aorta to the right internal carotid artery (ICA), and (b) the ascending aorta to the left ICA. The location of the measurements was recorded as follows: the ascending aorta, aortic

arch, proximal common carotid artery (CCA) (first two measurements in the CCA), distal CCA, proximal ICA (first two measurements in the ICA), distal ICA, carotid siphon and intracranial part of the ICA; measurements in the brachiocephalic trunk were considered to be measurements in the CCA.

One observer (C.d.M.) with 3 years of experience with CT angiography measured and recorded all data. The attenuation was measured by drawing a circular ROI in the center of the vessel lumen. The ROIs were drawn as large as the anatomic configuration of the lumen allowed in the transverse section.

The mean value of the measurements on the left and right side at each time point was calculated. Time-attenuation curves were generated for each patient. Subsequently, the attenuation at time 0; the mean, minimum and maximum attenuation; and the time to reach the maximum attenuation were assessed. Because attenuation above 200 HU was considered optimal, the number of measurements below 200 HU was counted.

The aforementioned analysis resulted in one to three measurements per location, depending on the size of the patient. To analyze the attenuation in these locations, the measurements obtained in these locations were averaged. The relationship between the mean attenuation and weight was analyzed in all three groups.

Statistical analysis

Differences between measurements on the left and right side were analyzed with paired Student t-test. Baseline characteristics and attenuation parameters (value at time 0, minimum and maximum attenuation, and time to maximum attenuation) in the three groups were compared with an one-way analysis of variance (ANOVA) test or Chi-square test. In case of a significant difference, a pair-wise comparison was performed with the Student t-test. The mean attenuation and the attenuation at different locations in the three groups were compared with repeated-measures ANOVA. In case of a significant difference, a pair-wise comparison with repeated measures ANOVA was performed. In addition, a pair-wise comparison of attenuation parameters with adjustment for differences in weight, age and sex was performed with a linear regression model. The relationship between weight and mean attenuation in the three groups was analyzed with linear regression analysis.

Statistical analysis was performed by using software (SPSS, version 9.0, SPSS, Chicago, Ill; and SAS Proc Mixed, SAS Institute, Cary, NC). $P < 0.05$ was considered to indicate a significant difference.

Results

Patients and procedures

More patients in group 3 received the contrast material (60 mL) and bolus chaser (40 mL) via the left antecubital vein than patients in groups 1 and 2 (32%, 4% and 12%, respectively; $p < 0.05$). Patient demographics, weight, scan delay, scan time, scan range and the number of images were not significantly different in the three groups (Table 1).

Left versus right injection side

Combination of data from all 75 patients revealed a slightly higher mean attenuation (2.5 HU ± 8.8) on the left side in comparison with the right side ($p < 0.05$)(Fig 2). In addition, the time to maximum attenuation was slightly shorter (0.3 second ± 1.3) on the left side ($p < 0.05$). The maximum and minimum attenuation on the left and right side were not different (Table 2).

Table 1 Patient and Scan Characteristics in Three Groups with Different Volumes of Contrast Material

Parameter	Group 1 80 mL CM	Group 2 80 mL CM + 40 mL BC	Group 3 60 mL CM + 40 mL BC
Number of patients	25	25	25
Gender: Male/Female	14/11	17/8	13/12
Age: mean (range) years	60 (36-81)	68 (27-84)	60 (22-85)
Weight: mean (range) kg	75 (58-107)	71 (55-92)	78 (56-103)
Injection site: right/left *	24/1	22/3	17/8
Scan delay: mean (range) sec	18 (12-26)	18 (15-24)	19 (14-27)
Scan time: mean (range) sec	14 (11-17)	13 (11-16)	13 (11-15)
Scan coverage mean (range) mm	331 (275-401)	325 (256-372)	316 (256-368)
Number of sections; mean (range)	553 (459-670)	546 (427-637)	527 (427-621)

Note: Data in parentheses are the range.
CM = contrast material; BC = bolus chaser; * = Chi-square test $p < 0.05$

Group 1: 80 mL contrast material

The mean arterial attenuation was 323 ± 39 HU. The minimum and maximum arterial attenuation was 240 ± 34 HU and 393 ± 53 HU, respectively. Two measurements in 2 of the 25 patients (330 measurements) had an attenuation of less than 200 HU. Both measurements were in the intracranial arteries.

Group 2: 80 mL contrast material with 40 mL saline

The mean arterial attenuation per patient was 351 ± 60 HU. The minimum and maximum arterial attenuation per patient was 264 ± 48 HU and 425 ± 76 HU, respectively. Five measurements in 2 of the 25 patients (330 measurements) had an attenuation of less than 200 HU. Two of these measurements were in the ascending aorta - aortic arch and three in the carotid siphon - intracranial arteries.

Table 2 Paired difference of attenuation parameters obtained on the left and right injection sides in 75 patients

Parameter	Paired difference	P Value
Mean attenuation (HU)	2.5 ± 8.8	< 0.05
Minimum attenuation (HU)	3.6 ± 24.9	Not significant
Maximum attenuation (HU)	0.7 ± 17.8	Not significant
Time to maximum attenuation (sec)	-0.3 ± 1.3	< 0.05

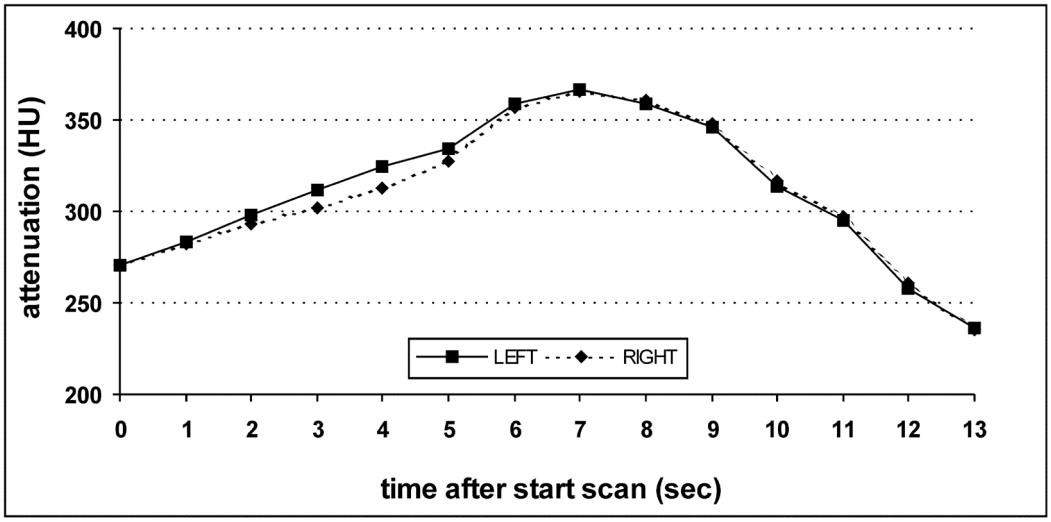

Figure 2. The time-attenuation curves show the mean intraluminal attenuation in left (n = 75) and right (n = 75) carotid arteries after start of scanning. There is a slightly higher mean attenuation on the left side in comparison to the right side.

Group 3: 60 mL contrast material with 40 mL saline

The mean arterial attenuation per patient was 273 ± 53 HU. The minimum and maximum arterial attenuation per patient was 185 ± 43 HU and 331 ± 64 HU, respectively. 53 of the measurements in 16 of the 25 patients (326 measurements) had an attenuation of less than 200 HU. These measurements were obtained in the ascending aorta, CCA, ICA, and

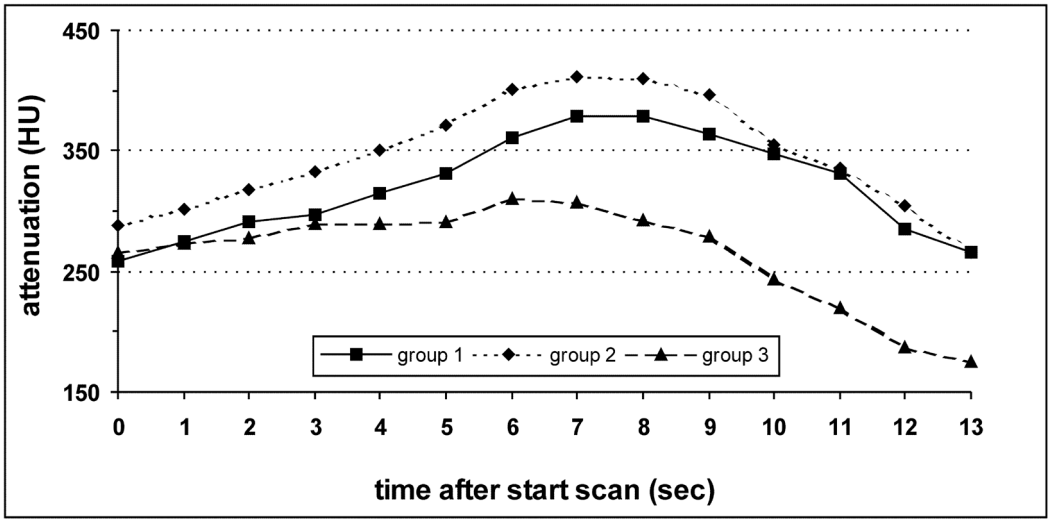

Figure 3. Time-attenuation curves show intraluminal attenuation after start of scanning in group 1 (80 mL contrast, n = 25), group 2 (80 mL contrast + 40 mL saline, n = 25) and group 3 (60 mL contrast + 40 mL saline, n = 25). A lower volume of contrast material resulted in lower attenuation.

intracranial arteries in 2, 15, 9 and 27 cases, respectively.

Comparison of time attenuation curves

The attenuation value at time 0 was significantly higher with the application of 40 mL bolus chaser (group 1 vs group 2); in addition, the maximum attenuation was higher (425 HU in group 2 vs 393 HU in group 1), although not significantly ($p = 0.09$). The minimum attenuation was significantly higher with the bolus chaser ($p < 0.05$). The time to maximum attenuation was shorter (6.9 seconds in group 2 vs 7.8 seconds in group 1, $p < 0.05$) (Table 3, Fig 3).

The group that received 60 mL of contrast material and 40 mL of bolus chaser had lower mean, maximum and minimum attenuations and time to maximum attenuation ($p < 0.001$) in comparison to the group that received 80 mL or contrast material without 40 mL of bolus chaser and the group that received 80 mL of contrast material with 40 mL of bolus chaser (Table 3). Adjustment for weight, age and sex in a regression model showed the same significant differences between the groups.

Comparison of locations

In all groups, the attenuation first increased to a maximum and then decreased during the course of the CT angiographic examination (Table 4, Fig 4). The maximum attenuation was reached in the proximal ICA in all three groups. The addition of a bolus chaser resulted in a higher attenuation at all locations, although no significant difference was reached except for the aortic arch ($p < 0.05$).

The group that received 60 mL contrast material and 40 mL bolus chaser had a lower attenuation ($p < 0.01$) at all locations, from the distal CCA to the intracranial arteries, in comparison to the group that received 80 mL of contrast material without 40 mL of bolus chaser and the group that received 80 mL of contrast material with 40 mL of bolus chaser (Table 4).

Table 3 Attenuation parameters in three groups with different volumes of contrast material

Parameter	Group 1	Group 2	Group 3	P Value	P Value	P Value
	80 mL CM	80 mL CM				
+						
40 mL BC	60 mL CM					
+						
40 mL BC	1 vs 2	2 vs 3	1 vs 3			
Time 0 value (HU) *	258 ± 32	288 ± 42	266 ± 48	< 0.01	NS	NS
Mean attenuation (HU) **	323 ± 39	351 ± 60	273 ± 53	NS	< 0.001	< 0.001
Minimum attenuation (HU) ***	240 ± 34	264 ± 48	185 ± 43	< 0.05	< 0.001	< 0.001
Maximum attenuation (HU) ***	393 ± 52	425 ± 76	331 ± 64	NS	< 0.001	< 0.001
Time to maximum attenuation (sec)***	7.8 ± 1.4	6.9 ± 1.4	5.0 ± 2.0	< 0.05	< 0.001	< 0.001

Note: Data are the mean ± standard deviation.
CM = contrast material; BC = bolus chaser; NS = not significant.
* = ANOVA, $p < 0.05$; ** = repeated-measures ANOVA, $p < 0.001$; *** = ANOVA, $p < 0.001$.

Table 4 Attenuation measurements at different locations in three groups with different volumes of contrast material

Location	Group 1	Group 2	Group 3	P Value	P Value	P Value
	80 mL CM	80 mL CM				
+						
40 mL BC	60 mL CM					
+						
40 mL BC	1 vs 2	2 vs 3	1 vs 3			
Ascending aorta (HU)	268 ± 34	292 ± 40	268 ± 48	NT	NT	NT
Aortic arch (HU) *	281 ± 36	309 ± 43	276 ± 46	< 0.05	< 0.05	NS
Proximal CCA (HU) **	311 ± 41	331 ± 52	286 ± 51	NS	< 0.01	NS
Distal CCA (HU) ***	357 ± 53	386 ± 70	301 ± 77	NS	< 0.001	< 0.01
Proximal ICA (HU) ***	376 ± 52	409 ± 82	301 ± 70	NS	< 0.001	< 0.001
Distal ICA (HU) ***	356 ± 59	387 ± 83	275 ± 65	NS	< 0.001	< 0.001
Carotid siphon (HU) ***	314 ± 53	342 ± 71	236 ± 57	NS	< 0.001	< 0.001
Intracranial ICA (HU) ***	274 ± 67	289 ± 63	190 ± 44	NS	< 0.001	< 0.001

Note: Data are the mean ± standard deviation.
CM = contrast material; BC = bolus chaser; NS = not significant; NT = not tested.
* = repeated-measures ANOVA, $p < 0.05$; ** = repeated-measures ANOVA, $p < 0.01$; *** = repeated-measures ANOVA, $p < 0.001$.

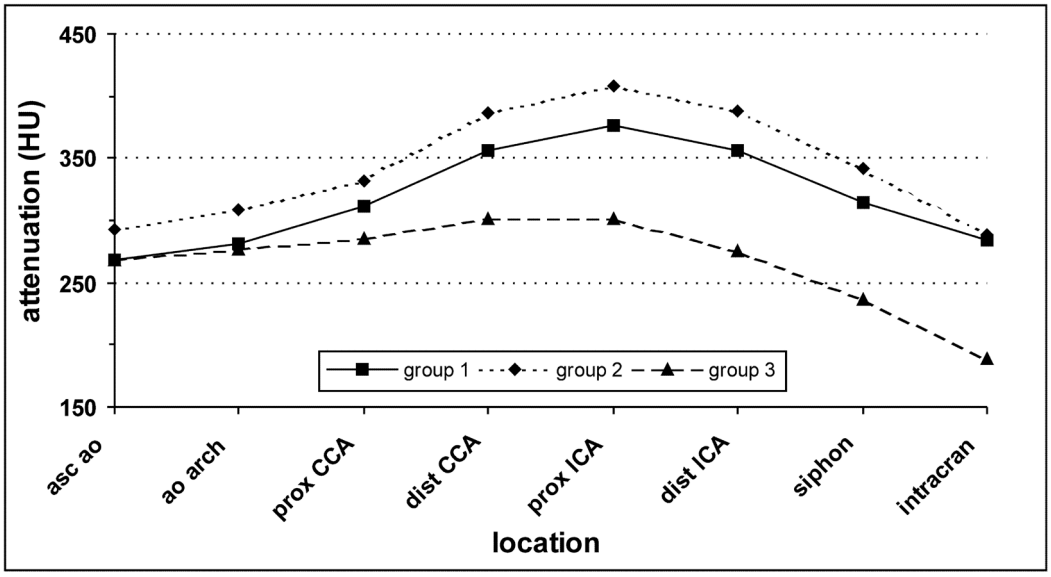

Figure 4. Intraluminal attenuation in group 1 (80 mL contrast, n = 25), group 2 (80 mL contrast 40 mL saline, n = 25) and group 3 (60 mL contrast 40 mL saline, n = 25) at different locations, from the ascending aorta to the circle of Willis. The maximum attenuation was reached in the proximal ICA in all three groups. The addition of a bolus chaser resulted in a higher attenuation at all locations, although no significant difference was reached, except for the aortic arch ($p < 0.05$). Group 3 had a lower attenuation at all locations, from the distal CCA to the intracranial arteries, in comparison with that in groups 1 and 2 ($p < 0.01$).

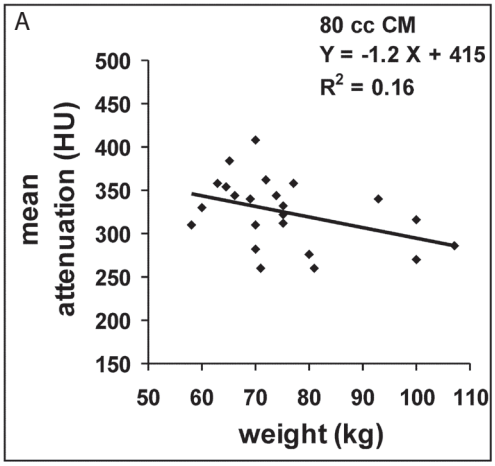

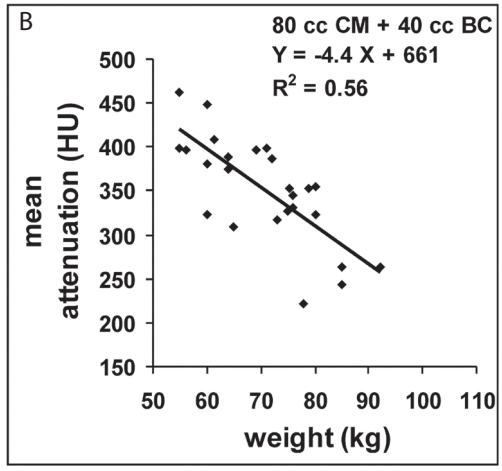

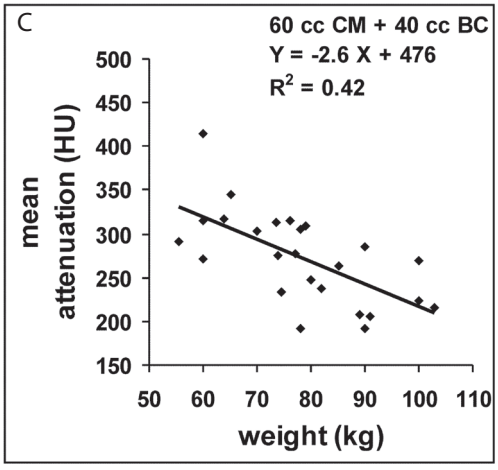

Figure 5. (a-c) Mean attenuation plotted against weight for each contrast material (CM) protocol. The addition of a bolus chaser (BC) makes the relationship between mean attenuation and weight stronger. The best correlation was found in the group that received 80 mL of contrast material and 40 mL of saline bolus chaser.

Relationship of weight and mean attenuation

In the group that received 80 mL of contrast material, there was a weak, though almost significant, relationship between weight and the mean attenuation (slope, –1.2; $p = 0.06$; $R2 = 0.16$). With the addition of a bolus chaser in groups 2 and 3, this relationship became stronger and more significant, with a slope of –4.4 and –2.6 ($p < 0.01$) and $R2 = 0.56$ and 0.42, respectively (Fig 5).

In the group that received 80 mL of contrast material and 40 mL of saline, a significant difference was found in the mean attenuation between patients weighing 75 kg or less and those wheighing more than 75 kg (381 HU ± 45 vs 305 HU ± 52, $p < 0.001$). In the group that received 60 mL of contrast material and 40 mL of saline, a significant difference was found in mean attenuation between patients weighing 75 kg or less and those weighing more than 75 kg (308 HU ± 49 vs 250 HU ± 43, $p < 0.01$). There was no significant difference in the mean attenuation between patients weighing 75 kg or less who received 60 mL of contrast material and patients weighing more than 75 kg who received 80 mL of contrast material ($p = 0.90$) (Fig 6).

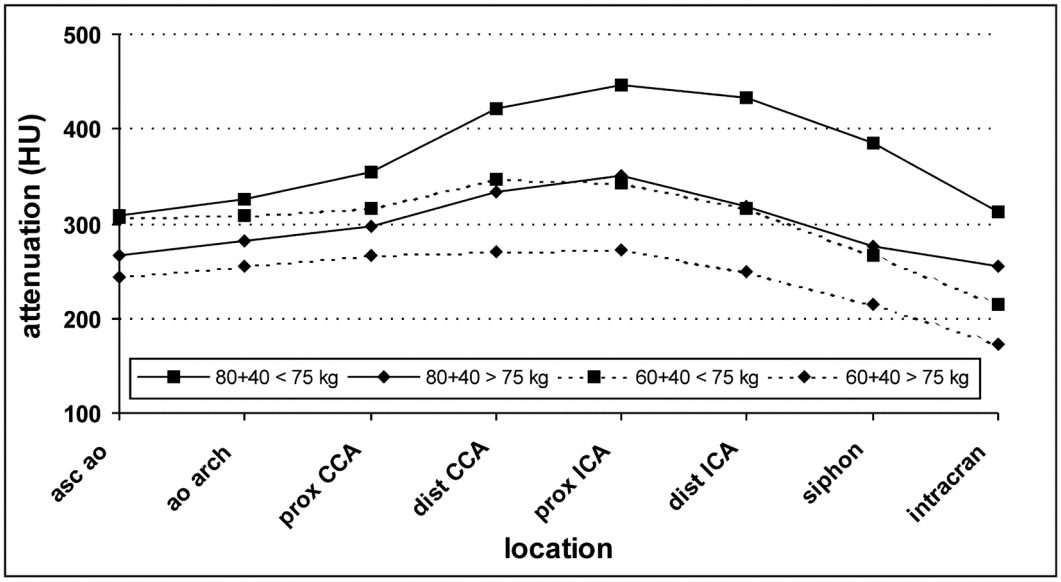

Figure 6. Intraluminal attenuation in the group that received 80 mL of contrast material and 40 mL of saline bolus chaser and the patient group that received 60 mL of contrast material and 40 mL of saline bolus chaser at different locations, from the ascending aorta to the circle of Willis. Subdivision was made between patients weighing 75 kg or less and patients weighing more than 75 kg. There is no significant difference in the mean attenuation between patients weighing 75 kg or less and who received 60 mL of contrast material and patients weighing more than 75 kg and who received 80 mL of contrast material ($p = 0.9$).

Discussion

Multi-detector row CT scanners allow performance of CT angiography of the carotid arteries with increased coverage from the aortic arch to the circle of Willis, improved spatial resolution, and shorter acquisition times. The short acquisition time may lead to lower doses of contrast material. It has been reported[16-20] that a saline bolus chaser after the injection of the contrast material may further reduce the volume of contrast material without an subsequent decrease in arterial attenuation. Yet, to our knowledge, no studies have been performed to determine the optimal contrast material administration protocol for CT angiography of the carotid arteries at multi-detector row CT.

When the left carotid artery was compared with the right carotid artery, a slightly higher mean attenuation and a shorter time to maximum attenuation were found on the left side. This may be caused by the way the time-attenuation curves were assessed. The time scale does not correspond to the length of the path the contrast material has passed through the vessel: the contrast material reaches the left carotid artery, which originates directly from the aortic arch, earlier than the right carotid artery, where the contrast material has to follow a longer path through the brachiocephalic trunk to reach the right carotid artery.

Injection of 80 mL of contrast material resulted in an attenuation above 200 HU in all but two measurements. Comparison of the mean time

attenuation curve of 80 mL of contrast material with and without a saline bolus chaser demonstrated higher mean and maximum attenuations along the carotid arteries, although the differences were not significant.

Hopper et al.[19] found higher attenuation in the ascending aorta with the addition of 50 mL saline bolus chaser to 75 or 100 mL of contrast material, although the differences were not significant. The results from their study can be explained by the lack of the analysis of a time-attenuation curve of the aorta, which allows the assessment of maximum and mean attenuations. However, Irie et al.[16], who did perform such an analysis, failed to demonstrate a significant increase in maximum attenuation with the application of a saline bolus chaser. Failure to demonstrate a significant effect of a bolus chaser on attenuation in these two studies and in our study may be explained by the small number of patients (n = 15-25) in the groups with different contrast material protocols.

On the basis of the attenuation curves of 80 mL of contrast material with and without a saline bolus chaser, we analyzed whether a decrease in the volume of contrast material was possible without compromising the attenuation. However, 60 mL of contrast material followed by 40 mL of saline bolus chaser resulted in a significantly lower mean and maximum attenuation in comparison to those with 80 mL of contrast material with and without a saline bolus chaser. Previous studies have not revealed such a decrease in attenuation with the replacement of contrast material by a saline bolus chaser. Haage et al.[18] found the same attenuation in the ascending aorta by comparing 60 mL of contrast material and 30 mL saline bolus chaser with 75 mL of contrast material (240 HU for both) . In another study, almost the same attenuation in the ascending aorta was observed by using 75 ml of contrast material with 50 ml saline bolus chaser and 125 ml of contrast material alone (254 HU vs 225 HU, respectively)[19]. In both studies, the attenuation was measured in one region instead of several levels. Irie et al.[16], who assessed the time attenuation curve in the aorta, found the same maximum attenuation with 75 mL of contrast material alone and with 63 mL of contrast material and a 25 mL saline bolus chaser. Cademartiri et al.[20] found the same mean and maximum attenuations in a time-attenuation curve in the descending aorta with 140 mL of contrast material alone and with 100 mL of contrast material followed by 40 mL saline bolus chaser. The discrepancy of our results could partly be explained by the difference, although not significant, in weight between the groups in our study, especially between group 2 and 3. However, adjustment for weight in a regression model still showed a difference in mean and maximum attenuation between group 3 and group 1 and 2.

Patient weight is inversely correlated with arterial enhancement[17, 21-23]. Our study revealed only a relationship between weight and mean attenuation in the patient groups with a bolus chaser. The best correlation was found in the group that received 80 mL contrast material and 40 mL saline bolus chaser. This could be explained by a better circulation of contrast material with the addition of a bolus chaser to the contrast material protocol. On the basis of

our results, a consideration could be made to adjust for weight; for example, use 60 mL of contrast material followed by a 40 mL saline bolus chaser in patients 75 kg or less and use 80 mL of contrast material followed by a 40 mL saline bolus chaser in patients weighing more than 75 kg to establish the mean and minimum attenuation of more than 250 HU and 200 HU, respectively.

The search for the lowest volume of contrast material necessary for optimal analysis has several motives. First, the high cost of contrast material forces the radiologist to search for ways to further decrease contrast material volume. However, one should realize that replacement of contrast material by saline necessitates the purchase of a dual-head power injector or an additional single-head power injector and the extra use of saline, a T connector and a syringe. Schoellnast et al.[24] showed that by taking these extra costs into account there is still a cost reduction. Second, the risk of nephrotoxicity is related to the volume of contrast material, and decreasing the volume of contrast material may influence the risk of subsequent nephrotoxicity[25-27]. Third, in patients with acute stroke, CT angiography of the carotid arteries has been combined with CT perfusion of the brain, which required an additional injection of 50 mL of contrast material[28, 29]. In such studies the total volume of contrast material should be restricted to what is necessary for optimal analysis. Finally, it may be possible that, in comparison to what is commonly thought, the best contrast material protocol is not the one with the highest intraluminal attenuation. Which attenuation in CT angiography allows the best evaluation of the presence and severity of vessel disease is not well studied. Attenuation levels obtained with 60 mL of contrast material followed by 40 mL of saline may be high enough for an excellent interpretation of the vessel, owing to a better contrast with calcifications in the vessel wall or atherosclerotic plaque. This may have an effect on both visual analysis as well as semi-quantitative analysis of the vessel dimensions.

Our study had several limitations. First, the patients were not randomly assigned to the groups. However, baseline characteristics were not significantly different except for injection site. The higher frequency of the left-sided injection in group 3 may have lead to a lower mean attenuation, because the longer path of the contrast material through the venous system may have diluted the contrast material. Second, the groups may be too small to lead to a significant result. Third, we analyzed attenuation from the aortic arch to the circle of Willis. Ideally, a single level dynamic CT will result in a more precise analysis of the contrast media dynamics[30]. Such a study will cause extra radiation exposure to the patients and we were reluctant to do this. Nevertheless, in clinical practice we are dealing with attenuation along the supra-aortic arteries, which reflects the way the contrast material passes through the vessels.

In conclusion, of the protocols we tested, the integration of a saline bolus chaser in the contrast material protocol for evaluation of the carotid arteries with 16-detector row CT leads to optimization of the attenuation but does not allow decrease in contrast material vol-

ume from 80 to 60 mL in all patients. Future studies may focus on a less strong reduction in contrast material volume, weight-adjusted dosage of contrast material or adjustment of the scan protocol; increase in pitch will shift the maximum attenuation distally.

References

1. Beneficial effect of carotid endarterectomy in symptomatic patients with high-grade carotid stenosis. North American Symptomatic Carotid Endarterectomy Trial Collaborators. N Engl J Med 1991; 325:445-53.
2. MRC European Carotid Surgery Trial: interim results for symptomatic patients with severe (70-99%) or with mild (0-29%) carotid stenosis. European Carotid Surgery Trialists' Collaborative Group. Lancet 1991; 337:1235-43.
3. Nederkoorn PJ, Mali WP, Eikelboom BC, Elgersma OE, Buskens E, Hunink MG, Kappelle LJ, Buijs PC, Wust AF, van der Lugt A, van der Graaf Y: Preoperative diagnosis of carotid artery stenosis: accuracy of noninvasive testing. Stroke 2002; 33:2003-8.
4. Napel S, Marks MP, Rubin GD, Dake MD, McDonnell CH, Song SM, Enzmann DR, Jeffrey RB, Jr.: CT angiography with spiral CT and maximum intensity projection. Radiology 1992; 185:607-10.
5. Katz DA, Marks MP, Napel SA, Bracci PM, Roberts SL: Circle of Willis: evaluation with spiral CT angiography, MR angiography, and conventional angiography. Radiology 1995; 195:445-9.
6. Hollingworth W, Nathens AB, Kanne JP, Crandall ML, Crummy TA, Hallam DK, Wang MC, Jarvik JG: The diagnostic accuracy of computed tomography angiography for traumatic or atherosclerotic lesions of the carotid and vertebral arteries: a systematic review. Eur J Radiol 2003; 48:88-102.
7. Dillon EH, van Leeuwen MS, Fernandez MA, Eikelboom BC, Mali WP: CT angiography: application to the evaluation of carotid artery stenosis. Radiology 1993; 189:211-9.
8. Cumming MJ, Morrow IM: Carotid artery stenosis: a prospective comparison of CT angiography and conventional angiography. AJR Am J Roentgenol 1994; 163:517-23.
9. Link J, Brossmann J, Grabener M, Mueller-Huelsbeck S, Steffens JC, Brinkmann G, Heller M: Spiral CT angiography and selective digital subtraction angiography of internal carotid artery stenosis. AJNR Am J Neuroradiol 1996; 17:89-94.
10. Marcus CD, Ladam-Marcus VJ, Bigot JL, Clement C, Baehrel B, Menanteau BP: Carotid arterial stenosis: evaluation at CT angiography with the volume-rendering technique. Radiology 1999; 211:775-80.
11. Leclerc X, Godefroy O, Lucas C, Benhaim JF, Michel TS, Leys D, Pruvo JP: Internal carotid arterial stenosis: CT angiography with volume rendering. Radiology 1999; 210:673-82.

12. Lell M, Wildberger JE, Heuschmid M, Flohr T, Stierstorfer K, Fellner FA, Lang W, Bautz WA, Baum U: CT-Angiographie der A. carotis: Erste Erfahrungen mit einem 16-Schicht-Spiral-CT. Rofo Fortschr Geb Rontgenstr Neuen Bildgeb Verfahr 2002; 174:1165-9.
13. Ertl-Wagner B, Hoffmann RT, Bruning R, Dichgans M, Reiser MF: Supraaortale Gefassdiagnostik mit dem 16-Zeilen-Multidetektor-Spiral-CT. Untersuchungsprotokoll und erste Erfahrungen. Radiologe 2002; 42:728-32.
14. Fleischmann D: Present and future trends in multiple detector-row CT applications: CT angiography. Eur Radiol 2002; 12 Suppl 2:S11-5.
15. Fleischmann D: Use of high concentration contrast media: principles and rationale-vascular district. Eur J Radiol 2003; 45 Suppl 1:S88-93.
16. Irie T, Kajitani M, Yamaguchi M, Itai Y: Contrast-enhanced CT with saline flush technique using two automated injectors: how much contrast medium does it save? J Comput Assist Tomogr 2002; 26:287-91.
17. Cademartiri F, van der Lugt A, Luccichenti G, Pavone P, Krestin GP: Parameters affecting bolus geometry in CTA: a review. J Comput Assist Tomogr 2002; 26:598-607.
18. Haage P, Schmitz-Rode T, Hubner D, Piroth W, Gunther RW: Reduction of contrast material dose and artifacts by a saline flush using a double power injector in helical CT of the thorax. AJR Am J Roentgenol 2000; 174:1049-53.
19. Hopper KD, Mosher TJ, Kasales CJ, TenHave TR, Tully DA, Weaver JS: Thoracic spiral CT: delivery of contrast material pushed with injectable saline solution in a power injector. Radiology 1997; 205:269-71.
20. Cademartiri F, Mollet N, van der Lugt A, Nieman K, Pattynama PM, de Feyter PJ, Krestin GP: Non-invasive 16-row multislice CT coronary angiography: usefulness of saline chaser. Eur Radiol 2004; 14:178-83.
21. Platt JF, Reige KA, Ellis JH: Aortic enhancement during abdominal CT angiography: correlation with test injections, flow rates, and patient demographics. AJR Am J Roentgenol 1999; 172:53-6.
22. Fleischmann D, Rubin GD, Bankier AA, Hittmair K: Improved uniformity of aortic enhancement with customized contrast medium injection protocols at CT angiography. Radiology 2000; 214:363-71.
23. Bae KT, Heiken JP, Brink JA: Aortic and hepatic contrast medium enhancement at CT. Part I. Prediction with a computer model. Radiology 1998; 207:647-55.
24. Schoellnast H, Tillich M, Deutschmann HA, Deutschmann MJ, Fritz GA, Stessel U, Schaffler GJ, Uggowitzer MM: Abdominal multidetector row computed tomography: reduction of cost and contrast material dose using saline flush. J Comput Assist Tomogr 2003; 27:847-53.
25. Rudnick MR, Goldfarb S, Wexler L, Ludbrook PA, Murphy MJ, Halpern EF, Hill JA, Winniford M, Cohen MB, VanFossen DB: Nephrotoxicity of ionic and nonionic contrast media in 1196 patients: a randomized trial. The Iohexol Cooperative Study. Kidney Int 1995; 47:254-61.

26. Manske CL, Sprafka JM, Strony JT, Wang Y: Contrast nephropathy in azotemic diabetic patients undergoing coronary angiography. Am J Med 1990; 89:615-20.
27. Rosovsky MA, Rusinek H, Berenstein A, Basak S, Setton A, Nelson PK: High-dose administration of nonionic contrast media: a retrospective review. Radiology 1996; 200:119-22.
28. Smith WS, Roberts HC, Chuang NA, Ong KC, Lee TJ, Johnston SC, Dillon WP: Safety and feasibility of a CT protocol for acute stroke: combined CT, CT angiography, and CT perfusion imaging in 53 consecutive patients. AJNR Am J Neuroradiol 2003; 24:688-90.
29. Nabavi DG, Kloska SP, Nam EM, Freund M, Gaus CG, Klotz E, Heindel W, Ringelstein EB: MOSAIC: Multimodal Stroke Assessment Using Computed Tomography: novel diagnostic approach for the prediction of infarction size and clinical outcome. Stroke 2002; 33:2819-26.
30. Bae KT, Heiken JP, Brink JA: Aortic and hepatic contrast medium enhancement at CT. Part II. Effect of reduced cardiac output in a porcine model. Radiology 1998; 207:657-62.

2.

OPTIMIZATION OF CT ANGIOGRAPHY OF THE CAROTID ARTERY WITH A 16-MDCT SCANNER: CRANIOCAUDAL SCAN DIRECTION REDUCES CONTRAST MATERIAL-RELATED PERIVENOUS ARTIFACTS

Cécile de Monyé • Filippo Cademartiri • Thomas T de Weert • Dorine AM Siepman • Diederik WJ Dippel • Aad van der Lugt

American Journal of Roentgenology 2006;186: 1737-45

Optimization of CT angiography of the carotid artery with a 16-MDCT scanner: craniocaudal scan direction reduces contrast material-related perivenous artifacts

Abstract

Objective

The objective of our study was to compare the effect of a caudocranial scan direction versus a craniocaudal scan direction on arterial enhancement and perivenous artifacts in 16-MDCT angiography of the supra-aortic arteries.

Materials and Methods

Eighty consecutive patients (51 men; mean age, 62 years; age range, 28-89 years) underwent scanning in the caudocranial direction (group 1; n=40) or craniocaudal direction (group 2; n=40). All patients received 80 mL of contrast material followed by a 40 mL saline bolus chaser, both administered IV at 4 mL/sec. Bolus tracking was used. Attenuation inside the arterial lumen was measured at intervals of 1 second throughout the data set. Attenuation in the superior vena cava (SVC) was measured. Contrast material-related perivenous artifacts were graded on a scale of 0-3 (none to extensive).

Results

Attenuation in the ascending aorta, carotid bifurcation and intracranial arteries were slightly lower in group 2 versus group 1 (231 ± 64 HU, 348 ± 52 HU and 258 ± 48 HU vs 282 ± 43 HU, 381 ± 73 HU and 291 ± 77 HU, respectively; $p<0.05$). Maximum and mean arterial attenuation were slightly lower in group 2 versus group 1 (369 ± 58 HU and 303 ± 48 HU vs 401 ± 71 HU and 334 ± 58 HU, respectively; $p<0.05$). Attenuation in the SVC was much lower in group 2 versus group 1 (169 ± 39 HU versus 783 ± 330 HU, respectively; $p<0.001$). Mean streak artifact score was much lower in group 2 versus group 1 (1.3 ± 0.9 versus 2.5 ± 0.6, respectively; $p<0.001$).

Conclusion

Use of a craniocaudal scan direction results in slightly lower attenuation of the carotid artery and much lower attenuation of the SVC. Streak artifacts are significantly reduced. This technique allows better evaluation of the ascending aorta and supraaortic arteries.

Introduction

Acute ischemic neurological symptoms are related to small vessel disease of the intracranial perforating arteries, thrombo-embolism from atherosclerotic disease in the supra-aortic arteries and cardiac embolism[1].

The most common source of thromboembolism is atherosclerotic disease of the carotid bifurcation. However, atherosclerotic lesions in the aorta, the origin of the supraaortic arteries, the common carotid artery (CCA), the internal carotid artery (ICA) distal to the bifurcation, and the vertebrobasilar circulation can cause transient ischemic attack or ischemic stroke due to thromboembolism[2, 3]. In the evaluation of patients with cerebrovascular disease, complete vascular imaging from the aorta to the circle of Willis must be performed before therapeutic decision-making can be undertaken.

With the introduction of MDCT, particularly 16-MDCT scanners, CT angiography (CTA) has become an attractive diagnostic method in the care of patients with cerebrovascular symptoms[4].

With bolus tracking, CTA scanning can be optimally synchronized with the passage of contrast material in the arteries[5]. The CTA scanning usually starts before the injection of contrast material ends. With this method, the presence of undiluted contrast material in the subclavian vein, brachiocephalic vein and superior vena cava (SVC) produces artifacts that project over the ascending aorta and the origin of the supraaortic

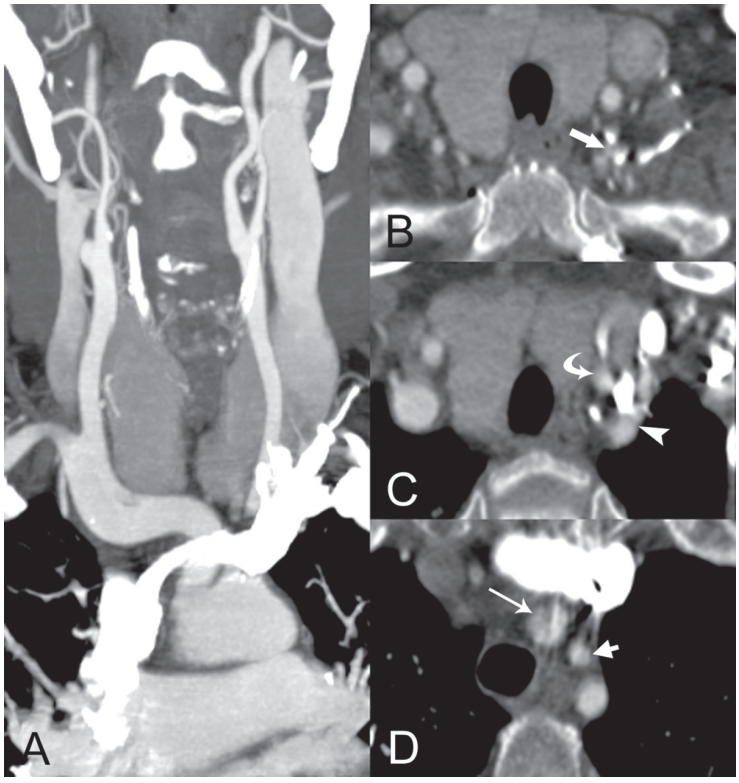

Figure 1. CT angiograms of supraaortic arteries in a 74-year-old woman scanned in caudocranial direction with left-sided injection of contrast material.
A: Coronal maximum intensity projection (15 mm). High-density contrast material in left subclavian vein and reflux of contrast material in neck veins give rise to artifacts over the origin of the supraaortic vessels.
B: Axial image at level of origin of left vertebral artery (arrow).
C: Axial image at level of proximal part of left common carotid artery (arrow) and left subclavian artery (arrowhead).
D: Axial image at level of first 1 cm of brachiocephalic trunk (long arrow) and left common carotid artery (short arrow). Evaluation of atherosclerotic disease is hampered by streak artifacts.

arteries[6,7]. Such artifacts can obscure adjacent structures and thus hide or suggest stenosis or occlusion of the proximal supraaortic arteries (Fig. 1). Addition of a bolus chaser to the main contrast bolus may reduce the frequency of these artifacts by clearing the veins of contrast material. However, the timing of the CTA scan is not altered by the addition of a bolus chaser and artifacts do occur. Use of a craniocaudal scan direction, opposite to the direction of blood flow, may reduce the number of artifacts caused by delayed scanning of the apex of the thorax (Fig. 2).

The purpose of this study was to compare the effects of a caudocranial scan direction versus a craniocaudal scan direction on enhancement of the carotid artery and on the presence of perivenous artifacts in CTA with a 16-MDCT scanner.

Materials and Methods

Study population

Between November 2002 and August 2003, 80 consecutive patients (51 men and 29 women; mean age, 62 years; range, 28-89 years), who underwent CTA of the carotid artery, were enrolled in the study. The indication for CTA was suspected atherosclerotic disease of the carotid or vertebrobasilar vascular system in

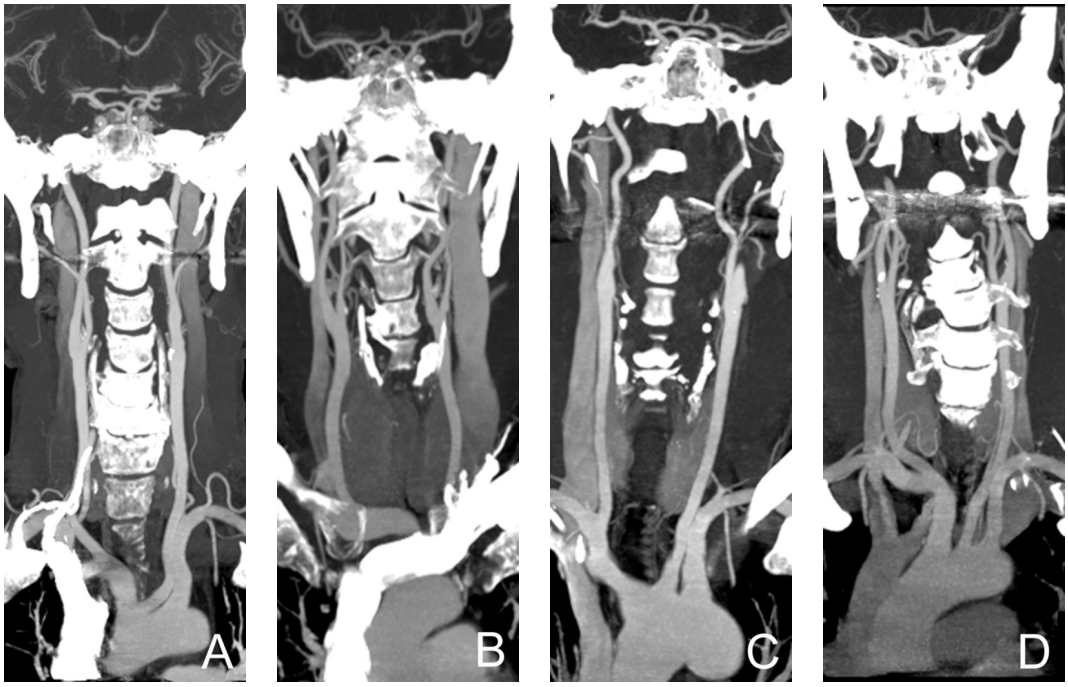

Figure 2. CT angiograms of supraaortic arteries. Four maximum intensity projections (30 mm) in coronal plane in four patients.
A and B, CT angiographic scans in caudocranial direction with right-sided (72-year-old man, A) and left-sided (B) injection of contrast material. Very high density of contrast material in the subclavian vein and superior vena cava hides the origin of the supraaortic arteries.
C and D, CT angiographic scans in craniocaudal direction with right-sided (48-year-old man, C) and left-sided (54-year-old man, D) injection of contrast material. High density of contrast material is not left in veins, and we all arteries are clearly depicted.

patients who had had a transient ischemic attack or minor ischemic stroke. Exclusion criteria were previous allergic reaction to iodine contrast medium, renal insufficiency (serum creatinine > 100 mmol/L), pregnancy, and age less than 18 years. Patients with occlusion of the carotid artery also were excluded. The Institutional Review Board approved the study, and patients gave informed consent in writing.

Each patient was allocated to one of two groups with different scan protocols. The first 40 patients (group 1) underwent scanning in the caudal to cranial direction, the second 40 patients (group 2) underwent scanning in the cranial to caudal direction. Age, sex, and body weight were recorded for each patient.

Scan protocol

The patients underwent CTA of the carotid artery with a 16-MDCT scanner (Sensation 16, Siemens Medical Solutions, Forchheim, Germany). Patients were positioned supine on the CT table with the arms along the chest. A lateral scout view including the thorax, neck and skull was acquired. The CTA scan range reached from the ascending aorta to the intracranial blood vessels (2 cm above the sella turcica). Scan parameters were as follows: number of detectors, 16; individual detector width, 0.75 mm; table feed per rotation, 12 mm (pitch of 1); gantry rotation time, 0.5 sec; 120 kV; 180 mAs; and scanning time, 10-14 sec, depending on patient's size and anatomic features). The entire examination took approximately 15 minutes.

The contrast material (iodixanol 320 mg I/ml [Visipaque, Amersham Health]) was injected with a double-head power injector (Stellant, MedRAD) through an 18- to 20-gauge IV cannula (depending on the size of the vein) in an antecubital vein. The right antecubital vein was preferentially used, because it provides the shortest path for contrast material through the venous system and therefore the least dilution. When venous access could not be achieved on the right side, the left antecubital vein was used. The saline bolus chaser was injected through the second head of the power injector immediately after injection of contrast material was completed. All patients received 80 mL of contrast material and a 40 mL saline bolus chaser, both at an injection rate of 4 mL/sec.

Synchronization between the passage of contrast material and data acquisition was achieved with real-time bolus tracking. The arrival of the injected contrast material was monitored in real time with a series of dynamic axial low-dose monitoring scans (120 kV, 20-40 mAs) at the level of the ascending aorta at intervals of 1 sec. The monitoring sequence started 5 sec after initiation of administration of contrast material. The CTA scan was triggered automatically by means of a threshold measured in a region of interest (ROI) set in the ascending aorta. The size of the ROI in the ascending aorta for the bolus triggering was adjusted to the size and composition of the ascending aorta, but was always greater than 5 mm in diameter. The trigger threshold was set at an increase in attenuation of 75 Hounsfield Units (HU) above baseline attenuation (≈ 150 HU in absolute HU value). When the threshold

was reached, the table was moved to the start position while the patient was instructed not to swallow. Breath-hold instructions were not given to the patient. CTA data acquisition was started automatically 4 sec (caudocranial scan direction) or 6 sec (craniocaudal scan direction) after the trigger threshold was reached. All bolus timing procedures and CTA scans were successfully completed. No significant adverse reactions to contrast material or other side effects occured.

Data collection and analysis

Images were reconstructed with an effective slice width of 1 mm, reconstruction interval of 0.6 mm, field of view of 100 mm, and convolution kernel B30f (medium smooth). The images were transferred to a stand-alone workstation and evaluated with dedicated analysis software (Leonardo, Siemens Medical Solutions).

For each patient, site of injection and scan delay (in seconds) were recorded. Axial images were used for the attenuation measurements. On each 40th slice (1-sec interval), beginning with the most caudal slice, an ROI was drawn throughout the data sets in two regions: the ascending aorta to the right ICA, and the ascending aorta to the left ICA. Measurements were recorded at the following locations: ascending aorta, aortic arch, proximal CCA (first two measurements in the CCA), distal CCA, proximal ICA (first two measurements in the ICA), distal ICA, carotid siphon, and intracranial part of the ICA. Measurements in the brachiocephalic trunk were considered to be measurements in the CCA.

Two observers measured and recorded all data. Attenuation was measured by drawing a circular ROI in the center of the vessel lumen. The ROI was drawn as large as the anatomic configuration of the lumen allowed in the axial slice. The mean value of the measure-

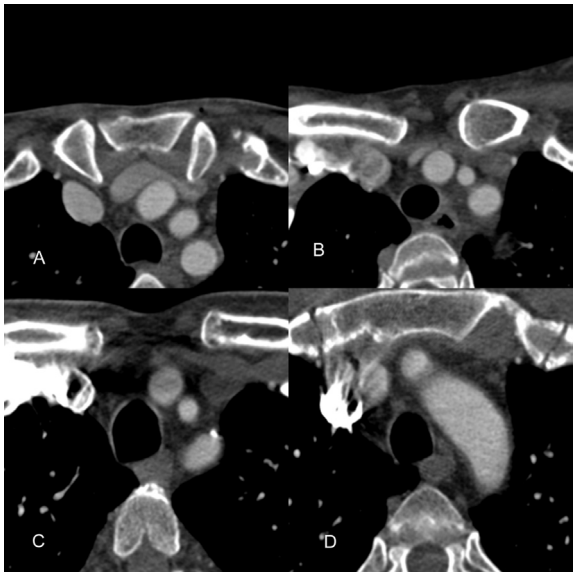

Figure 3. Contrast material-related perivenous artifacts graded on four-point scale in four different patients.
A, Score of 0 indicates no streak artifacts and clear anatomic detail in 39-year-old man.
B, score of 1 indicates minimal streak artifacts without notable obscuration of adjacent arteries in 40-year-old woman.
C, score of 2 indicates moderate streak artifacts partially obscuring adjacent arteries in 59-year-old man.
D, score of 3 indicates extensive streak artifacts completely obscuring adjacent arteries in 63-year-old man. Figure 3.
Contrast material-related perivenous artifacts graded on four-point scale in four different patients.
A, Score of 0 indicates no streak artifacts and clear anatomic detail in 39-year-old man.
B, score of 1 indicates minimal streak artifacts without notable obscuration of adjacent arteries in 40-year-old woman.
C, score of 2 indicates moderate streak artifacts partially obscuring adjacent arteries in 59-year-old man.
D, score of 3 indicates extensive streak artifacts completely obscuring adjacent arteries in 63-year-old man.

ments on the left and right side at each time point was calculated. Time-attenuation curves were generated for each patient, and mean, minimum and maximum attenuation were assessed. Because attenuation greater than 200 HU was considered optimal, the number of measurements less than 200 HU was counted. The analysis resulted in one to three measurements per location depending on the size of the patient. For analysis of attenuation, the measurements obtained in these locations were averaged.

Contrast material-related perivenous artifacts were graded on a four-point scale adjusted from Rubin et al[6] and Vogel et al[8] (Fig. 3). A score of 0 indicated no streak artifacts and clear anatomic detail; 1, minimal streak artifacts without notable obscuration of adjacent arteries; 2, moderate streak artifacts partially obscuring adjacent arteries; and 3, extensive streak artifacts completely obscuring adjacent arteries. The artifact score was assessed by two observers blinded to scan protocol. In case of a lack of congruence, consensus was reached. Attenuation in the SVC was measured in the most caudal slice. Reflux of contrast material in the veins of the neck was measured in centimeters on a coronal maximum-intensity-projection image.

Statistical analysis

Baseline characteristics, attenuation parameters and artifact parameters in the two groups were compared using Student's t-test, chi-square test or Mann Whitney test. In the pairwise comparison of attenuation parameters, a linear regression model was used to adjust for weight and age. The Spearman's rank correlation test was used for assessment of the relation between artifact parameters.

The software used for statistical analysis was SPSS 11.5 (SPSS). A p-value of < 0.05 was considered statistically significant.

Results

Patients and procedures

Patient demographics were not significantly different in the two groups (Table 1). Scan delay was significantly higher in group 2 ($p < 0.01$) because of the extra 2 sec necessary after the threshold was reached for the table to

Table 1 Patient and Scan Characteristics

Characteristic	Caudocranial scan direction (Group 1)	Craniocaudal scan direction (Group 2)
Number of patients	40	40
Sex (Male/Female)	26/14	25/15
Age (years): mean (range)	65 (28-85)	59 (32-89)
Weight (kg): mean (range)	74 (55-97)	75 (54-96)
Injection side (right/left)	34/6	29/11
Scan delay (sec): mean (range) *	18 (14-22)	20 (14-30)
Number of slices: mean (range) **	532 (427-637)	500 (430-564)

* = Student's t-test: $p < 0.01$; ** = Student's t-test: $p < 0.001$

move to a cranial start position in comparison with a caudal start position. After correction for those 2 sec, there was no significant difference in scan delay between the two groups.

Caudocranial scan direction

Mean arterial attenuation for the caudocranial scan direction was 334 ± 58 HU (Table 2). The minimum and maximum arterial attenuation per patient were 255 ± 50 HU and 401 ± 71 HU, respectively. Fifteen measurements in five of the 40 patients (513 measurements) had an attenuation of less than 200 HU. These measurements were obtained in the ascending aorta (n=2), aortic arch (n=2), CCA (n=3), ICA (n=1), carotid siphon (n=2), and intracranial arteries (n=5).

Craniocaudal scan direction

The mean arterial attenuation per patient was 303 ± 48 HU (Table 2). The minimum and maximum arterial attenuation per patient were 212 ± 49 HU and 369 ± 58 HU, respectively. Sixty-nine of the measurements in 16 of the 40 patients (493 measurements) had an attenuation less than 200 HU. These measurements were obtained in the ascending aorta (n=23), aortic arch (n=12), CCA(n=15), ICA (n=8), carotid siphon (n=5), and intracranial arteries (n=6).

Comparison of attenuation curves

Group 2, in whom the craniocaudal scan direction was used, had lower mean, maximum,

Table 2 Attenuation Levels

Parameter	Attenuation (HU)		P Value*	P Value** After adjustment for age and weight
	Caudocranial scan direction (Group 1)	Craniocaudal scan direction (Group 2)		
Mean	334 ± 58	303 ± 48	< 0.05	NS
Maximum	401 ± 71	369 ± 58	<0.05	NS
Minimum	255 ± 50	212 ± 49	<0.001	<0.01

NS = not significant.
* = Student's t-test; ** = multiple linear regression.

Table 3 Attenuation by Location

Location	Mean attenuation ± SD (HU)		P Value*	P Value** After adjustment for age and weight
	Caudocranial scan direction (Group 1)	Craniocaudal scan direction (Group 2)		
Ascending aorta	282 ± 43	231 ± 64	<0.001	<0.01
Aortic arch	293 ± 44	259 ± 62	<0.01	NS
Proximal CCA	310 ± 52	299 ± 64	NS	NS
Distal CCA	363 ± 65	334 ± 59	<0.05	NS
Proximal ICA	381 ± 73	348 ± 52	<0.05	NS
Distal ICA	368 ± 75	331 ± 50	<0.05	NS
Carotid siphon	333 ± 71	288 ± 46	<0.01	<0.01
Intracranial ICA	291 ± 77	258 ± 48	<0.05	<0.05

CCA = common carotid artery; ICA = internal carotid artery; NS = not significant.
* = Student's t-test; ** = multiple linear regression

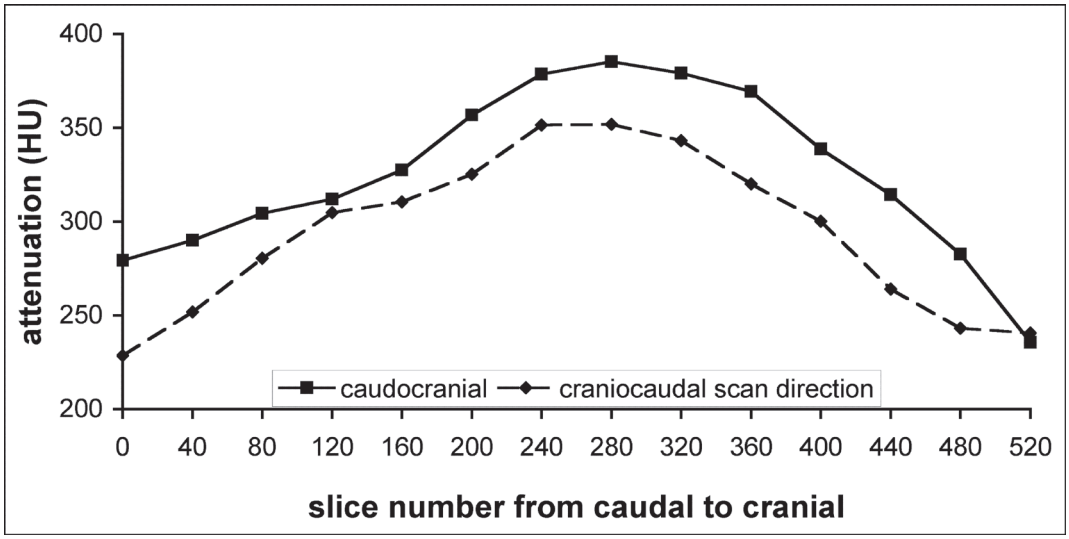

Figure 4. Time-attenuation curves show intraluminal attenuation at slice number from caudal to cranial. Slightly lower attenuation is evident for craniocaudal scan direction in comparison with caudocranial scan direction.

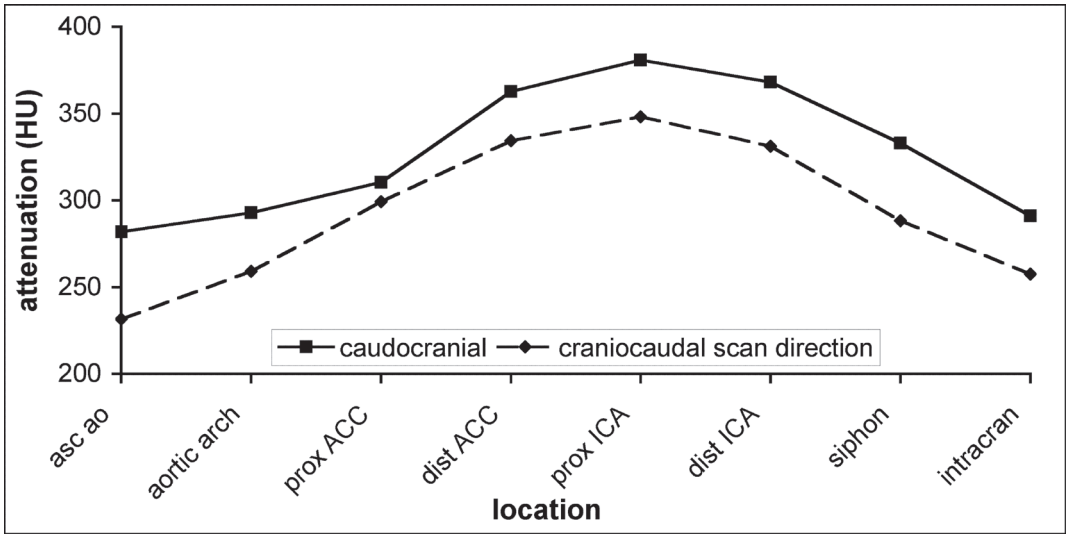

Figure 5. Intraluminal attenuation of group 1 (caudocranial scan direction) and group 2 (craniocaudal scan direction) at different locations from ascending aorta (asc ao) to circle of Willis. Maximum attenuation was reached in proximal internal carotid artery (ICA) in both groups. Prox = proximal, CCA = common carotid artery, Dist = distal, Intracran = intracranial arteries.

and minimum attenuations ($p < 0.05$) than group 1, in whom the caudocranial scan direction was used (Tables 2 and 3, Figs. 4 and 5). After adjustment for age and weight, no significant difference was found in mean ($p = 0.07$) or maximum ($p = 0.26$) attenuation. Minimum attenuation remained significantly different ($p < 0.01$). In both patient groups, maximum attenuation was reached in the proximal ICA.

The craniocaudal scan direction resulted in

Table 4 Attenuation in Relation to Artifacts

Parameter	Mean ± SD		P Value
	Caudocranial scan direction (Group 1)	Craniocaudal scan direction (Group 2)	
Superior Vena Cava attenuation (HU)	782 ± 330	169 ± 39	<0.001
Streak-artifact score	2.5 ± 0.6	1.3 ± 0.9	<0.001
Reflux neck veins (cm)	2.9 ± 2.4	1.2 ± 1.5	<0.001

significantly lower attenuation in all locations ($p < 0.05$), except for the proximal CCA ($p = 0.39$). After adjustment for age and weight, no significant difference was found for the aortic arch ($p = 0.07$), proximal CCA ($p = 0.87$), distal CCA ($p = 0.17$), proximal ICA ($p = 0.21$), or distal ICA ($p = 0.16$). Attenuation in the ascending aorta, carotid siphon, and intracranial arteries remained significantly different ($p < 0.05$).

Comparison of artifacts

Attenuation in the SVC was much higher in group 1 (caudocranial) than in group 2 (craniocaudal): 782 ± 330 HU (range 183 – 2083 HU) and 169 ± 39 HU (range 102-288 HU), respectively ($p < 0.001$) (Table 4).

The mean artifact scores were 2.5 ± 0.6 and 1.3 ± 0.9 for groups 1 and 2, respectively ($p < 0.001$). All but one of the patients in group 1 had an artifact score of 2 or more. Extensive streak artifacts completely obscuring adjacent arteries (score 3) were seen in 21 (53%) of the patients in group 1 and in three (8%) of the patients in group 2.

Reflux of contrast material in the neck veins measured 2.9 ± 2.4 cm (range 0 - 14.4 cm) and 1.2 ± 1.5 cm (range 0 - 5.1 cm) in groups 1 and 2 ($p < 0.001$). Reflux of contrast material in the neck veins measuring more than 2 cm was seen in group 1 in 24 (60%) of the patients and in group 2 in 11 (28%) of the patients ($p < 0.001$).

Table 5 Artifact Parameters According to Injection Side

Parameter	Mean ± SD		P Value
	Left Injection (n=17)	Right Injection (n=63)	
Caudocranial scan direction (Group 1)			
SVC (HU)	732 ± 265	791 ± 343	NS
Artifact score	2.7 ± 0.5	2.4 ± 0.7	NS
Reflux (cm)	2.9 ± 1.6	2.9 ± 2.6	NS
Craniocaudal scan direction (Group 2)			
SVC (HU)	167 ± 56	170 ± 32	NS
Artifact score	1.7 ± 1.0	1.2 ± 0.8	NS
Reflux (cm)	2.2 ± 1.9	0.8 ± 1.1	<0.01

SVC = Superior vena cava; NS = not significant.

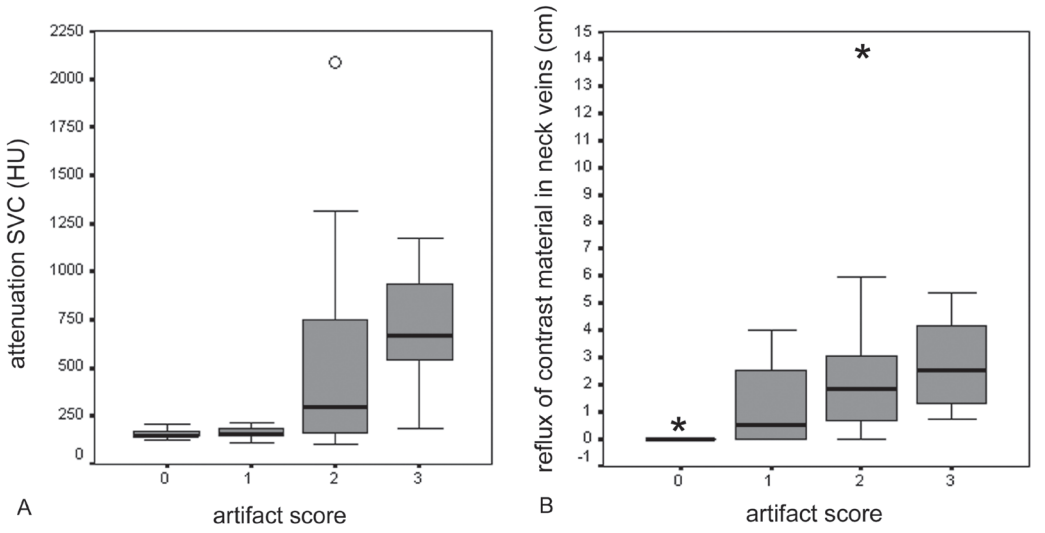

Figure 6. Box –and-whisker plots of attenuation in the superior vena cava (SVC) and of reflux of contrast material in neck veins according to artifact score.
A, Plot shows clear cutoff point at ± 200 HU attenuation of SVC. Above this level artifacts interfered with evaluation of arteries. Circle indicates outlier.
B, Plot shows greater amount of reflux is associated with higher artifact score. Stars indicate extreme.

Comparison of left and right injection sides

In group 2 (craniocaudal scan direction) there was more reflux and a higher artifact score in left-sided injection than with right-sided injection, although the difference was significant only for reflux ($p < 0.01$) and almost significant for artifact score ($p = 0.08$) (Table 5). Attenuation of the SVC was higher in patients who received a right-sided injection, although the difference was not significant ($p = 0.19$).

Relationships among artifact parameters

There was a significant relation between the attenuation of the SVC and artifact score (Spearman's $r = 0.62$, $p < 0.001$) (Fig. 6). A clear cut-off point was seen at an attenuation of the SVC of ± 200 HU. Above this level, artifacts interfered with evaluation of the arteries. There was also a significant relation between reflux in the neck veins and artifact score (Spearman's $r = 0.52$, $p < 0.001$).

Discussion

Artifacts caused by the inflow of undiluted high density contrast material in the SVC during thoracic helical CT have been described[5-7,9]. These artifacts can cause obscuration of enlarged lymph nodes, incomplete characterization of axillary and mediastinal masses, and obscuration of vascular lesions. During CTA, artifacts can especially obscure the ascending aorta and proximal supraaortic arteries and thus hide or suggest stenosis or occlusion of the origin of the supraaortic arteries. Perivenous artifacts are frequently seen when the start of the CT scan occurs before injec-

tion of contrast material ends. In case of delayed start of data acquisition, after the end of contrast material injection, stasis of contrast material in the major thoracic veins can cause artifacts.

Rubin et al.[6], who performed helical CT with an injection duration of 40 sec and a scan delay of 25 sec, found that 3:1 dilution of contrast material resulted in diminished perivenous artifacts. To keep the same total injected iodine dose with a 3:1 dilution, the total injected volume and the injection rate have to be increased 4 times. In CTA, however, dilution of contrast material is not an option because the already high injection rate should be increased to more than 10 mL/sec in maintaining the injected iodine dose.

Haage et al.[5] tested the effect of the addition of a bolus chaser to the main contrast material bolus and subsequent reduction of contrast material. They found a reduction in perivenous artifacts. This result can be explained by the reduction in total iodine concentration and shorter contrast material injection time rather than use of a bolus chaser after the main bolus.

In theory, to prevent perivenous artifacts, a bolus chaser is useful in CTA only when the scan starts after injection of contrast material ends. In our study the optimal scan delay was within the injection period of 20 seconds in most of the patients. Although use of a bolus chaser in CTA of the supraaortic arteries leads to optimal use of contrast material[4], it does not decrease perivenous artifacts.

To synchronize data acquisition relative to optimal arterial enhancement, the scan direction in CTA usually is in the direction of the blood flow[10]. With 16-MDCT, scanning time in CTA of the supraaortic arteries has decreased to less than 15 sec. This change may allow reversal of the scan direction without a compromise in vascular attenuation. In addition, perivenous artifacts may decrease because of the delay in scanning of the apex of the thorax when a craniocaudal scan direction is used.

Our study showed that a craniocaudal scan direction resulted in slightly lower attenuation of the carotid artery, although attenuation remained high enough for good evaluation, in comparison with a caudocranial scan direction. With both scan directions, peak attenuation is at the level of the proximal ICA, which is the most relevant site. After adjustment for age and weight, no significant difference in mean or maximum attenuation was found for the two scan directions. Minimum attenuation, however, was significantly lower for the craniocaudal scan direction. The explaination is that the scan direction is the opposite of the direction of blood flow, and to have maximal enhancement at the halfway point (the level of the proximal ICA), the scan is at the cranial level a little too early and at the caudal part a little too late for optimal enhancement. Therefore, attenuation at the beginning and at the end of the craniocaudal scan, and thus minimum attenuation, is lower than for a caudocranial scan. This factor is also reflected in the significantly lower attenuation, after adjustment for age and weight, at the ascending aorta, carotid siphon and intracranial arteries

and the lack of difference in attenuation at locations in between.

We found that a craniocaudal scan direction resulted in a much lower attenuation of the SVC, which resulted in fewer perivenous artifacts. By the time the craniocaudal scan reaches the apex of the thorax, injection of contrast material has ended, and contrast material has been flushed from the veins by the bolus chaser.

There was a tendency to increased artifacts with left-sided injection compared with right-sided injection, although this difference was not significant ($p=0.08$ for the craniocaudal scan direction). The explaination is that venous return in the left subclavian vein, because of its transverse course into the SVC, may be more likely to be affected by changes in intrathoracic pressure and to be compressed by normal structures, such as the aorta. These effects can cause more pooling of contrast material in the subclavian vein and more reflux in the neck veins with left-sided injection than occurs with right-sided injection[11]. We found more reflux in patients in the craniocaudal scan direction group who received a left-sided injection ($p<0.01$) and a significant relationship between reflux and artifacts ($p<0.01$).

A limitation of our study is that the groups were not randomly allocated. Baseline characteristics, however, were not significantly different.

Another limitation was that our results probably will not apply when bolus triggering is not used to optimize the timing of the data acquisition. The timing for a craniocaudal scan direction has to be more precise than for a caudocranial scan direction. Without bolus triggering data acquisition may be too early for good arterial attenuation in the intracranial arteries and too late for good attenuation in the aorta.

In conclusion, we advocate the use of a craniocaudal scan direction in 16-MDCT angiography of the supraaortic arteries. Right-sided injection is preferred over left-sided injection. This protocol results in good arterial attenuation, low attenuation of the SVC, and few perivenous artifacts, and facilitates evaluation of the ascending aorta and supraaortic arteries.

References

1. Warlow C, Sudlow C, Dennis M, Wardlaw J, Sandercock P. Stroke. Lancet 2003;362:1211-1224
2. Ersoy H, Watts R, Sanelli P, et al. Atherosclerotic disease distribution in carotid and vertebrobasilar arteries: clinical experience in 100 patients undergoing fluoro-triggered 3D Gd-MRA. J Magn Reson Imaging 2003;17:545-558
3. Rouleau PA, Huston J, 3rd, Gilbertson J, Brown RD, Jr., Meyer FB, Bower TC. Carotid artery tandem lesions: frequency of angiographic detection and consequences for endarterectomy. AJNR Am J Neuroradiol 1999;20:621-625

4. de Monyé C, Cademartiri F, de Weert TT, Siepman DAM, D.W.J. D, van der Lugt A. CT Angiography of the carotid artery with a 16-multidetector-row CT scanner: comparison of different volumes of contrast material with and without bolus chaser. Radiology 2005 in press
5. Haage P, Schmitz-Rode T, Hubner D, Piroth W, Gunther RW. Reduction of contrast material dose and artifacts by a saline flush using a double power injector in helical CT of the thorax. AJR Am J Roentgenol 2000;174:1049-1053
6. Rubin GD, Lane MJ, Bloch DA, Leung AN, Stark P. Optimization of thoracic spiral CT: effects of iodinated contrast medium concentration. Radiology 1996;201:785-791
7. Loubeyre P, Debard I, Nemoz C, Minh VA. High opacification of hilar pulmonary vessels with a small amount of nonionic contrast medium for general thoracic CT: a prospective study. AJR Am J Roentgenol 2002;178:1377-1381
8. Vogel N, Kauczor HU, Heussel CP, Ries BG, Thelen M. [Artefact reducing in diagnosis of lung embolism using spiral CT with saline bolus]

Artefaktreduzierung bei der Lungenemboliediagnostik mittels Spiral-CT unter Verwendung eines Kochsalzbolus. Rofo Fortschr Geb Rontgenstr Neuen Bildgeb Verfahr 2001;173:460-465

9. Nakayama M, Yamashita Y, Oyama Y, Ando M, Kadota M, Takahashi M. Hand exercise during contrast medium delivery at thoracic helical CT: a simple method to minimize perivenous artifact. J Comput Assist Tomogr 2000;24:432-436
10. Fleischmann D. Use of high concentration contrast media: principles and rationale-vascular district. Eur J Radiol 2003;45 Suppl 1:S88-93
11. Sakai O, Nakashima N, Shibayama C, Shinozaki T, Furuse M. Asymmetrical or heterogeneous enhancement of the internal jugular veins in contrast-enhanced CT of the head and neck. Neuroradiology 1997;39:292-295

3

IN VITRO CHARACTERIZATION OF ATHEROSCLEROTIC CAROTID PLAQUE WITH MULTIDETECTOR COMPUTED TOMOGRAPHY AND HISTOPATHOLOGICAL CORRELATION

Thomas T de Weert • Mohamed Ouhlous • Pieter E Zondervan • Johanna M Hendriks •
Diederik WJ Dippel • Marc RHM van Sambeek • Aad van der Lugt

European Radiology 2005;15: 1906-14

In vitro characterization of atherosclerotic carotid plaque with multidetector computed tomography and histopathological correlation

Abstract

Objective

This in vitro study evaluated the performance of 16-slice multidetector computed tomography (MDCT) in the assessment of carotid plaque components, with histology as the gold standard.

Materials and Methods

Twenty-one specimens (n=21) were scanned and reconstructed after optimization of the protocol. Three corresponding MDCT images and histologic sections were selected from each specimen. The Hounsfield values (HV) of the major plaque components (calcifications, fibrous tissue and lipid) were assessed. Plaque areas (mm^2) assessed with MDCT were compared with the results from histologic analysis.

Results

A value of 140 kVp and an intermediate reconstruction algorithm was the optimal protocol. In 15 out of 21 specimens it was possible to match MDCT images with histology. The HV of calcifications, fibrous tissue and lipid were 45 ± 21 HU, 79 ± 20 HU and 960 ± 491 HU ($P < 0.001$), respectively. Plaque areas were compared in 27 matched levels. The calcified and lipid areas on MDCT and histology correlate well ($R^2 = 0.83$ and $R^2 = 0.68$, respectively). The mean difference in lipid area was 0.1 mm^2 (95% CI = -2.1 – 2.3 mm^2).

Conclusions

This in vitro study showed that MDCT is capable of characterizing and quantifying the lipid rich portion of the atherosclerotic plaque.

Introduction

Studies on carotid atherosclerotic plaque have suggested that atherosclerotic plaque rupture can lead to distal thromboembolization. These rupture-prone vulnerable plaques have specific morphological features: the most frequently seen vulnerable plaque type has a large lipid-rich core with a thin fibrous cap.[1]

Since computed tomography (CT) angiography of the carotid artery may replace ultrasound and invasive angiography in the assessment of stenosis in stroke patients[2], evaluation of plaque composition would provide important additional information.

In 1984, it was demonstrated that single-slice CT was able to detect intimal disease in the carotid bifurcation.[3] In later studies, in which 3-mm thick CT slices were compared with histology sections of endarterectomy specimens, Estes et al.[4] and Oliver et al.[5] concluded that hyperdense structures corresponded with calcifications, hypodense regions with lipid or hemorrhage, and isodense regions with fibrosis. However, Walker et al.[6] concluded that CT fails to reliably indicate the presence of lipid or fibrous tissue and suggested the need of multidetector technology.

Multidetector CT (MDCT) allows the evaluation of carotid atherosclerosis with thinner slices (0.5-1.0 mm) and less volume averaging. More detailed analysis of plaque composition is now expected to be possible based on differences in Hounsfield values (HV). Although MDCT is a robust technique, the HV in MDCT images are influenced by a number of scan and image reconstruction parameters; only some of these (collimation and contrast concentration) have been evaluated.[7] Furthermore, there are concerns about the limiting effect of blooming artifacts of calcifications on the characterization of the non-calcified part of the plaque.[8]

The aim of this in vitro study was to assess the ability of thin section MDCT to characterize and quantify plaque components in carotid endarterectomy specimens, with histology as gold standard. In addition, the effects of voltage setting (kVp) and reconstruction algorithms on image quality and the depiction of calcifications were analyzed.

Methods

Subjects

Twenty-one patients (17 male, four female; mean age 65 years, range 41-81 years) undergoing carotid endarterectomy (CEA) for a symptomatic angiographically detected stenosis (> 70%), were included in the study. The Institutional Review Board approved the study and patients gave written informed consent. After CEA, the plaque specimens were stored in 4% formaldehyde.

Optimization of protocol

In order to optimize scanning and reconstructing parameters five out of 21 specimens were taken out the formaldehyde and scanned on an MDCT scanner (Siemens, Sensation 16, Erlangen, Germany) with a standardized protocol (tube current 180 mAs, collimation 16x0.75 mm, table feed 12 mm/rotation, pitch

of 1). Four scans were made with 80, 100, 120 and 140 kVp, respectively. Axial reconstructions were made with 50-mm field of view, matrix size 512 x 512 (yielding interpolated pixels of 0.10 x 0.10 mm; true in-plane resolution is about 0.5x 0.5 mm), slice thickness 1.0 mm, increment 0.5 mm and four different types of reconstruction algorithms (B20: smooth, B36: heart view smooth, B46: heart view sharp and B70: very sharp). Hereafter, from each of the 5 selected specimens the corresponding 16 MDCT images of the most stenotic site (= CT image with the largest amount of plaque) were compared with each other (Fig. 1). The optimal protocol was determined based on image quality and the depiction of the calcified area in the atherosclerotic plaque.

Evaluation of image quality was done by two observers (AvdL and TdW) in one consensus reading and focused on the presence of artifacts (averaging of HV, edge-enhancement artifacts). To evaluate the effect on the depiction of calcifications, the calcified area (number of pixels with HU >150) and the total plaque area (number of pixels with HU ≥0) in each MDCT image was determined using the freely available software package ImageJ (Rasband, National Institute of Mental Health, Bethesda, USA); in addition the percentage of calcified plaque area was calculated. Since, the specimens were surrounded by air (-1000 HU) during scanning, manual tracing of the total plaque area was not needed: all pixels above 0 HU were considered to be part of the atherosclerotic plaque.

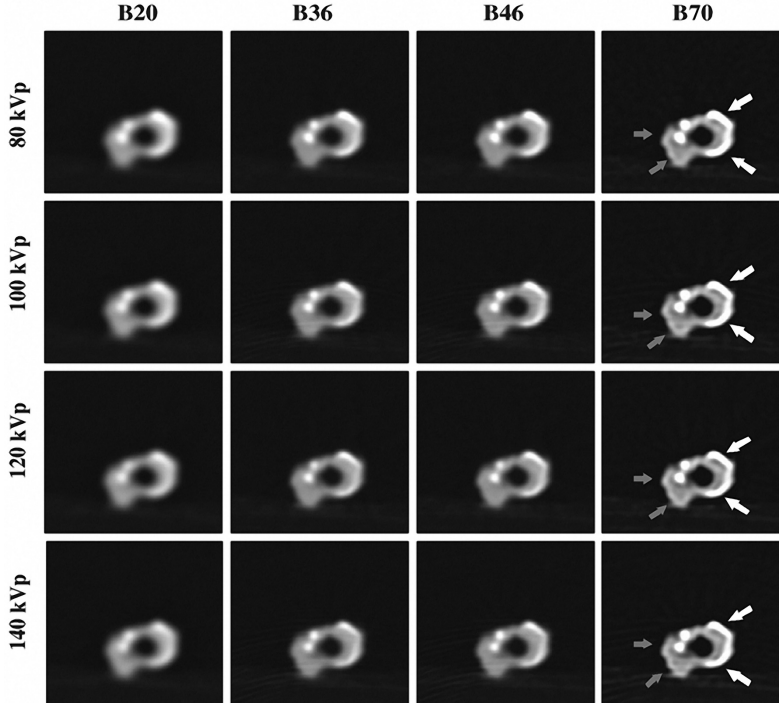

Figure 1. MDCT images of an atherosclerotic specimen from the carotid artery obtained at the same location in the specimen with different kVp settings (80 kVp, 100 kVp, 120 kVp, 140 kVp) and different reconstruction algorithms (B20 = smooth, B36 = heart view smooth, B46 = heart view sharp, B70 = sharp). Gray arrows show a high intensity ring at the air-tissue interface and the white arrows show a low intensity ring around calcifications.

Once, the optimal protocol was determined, the other 16 specimens were scanned and the MDCT images were reconstructed according to this protocol. Subsequently, the specimens were stored again in 4% formaldehyde and sent for histopathological analysis.

Histology preparation

The specimens were decalcified in Goodings and Stewarts solution. After paraffin embedding, histologic sections (5 µm thick) were cut at 1-mm intervals. Three histologic sections obtained per 1-mm were stained with hematoxyline-eosin (HE), Sirius Red (SR) and elastic-Van Gieson (EVG), respectively.

Data analysis

The stack of MDCT images and histologic sections at 1-mm intervals were matched. The shape of the specimen, the location of the bifurcation and calcifications in the plaque were used for matching. For each specimen three corresponding MDCT images and histologic sections were selected for analysis: the most stenotic site, defined as the histologic section with the largest amount of plaque (the stenosis), and one site proximal and one site distal within 4 to 10 mm to the stenosis.

Measurements of different plaque components

Regions within the selected histologic sections with one predominant plaque component (calcifications, fibrous tissue or lipid) were selected by 2 observers (AvdL and TdW) during a consensus reading. The HV of these plaque components were measured by drawing a region of interest (ROI) in the center of the same region in the corresponding MDCT image. For each measurement the same Swiss-cross shaped ROI (size: 5 pixels) was used.

The fibrous tissue and lipid measurements were put in a frequency table from which an ROC curve was created based on the sensitivity and specificity to differentiate fibrous tissue from lipid when using different cut-off points of HV. The optimal cut-off point was considered to have the highest paired sensitivity and specificity.

Size of different plaque components

The size of the three plaque components (calcifications, fibrous tissue, lipid) was assessed in both selected histologic sections and corresponding MDCT images.

Since in the MDCT images, HV at the borders of the specimens can not be considered representative for the underlying tissue, due to partial volume effects at the air-tissue interface, thin and split plaque sections, which have relatively large air-tissue borders, were discarded.

The size of the plaque components in the selected histologic sections was assessed during a consensus reading by two observers (AvdL and TdW), prior to and blinded for the plaque component size assessment in the corresponding MDCT images.

The histologic sections were analyzed with a microscopy image analysis system (Clemex vision 3.5, Clemex Technologies Inc., Longueuil, Canada) (Fig. 2). This system made it possible to assess automatically with a color threshold within SR stained histologic sections the area

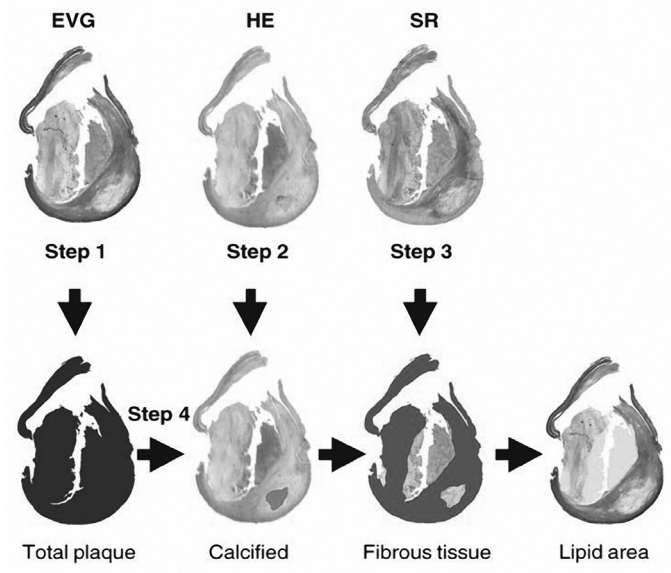

Figure 2. Assessment in histologic sections of plaque component areas with a microscopy image analysis system (Clemex vision 3.5). Step 1, total plaque area was determined with a color threshold (any color = plaque). Step 2, calcified areas were manually drawn. Step 3, fibrous tissue was determined automatically with color threshold (red = collagen) and manually (tunica media). Step 4, remaining tissue was considered to be lipid. (A full color version of this illustration can be found in the color section)

percentage of collagen. The fibrous area was considered to be equal to this collagen area percentage and the area of the media, which was manually outlined and automatically calculated. The calcified area percentage was determined in the HE stained sections; calcified areas show purple in this staining or appear as holes in the tissue (due to decalcification). The purple areas and, or holes in the tissue were manually outlined and automatically calculated. The remaining tissue (lipid, hemorrhage and culprit) in the histologic sections was then considered all to be lipid tissue. We consider this fair since lipid, hemorrhage and culprit are all destabilizing features of an atherosclerotic plaque. Furthermore, these plaque constituents have been described as having the same HV.[4-6]

In the corresponding MDCT images, the total plaque area and the area of each plaque component were calculated by counting the number of pixels within a certain HV range, which was subsequently multiplied by the pixel size.

The cut-off point between fibrous tissue and calcification was set at 150 HU. The cut-off point between fibrous tissue and lipid was based on the optimal cut-off point as assessed in the present study.

Statistical analysis

Data are presented as the mean ± standard deviation (SD). Data on the HV measurements of the three plaque components were compared with Student's t-tests. Data on the HV of fibrous tissue and lipid measured in the same image were compared with paired Student's t-tests.

To assess systematic differences between MDCT and histology, the area measurements were compared with paired Student's t tests. To assess a relationship between the measurements a linear regression analysis was performed. Differences in area measurements on MDCT and histology were plotted against the mean value of the measurements (Bland Altman plot).[9]

Results

Optimization of protocol

Direct visual comparison of the 16 MDCT images showed that plaque composition is influenced by the reconstruction algorithm but is not clearly influenced by kVp setting. Smooth (B20) reconstructed images resulted in less interpretability due to averaging of contrast differences. Sharp (B70) reconstructed images resulted in less interpretability due to image degradation caused by edge-enhancement artifacts. This resulted in a high intensity ring at the air-tissue interface and a low intensity ring around calcifications. The images reconstructed with an intermediate (B36 and B46) algorithm showed good interpretability (Fig. 1).

Measurement of the absolute and relative size of the calcifications revealed that the application of intermediate algorithms led to the smallest size of calcifications (Table 1) and that an increase in kVp setting resulted in a gradual decrease in the size of calcifications (Table 2). The smaller depiction of calcifications with intermediate algorithms and higher kVp setting was observed in every analyzed image.

Since, the B46 reconstruction algorithm has an expected better soft tissue contrast due to a sharper reconstruction algorithm, 140 kVp and a B46 reconstruction algorithm was considered the optimal protocol.

Table 1. Effect of reconstruction algorithm on the amount of calcified tissue expressed in the number of pixels >150 HU and as a percentage of the total plaque area. Data are mean values of measurements in CT images obtained with 80, 100, 120 and 140 kVp.

Reconstruction algorithm	Total plaque area (0-max HU)	Calcified area (>150 HU)	% Calcified area (>150 HU)
B20	2587	695	26,9
B36	2572	601	23,4
B46	2771	623	22,5
B70	4172	2200	52,7

Table 2. Effect of kVp setting on the amount of calcified tissue expressed in the number of pixels >150 HU and as a percentage of the total plaque area. Data are mean values of measurements in CT images reconstructed with B46 reconstruction algorithm.

kVp	Total plaque area (0-max HU)	Calcified area (>150 HU)	% Calcified area (>150 HU)
80	2693	695	25,8
100	2794	637	22,8
120	2852	596	20,9
140	2743	565	20,6

Measurement of different plaque components

In 15 out of 21 specimens it was possible to match MDCT images with corresponding histology sections. Six specimens were excluded due to poor histologic quality. Thus, 45 matched levels (15 specimens x 3) were available for evaluation.

Regions with predominant calcifications, fibrous tissue or lipid were present in 34, 28 and 35 histologic sections, respectively. The measured HV were 960 ± 491 HU for calcifications, 79 ± 20 HU for fibrous tissue and 45 ± 21 HU for lipid tissue. The difference in HV between fibrous tissue and lipid was significant ($p < 0.001$). In 23 histologic sections both fibrous tissue and lipid were present and the HV could be measured on the corresponding MDCT images. In all cases the HV of lipid was lower than the HV of fibrous tissue (mean difference = 31 ± 17 HU; $p < 0.001$).

Figure 3a shows the distribution of HV of lipid and fibrous tissue. The ROC curve (Fig. 3b) revealed 60 HU as the optimal cut-off point to differentiate lipid from fibrous tissue, with a sensitivity and specificity of 89% and 93%, respectively. The range for lipid tissue was therefore set at 0-60 HU during further analysis.

Size of different plaque components

In total 27 matched levels from 13 specimens were analyzed. Eighteen levels were discarded, because the atherosclerotic plaque was thin or split.

The area measurements of the different plaque components on MDCT and on histology are shown in Table 3. Linear regression plots show the relationship between the results of both modalities (Fig. 4a-d). The total plaque area on MDCT was significantly smaller than on histology, the correlation ($R^2 = 0.81$) was good. The calcified area on MDCT was significantly larger than on histology, the correlation ($R^2 = 0.83$) was good. The mean lipid area on MDCT was not significantly different from histology, the correlation ($R^2 = 0.68$) was good. The Bland-Altman plots showed that the difference in lipid area measurements between MDCT and histology was not dependent on the size of the lipid area (Fig. 4e), while the difference in calcified area measurements increased in larg-

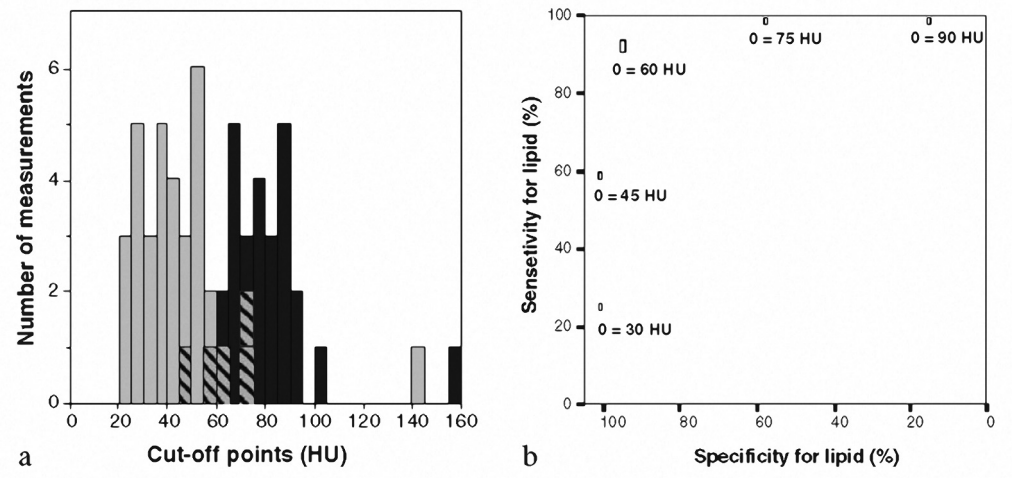

Figure 3. a Frequency distribution of Hounsfield values of lipid (gray bars) and fibrous tissue (black bars). Gray and black striped bars count for both tissues. b ROC curve of various cut-off points (in HU) between lipid and fibrous tissue. With a range for lipid tissue of 0-60 HU, sensitivity and specificity for lipid tissue are 89% and 93%, respectively.

Table 3. Mean areas, standard deviations and P-values of total plaque and plaque component areas in 27 corresponding MDCT images and histologic sections.

	Total plaque area	Lipid area	Fibrous area	Calcified area
MDCT	32.7 ± 14.4 mm^2	14.5 ± 10.1 mm^2	7.0 ± 4.0 mm^2	11.2 ± 12.2 mm^2
Histology	44.9 ± 19.3 mm^2	14.6 ± 9.6 mm^2	26.8 ± 11.5 mm^2	3.6 ± 6.8 mm^2
P-value	< 0.0001	0.94	< 0.0001	< 0.0001

er calcifications (Fig. 4f). Therefore, the mean difference in lipid area between MDCT and histology was taken as a summary measure of the concordance between histologic and MDCT areas: it amounted to 0.1 mm^2 (95% CI = -2.1 – 2.3 mm^2). The fibrous tissue area on MDCT was significantly smaller than on histology, the correlation (R^2 = 0.26) was poor.

Discussion

This in vitro study evaluated the capability of thin section MDCT to characterize plaque components in carotid endarterectomy specimens. It showed that image quality and the depiction of calcifications were influenced by reconstruction algorithm and kVp setting; that fibrous rich regions and lipid rich regions could be differentiated based on differences in HV; and that besides the already commonly used quantification of calcified tissue, MDCT was capable of quantifying the lipid rich portion of carotid atherosclerotic plaque.

To our knowledge, this is the first study that correlates MDCT images of carotid endarterectomy specimen to histology. The in vitro approach has the major advantage that MDCT images and histologic sections easily and accurately can be correlated.

Analysis of different reconstruction algorithms revealed that smooth (B20) reconstructed images showed larger calcifications and less differentiation between lipid and fibrous tissue, due to averaging of contrast differences. It is expected that this will also be observed in patient studies. Sharp (B70) reconstructed images showed high intensity rings at the air-tissue interface and low intensity rings around calcifications. Since these intensity rings did not correlate with specific tissue regions in histology, they may be considered as edge-enhancement artifacts. During in vivo experiments low intensity rings will still worsen image quality and hamper differentiation of the non-calcified parts of the plaque. The intermediate reconstruction algorithms (B36 and B46) produced better quality images with almost no difference in the size of calcifications. The B46 reconstruction algorithm was preferred to the B36 based on an expected better soft tissue contrast due to a sharper reconstruction algorithm.

Since calcifications are overestimated in MDCT images and hinder the characterization of the non-calcified part of the plaque, this study analyzed the effect of kVp on the blooming effect of calcifications. This effect was best minimized with the highest kVp setting. However, the differences between 140 kVp and 120 kVp were small (Table 2) and therefore it seems,

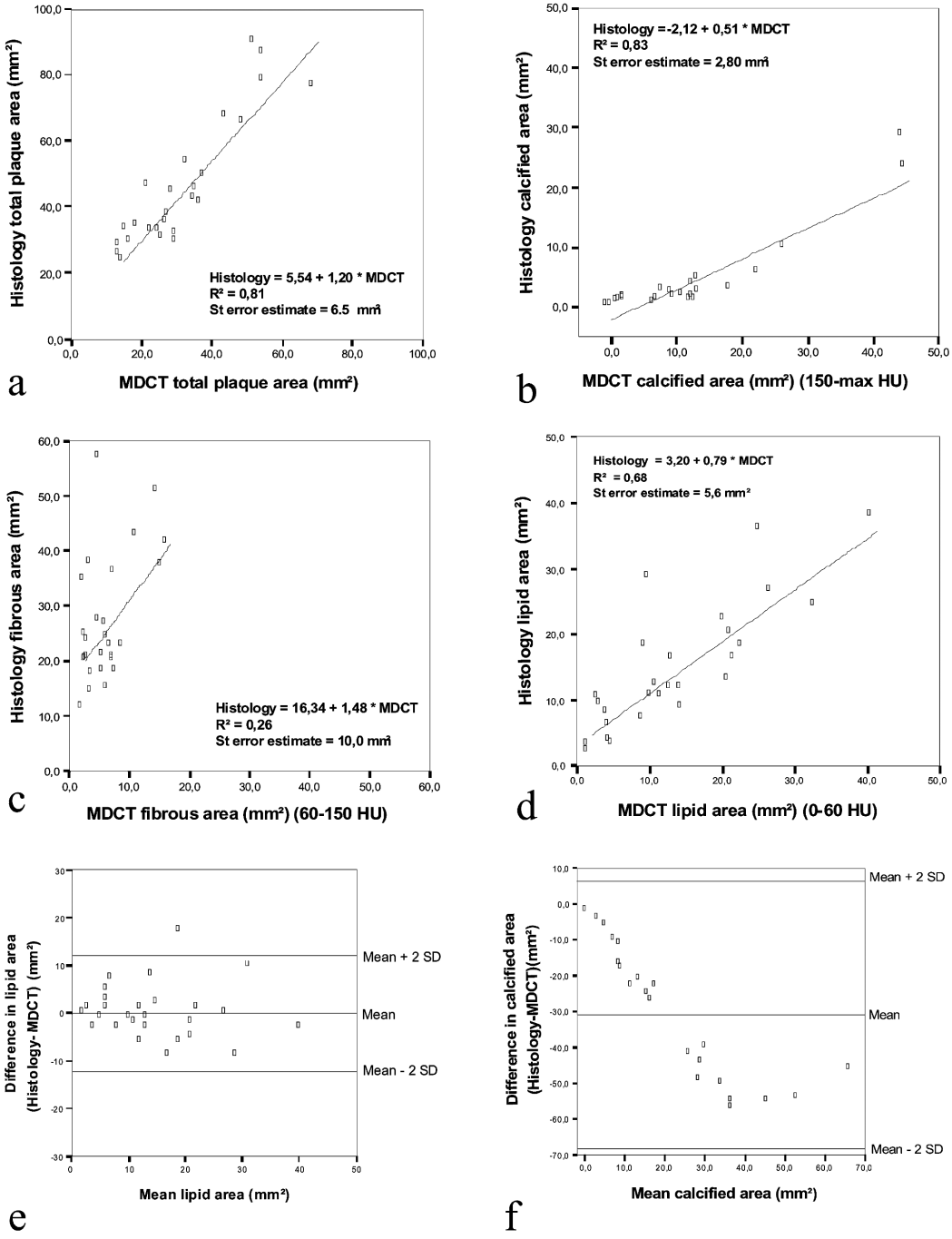

Figure 4. a-d Linear regression analysis of total plaque area and plaque component areas on MDCT images and histologic sections. e Bland-Altman plot of lipid area assessed in MDCT images and in histologic sections. f Bland-Altman plot of calcified area assessed in MDCT images and in histologic sections.

in our opinion, reasonable to choose 120 kVp during in vivo studies, with respect to patient dose.

The present study showed that the HV of the three major plaque components (calcifications, fibrous tissue and lipid) differed significantly from each other. This is in concordance with the observations of Oliver et al.[5] and Estes et al..[4] However, the study from Walker et al.[6] reported that CT could not differentiate between fatty and fibrous plaques. This disappointing result can be contributed to the nature of the study: HV measurements were done in the predominant plaque area and correlated to the fibrous tissue-to-lipid ratio of that plaque area, while in the other two studies (like in our study) predominant tissue components at specific regions in the histological sections were correlated to the measured HV in the CT images at these specific regions.

A few studies have focused on atherosclerotic plaque characterization in the coronary arteries. Becker et al.[10] used histology as a reference for their MDCT findings and found significant differences in mean attenuation of the non-calcified part of the plaque between classified on histology as predominant lipid-rich plaques, and predominant fibrous-rich plaques (47 ± 9 HU and 104 ± 28 HU, respectively). Other coronary studies used IVUS as a reference and found a significant difference on MDCT images in mean attenuation of the non-calcified part of the plaque between plaques classified on IVUS as soft, intermediate and calcified.[11, 12]

The fact that the HV of the major plaque components differed significantly from each other is of great interest, because these differences allow the plaque components to be quantified. For calcifications this quantification has already been extensively reported13, in contrast to the quantification of lipid. Quantification of lipid would be of utmost interest because lipid is one of the conclusive features of an unstable plaque and thus of major importance for risk assessment. A high lipid plaque volume, over 40%, will suffer from a high wall stress and will be more prone to rupture; additionally, the lipid content is highly thrombogenic after disruption.[14] Duplex ultrasonography studies confirmed this idea about the risk of lipid, by demonstrating that echolucent plaques are associated with a higher risk for future ischemic stroke. They failed, however, in quantifying lipid or other plaque components.[15, 16] The important role of lipid is also strengthened by the success of lipid-lowering therapy in preventing acute atherosclerotic-related events. This success could be explained by the reduction of the lipid content of vulnerable plaques.[17]

In the present study, the amount of major plaque components assessed with MDCT was validated by comparison with histology. The total plaque area assessed with MDCT was smaller than the histologic plaque area. This is in conflict with previous studies which show that histologic preparation leads to plaque shrinkage of 19-25%.[18] This conflict is explained by the air-tissue interface which resulted in partial volume effects at the borders of the plaque (fibrous tissue) and thus in smaller plaque sizes and underestimation

of fibrous tissue areas. As in previous studies, calcifications were overestimated with MDCT due to the blooming effect, but the correlation with histologic findings was strong.[19, 20] Besides blooming, decalcification may have contributed to this overestimation. The lipid plaque area detected with MDCT was not significantly different from the lipid area found in histologic sections and the correlation was good.

Limitations

Correlation of MDCT images of carotid endarterectomy specimens with histologic sections has several limitations. Firstly, the air-tissue interface leads to lower HV (< 0 HU) at the tissue borders of the specimens, due to partial volume effects. This deteriorates the correlation between fibrous tissue on MDCT images and histology. We have tried to avoid this effect by scanning the specimens in water. However, in water were no clear differences encountered between water and soft tissue, which resulted in difficulties during the matching of MDCT images and histologic sections. A second limitation is the absence of a contrast agent. Such an agent is present during in vivo plaque characterization and may affect HV measurements. However, the first step towards carotid plaque characterization with MDCT is assessment of HV of plaque components in the absence of contrast agents; the second step is the assessment of the HV in the presence of contrast agents. A third limitation regards the fact that histology sections were 5 μm thick while the MDCT sections were 1 mm thick. This may affect the correlation between area measurements. Finally, one may argue whether it is possible to differentiate between fibrous tissue and the lipid rich portion of the atherosclerotic plaque with MDCT based on a clear cut-off point. The HV measurements of fibrous tissue and the lipid rich portion of the plaque were done in regions with a predominant type of tissue, while in practice the atherosclerotic plaque is often very heterogeneous. Nevertheless, the difference in HV measurements is caused by differences in plaque composition. The cut-off point in this study has not separated completely fibrous tissue from the lipid rich portion of the plaque. It is based on an ROC analysis and is a compromise between a high sensitivity or a high specificity.

Until now studies have reported the ability of MDCT to quantify calcified tissue within the atherosclerotic plaque.[13] These quantities have been used to predict all-cause mortality21 and the risk of acute atherosclerotic-related events.[22] The present study is the first that demonstrates that MDCT is able to quantify the amount of lipid in an in vitro setting. Further studies must be performed to determine if MDCT is also capable of quantifying lipid in an in vivo setting, in order to establish, besides a calcification score, a lipid score which may prove to be an interesting predictor for stroke risk and myocardial infarction and which may function as a parameter in studies of lipid regression.

References

1. Golledge J, Greenhalgh RM, Davies AH. The symptomatic carotid plaque. Stroke. 2000;31:774-781
2. Koelemay MJ, Nederkoorn PJ, Reitsma JB, Majoie CB. Systematic review of computed tomographic angiography for assessment of carotid artery disease. Stroke. 2004;35:2306-2312
3. Heinz ER, Pizer SM, Fuchs H, Fram EK, Burger P, Drayer BP, Osborne DR. Examination of the extracranial carotid bifurcation by thin-section dynamic ct: Direct visualization of intimal atheroma in man (part 1). AJNR Am J Neuroradiol. 1984;5:355-359
4. Estes JM, Quist WC, Lo Gerfo FW, Costello P. Noninvasive characterization of plaque morphology using helical computed tomography. J Cardiovasc Surg (Torino). 1998;39:527-534
5. Oliver TB, Lammie GA, Wright AR, Wardlaw J, Patel SG, Peek R, Ruckley CV, Collie DA. Atherosclerotic plaque at the carotid bifurcation: Ct angiographic appearance with histopathologic correlation. AJNR Am J Neuroradiol. 1999;20:897-901
6. Walker LJ, Ismail A, McMeekin W, Lambert D, Mendelow AD, Birchall D. Computed tomography angiography for the evaluation of carotid atherosclerotic plaque: Correlation with histopathology of endarterectomy specimens. Stroke. 2002;33:977-981
7. Schroeder S, Flohr T, Kopp AF, Meisner C, Kuettner A, Herdeg C, Baumbach A, Ohnesorge B. Accuracy of density measurements within plaques located in artificial coronary arteries by x-ray multislice ct: Results of a phantom study. J Comput Assist Tomogr. 2001;25:900-906
8. Nikolaou K, Becker CR, Muders M, Babaryka G, Scheidler J, Flohr T, Loehrs U, Reiser MF, Fayad ZA. Multidetector-row computed tomography and magnetic resonance imaging of atherosclerotic lesions in human ex vivo coronary arteries. Atherosclerosis. 2004;174:243-252
9. Bland JM, Altman DG. Statistical methods for assessing agreement between two methods of clinical measurement. Lancet. 1986;1:307-310
10. Becker CR, Nikolaou K, Muders M, Babaryka G, Crispin A, Schoepf UJ, Loehrs U, Reiser MF. Ex vivo coronary atherosclerotic plaque characterization with multi-detector-row ct. Eur Radiol. 2003;13:2094-2098
11. Leber AW, Knez A, Becker A, Becker C, von Ziegler F, Nikolaou K, Rist C, Reiser M, White C, Steinbeck G, Boekstegers P. Accuracy of multidetector spiral computed tomography in identifying and differentiating the composition of coronary atherosclerotic plaques: A comparative study with intracoronary ultrasound. J Am Coll Cardiol. 2004;43:1241-1247
12. Kopp AF, Schroeder S, Baumbach A, Kuettner A, Georg C, Ohnesorge B, Heuschmid M, Kuzo R, Claussen CD. Non-invasive characterisation of coronary lesion morphology and composition by multislice ct: First results in comparison with intracoronary ultrasound. Eur Radiol. 2001;11:1607-1611

13. Agatston AS, Janowitz WR, Hildner FJ, Zusmer NR, Viamonte M, Jr., Detrano R. Quantification of coronary artery calcium using ultrafast computed tomography. J Am Coll Cardiol. 1990;15:827-832
14. Davies MJ, Woolf N, Rowles P, Richardson PD. Lipid and cellular constituents of unstable human aortic plaques. Basic Res Cardiol. 1994;89 Suppl 1:33-39
15. Montauban van Swijndregt AD, Elbers HR, Moll FL, de Letter J, Ackerstaff RG. Ultrasonographic characterization of carotid plaques. Ultrasound Med Biol. 1998;24:489-493
16. Liapis CD, Kakisis JD, Kostakis AG. Carotid stenosis: Factors affecting symptomatology. Stroke. 2001;32:2782-2786
17. Zhao XQ, Yuan C, Hatsukami TS, Frechette EH, Kang XJ, Maravilla KR, Brown BG. Effects of prolonged intensive lipid-lowering therapy on the characteristics of carotid atherosclerotic plaques in vivo by mri: A case-control study. Arterioscler Thromb Vasc Biol. 2001;21:1623-1629
18. Dobrin PB. Effect of histologic preparation on the cross-sectional area of arterial rings. J Surg Res. 1996;61:413-415
19. Zhang Z, Berg MH, Ikonen AE, Vanninen RL, Manninen HI. Carotid artery stenosis: Reproducibility of automated 3d ct angiography analysis method. Eur Radiol. 2004;14:665-672
20. Ulzheimer S, Kalender WA. Assessment of calcium scoring performance in cardiac computed tomography. Eur Radiol. 2003;13:484-497
21. Shaw LJ, Raggi P, Schisterman E, Berman DS, Callister TQ. Prognostic value of cardiac risk factors and coronary artery calcium screening for all-cause mortality. Radiology. 2003;228:826-833
22. Raggi P, Cooil B, Callister TQ. Use of electron beam tomography data to develop models for prediction of hard coronary events. Am Heart J. 2001;141:375-382

PART 2

VALIDATION STUDIES

4 In vivo characterization and quantification of atherosclerotic carotid plaque components with multidetector computed tomography and histopathological correlation

Thomas T de Weert • Mohamed Ouhlous • Erik Meijering • Pieter E Zondervan • Johanna M Hendriks • Marc RHM van Sambeek • Diederik WJ Dippel • Aad van der Lugt

Arteriosclerosis, Thrombosis and Vascular Biology 2006; 26: 2366-72.

In vivo characterization and quantification of atherosclerotic carotid plaque components with multidetector computed tomography and histopathological correlation

Abstract

Objective

In a previous in vitro study we have demonstrated that atherosclerotic plaque components can be characterized with multidetector computed tomography (MDCT) based on differences in Hounsfield values (HV). Now we evaluated the use of MDCT in vivo to characterize and quantify atherosclerotic carotid plaque components compared with histology as reference standard.

Materials and Methods

Fifteen symptomatic patients with carotid stenosis (>70%) underwent MDCT angiography prior to carotid endarterectomy (CEA). From each CEA specimen 3 histological sections and corresponding MDCT images were selected. The Hounsfield values (HV) of the major plaque components were assessed.

Results

The measured HV were: 657±416HU, 88±18HU and 25±19HU for calcifications, fibrous tissue and lipid core, respectively. The cut-off value to differentiate lipid core from fibrous tissue and fibrous tissue from calcifications was based on these measurements and set at 60 HU and 130 HU, respectively. Regression plots showed good correlations (R^2>0.73) between MDCT and histology except for lipid core areas, which had a good correlation (R^2=0.77) only in mildly calcified (0-10%) plaques.

Conclusions

MDCT is able to quantify total plaque area, calcifications and fibrous tissue in atherosclerotic carotid plaques in good correlation with histology. Lipid core can only be adequately quantified in mildly calcified plaques.

Introduction

The severity of luminal stenosis, caused by the atherosclerotic plaque in the carotid bifurcation, is an important risk factor for (recurrent) stroke and is used in therapeutic decision making: i.e. patients with symptomatic or asymptomatic carotid stenosis above a certain degree are considered candidates for carotid intervention such as carotid endarterectomy (CEA) or stent placement.[1]

However, morphology studies on carotid atherosclerotic plaque have revealed that plaque morphology could be an important additional feature in the risk assessment of patients with carotid stenosis.[2, 3]

Computed tomography angiography (CTA) is an accurate modality to grade the severity of stenosis,[4] and is increasingly used in the evaluation of stroke patients. The question then arises whether CT can also provide detailed information about plaque morphology.

Earlier studies in which 3-mm thick single-slice CT images were compared with histology sections of CEA specimens, yielded confusing results.[5,6] Multidetector CT (MDCT) allows evaluating carotid atherosclerosis with thinner slices (0.5-1.0 mm) and less volume averaging. More detailed analysis of plaque composition may now become possible.

A previous in vitro validation study showed that thin-section MDCT is capable of characterizing and quantifying calcifications and lipid core regions in CEA specimens based on differences in Hounsfield values (HV).[7] However, in vitro studies have inherent limitations due to the presence of air around the specimen and the absence of contrast in the vessel lumen. The purpose of this study was to assess the ability of in vivo thin-section MDCT to characterize and quantify carotid plaque compared with histology as reference standard.

Materials and Methods

Subjects

Fifteen patients (6 male, 9 female; mean age 70.3 years, range 62-84 years) with a transient ischemic attack (TIA) or minor stroke and with severe ipsilateral carotid atherosclerotic disease (>70%) on CTA underwent CEA within three months (mean: 2.2±0.9 months) after CTA. All but one patient (who experienced a TIA) were asymptomatic between CTA and CEA. The CEA specimens were collected and stored in 4% formaldehyde. The Institutional Review Board approved the study and patients gave written informed consent.

Scanning and image reconstruction

Scanning was performed on a 16-slice MDCT scanner (Siemens, Sensation 16, Erlangen, Germany) with a standardized optimized contrast-enhanced protocol (120 kVp, 180 mAs, collimation 16 x 0.75 mm, table feed 12 mm/rotation, pitch 1).[8]

Image reconstructions were made with field of view 100 mm, matrix size 512 x 512 (real in-plane resolution 0.6 x 0.6 mm), slice thickness 1.0 mm, increment 0.6 mm and with an intermediate reconstruction algorithm.[7]

Histology preparation

The 15 CEA specimens were partly decalcified and embedded in paraffin. Three histological sections were obtained per 1-mm and stained with haematoxylin-eosin, Sirius Red and elastic-Van Gieson, respectively.

MDCT and histology matching

The shape of the lumen and vessel wall, the location of the bifurcation and the presence of calcifications in the plaque were used for matching. From each specimen three histological sections and corresponding MDCT images were selected for analysis: the most stenotic site and one site proximally and one site distally within 5 to 10 mm. A minimum distance of 5 mm between histological sections was chosen in order to obtain a heterogeneous data set and to minimize selection bias.[9] Since not every histological section was of good quality, some sections had to be chosen at a larger distance than the preferred 5 mm.

Differentiation of plaque components

Within the selected histological sections, regions with one predominant plaque component (calcifications, fibrous tissue or lipid core) were determined. The HV of these regions were measured by drawing a region of interest (ROI) in the centre of the same region in the corresponding MDCT images. Care was taken to place the ROI in lipid core and fibrous tissue regions at a distinct distance from calcified tissue and vessel lumen, to avoid partial volume effects. Based on these measurements a cut-off value was determined to differentiate lipid core from fibrous tissue.

Size of different plaque components

The size of the three predominant plaque components was assessed. One observer measured the areas within the histological sections, after reviewing them with a histopathologist. One month later the same observer, who was blinded for the histology results, assessed the areas within the MDCT images. Plaque component areas were expressed as percentages of the total plaque area, since histological preparation leads to plaque shrinkage.[10]

The histological sections were analyzed with a microscopy-image-analysis-system (Clemex vision 3.5, Clemex Technologies Inc., Longueuil, Canada). This system allows to assess (in a semi-automatic way) the total plaque area, calcified area and fibrous tissue area (which included also the tunica media); the remaining tissue (lipid, haemorrhage and necrotic debris) was then considered to be lipid core.[7]

In the corresponding MDCT images, the total plaque area and the area of each plaque component was determined, using a custom-made plug-in for the freely available software ImageJ (Rasband, National Institute of Mental Health, Bethesda, USA). This plug-in assessed the total number of pixels (= plaque + lumen area) and the number of pixels of different HV ranges (= different plaque component areas) within a manually drawn ROI (Figure 1). Each HV range was considered to represent a different plaque component and was given a different colour within the MDCT image. By multiplying the number of pixels of each HV range by the pixel size, total plaque area and plaque component areas were determined.

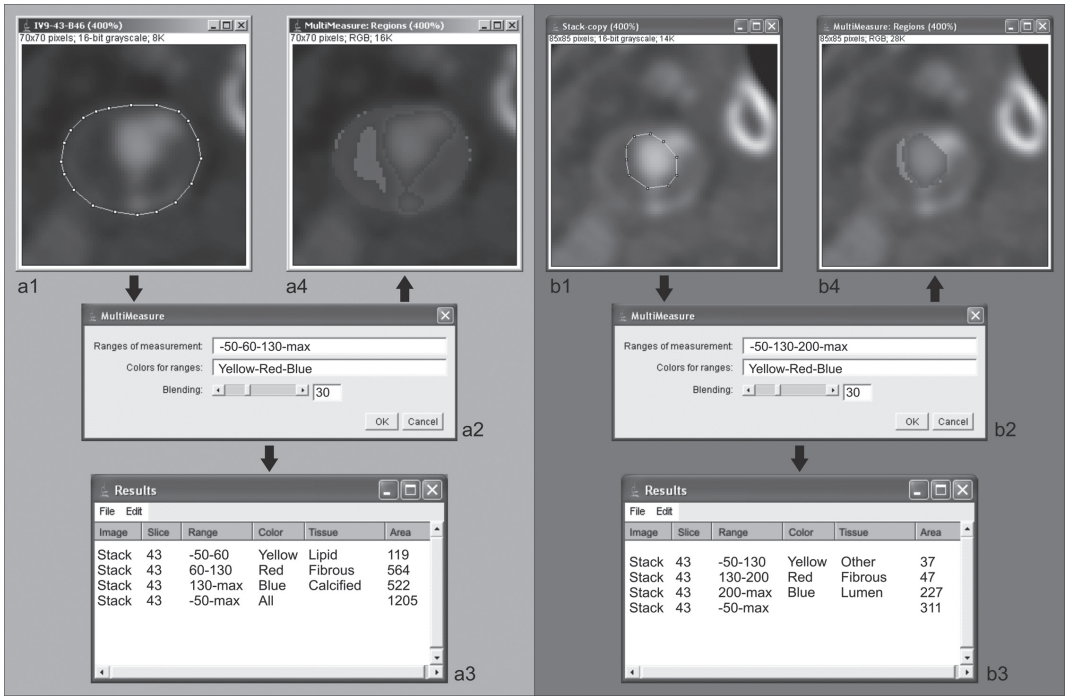

Figure 1. Semi-automatic assessment of plaque component areas in MDCT images with the ImageJ plug-in 'MultiMeasure'. (a1.) This plug-in allows an observer to draw a region of interest (ROI) (=vessel outline). (a2.) After the input of specific ranges of Hounsfield values (HV), which should represent specific plaque components, the amount of pixels (a3.) within each range of HV is assessed. (a4.) Each range of HV is given a different colour and a MDCT-based plaque morphology image is produced. (b1.) To differentiate lumen from the atherosclerotic plaque and from calcified tissue, a second ROI is drawn. (b2.) After the input of specific ranges of HV, which should differentiate lumen and fibrous tissue located at the border of the lumen, the amount of pixels (b3.) within each range of HV is assessed. (b4.) Each range of HV is given a different colour and a second MDCT-based plaque morphology image is produced. The number of lumen pixels has now been calculated (b3). The exact number of fibrous and calcified pixels can now be determined (fibrous = fibrous measurement a (60 to 130 HU) plus fibrous measurement b (130 to 200HU); calcified = calcified measurement a (>130 HU) minus lumen measurement b (>200HU) minus fibrous measurement b (130-200HU)). (A full color version of this illustration can be found in the color section)

The cut-off point between lumen and atherosclerotic vessel wall was set at 200 Hounsfield Units (HU). This cut-off point was chosen to compensate for partial volume effects that appear at the border between atherosclerotic plaque and contrast-enhanced lumen, which has a mean HV at the carotid bifurcation of approximately 400 HU with the described scan protocol.[8] The cut-off point between calcifications and non-calcified tissue was set at 130 HU, the value currently used in calcium scoring.[11] When calcified areas bordered the lumen and merged with the lumen, lumen area and calcifications were separated by manual drawing. The cut-off point between fibrous tissue and lipid was based on the HV measurements in the present study in regions that showed predominant lipid core or fibrous tissue.

To evaluate inter- and intra-observer variability in MDCT area measurements, a second observer independently performed the area measurements whereas the first observer reassessed the areas after 4 months.

Detection of lipid core in MDCT images

To investigate the interpretation of hypodense regions within atherosclerotic plaque in MDCT images, each hypodense region was divided in three different regions based on a range of HV (<0 HU, 0-30 HU, 30-60 HU). For each range of HV the number of hypodense regions in the MDCT images was assessed and the results were subsequently compared with the histological section. On histology, hypodense regions were true-positive for lipid core if the whole region fell within a lipid core area (i.e. lipid, haemorrhage or necrotic debris) and false-positive for lipid core if these regions included (besides lipid core) calcified or fibrous tissue. Hypodense regions along the vessel wall border were counted separately because they were caused by inadequate positioning of the outer contour with inclusion of periarterial fat in the analysis.

Statistics

Data are presented as the mean ± standard deviation (SD). Continuous data were compared with Student's t-test or paired Student's t-test. A p-value < 0.05 was considered to indicate statistical significance. Relationships between area measurements in MDCT images and histology were evaluated with linear regression analysis and Bland-Altman plots. The degree of observer variability is presented both with Bland-Altman plots and a coefficient of variation.

Results

In 14 out of 15 endarterectomy specimens it was possible to match MDCT images with corresponding histological sections. One specimen had to be excluded because of dental streak artefacts in the MDCT images. In another specimen, due to its limited length, only two matched histological sections and MDCT images could be evaluated. Hence, 41 matched levels were available for evaluation.

Differentiation of plaque components

Table 1. Number of Hounsfield value (HV) measurements in predominant calcified, fibrous tissue and lipid core regions per histological section. Total number of HV measurements and mean HV (mean ± SD) for predominant calcified, fibrous tissue and lipid core regions. The difference in HV between fibrous tissue and lipid core is significant ($p < 0.001$).

Number of Measurements per section	Calcified	Fibrous	Lipid core
0x	15	3	19
1x	20	23	14
2x	6	15	7
3x	---	---	1
Total number of measurements	32	53	31
Mean HV (HU)	**657 ± 416**	**88 ± 18**	**25 ± 19**

In Table 1 the number of HV measurements in predominant calcified, fibrous tissue and lipid core regions per histological section, the total number of HV measurements and the mean HV of each plaque component are given. A significant difference in HV between fibrous

tissue and lipid core was found ($p < 0.001$). In 21 histological sections from 11 different CEA specimens, predominant regions of both fibrous tissue and lipid core were present in the same slice. In all cases the HV of lipid core was lower than the HV of fibrous tissue.

Based on the distribution of measured HV of lipid core (range: -20 to 60 HU) and fibrous tissue (range: 60 to 140 HU) in the MDCT images, 60 HU was determined as the cut-off point to differentiate lipid core from fibrous tissue.

Size of different plaque components

All 41 matched levels of histological sections and MDCT images were used for area measurements (Table 2). Total plaque area and calcified area in MDCT images were significantly larger than the histological total plaque area and calcified area ($p < 0.001$), while fibrous area in MDCT images was significantly smaller than the histological fibrous area. There was no significant difference between MDCT and histology for lipid core area measurements.

The correlation between histology and MDCT for total plaque area, calcified area and fibrous tissue area was good ($R^2 = 0.73$; 0.74; 0.76, respectively; $p < 0.001$), whereas the correlation for lipid core area was poor ($R^2 = 0.24$; $p < 0.002$) (Figure 2a). However, when we performed an exploratory analysis by evaluating the lipid core area data in severely and mildly calcified plaques and changed the cut-off value between severely and mildly calcified plaques (<30%, <20%, <10% or 0% calcified, respectively) the correlation between lipid core areas on histological sections and in MDCT images improved for the mildly calcified plaques ($R^2 = 0.50$, 0.62, 0.77 and 0.81, respectively; $p < 0.001$), while it remained poor for the severely calcified plaques (Figure 2b).

Table 2. Total plaque area and plaque component areas (mean ± SD) in 41 matched MDCT images and histological sections. All area measurements in the MDCT images, except the lipid core measurements, were significantly different ($p < 0.001$) from the histological data.

	Total plaque area (mm^2)	Calcified area (%)	Fibrous area (%)	Lipid core area (%)
MDCT	50.1 ± 22.4	24.2 ± 22.9	52.9 ± 19.4	22.9 ± 16.0
Histology	34.7 ± 12.3	8.1 ± 10.3	66.6 ± 17.2	25.8 ± 15.3

The difference between MDCT measurements and histological measurements of total plaque area and calcified area became larger as the total plaque area and the calcified area increased, respectively. The latter is explained by the fact that the blooming effect of calcifications leads to overestimation of calcifications. In addition, this effect increases with the size of the calcification. However, the measurement of the size of the total plaque area is less affected by this blooming effect. The difference between fibrous tissue and lipid core areas assessed on histology and in MDCT images could not be related to their size (Figure 3).

Inter- and intraobserver variability

The MDCT area measurements of the two observers showed significant differences

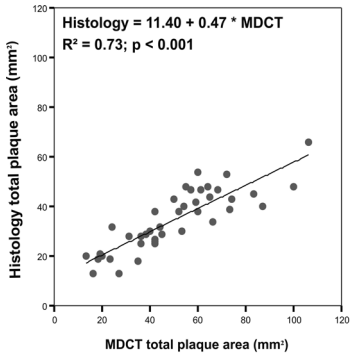

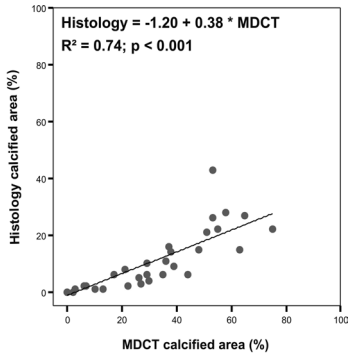

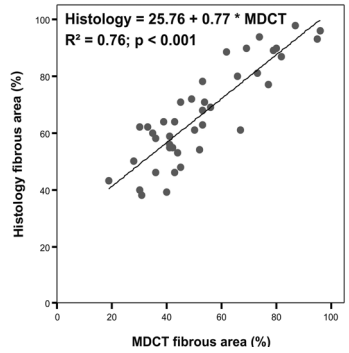

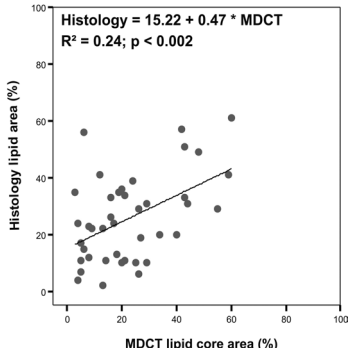

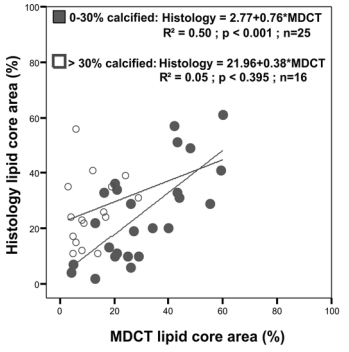

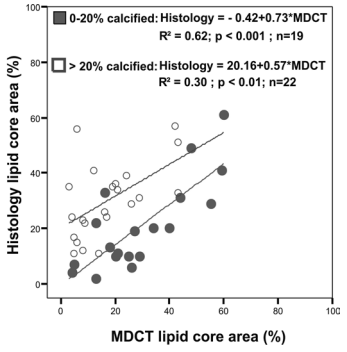

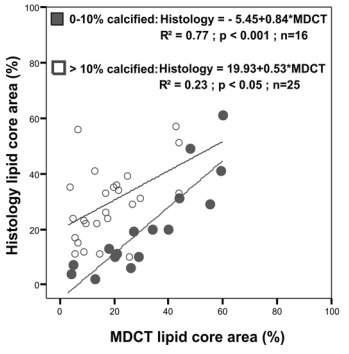

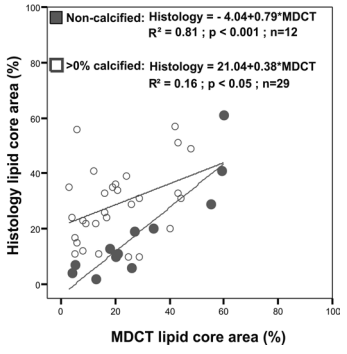

(p<0.05) for the assessment of total plaque area, fibrous tissue area and lipid core area. The lumen area and calcified area were assessed with no significant difference (p>0.05). The intraobserver measurements showed significant differences (p<0.05) for the assessment of total plaque area. The lumen area, calcified area, fibrous tissue area and lipid core area were assessed with no significant difference (p>0.05).

The Bland-Altman plots of the area measurements of the two observers showed that observer variability is mainly caused by variability in the manual outlining of the outer vessel wall (Figure 4). The inter-observer coefficients of variation for the absolute measurement of lumen, plaque, calcified, fibrous tissue and lipid core areas were: 4%, 19%, 16%, 21% and 40%, respectively, and

Figure 2a. Linear regression analysis of total plaque area and plaque component areas in MDCT images and histological sections. **Figure 2b**. Linear regression analysis of lipid core areas in MDCT images and histological sections, for different levels of calcification.

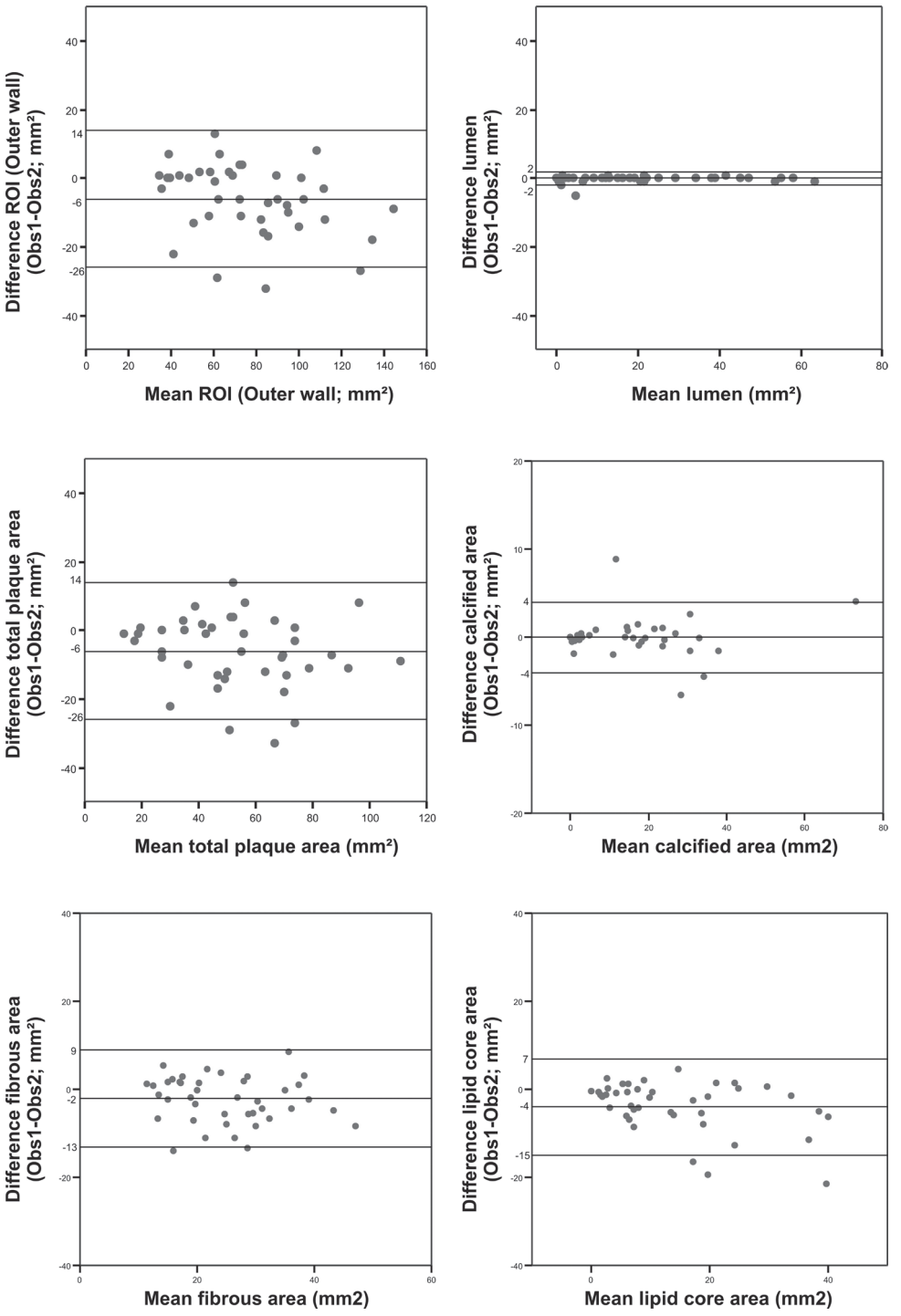

Figure 3. Bland-Altman plot of total plaque area and plaque component areas in MDCT images and histological sections. The horizontal lines express the mean difference and the mean difference ± 2 standard deviations.

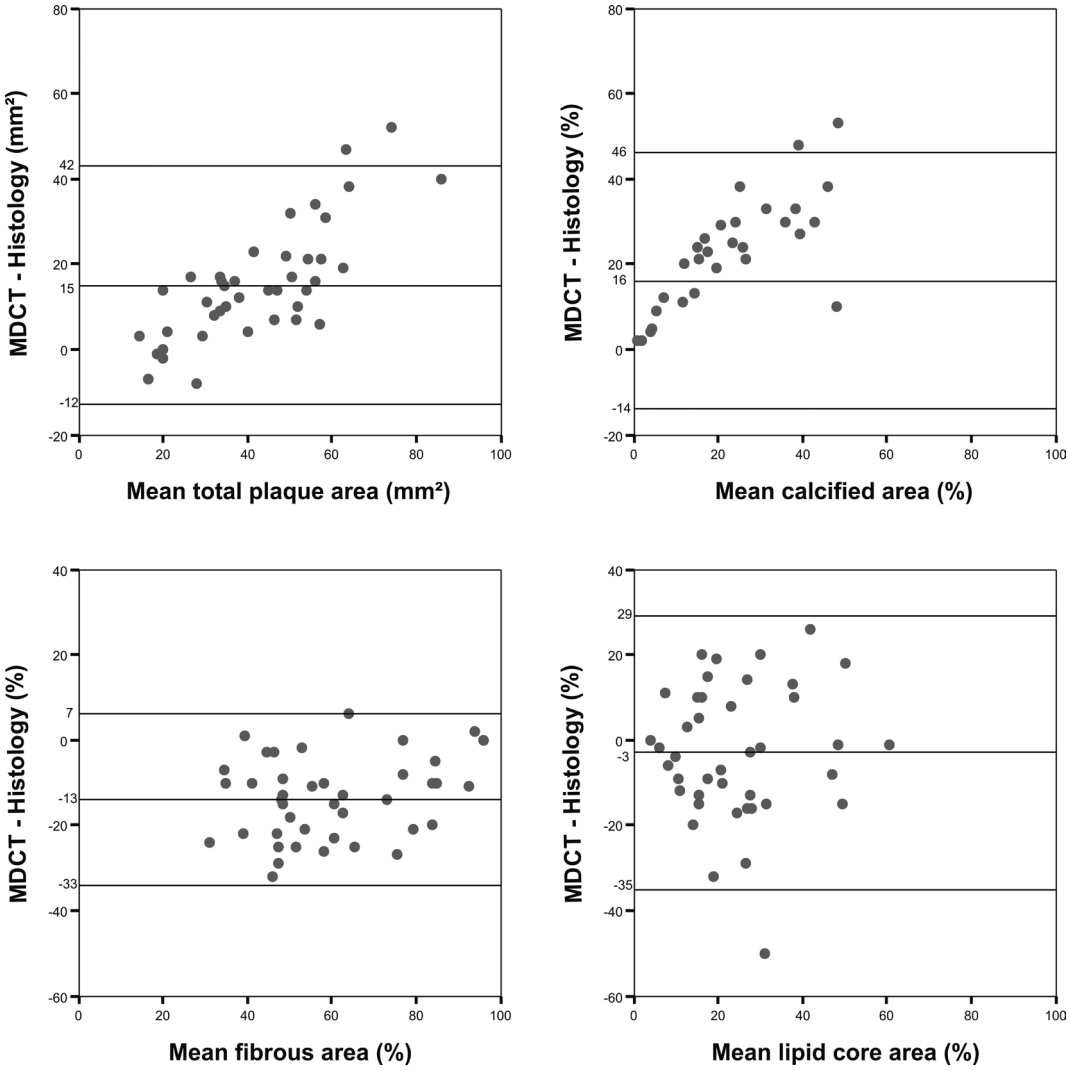

Figure 4. Bland-Altman plot of total plaque area and plaque component areas assessed by two observers. The horizontal lines express the mean difference and the mean difference ± 2 standard deviations.

the inter-observer coefficients of variation for the relative measurement (%) of calcified, fibrous tissue and lipid core areas were: 26%, 10% and 20%, respectively. The intra-observer coefficients of variation for the absolute measurement of lumen, plaque, calcified, fibrous tissue and lipid core areas were: 3%, 8%, 8%,11% and 15 %, respectively, and the intra-observer coefficients of variation for the relative measurement (%) of calcified, fibrous tissue and lipid core areas were: 14%, 7% and 14%, respectively.

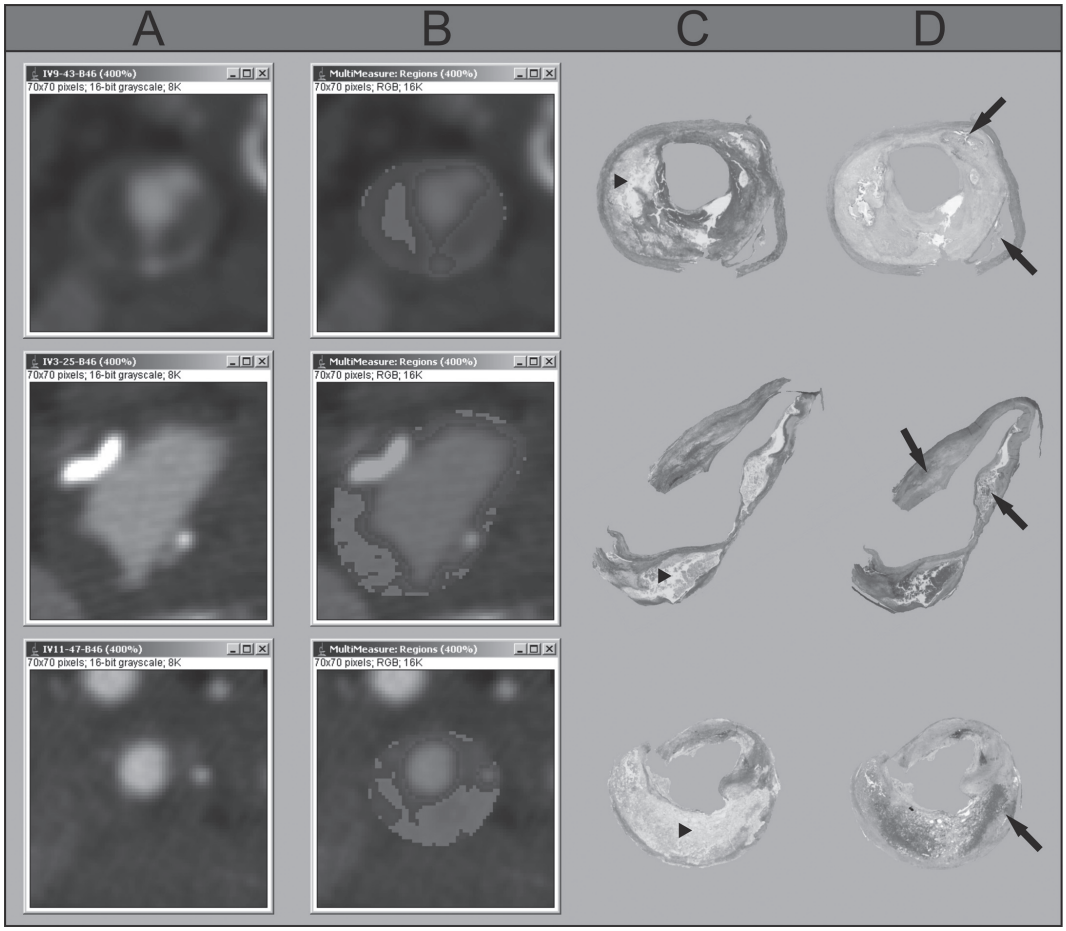

Figure 5. Column A: three axial MDCT images of the carotid artery with atherosclerotic plaque. Column B: MDCT plaque morphology images based on differences in Hounsfield Units. Column C and D: Corresponding histological sections with Sirius Red (SR) and haematoxylin eosin (HE) staining, respectively). The blue regions in the MDCT morphology images correspond well with the lumen and calcifications (arrow) on HE stained histological sections. The red regions in the MDCT morphology images correspond well with the red collagen-rich regions in the SR stained histological sections. The yellow regions in the MDCT morphology images correspond well with lipid core (i.e. lipid, haemorrhage and necrotic debris) (arrowhead) regions on histology (the non-red regions on the SR stained sections that are not calcified areas on the HE stained sections). (A full color version of this illustration can be found in the color section)

Detection of lipid core in MDCT images

Analysis of hypodense regions showed that 54 hypodense regions were present in the HV range of <0 HU: 28 regions were true positive for lipid core and 26 regions were located at the vessel wall borders. With a HV range of 0-30 HU, 118 hypodense regions were present: 49 regions were true positive, 3 regions false positive and 66 regions were located at the vessel wall borders. With a HV range of 30-60 HU, 144 hypodense regions were present: 28 regions were true positive, 95 were false positive and 21 regions were located at the vessel wall borders.

Discussion

This study shows that the HV measured in the centre of fibrous-rich regions and lipid core is significantly different. This confirms the results of our earlier in vitro study.[7] In addition, the present study reveals how to interpret very hypodense regions (< 30 HU) in the centre of atherosclerotic carotid plaque in MDCT images; these regions are associated with the presence of a lipid core (i.e. lipid, haemorrhage or necrotic debris). To our knowledge, this in vivo MDCT study is the first to use differences in HV between plaque components to quantify atherosclerotic carotid plaque and its components, and to correlate the findings with histology: MDCT was capable of quantifying total plaque area, calcified area and fibrous tissue area and lipid core area in mildly calcified plaques. The inter-observer variability in area measurements was moderate (range:4-40 %), and the intra-observer variability was good (range 3-15 %).

The present study shows that the HV of calcifications, fibrous tissue and lipid core differ significantly from each other, which is in concordance with earlier carotid[5] and coronary[12, 13] CT studies. These differences allow quantification of total plaque area and plaque component areas.

Total plaque area acquired in MDCT images was 30% larger than the histological total plaque area; this is in accordance with reported plaque shrinkage of 19-25% due to histological preparation.[10] The correlation between total plaque area measurements is strong, while observer variability can be improved when using new methods of measurement (e.g. automated vessel-wall contour detection, volume measurements instead of area measurements). Therefore, MDCT-based plaque volume assessment may prove to be ready for use in follow-up studies and the predictive value of plaque volume for stroke might be assessed.

The quantification of calcifications has been extensively reported[11] and although the calcified mass is reported to be overestimated with CT[14] accurate event prediction has been described in the coronaries: the greater the calcified mass, the higher the risk of an acute event.[15]

However, a similar study in the carotid arteries describes the protective value of a higher degree of calcification.[16] This suggests that the degree of calcification should be regarded as a reflection of the presence of more localizations of atherosclerosis rather than the instability of calcified plaques. In our study calcifications were also overestimated. Nevertheless, there was a strong correlation with histology. The main problem with the overestimation of calcifications (mainly attributed to the blooming effect of calcifications), is not the imprecise quantification of the calcium mass but its influence on optimal characterization of the non-calcified part of the plaque.

Quantification of fibrous tissue has not been done previously with MDCT. The present study shows however that this is possible with a strong correlation to histology. Due to the fact that fibrous tissue is a stabilizing feature of an atherosclerotic plaque[17], the quantifica-

tion could qualify fibrous tissue as an important predictor of plaque stability.

Accurate assessment of the presence of lipid core is of interest for risk prediction because lipid core is one of the conclusive features of an unstable plaque.[17] The present study shows that very hypodense regions are associated with the presence of a lipid core. Nevertheless, the correlation between histological sections and MDCT images for lipid core area measurements was poor, although only for heavily calcified plaques. The lack of correlation is explained in our opinion by the blooming effect of calcifications in the MDCT images. This blooming effect, as earlier explained, overshadows parts of the soft plaque and hampers the correct characterization of those parts. The exploratory analysis we performed shows indeed a better correlation for soft plaque regions (lipid core and fibrous regions) when less calcifications are present and more of the soft plaque can be correctly classified. In addition, the lack of correlation in lipid core area measurements can be explained by the relatively high observer variability for these measurements. This might be a result of possible inclusion of peri-arterial fat in the analysis by drawing too large outer vessel wall contours by the observers.

A recent prospective MRI study by Takaya et al.[18] showed a positive association between a higher percentage lipid-necrotic core and a higher event rate. Whether the same association exists between with MDCT identified and/or quantified lipid core needs to be established in prospective MDCT studies. For clinical decision-making especially risk assessment in patients with lesions of moderate degree of stenosis will be important. Fortunately, these patients have less calcifications.[19] Thus, MDCT based lipid core evaluation should not be problematic.

Limitations

The first limitation of this study concerns histology, which is considered the reference standard for the assessment of plaque components with MDCT. However, it is limited for this purpose, because of several reasons: 1) Surgical plaque extirpation is not always done in toto, therefore small parts of the vessel wall can not be taken into account during histological analysis. 2) During slicing histological sections can become damaged and this may result in underestimation of histological plaque burden. 3) Due to necessary routinely performed decalcification small calcifications may be missed and larger calcifications may be underestimated by histological area measurements. However, no hyperdense regions in the MDCT images (besides the contrast filled lumen) were determined that could not be correlated to the presence of calcifications. If small calcifications have been missed on histology due to decalcification, they were also too small to be depicted in MDCT images. The strong correlation between calcified areas in MDCT images and histology and the systematic overestimation of calcium in MDCT images clarifies that the possible underestimation of larger calcifications is of little influence. 4) Since the resolution of histological sections (± 7x7x5 μm) can not be achieved with MDCT (± 0.6x0.6x0.6 mm), histological morphology will show too much detail compared with MDCT-based morphology. 5) Plaque shrinkage that

occurs during histological preparation alters the gross morphology of the plaque and it is unknown to what extent each component contributes to the plaque shrinkage.

The second limitation concerns atherosclerotic plaques with severe calcifications. These calcifications will hamper correct quantification of lipid core. However, our exploratory analysis has shown that these hampering effects are less in moderately calcified plaques. Fortunately, this will be the main plaque type in the patient population that will benefit most of stroke prediction based on plaque morphology.

A third limitation concerns the identification of haemorrhage and thrombus as recommended in a recent review[20] on the performance and reporting of studies on carotid plaque imaging versus histology. MDCT can differentiate between calcifications, fibrous tissue and lipid core, but because haemorrhage and thrombus can not be distinguished reliably from lipid they are not reported seperately.[5, 6]

A fourth limitation lies in the fact that the assessment of the cut-off value between fibrous tissue and lipid core was performed in the same data set in which the quantification of components was performed. We choose this approach, since availability of specimens was low and we did not want to lower the number of specimens available for quantification. We recognize that by doing this we report the highest achievable level of correlation.

The last limitation concerns the passing of 2.2 months between CTA and CEA. During this period the atherosclerotic plaque can have changed from what was recorded in the MDCT images. However, these changes will have had a negative effect on the found correlations and the actual correlations might therefore be even better.

Conclusions

Although CTA is established as an accurate modality to grade the severity of stenosis, the results regarding the characterization of atherosclerotic disease in the carotid bifurcation are confusing. The present study shows that MDCT is capable of characterizing and quantifying plaque burden, calcifications and fibrous tissue in atherosclerotic carotid plaque in good correlation with histology, and that lipid core can be adequately quantified in mildly calcified plaques. Furthermore the MDCT-based assessment of atherosclerotic plaque component quantities was possible with a moderate observer variability. Further studies are required to determine whether MDCT-assessed plaque parameters are important predictors of stroke, or can function as secondary endpoints in pharmacological studies of plaque regression.

Acknowledgements

The authors thank Heleen van Beusekom for the use of and help with the histology analysis system.

Funding: Aad van der Lugt is recipient of a fellowship from the Netherlands Organisation for Health Research and Development (NWO-KF grant no. 907-00-122).

References

1. Rothwell PM, Eliasziw M, Gutnikov SA, Warlow CP, Barnett HJ. Endarterectomy for symptomatic carotid stenosis in relation to clinical subgroups and timing of surgery. Lancet. 2004;363:915-924.
2. Rothwell PM, Gibson R, Warlow CP. Interrelation between plaque surface morphology and degree of stenosis on carotid angiograms and the risk of ischemic stroke in patients with symptomatic carotid stenosis. On behalf of the European Carotid Surgery Trialists' Collaborative Group. Stroke. 2000;31:615-621.
3. Lovett JK, Gallagher PJ, Hands LJ, Walton J, Rothwell PM. Histological correlates of carotid plaque surface morphology on lumen contrast imaging. Circulation. 2004;110:2190-2197.
4. Koelemay MJ, Nederkoorn PJ, Reitsma JB, Majoie CB. Systematic review of computed tomographic angiography for assessment of carotid artery disease. Stroke. 2004;35:2306-2312.
5. Estes JM, Quist WC, Lo Gerfo FW, Costello P. Noninvasive characterization of plaque morphology using helical computed tomography. J Cardiovasc Surg (Torino). 1998;39:527-534.
6. Walker LJ, Ismail A, McMeekin W, Lambert D, Mendelow AD, Birchall D. Computed tomography angiography for the evaluation of carotid atherosclerotic plaque: correlation with histopathology of endarterectomy specimens. Stroke. 2002;33:977-981.
7. de Weert TT, Ouhlous M, Zondervan PE, Hendriks JM, Dippel DW, van Sambeek MR, van der Lugt A. In vitro characterization of atherosclerotic carotid plaque with multidetector computed tomography and histopathological correlation. Eur Radiol. 2005;15:1906-1914.
8. de Monye C, Cademartiri F, de Weert TT, Siepman DA, Dippel DW, van Der Lugt A. Sixteen-detector row CT angiography of carotid arteries: comparison of different volumes of contrast material with and without a bolus chaser. Radiology. 2005;237:555-562.
9. Lovett JK, Gallagher PJ, Rothwell PM. Reproducibility of histological assessment of carotid plaque: implications for studies of carotid imaging. Cerebrovasc Dis. 2004;18:117-123.
10. Dobrin PB. Effect of histologic preparation on the cross-sectional area of arterial rings. J Surg Res. 1996;61:413-415.
11. Agatston AS, Janowitz WR, Hildner FJ, Zusmer NR, Viamonte M, Jr., Detrano R. Quantification of coronary artery calcium using ultrafast computed tomography. J Am Coll Cardiol. 1990;15:827-832.
12. Kopp AF, Schroeder S, Baumbach A, Kuettner A, Georg C, Ohnesorge B, Heuschmid M, Kuzo R, Claussen CD. Non-invasive characterisation of coronary lesion morphology and composition by multislice CT: first results in comparison with intracoronary ultrasound. Eur Radiol. 2001;11:1607-1611.

13. Leber AW, Knez A, Becker A, Becker C, von Ziegler F, Nikolaou K, Rist C, Reiser M, White C, Steinbeck G, Boekstegers P. Accuracy of multidetector spiral computed tomography in identifying and differentiating the composition of coronary atherosclerotic plaques: a comparative study with intracoronary ultrasound. J Am Coll Cardiol. 2004;43:1241-1247.
14. Moselewski F, Ropers D, Pohle K, Hoffmann U, Ferencik M, Chan RC, Cury RC, Abbara S, Jang IK, Brady TJ, Daniel WG, Achenbach S. Comparison of measurement of cross-sectional coronary atherosclerotic plaque and vessel areas by 16-slice multidetector computed tomography versus intravascular ultrasound. Am J Cardiol. 2004;94:1294-1297.
15. Shaw LJ, Raggi P, Schisterman E, Berman DS, Callister TQ. Prognostic value of cardiac risk factors and coronary artery calcium screening for all-cause mortality. Radiology. 2003;228:826-833.
16. Shaalan WE, Cheng H, Gewertz B, McKinsey JF, Schwartz LB, Katz D, Cao D, Desai T, Glagov S, Bassiouny HS. Degree of carotid plaque calcification in relation to symptomatic outcome and plaque inflammation. J Vasc Surg. 2004;40:262-269.
17. Seeger JM, Barratt E, Lawson GA, Klingman N. The relationship between carotid plaque composition, plaque morphology, and neurologic symptoms. J Surg Res. 1995;58:330-336.
18. Takaya N, Yuan C, Chu B, Saam T, Underhill H, Cai J, Tran N, Polissar NL, Isaac C, Ferguson MS, Garden GA, Cramer SC, Maravilla KR, Hashimoto B, Hatsukami TS. Association between carotid plaque characteristics and subsequent ischemic cerebrovascular events: a prospective assessment with MRI--initial results. Stroke. 2006;37:818-823.
19. Nandalur KR, Baskurt E, Hagspiel KD, Finch M, Phillips CD, Bollampally SR, Kramer CM. Carotid artery calcification on CT may independently predict stroke risk. AJR Am J Roentgenol. 2006;186:547-552.
20. Lovett JK, Redgrave JN, Rothwell PM. A critical appraisal of the performance, reporting, and interpretation of studies comparing carotid plaque imaging with histology. Stroke. 2005;36:1091-1097.

5

ASSESSMENT OF ATHEROSCLEROTIC CAROTID PLAQUE VOLUME WITH MULTIDETECTOR COMPUTED TOMOGRAPHY ANGIOGRAPHY

Thomas T de Weert • Cécile de Monyé • Erik Meijering • Ronald Booij • Wiro J Niessen • Diederik WJ Dippel • Aad van der Lugt

International Journal of Cardiovascular Imaging 2008; 24: 751-9

Assessment of atherosclerotic carotid plaque volume with multidetector computed tomography angiography

Abstract

Objective

The amount of atherosclerotic plaque and its components (calcifications, fibrous tissue, and lipid core) could be better predictors of acute events than the now currently used degree of stenosis. Therefore, we evaluated a dedicated software tool for volume measurements of atherosclerotic carotid plaque and its components in multidetector computed tomography angiography (MDCTA) images.

Materials and Methods

Data acquisition was approved by the Institutional Review Board and all patients gave written informed consent. MDCTA images of 56 carotid arteries were analyzed by three observers. Plaque volumes were assessed by manual drawing of the outer vessel contour. The luminal boundary was determined based on a Hounsfield-Unit (HU) threshold. The contribution of different components was measured by the number of voxels within defined ranges of HU-values (calcification >130 HU, fibrous tissue 60-130 HU, lipid core <60 HU). Interobserver variability (IOV) was assessed.

Results

Plaque volume was 1259±621 mm^3. The calcified, fibrous and lipid volumes were 238±252 mm^3, 647±277 mm^3 and 376±283 mm^3, respectively. IOV was moderate with interclass correlation coefficients (ICC) ranging from 0.76-0.99 and coefficients of variation (COV) ranging from 3-47%.

Conclusion

In conclusion atherosclerotic carotid plaque volume and plaque component volumes can be assessed with MDCTA with a reasonable observer variability.

Introduction

It is well known that the severity of stenosis is an unreliable estimation of the amount of atherosclerotic plaque. In case of carotid atherosclerotic disease, this is both related to the carotid bulb, in which atherosclerotic plaque accumulates before it compromises the lumen, and to positive remodeling, the phenomenon that an artery may or may not enlarge in response to plaque accumulation.[1] Furthermore, it is current opinion that atherosclerotic plaque rupture plays an important role in acute events, like transient ischemic accidents (TIA) and minor stroke.[2] Rupture-prone plaques have specific morphological features: the most frequently seen vulnerable plaque type has a large lipid-rich core with a thin fibrous cap[2] and has proved to be an independent predictor of ischemic cerebrovascular events.[3]

It is therefore hypothesized that the amount of atherosclerotic plaque and its components (calcifications, fibrous tissue, and lipid core) could be better predictors of acute events than the now clinically used degree of stenosis, and may be useful in the selection of patients who could benefit from therapeutic intervention.

Computed tomography angiography (CTA) has been established as an accurate modality to assess the presence of carotid atherosclerotic plaque and grade the severity of stenosis.[4] A recent in vitro and in vivo study showed that quantification of the area (two dimensional) of atherosclerotic carotid plaque and its components is possible in axial thin section multidetector computed tomography angiography (MDCTA) images, in good correlation (R^2>0.73) with histology.[5,6] Further developments in the quantification software now enable to quantify the volume of atherosclerotic plaque and the volume of different plaque components (three dimensional).

The aim of this study was to evaluate this software tool for atherosclerotic plaque and plaque component volume measurements in MDCTA images of the carotid artery and to assess the observer variability of these measurements.

Materials and Methods

Subjects

Twenty patients with a 0-29% stenosis grade (based on NASCET[7] criteria) and twelve patients for each of the three other stenosis grades (30-49%; 50-69% and 70-99%) at the symptomatic side were retrieved at random from a database (n=421) of MDCTA examinations of patients with transient ischemic attack or minor stroke. In all 56 patients MDCTA had been performed as part of a research protocol that was approved by the Institutional Review Board and for which all patients had given written informed consent.

Scanning and image reconstruction

Scanning was performed on a 16-slice MDCT scanner (Siemens, Sensation 16, Erlangen, Germany) with a standardized protocol (120 kVp, 180 mAs, collimation 16x0.75 mm, table feed 12 mm/rotation, pitch 1).[8] All patients received 80 ml contrast material (320 mg/ml), followed by 40 ml saline, both with an injec-

tion rate of 4 ml/sec.[9] The radiation dose was 2.6 mSv.

Image reconstructions were made with field of view 120 mm, matrix size 512x512 (yielding interpolated pixels of 0.2x0.2 mm, real in-plane resolution is 0.6x0.6 mm), slice thickness 1.0 mm, increment 0.6 mm and with an intermediate reconstruction algorithm (B46: heart-view sharp).[6]

Quantification and characterization

Three observers independently assessed the presence of an atherosclerotic lesion, the length of the atherosclerotic lesion, the location of the bifurcation, lumen attenuation, and plaque volume and plaque component volumes. One of the observers assessed after four months for a second time the volumes in a subset of patients (half the population per stenosis degree, randomly chosen).

The criterion used for the presence of an atherosclerotic lesion was: the presence of a calcification and/or thickening of the vessel wall. The length of the atherosclerotic lesion was defined as the distance between the first (most proximal) image and the last (most distal) image on which the atherosclerotic lesion was present. The location of the bifurcation was defined as the first image with two separate lumina. Lumen attenuation was measured in the most proximal and distal image with atherosclerosis, and the mean lumen attenuation was calculated.

Plaque and plaque component areas were measured with a polymeasure plug-in developed by one of the co-authors (E.M.) for the freely available software package ImageJ (Rasband, National Institute of Mental Health, Bethesda, USA). This plug-in made it possible to draw manually regions of interest (ROI) in consecutive axial MDCT images and to automatically calculate the total number of pixels and the number of pixels of different Hounsfield value (HV) ranges within these ROI (Figure 1). The ROI was placed over the outer vessel wall contour and therefore equals plaque area plus lumen area. The different HV ranges are considered to represent the different plaque components; calcification >130 HU, fibrous tissue 60-130 HU and lipid core <60 HU.

The cut-off value between calcifications and fibrous tissue was set at 130 HU; the value currently used for calcium scoring. The cut-off value between fibrous tissue and lipid core was set at 60 HU as assessed in previous studies.[5,6] The cut-off value between atherosclerotic plaque and lumen was adjusted for each patient and based on the full-width-half-maximum principle (mean lumen attenuation plus mean fibrous tissue attenuation ($\approx$ 88 HU) divided by two). To compensate for partial volume effects, related to a high lumen attenuation at the plaque-lumen border, the pixels around the lumen with a HV between 130 HU and the adjusted cut-off value were considered to be fibrous tissue. To assess the border between lumen and atherosclerotic plaque it was necessary to draw a second ROI close to the lumen in each image. Normally, the lumen area was then automatically differentiated from atherosclerotic plaque based on the adjusted cut-off value. But in those plaques in which calcifications bordered the lumen and the two dense structures merged with each

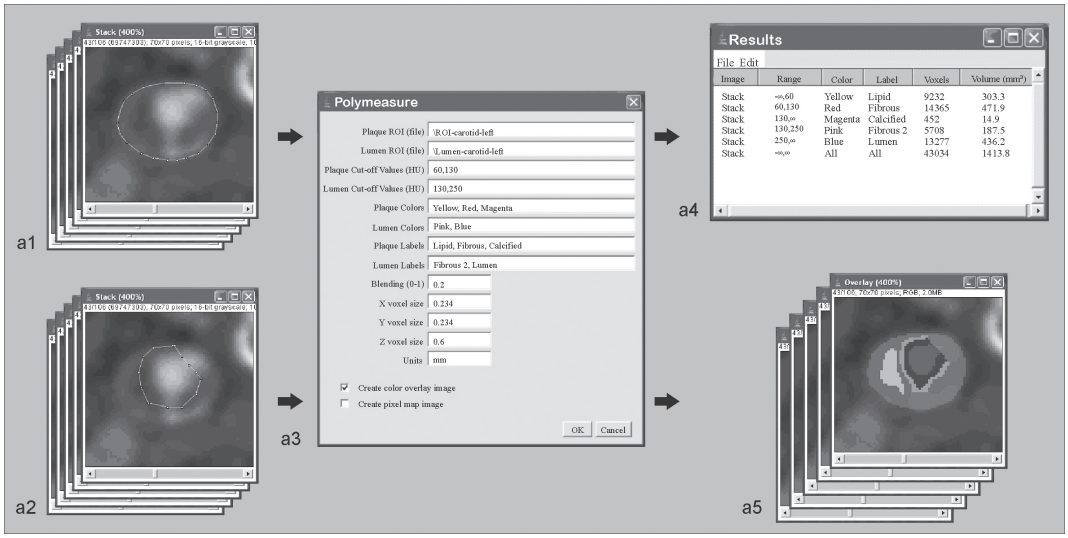

Figure 1. Semi-automatic assessment of plaque component volumes in a stack of MDCTA images with the ImageJ plug-in 'PolyMeasure'. (a1.) This plug-in allows an observer to draw a region of interest (ROI) on consecutive axial MDCTA images. This ROI represents lumen area and atherosclerotic plaque area. (a2.) To differentiate lumen area from the atherosclerotic plaque area and from calcified tissue, a second ROI is drawn. This second ROI should include the attenuated lumen area, but should not include any calcifications.(a3.) After the input of the cut-off values that differentiate the specific plaque components and the lumen, the plaque components and the lumen can be labeled with a color. After the input of the voxel sizes, (a4.) atherosclerotic plaque component volumes and lumen volume are automatically calculated, and (a5.) color overlay images are produced on which the plaque components and the lumen have a specific color.

other, lumen area and calcifications had to be separated by manual drawing.

The volumes were calculated as the product of the number of pixels, the pixel size and the increment.

Analysis

Firstly, the difference between observers in the assessment of the presence of an atherosclerotic lesion was assessed. Hereafter, consensus on the presence of an atherosclerotic lesion was achieved by a consensus reading between all three observers. Those image series that were appointed as having atherosclerosis were used for further analysis.

Secondly, differences between observers in the assessment of the length of the atherosclerotic lesion, the location of the bifurcation, lumen attenuation and plaque and plaque component volumes, were calculated.

After assessment of the differences, a second consensus reading was held in order to achieve consensus about the length of the atherosclerotic lesion, the location of the bifurcation and lumen attenuation because these features influence the volume measurements. All observers had to adapt their assessments on grounds of this second consensus reading and hereafter plaque and plaque component volumes were calculated again and differences were evaluated. This recalculation provides observer variability measurements due to differences in the assessment of the outer vessel wall contour only.

In order to assess not only the variability in volume measurements, the overlap (similarity index) between the ROIs (outer contour) of the observers was assessed and expressed as a percentage (2 x pixels with overlap / (pixels ROI observer A + pixels ROI observer B)x 100 %).
Finally, the intra-observer differences in plaque and plaque component volume measurements were assessed.

Statistics

Continuous data were compared with a paired Student's t-test for which a p-value <0.05 was considered to indicate statistical significance.
Inter-observer differences in the assessment of the length of the atherosclerotic lesion, the location of the bifurcation and lumen attenuation were expressed as the mean ± the standard deviation (SD), and as a coefficient of variation defined by the SD of the paired difference divided by the mean of the absolute values.

Inter- and intra-observer differences in plaque and plaque component volume measurements were presented with a mean ± SD, an interclass correlation coefficient (ICC) with 95% confidence interval and a coefficient of variation. The differences were also plotted against the mean value of the measurements (Bland-Altman plot).

Results

In the 36 patients with a stenosis degree of 30% or higher, all observers agreed on the presence of an atherosclerotic lesion. In the 20 patients with 0-29% stenosis, the presence of an atherosclerotic lesion was determined in 9 patients by three observers, in 1 patient by two observers, and in 1 patient by one observer. The consensus reading appointed 10 patients as having atherosclerosis, thus 46 patients were selected for further analysis.

The mean time used by an observer for the analysis of one artery was about 1 hour, almost entirely taken by the drawing of the outer vessel wall.

The assessment of the length of an atherosclerotic lesion was significantly different between observers, while the assessment of the location of the bifurcation and lumen attenuation was not significantly different ($p>0.27$ and $p>0.49$, respectively).

The ICC was good for all volume measurements (range 0.53-0.96). The plaque and plaque component volumes measured by the three observers were significantly different and the coefficients of variation were moderate (range 13-58%) (Table 1).

After the second consensus reading in which consensus was achieved about the length of the atherosclerotic lesion, the location of the bifurcation and lumen attenuation, the ICC improved and was excellent for all volume measurements (ICC>0.80), except for the lipid core volume measurements (ICC=0.76 (0.54-0.87)), for which it was good (Table 2). The coefficients of variation between observers improved for all measurements: plaque volume (17-24%), calcified volume (13-33%), fibrous tissue volume (18-24%), lipid core volume

Table 1. Mean values, inter-observer differences, interclass correlation coefficients, coefficients of variation of atherosclerotic plaque features and volume measurements from 46 CTA datasets in which atherosclerosis was considered to be present.

	Mean ± SD	Diff Obs 1-2	Diff Obs 1-3	Diff Obs 2-3	ICC (95% CI)	CoV (range)
Lesion length (mm)	27.3±10.6	6.1±4.4*	1.7±5.2*	4.3±6.2*	-	-
Image with bifurcation(mm²)	-	0.5±3.6	0.3±1.7	0.2±3.2	-	-
Lumen attenuation (HU)	217.4±36.9	0.4±5.9	0.7±3.9	0.2±5.8	-	-
Plaque volume (mm³)	1259±621	167±278*	247±381*	80±446	0.79 (0.65-0.87)	23-34%
Calcified volume (mm³)	238±252	37±68*	3±38	40±82*	0.96 (0.93-0.98)	13-34%
Fibrous volume (mm³)	647±277	77±144*	92±191*	15±210	0.76 (0.63-0.85)	23-31%
Lipid volume (mm³)	376±283	48±141*	153±204*	105±236*	0.70 (0.51-0.82)	42-58%
Luminal volume (mm³)	879±459	182±206*	51±226	132±240*	0.84 (0.71-0.91)	23-27%
Calcified volume (%)	19±15	1±9	4±9*	2±6*	0.85 (0.77-0.91)	33-48%
Fibrous volume (%)	54±12	2±14	0±13	2±7*	0.53 (0.36-0.69)	13-27%
Lipid volume (%)	27±13	1±11	3±11*	5±8*	0.68 (0.53-0.80)	30-44%

* = t-test p value < 0.05; Diff = Difference; Obs = Observer; CoV = Coefficient of variation; ICC = Interclass correlation; CI = Confidence interval

Table 2. Mean values, inter-observer differences, interclass correlation coefficients, coefficients of variation of volume measurements from 46 CTA datasets in which atherosclerosis was considered to be present and consensus was reached with regard to the lesion length, location of bifurcation and lumen attenuation.

	Mean ± SD	Diff Obs 1-2	Diff Obs 1-3	Diff Obs 2-3	ICC (95 % CI)	CoV (range)
Plaque volume (mm³)	1223±606	26±194	218±255*	192±300*	0.88 (0.75-0.94)	17-24%
Calcified volume (mm³)	235±250	28±60*	4±28	31±78*	0.97 (0.95-0.98)	13-33%
Fibrous volume (mm³)	619±264	21±72*	67±88*	87±106*	0.90 (0.78-0.95)	18-24%
Lipid volume (mm³)	369±278	20±120	150±168*	130±186*	0.76 (0.54-0.87)	37-47%
Luminal volume (mm³)	830±421	13±76	6±21	18±86	0.99 (0.98-0.99)	3-10%
Calcified volume (%)	18±15	2±4*	2±3*	4±5*	0.95 (0.89-0.98)	15-26%
Fibrous volume (%)	54±12	2±6	3±5*	1±8	0.84 (0.76-0.91)	10-15%
Lipid volume (%)	27±13	0±7	5±6*	5±8*	0.81 (0.66-0.89)	21-30%

* = t-test p value < 0.05; Diff = Difference; Obs = Observer; CoV = Coefficient of variation; ICC = Interclass correlation; CI = Confidence interval

(37-47%) and lumen volume (3-10%) (Table 2). The coefficients of variation between observers for the assessment of calcified volume percentage (15-26%), fibrous volume percentage (10-15%) and lipid core volume percentage (21-30%) were also improved (Table 2).

From the Bland-Altman plots it can be observed that especially the differences between observers in plaque volume, fibrous tissue volume and lipid core volume measurements increase with a larger volume (Figure I).

The similarity indices (±SD) between the ROIs assessed by observer 1 and 2, observer 1 and 3, and observer 2 and 3 were 91.3±3.0%, 90.9±2.9% and 90.0±4.5%, respectively.

Intra-observer analysis was good with excellent ICC (all >0.94) and moderate to good coefficients of variation for the assessment of plaque volume (11%), calcified volume (8%), fibrous tissue volume (8%), lipid core volume (25%) and lumen volume (5%) (Table 3). The intra-observer coefficients of variation for the assessment of calcified volume percentage (10%), fibrous volume percentage (6%) and lipid core volume percentage (14%) were also good (Table 3).

The similarity index (± SD) between the two series of independently assessed ROIs by observer 1 was 93.7±1.8%.

Discussion

Non-invasive in vivo assessment of atherosclerotic plaque volume and the relative contribution of the different plaque components will have important clinical implications: it provides new and probably better parameters, together with the severity of stenosis, for cardiovascular risk assessment, and furthermore the natural history of atherosclerotic disease and the effect of pharmacological intervention can be studied[10]. MDCTA has extensively been used to assess the severity of luminal narrowing, and nowadays attention is increasingly paid to the potential role of MDCTA in qualitative and quantitative evaluation of the atherosclerotic plaque itself. Validation studies in which image-based plaque features are compared with histology, as well as assessment of observer variability, are necessary to

Table 3. Mean values, intra-observer differences, interclass correlation coefficients, coefficients of variation of volume measurements from 46 CTA datasets in which atherosclerosis was considered to be present and consensus was reached with regard to the lesion length, location of bifurcation and lumen attenuation.

	Mean ± SD	Difference	ICC (95 % CI)	CoV
Plaque volume (mm^3)	1098±459	1±120	0.97 (0.93–0.99)	11%
Calcified volume (mm^3)	218±186	7±18	0.99 (0.99–1.00)	8%
Fibrous volume (mm^3)	591±229	10±49	0.98 (0.95–0.99)	8%
Lipid volume (mm^3)	289±205	2±72	0.94 (0.87–0.97)	25%
Luminal volume (mm^3)	824±413	14±40	1.00 (0.99–1.00)	5%
Calcified volume (%)	20±16	1±2	0.99 (0.98–1.00)	10%
Fibrous volume (%)	56±12	1±3	0.96 (0.91–0.98)	6%
Lipid volume (%)	24±11	0±3	0.96 (0.91–0.96)	14%

* = t-test p value < 0.05; ICC = Interclass correlation; CI = Confidence interval; CoV = Coefficient of variation

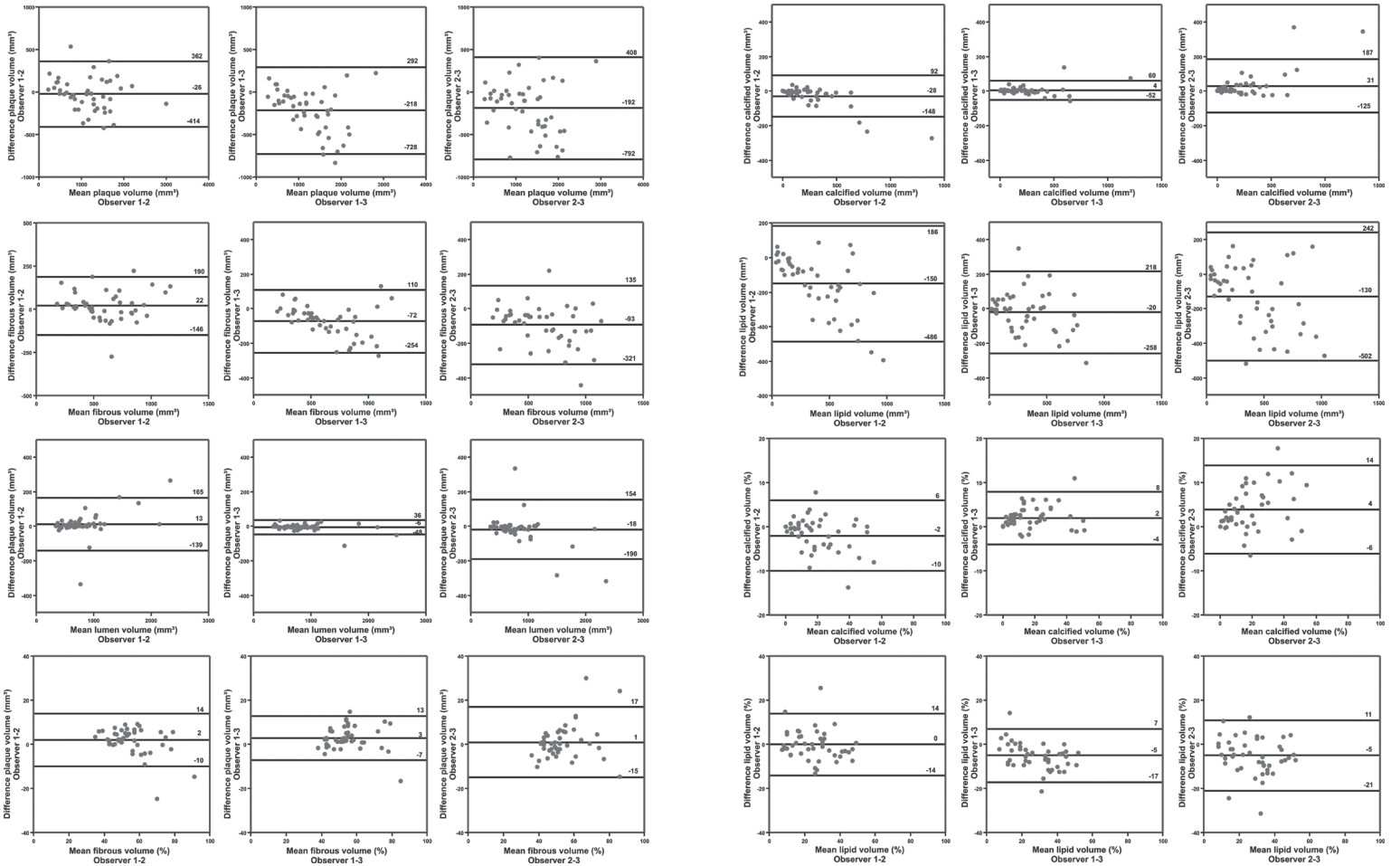

Figure I. Bland-Altman plots of plaque volume and plaque component volumes assessed by three observers. The horizontal lines express the mean difference and the mean difference ± 2 standard deviations.

establish the final role of MDCTA in qualitative and quantitative atherosclerotic plaque evaluation.

Until now a few coronary in vivo studies have compared the plaque volume assessed with MDCTA and intravascular ultrasound (IVUS). One study found a strong correlation (r = 0.8) and an underestimation of the coronary plaque volume assessed with MDCT compared to IVUS.[11] Another study found a moderate correlation (r = 0.55) and an overestimation of coronary plaque area assessed with MDCTA compared to IVUS.[12] The discrepancies between these studies might be explained by the results of a third study that found a strong correlation coefficient (r^2=0.69) with an underestimation of mixed and noncalcified plaque volumes, and a trend to overestimate calcified plaque volumes with MDCTA. In addition, they reported a moderate reproducibility in the assessment of plaque volume, with a coefficient of variation of 37%.[13]

An in vivo study[5] on carotid atherosclerotic plaques revealed a strong correlation between MDCTA and histology for the assessment of plaque area (r^2=0.73); in addition, the inter- and intra-observer variability of plaque area measurements with MDCTA was reasonable with coefficients of variation of 19% and 8%, respectively.

To our knowledge, the present study is the first study that shows that in vivo quantification of the volume of atherosclerotic carotid plaque and its components is possible with MDCTA (Figure 2.). Inter-observer variability was moderate with ICC ranging from 0.53-0.96 and coefficients of variation ranging from 13-58%. To evaluate the inter-observer variability caused by the manual drawing of the contours we re-evaluated the data after consensus was reached with regard to the length of atherosclerotic disease, the location of the bifurcation and lumen attenuation, because all these features also influenced the volume measurements. This led to a decreased variability with ICC ranging from 0.76-0.99 and coefficients of variation ranging from 3-47%. Intra-observer variability was less with ICC ranging from 0.94-1.00 and coefficients of variation ranging from 5-25%.

The first problem which causes a variability in volume measurements is the differentiation between a normal vessel wall and a slightly thickened (diseased) vessel wall. In a number of cases, observers disagree with regard to the presence of atherosclerotic disease in carotid arteries with a stenosis of 0-29%. In such cases, the assessed plaque volume in such patients will be very low; the measured plaque volume in the two arteries in which the observers disagree on the presence of atherosclerotic disease was 609 and 245 mm^3, while the mean plaque volume of all patients was 1259±621 mm^3.

Furthermore, the difficulty in differentiation between a normal vessel wall and a slightly thickened (diseased) vessel wall, influences the assessment of the most proximal and distal image with atherosclerosis and thus the length of the atherosclerotic lesion. Because the plaque volume measurements include the original vessel wall, inclusion of additional

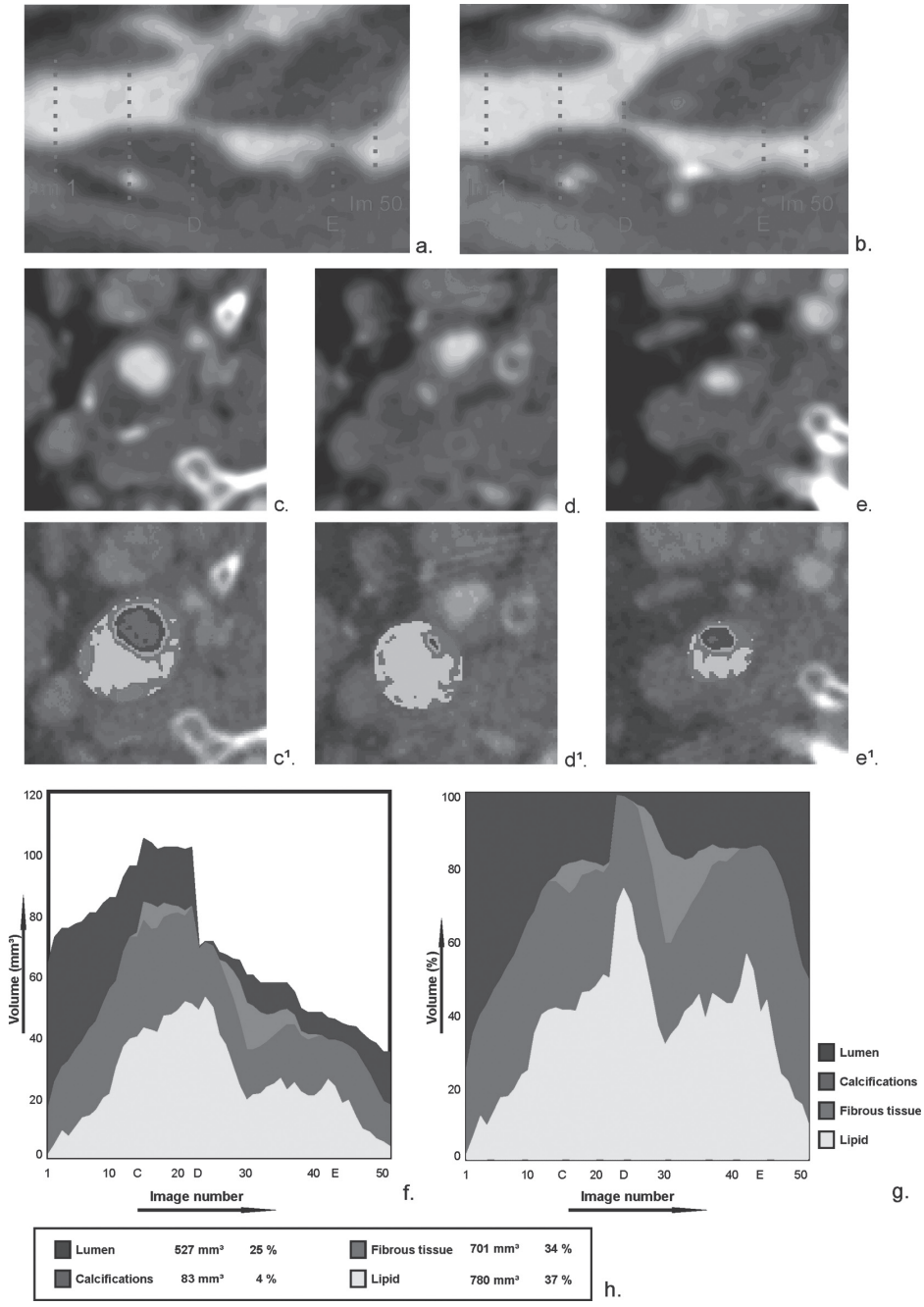

Figure 2. One mm multiplanar reformat (a.) and 2 mm maximum intensity projection (b.) in the sagittal plane depicts the carotid bifurcation with an atherosclerotic plaque. The startpoint (Im 1) and endpoint (Im 50) of atherosclerotic plaque volume assessment in this patient, and the position (C, D, E) of the three thin sliced (0.75 mm) axial MDCT images (c., d. and e.) of the internal carotid artery and their associated color overlay images (c'., d'. and e'.) are indicated. A graphical representation of the absolute (f.) and relative (g.) volume measurements of lumen, calcifications, fibrous tissue, and lipid per MDCT image. The x-axis represents the consecutive MDCT images, the y-axis represents the volume. (h.) A table with the total lumen, total calcified, total fibrous tissue and total lipid volume. (A full color version of this illustration can be found in the color section)

images with normal vessel wall increases the amount of measured volumes considerably.

The second problem is the manual outlining of the outer border of the vessel wall. Some parts of the vessel wall can easily be differentiated from the surrounding tissue due to the low density of peri-arterial fat or the presence of calcifications at the outer border of the plaque. However, other parts have the same density as the peri- and paravertebral and sternocleidomastoid muscle, which are frequently positioned along the artery. The erroneous manual inclusion of peri-arterial fat in the ROI leads to the classification of this fat as lipid in the plaque. This inclusion will vary between the observers which explains the moderate ICC and the high observer variability in the assessment of lipid volume. The Bland-Altman plots confirm this by showing that the differences in lipid volume between observers 1 and 3, and 2 and 3 depend on the size of the assessed volume, suggesting that observer 3 systematically draws a larger outer contour than the other observers and thus includes more peri-arterial low density tissues. An additional problem in the assessment of the outer border of the vessel wall is, that the size of calcifications is influenced by differences in window-level setting. Because these calcifications are often located at the border of an atherosclerotic plaque, different window-level settings between observers will influence the assessment of the outer vessel wall between observers, and thereby introduce variability in the assessment of plaque volume and calcified volume.

The third problem is the differentiation of contrast-enhanced lumen from atherosclerotic plaque. In some plaque without calcifications at the inner border of the plaque the differentiation is automated and based on a threshold and the only variability is caused by a difference in the measurement of luminal attenuation, which was fortunately low. In case a calcification borders the lumen, a threshold based approach would merge the lumen with the calcification. In such cases manual drawing of the border between lumen and calcification was necessary which introduced a variability in plaque volume and calcium volume measurements.

We expect that improvements in the measurement software will improve the observer variability. Although in our method we assessed volumes, the analysis was performed in axial two-dimensional images. Evaluating the artery both in axial slices and using longitudinal reformats will provide more information on the borders of the vessel wall. This would enable a better continuation of transversal contours in adjacent slices. Also, highlighting specific parts of the vessel outer contour in axial images based on outer vessel contour assessment in longitudinal planes might be helpful. Finally, the differentiation between normal vessel wall and slightly thickened vessel wall can be based on wall thickness measurements, and the length of the atherosclerotic disease can be assessed more reproducibly.

Besides MDCTA, MRI has been used for non-invasive atherosclerotic carotid plaque characterization and quantification. Studies have shown that there is good agreement between

in vivo MRI and histology for qualitative[14-16] and quantitative[17] assessment of plaque components, while observer reproducibility has shown to be good to excellent for plaque area[14-16,18] and plaque component areas.[19] ICC for plaque area were 0.90-0.96 and for lipid core 0.88-0.89. The reproducibility of MRI-based plaque volume measurements has not been extensively studied. One study reported a coefficient of variation for an averaged (over 5 slices) plaque area of 3.5%[20], while another study reported a coefficient of variation of 9.8% for plaque volume.[20]

Until now carotid intima-media thickness (CIMT) is a validated endpoint in progression/regression studies. CIMT has shown to be an independent risk factor for future myocardial infarction and stroke risk.[21,22] In addition, CIMT has been related to the presence of future carotid plaque.[23] Lifestyle changes[24] and statin therapy[25] has a beneficial effect on CIMT. Ultrasound assessment of CIMT is accurate when compared with histology[26,27], and has a very good reproducibility (coefficient of variation 2.4-10.6%).[28] Interscan coefficient of variation is 5.6%,[28] making it a potential valuable tool to evaluate the effectiveness of prevention therapy. Unfortunately, CIMT does not provide us with area and volumetric measurements of the plaque and ignores the presence of different plaque components. This makes CIMT unsuitable for the precise evaluation of pharmacological effects on the advanced atherosclerotic plaque.

The present study investigated the reproducibility of MDCTA-based atherosclerotic plaque volume measurements. It is a limitation that validation with histology has not been performed. Because we investigated a range of carotid artery stenoses, atherosclerotic specimens were not available in most of the patients. In the patients with a stenosis of more than 70% stent placement or surgery was performed. Previous studies[5,6], however, have demonstrated a good correlation between area measurements with MDCTA and histology. A second limitation is the inclusion of the vessel wall (tunica media) in the plaque volume measurements. With MDCTA it is not possible to differentiate between the atherosclerotic plaque and the tunica media. This will lead to a systematic overestimation of plaque volume measurements. It is not expected that this overestimation will be a problem for serial evaluation or risk prediction.

Conclusion

In vivo assessment of atherosclerotic plaque and plaque component volumes in carotid arteries with MDCTA is feasible with a moderate reproducibility. A prospective longitudinal study which examines the relationship between cardiovascular risk factors, plaque and plaque component volumes and outcome may determine the value of MDCTA-based stroke risk predictors.

References

1. Glagov S, et al. Compensatory enlargement of human atherosclerotic coronary arteries. N Engl J Med. 1987;316:1371-5.
2. Naghavi M, et al. From vulnerable plaque to vulnerable patient: a call for new definitions and risk assessment strategies: Part I. Circulation. 2003;108:1664-72.
3. Polak JF, et al. Hypoechoic plaque at US of the carotid artery: an independent risk factor for incident stroke in adults aged 65 years or older. Cardiovascular Health Study. Radiology. 1998;208:649-54.
4. Koelemay MJ, et al. Systematic review of computed tomographic angiography for assessment of carotid artery disease. Stroke. 2004;35:2306-12.
5. de Weert TT, et al. In vivo characterization and quantification of atherosclerotic carotid plaque components with multidetector computed tomography and histopathological correlation. Arterioscler Thromb Vasc Biol. 2006;26:2366-72.
6. de Weert TT, et al. In vitro characterization of atherosclerotic carotid plaque with multidetector computed tomography and histopathological correlation. Eur Radiol. 2005;15:1906-14.
7. Beneficial effect of carotid endarterectomy in symptomatic patients with high-grade carotid stenosis. North American Symptomatic Carotid Endarterectomy Trial Collaborators. N Engl J Med. 1991;325:445-53.
8. de Monye C, et al. Optimization of CT angiography of the carotid artery with a 16-MDCT scanner: craniocaudal scan direction reduces contrast material-related perivenous artifacts. AJR Am J Roentgenol. 2006;186:1737-45.
9. de Monye C, et al. Sixteen-detector row CT angiography of carotid arteries: comparison of different volumes of contrast material with and without a bolus chaser. Radiology. 2005;237:555-62.
10. Pulido MA, et al. Imaging of atherosclerotic plaque. Int J Cardiovasc Imaging. 2004;20:553-9.
11. Achenbach S, et al. Detection of calcified and noncalcified coronary atherosclerotic plaque by contrast-enhanced, submillimeter multidetector spiral computed tomography: a segment-based comparison with intravascular ultrasound. Circulation. 2004;109:14-7.
12. Moselewski F, et al. Comparison of measurement of cross-sectional coronary atherosclerotic plaque and vessel areas by 16-slice multidetector computed tomography versus intravascular ultrasound. Am J Cardiol. 2004;94:1294-7.
13. Leber AW, et al. Accuracy of 64-slice computed tomography to classify and quantify plaque volumes in the proximal coronary system: a comparative study using intravascular ultrasound. J Am Coll Cardiol. 2006;47:672-7.
14. Cai J, et al. In vivo quantitative measurement of intact fibrous cap and lipid-rich necrotic core size in atherosclerotic carotid plaque: comparison of high-resolution, contrast-enhanced magnetic resonance imaging and histology. Circulation. 2005;112:3437-44.

15. Trivedi RA, et al. Multi-sequence in vivo MRI can quantify fibrous cap and lipid core components in human carotid atherosclerotic plaques. Eur J Vasc Endovasc Surg. 2004;28:207-13.
16. Saam T, et al. Quantitative evaluation of carotid plaque composition by in vivo MRI. Arterioscler Thromb Vasc Biol. 2005;25:234-9.
17. Yuan C, et al. Measurement of atherosclerotic carotid plaque size in vivo using high resolution magnetic resonance imaging. Circulation. 1998;98:2666-71.
18. Takaya N, et al. Intra- and interreader reproducibility of magnetic resonance imaging for quantifying the lipid-rich necrotic core is improved with gadolinium contrast enhancement. J Magn Reson Imaging. 2006;24:203-10.
19. Corti R, et al. Effects of lipid-lowering by simvastatin on human atherosclerotic lesions: a longitudinal study by high-resolution, noninvasive magnetic resonance imaging. Circulation. 2001;104:249-52.
20. Adams GJ, et al. Tracking regression and progression of atherosclerosis in human carotid arteries using high-resolution magnetic resonance imaging. Magn Reson Imaging. 2004;22:1249-58.
21. O'Leary DH, et al. Carotid-artery intima and media thickness as a risk factor for myocardial infarction and stroke in older adults. Cardiovascular Health Study Collaborative Research Group. N Engl J Med. 1999;340:14-22.
22. Touboul PJ, et al. Carotid intima-media thickness, plaques, and Framingham risk score as independent determinants of stroke risk. Stroke. 2005;36:1741-5.
23. Zureik M, et al. Cross-sectional and 4-year longitudinal associations between brachial pulse pressure and common carotid intima-media thickness in a general population. The EVA study. Stroke. 1999;30:550-5.
24. Markus RA, et al. Influence of lifestyle modification on atherosclerotic progression determined by ultrasonographic change in the common carotid intima-media thickness. Am J Clin Nutr. 1997;65:1000-4.
25. Probstfield JL, et al. Results of the primary outcome measure and clinical events from the Asymptomatic Carotid Artery Progression Study. Am J Cardiol. 1995;76:47C-53C.
26. Wong M, et al. Ultrasonic-pathological comparison of the human arterial wall. Verification of intima-media thickness. Arterioscler Thromb. 1993;13:482-6.
27. Pignoli P, et al. Intimal plus medial thickness of the arterial wall: a direct measurement with ultrasound imaging. Circulation. 1986;74:1399-406.
28. Sramek A, et al. Ultrasound assessment of atherosclerotic vessel wall changes: reproducibility of intima-media thickness measurements in carotid and femoral arteries. Invest Radiol. 2000;35:699-706.

6 CT OF THE PLAQUE

Thomas T de Weert • Mohamed Ouhlous • Marc RHM van Sambeek • Aad van der Lugt

In: *Imaging carotid disease:* J Gillard, M Graves, T Hatsukami, C Yuan (Eds): Cambridge University Press, 2006.

CT of the plaque

Introduction

Stroke is the most common cause of disability in adults in Western societies. Infarction and ischemia account for 80% of all strokes and about 20%-30% of ischemic stroke can be linked to carotid artery stenosis.[1] The degree of carotid luminal stenosis is used in therapeutic decision making: patients with symptomatic or asymptomatic carotid stenosis above a certain degree are considered candidates for carotid intervention, such as carotid endarterectomy or stent placement.

However, the fact that most symptomatic patients have only mild stenotic lesions and that most patients with severe carotid stenosis are asymptomatic[2, 3], show that apart from the degree of stenosis other features may play a role in an acute ischemic event and in the assessment of stroke risk.

Morphology studies on carotid and coronary atherosclerotic plaque have lead to the consensus opinion that atherosclerotic plaque morphology and luminal plaque surface could be these important features.[4] An atherosclerotic plaque with specific morphological features (e.g. a large lipid core with a thin fibrous cap; outward remodeling) is more prone to rupture, and irregular luminal plaque surfaces (caused by ruptured or eroded plaques) are more prone to thrombus formation, thromboembolization and consequent acute events (Fig. 1)[4].

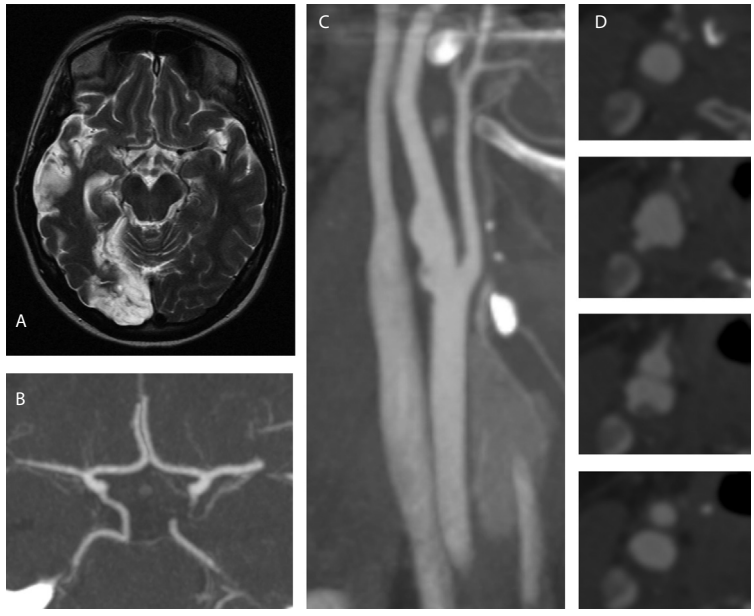

Figure 1. MR image of a 37-year-old woman with infarcts in the territory of the medial and posterior cerebral artery (A). MDCT image, showing the circle of Willis with a fetal origin of the posterior cerebral artery demonstrating that both infarcts are in the territory of the right internal carotid artery (B). MDCT image of the right carotid artery shows mild atherosclerotic plaque formation at the level of the carotid bifurcation. In addition, it shows an ulcer with extension of contrast material beyond the vascular lumen into the surrounding plaque (arrow) (C). Four axial MDCT images at the level of the right carotid bifurcation with an eccentric plaque and confirmation of the presence of an ulcer (arrow) (D).

Because computed tomography angiography (CTA) can accurately grade the severity of carotid luminal stenosis5 computed tomography (CT) is increasingly used in the evaluation of stroke patients. The question then arises whether CT can also provide detailed information about atherosclerotic plaque morphology and luminal plaque surface.

History

Single slice CT

In 1984 it was demonstrated that single-slice CTA was able to detect the presence of intimal atherosclerotic disease in the carotid bifurcation.[6] Later studies showed that CTA had a high degree of correlation with results of digital subtraction angiography (DSA) in the evaluation of carotid luminal stenosis.[7, 8] In addition, CTA more frequently depicted luminal surface irregularities than either DSA or magnetic resonance angiography (MRA).[9] It was also shown that electron-beam CT (EBCT) was an excellent tool for detecting and quantifying vessel wall calcifications in the coronary arteries10 as well as in the carotid arteries.[11]

Validation studies compared 3-mm thick CT images with histologic sections of carotid endarterectomy specimens. The results were, however, confusing. Two studies reported that the major plaque components could be differentiated based on differences in measured density expressed in Hounsfield units (HU): hyperdense structures correspond with calcifications, hypodense regions with lipid or hemorrhage, and isodense regions with fibrosis.[12, 13] However, another study concluded that CT failed to reliably indicate the presence of lipid or fibrous tissue and suggested the need of multislice technology.[14]

Multislice CT

Multislice CT (MSCT) allows full vascular imaging (from the aorta to the circle of Willis). By providing this large coverage with an evaluation of other important atherosclerotic predilection sites, MS-CTA can now compete with DSA and MRA in the evaluation of stroke patients. However, the main advantage of MSCT for carotid atherosclerotic plaque evaluation is the increased in-plane resolution, the decreased slice thickness (<0.75 mm) and the subsequent ability to obtain near isotropic voxels. More detailed analysis of atherosclerotic plaque morphology (based on differences in HU) and luminal plaque surface may now be possible.

Influence of scanning and reconstruction parameters

Slice thickness

In single-slice CT, slice thickness and detector collimation (defined as the width of the individual detector) are the same; However, the effective slice thickness is larger than the reconstructed slice thickness. In MSCT the reconstructed slice thickness is independent of the detector collimation and is equal to or larger than the single detector collimation. In addition, the effective slice thickness reaches the reconstructed slice thickness. Reconstruction of thin slices is important in plaque imaging

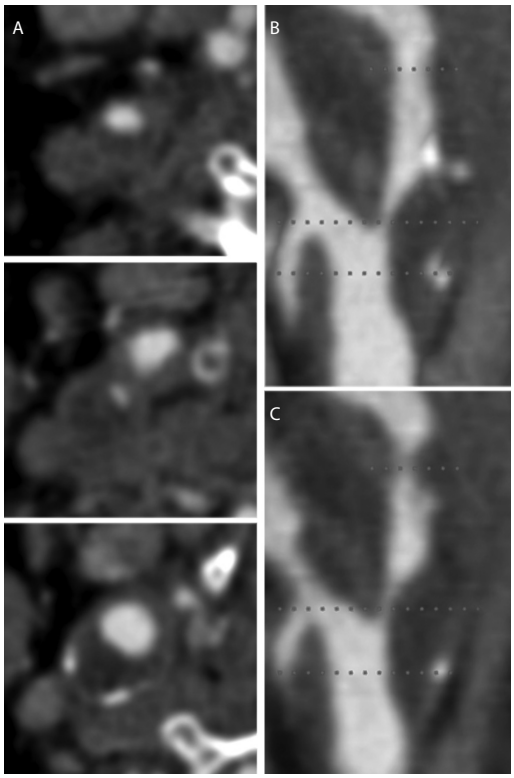

Figure 2. Three axial thin-slice (0.75 mm) MDCT images of the internal carotid artery (A). The true volumetric data sets with (nearly) isotropic voxels allow reconstruction in other planes, like the sagittal and coronal plane. One mm multiplanar reformat (B) and 2 mm minimum intensity projection (C) in the sagittal plane depicts the carotid bifurcation with an eccentric plaque.

for two reasons. First, with thinner slices true volumetric data sets can be acquired which allows reconstruction in other planes (Fig. 2). Secondly, as atherosclerotic plaques are very small and heterogenous, thinner slices lead to less volume averaging and may therefore enhance the differentiation of plaque components. This is especially important for differentiation of lipid and fibrous tissue.

The latter phenomenon has been confirmed in a phantom study in which silicon tubes with two different plaque types (resembling lipid and fibrous tissue) were scanned with two different detector widths (4 x 1.0 mm vs 4 x 2.5 mm). A larger slice thickness increased the density measurements of both plaque types; an effect that was even more evident in the plaques with lower densities (resembling lipid).[15]

Tube energy (kVp)

The voltage across the x-ray tube determines the effective energy of the x-ray beam, which influences the type and amount of interactions of the x-ray beam in the tissue. The most commonly used tube energy is 120 kVp, although current MSCT scanners allow other tube energy settings in the range of 60-140 kVp. With higher kVp almost all interaction in the tissue occurs by Compton scattering. Lowering the kilovolt peak from 140 to 80 kVp will increase the number of photoelectric interactions. Therefore for calcium and contrast material, lowering the tube energy will increase the x-ray attenuation coefficient, as reflected by the measured density.

The high density calcifications normally lead to overestimation of the true volume of the calcium and can lead to overestimation of plaque size with an increase in the severity of luminal stenosis. This so-called blooming artifact is caused by the large difference in density between calcifications and surrounding tissue. This difference causes partial volume averaging effects due to the finite spatial resolution of CT.

The main problem of this blooming artifact is hampering of the optimal characterization of the non-calcified part of the plaque. Increas-

ing the tube energy will reduce the size of the already overestimated calcifications. An ex vivo study in which carotid specimens were scanned with MSCT revealed that the calcium volume decreased by 14.0%, 17.3% and 20.2% with 100-, 120-, and 140-kVp settings, respectively, as compared with the volume measured with 80-kVp acquisition16. The same results were found in a second ex vivo study (Fig. 3)[17]. The effects on plaque analysis of an increase in the density values of the contrast material in the lumen with lower tube energy are discussed below (see Contrast material).

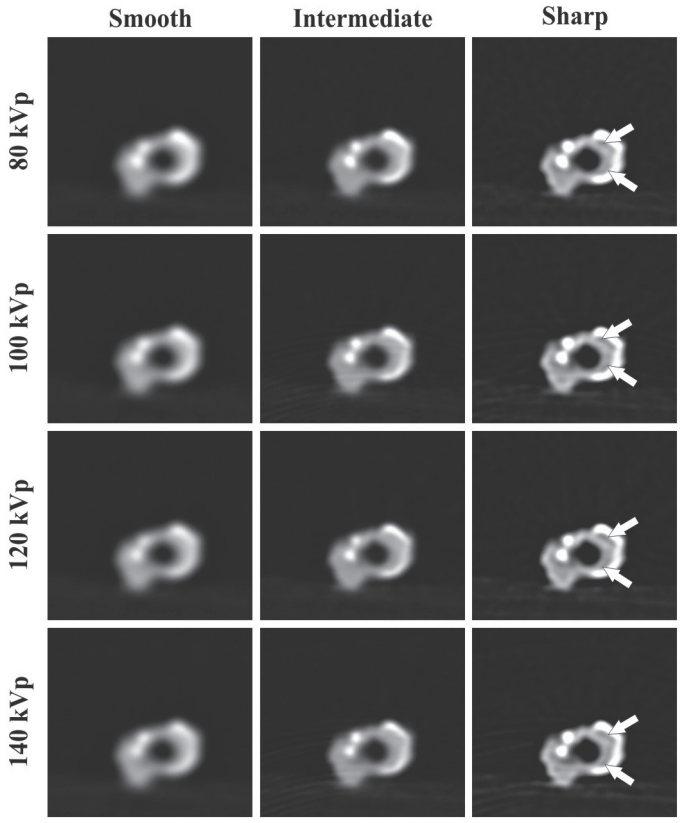

Figure 3. MDCT images of a carotid endarterectomy specimen. All images are obtained at the same location in the specimen, but with different kVp settings (80 kVp, 100 kVp, 120 kVp or 140 kVp) and different reconstruction algorithms (smooth, intermediate or sharp). Higher kVp settings decrease the calcium volume up to 20.2% (140 kVp). Furthermore, the evaluation of plaque composition is influenced by the reconstruction algorithm. Sharp algorithms produce low intensity rings around calcifications (white arrows) that hamper plaque characterization. (Reprinted with permission from De Weert et al., European Radiology 2005, 15: 1906.)

Tube current (mAs)

Radiographic exposure (the product of tube current and exposure time) is the main determinant of image quality, more specifically the signal-to-noise ratio (SNR) in the CT image. Normally, the small size of the neck region leads to sufficient SNR in the CT image for clinical evaluation. However, the size of the atherosclerotic plaque (< 10 mm) means that a reconstructed CT image needs a thin slice thickness and a small field-of-view necessary. The resultant decrease in SNR demands a higher exposure since only a high SNR allows differentiation of tissues with a small difference in density.

Contrast material

To differentiate lumen from plaque, contrast material in the patent lumen is a prerequisite (Fig .4). In CTA, in which assessment of the severity of stenosis was the main indication, the aim is to have a high dose of contrast material in the artery under study. To achieve this high dose a high concentration of iodine is injected with a high injection rate into the anticubital vein.[18] With higher densities in the contrast-filled lumen, the cut-off point for the dif-

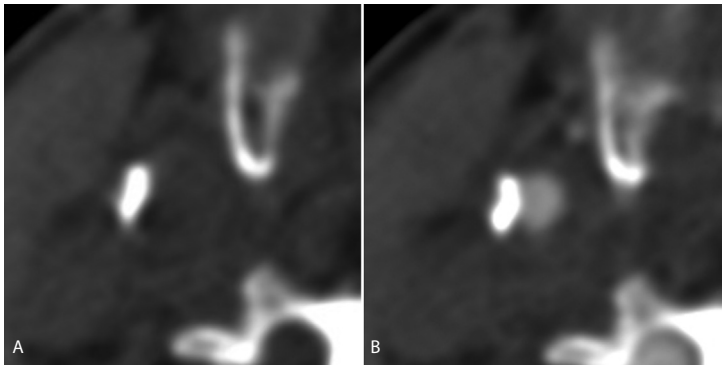

Figure 4. Two MDCT images of an atherosclerotic carotid artery of the same patient at the same level, one without (A) and one with contrast material in the lumen (B). Contrast material in the patent lumen is a prerequisite to visualize the atherosclerotic wall thickening.

and colleagues concluded that it is difficult to identify absolute ranges of attenuation that relate to specific plaque characteristics. They suggested that when plaque density measurements are performed, intraluminal attenuation should be reported, and that a calibration factor should be introduced to address this issue.[19]

ferentiation of lumen from plaque is subsequently higher. Therefore, fixed cut-off points will lead to an underestimation of the size of the atherosclerotic plaque and the severity of stenosis.

Higher densities in the lumen may also influence the density measurements in the atherosclerotic plaque, especially in small arteries. A phantom study in which silicon tubes with two different plaque types (resembling lipid and fibrous tissue) were scanned with different contrast medium concentrations (258 HU, 280 HU and 336 HU) revealed an increase in the measured plaque density with higher contrast medium concentrations.[15] This was explained by the presence of partial volume effects, a problem that might be reduced by further technical improvements in collimation width (e.g. thinner). An ex vivo study in which coronary arteries filled with different contrast material concentrations were scanned, demonstrated that the intraluminal attenuation significantly modifies the attenuation of plaques.[19] Based on this study, Cademartiri

Whether this is also a problem in the evaluation of the carotid atherosclerotic plaque has not yet been explored. Since the size of the plaque in carotid arteries is much larger than in coronary arteries, partial volume effects will only influence the density measurements in plaque near the luminal border. However, another explanation for the increased density in the plaque in the presence of intraluminal contrast, is that the plaque may be enhanced by the entrance of contrast material via the vasa vasorum. In that case plaque evaluation will not be hampered but improved, since perfusion studies may provide additional information on the plaque composition.

Reconstruction algorithms

In CT raw data are collected from multiple directions. In the reconstruction of a CT image from the raw data a so-called convolution-backprojection procedure is used.

Each projection has to be convoluted before backprojection with a mathematical function, the convolution kernel. The choice and design

of the convolution kernel allows to influence image characteristics: i.e. a smooth algorithm will reduce spatial resolution as well as SNR, whereas a sharp algorithm has the opposite effect.[20]

Plaque characterization and quantification of the different plaque components based on measured densities is strongly influenced by the type of convolution kernel used in the reconstruction algorithm. "Smooth" kernels decrease SNR but also lead to less interpretability due to averaging of contrast differences. This is especially important when the density differences between tissues are small, which is the case for lipid and fibrous tissue.[21] "Sharp" kernels increase the contrast differences between these tissues, but they also lead to an increase in calcium size and low intensity rings around calcifications (edge-enhancement artifacts) which hamper interpretation.[21, 22] Therefore, CT images reconstructed with an intermediate kernel will lead to an optimal CT image (Fig. 3).

Window-Level setting

In the CT image, density values are represented as gray scale values. With windowing, the density range of diagnostic relevance is assigned the whole range of discernible gray values. With window-level setting, it is first defined which density (expressed in HU) the central gray scale value is to be assigned to. By setting the window width, it is then defined which densities above and below the central gray value can still be discriminated by varying shades of gray, with black representing tissue of the lowest density and white representing tissue of the highest density. Normally, in evaluation of CTA a large window width (± 500 to1000 HU) is used to differentiate the contrast-filled lumen from the plaque with calcifications. In such images the non-calcified plaque looks rather homogenous. For evaluation of the plaque, smaller windows are more optimal to discern the small differences in densities inside the non-calcified part of

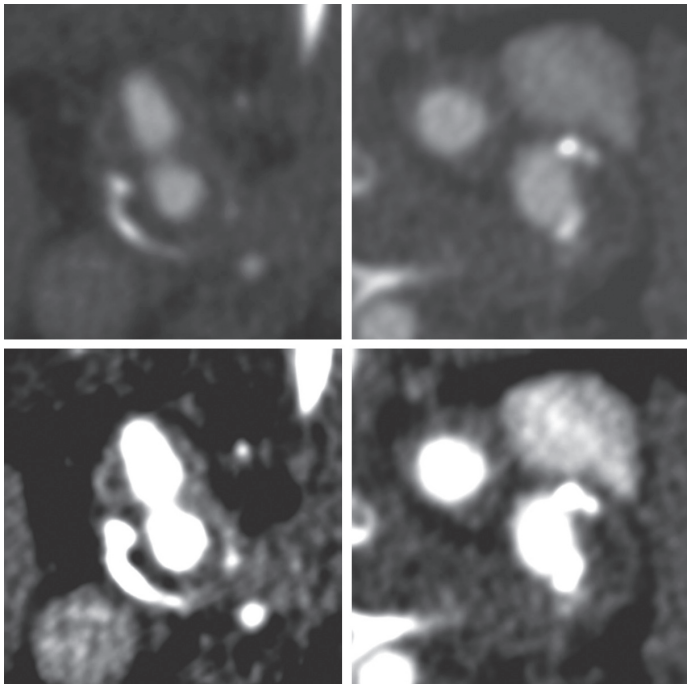

Figure 5. Four MDCT images, two with a large window setting and two with a small window setting. With the large window width setting (500/200) (A, B) the contrast-filled lumen can more easily be differentiated from calcifications. Calcifications appear (often) brighter. However, the non-calcified plaque looks rather homogenous. For evaluation of the plaque smaller window widths (120/50) (C, D) are more optimal to discern the small differences in densities inside the non-calcified part of the plaque.

the plaque (Fig. 5). Drawbacks are the effects on differentiation of contrast-filled lumen and calcification, and the size of the patent lumen and subsequently the size of the plaque.

Scan protocol

Because the plaque density measurements are affected by scanning and image reconstruction parameters it is essential that scanning and reconstruction protocols are standardized. Normally, a carotid plaque imaging protocol is part of a carotid CTA protocol which is used in the workup of patients with a transient ischemic attack or stroke.[23] This protocol requires an injection of 80 cc of contrast material and 40 cc bolus chaser with an injection rate of 4cc/sec. The contrast material is injected using a double-head power injector in an antecubital vein. The CTA scan range reaches from the ascending aorta to the intracranial circulation. Scan direction is craniocaudal to reduce perivenous artifacts.[24] Scan parameters are: number of detector rows 16, individual detector width 0.75 mm, table feed per rotation 12 mm (pitch 1), gantry rotation time 0.37-0.5 sec, kVp 120, effective mAs 180, and scan time 10-14 sec (depending on the individual patient's size and anatomy). Synchronization between the passage of contrast material and data acquisition is achieved by realtime bolus tracking. With this protocol a relatively homogenous luminal attenuation is reached (368 ± 92 HU) with a small density difference between the lumen attenuation at the proximal and distal border of the plaque (5 ± 17 HU). CT images are reconstructed with slice width of 1 mm, reconstruction interval 0.6 mm, field-of-view 120 mm, and intermediate convolution kernel.

Validation

Lumen surface morphology

CTA allows to analyse the surface of the atherosclerotic plaque whereby a differentiation can be made between plaque irregularities and plaque ulceration (Fig. 6). A plaque ulcer is defined as an ulcer niche with extension of contrast material beyond the vascular lumen into the surrounding plaque.[14] The accuracy of DSA in the detection of ulceration, with surgical observations as reference, has been reported to be low (sensitivity 46% and specificity

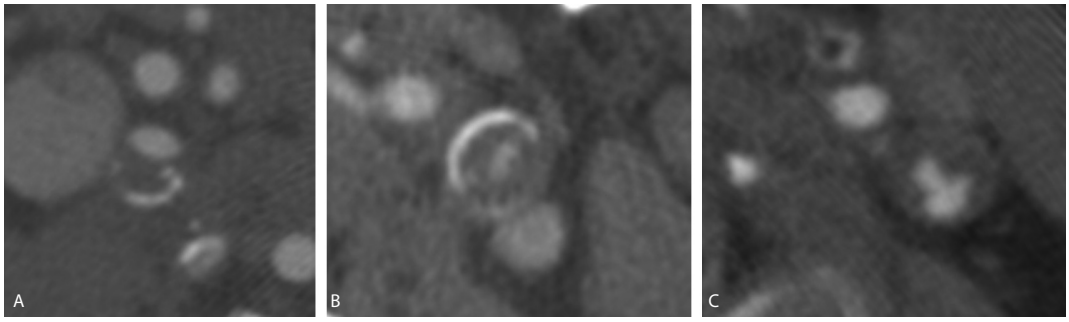

Figure 6. Three MDCT images with atherosclerotic carotid plaque formation. The plaque surface appears smooth (A), irregular (B) or ulcerated (C).

74%).[25] However, with microscopic evaluation of the plaque it became clear that plaque surface morphology assessed on DSA is strongly associated with the presence of plaque rupture, plaque hemorrhage, lipid core size and proportion of fibrous tissue, i.e. features that are all closely related with the concept of a vulnerable plaque.[26]

The first reports on the accuracy of CTA compared with DSA in the assessment of plaque ulcers were disappointing, but this might be explained by the rather thick slice thickness used with single section CT.[13] A later report demonstrated that MS-CTA was superior to DSA in the detection of plaque irregularities and ulcerations.[9] Walker and colleagues evaluated 165 CTA studies, compared them with endarterectomy specimens, and reported a sensitivity of 60% and a specificity of 74%.[14]

Calcifications

The presence of calcifications in atherosclerotic plaques can easily be detected with CT due to the high attenuation of the x-rays by calcium hydroxyapatite which leads to a high density structure in the plaque. Agatston and colleagues were the first to show that coronary calcifications could be detected and quantified with EBCT.[10] Later on this principle of calcium quantification was also used in the carotid arteries.[11, 27] The threshold for calcification is normally set at a density of 130 HU having an area ≥ 1 mm^2. Calcifications can be detected and quantified without the presence of intraluminal contrast media. In the presence of intraluminal contrast media the threshold value has to be higher to differentiate between calcifications and contrast media.[28] The main problem with the Agatson score for coronary calcifications is the substantial measurement variability (up to 30%); the variability for carotid calcifications is not yet known. Calcifications can also be quantified with MSCT using the Agatston score or new alternative scorings methods (volume or mineral mass score). Phantom studies and an ex vivo study with atherosclerotic carotid specimens have shown that the mineral mass score is the most precise and best reproducible scoring method.[16, 28]

Non-calcified plaque components

Because the presence of non-calcified parts of the atherosclerotic plaque is considered to be important for the (in)stability of the plaque much attention has been given to the ability of MSCT to further classify the plaques. Several studies have compared the densities values obtained in different type of plaques (Table 1). The classification scheme normally used for these studies is based on the (modified) criteria set by the American Heart Association Committee on vascular lesions29-31 which is sometimes simplified to predominantly lipid-rich plaques, intermediate (fibrous) plaques, and predominantly calcified plaques. These studies have mainly been performed in coronary arteries.

Because the atherosclerotic plaques in the carotid artery are larger than those in the coronary arteries, it should be possible not only to characterize a whole plaque as lipid-rich, fibrous-rich or calcified, but also to characterize regions within the plaque as predominantly lipid-rich, fibrous-rich or calcified and then to measure the density of that region. The sec-

Table 1. Results of validation studies in carotid/coronary arteries using histology/IVUS as reference.

	Type of artery	Type of study	Number of patients	Histology (reference)		p-value
				Lipid-rich	Fibrous-rich	
Estes[12]	Carotid	in vivo	21	39±12 (n=11)	90±24 (n=15)	<0.001
De Weert[21]	Carotid	ex vivo	15	45 ±21 (n=35)	79±20 (n=28)	<0.001
De Weert	Carotid	in vivo	15	25±19 (n=31)	88±18 (n=53)	<0.001
Becker[33]	Coronary	ex vivo	11	47±9 (n=15)	104±28 (n=16)	<0.01
Schroeder34	Coronary	ex vivo	12	42± 22 (n=6)	71±21 (n=6)	<0.001
Nikolaou17	Coronary	ex vivo	13	47 ±13 (n=10)	87±29 (n=11)	<0.01
				IVUS (reference)		
				Soft (hypoechoic)	Intermediate (hyperechoic)	
Schroeder[36]	Coronary	in vivo	15	14 ±26 (n=12)	91±21 (n=5)	<0.0001
Leber[35]	Coronary	in vivo	58	49±22 (n=62)	91±22 (n=87)	<0.02

(n) = number of measurements
Data, expressed in Hounsfield units (HU), are mean ± SD

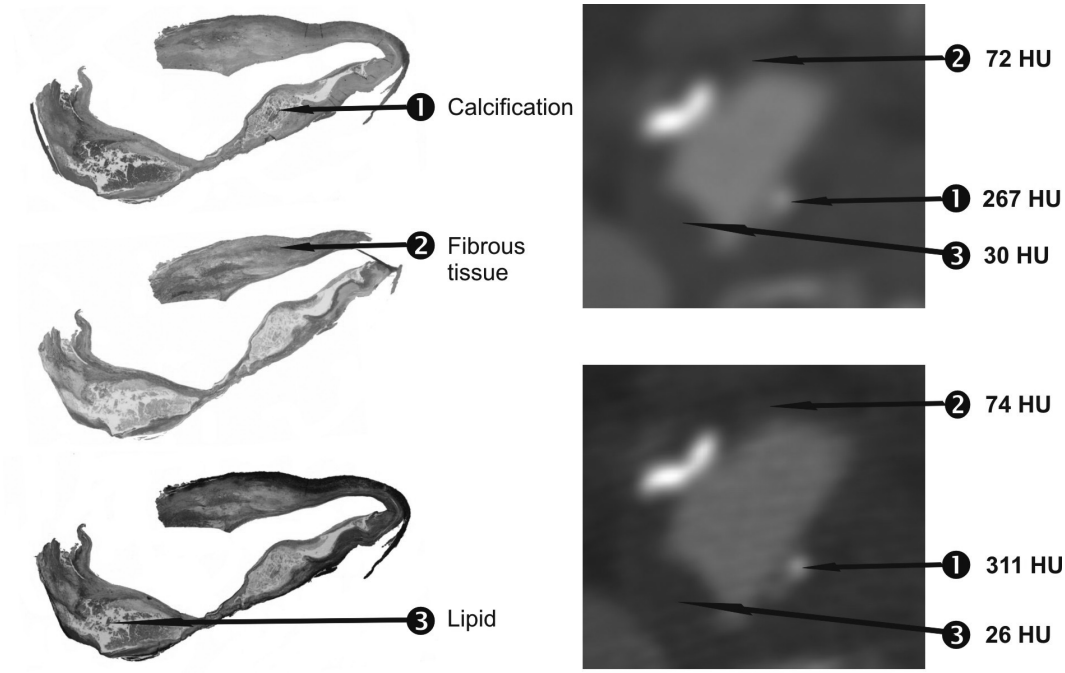

Figure 7. Three differently stained histologic sections (HE = hematoxylin eosin; SR = Sirius Red; EVG = elastic van Gieson) and two corresponding differently reconstructed MDCT images (intermediate smooth, intermediate sharp) of atherosclerotic carotid plaque. The Hounsfield value was measured in the MDCT images in regions with one predominant plaque component on histology.

ond advantage of carotid studies compared with coronary studies is the possibility to perform the MSCT in vivo and to acquire the surgical carotid endarterectomy specimen for histologic correlation, whereas coronary studies in vivo are correlated with intravascular ultrasound (IVUS).

With single slice CT (3-mm slice thickness) it was already possible to differentiate between lipid and fibrous tissue in the carotid atherosclerotic plaque. Density measurements revealed a significant difference for lipid and fibrous tissue (39 ± 13 HU and 90 ±24 HU, respectively).[12]

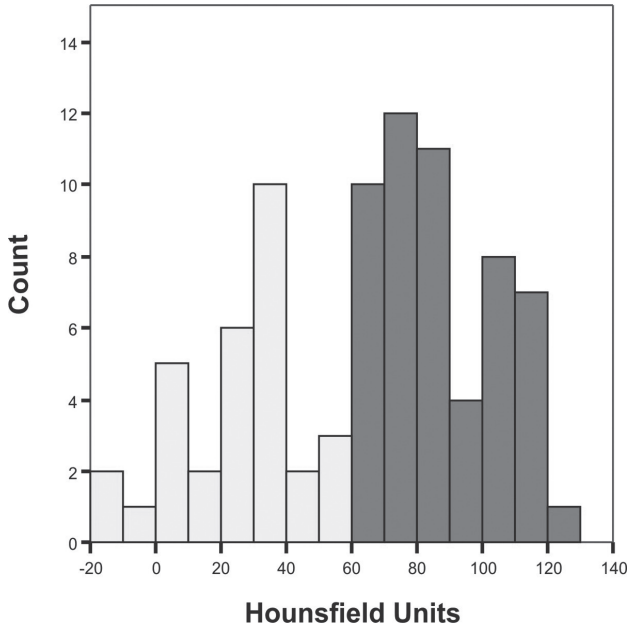

Figure 8. Frequency distribution of measured density values of lipid-rich regions (light bars) and fibrous-rich regions (dark bars) in MDCT images. The most optimal cut-off point to differentiate lipid-rich from fibrous-rich tissue in MDCT images was 60 HU, with 100% sensitivity and specificity.

De Weert and colleagues performed an ex vivo study in which carotid endarterectomy specimens were scanned and the MSCT images were compared with histologic sections (Fig. 7). 21 Lipid-rich and fibrous-rich regions within plaques had significantly different density values (45 ± 21 HU and 79 ± 20 HU, respectively). The histograms revealed a small overlap in the distribution of the lipid and fibrous tissue density measurements (Fig. 8). Based on this distribution a receiver-operating-characteristic curve was created, which revealed 60 HU as the optimal cut-off point to differentiate lipid-rich from fibrous-rich tissue, with a sensitivity and specificity of 89% and 93%, respectively.[21]

Such a validation study was subsequently performed with MSCT images acquired in vivo, and the density values for lipid-rich and fibrous-rich regions in the plaques were 25 ± 19 HU and 88 ± 18 HU, respectively. The distribution of density values of lipid-rich and fibrous-rich regions again showed an optimal cut-off point at 60 HU to differentiate lipid from fibrous tissue, with 100% sensitivity and specificity.[32]

The density values of lipid-rich regions measured in vivo are lower than those measured ex vivo, and some of them reached values below zero (Fig. 9). Prospective analysis of the MSCT images in which all hypodense (<60 HU) regions were detected based on thresholding revealed that the positive predictive value of a hypodense region in the plaque with a density value < 30 HU for a lipid-rich region was 97%, while the positive predictive value of a

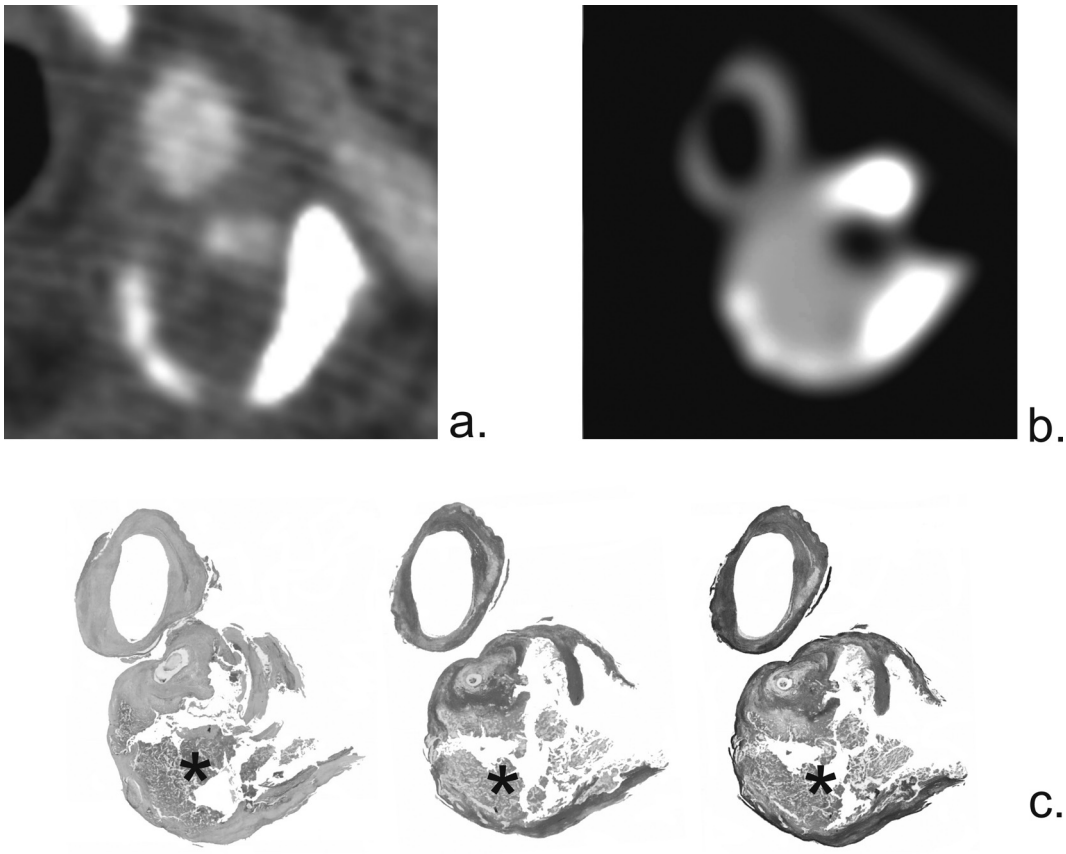

Figure 9. MDCT images of an atherosclerotic plaque obtained in vivo (A) and ex vivo (B). The density value of a lipid-rich region measured in vivo (5 HU) was lower than measured ex vivo (32 HU).

hypodense region with a density value between 30 - 60 HU was 23%.[32]

The results of the carotid validation studies are confirmed by the results of several ex vivo coronary validation studies (Table 1). All these studies showed a significant difference in density values between lipid-rich plaques and fibrous-rich plaques.[17, 33, 34] Other coronary studies used IVUS as a reference and found a significant difference in the density values of soft (hypoechoic) and intermediate (hyperechoic) plaques.[35, 36]

Due to the relatively small size of the atherosclerotic plaques in coronary arteries, plaques have to be characterized by their predominant tissue which ignores the fact that atherosclerotic disease is often very heterogenic and that a solitary plaque might contain areas with different morphology. Furthermore, some studies revealed a considerable overlap in density values of lipid-rich and fibrous-rich plaques, which decreases the accuracy of MSCT in coronary plaque analysis.[15, 35]

Quantification

Plaque volume quantification

The cross-sectional nature of CT allows the measurement of both luminal and vessel area. Plaque area is calculated by subtracting luminal area from vessel area. Plaque volumes are calculated by multiplying plaque area and slice increment. Outlining the luminal area can be performed by (semi-)automated measures based on a threshold to separate lumen from plaque. Calcifications (which also have a high density) nearby the lumen may be included in the lumen but then and manual correction should be performed. The vessel area is currently drawn manually because the carotid vessel is not surrounded circumferentially by a tissue with a homogenous lower or higher density to allow a threshold based semi-automated technique to outline this boundary. Semi-automated measurements are influenced by the thresholds, which should vary depending on the density of the intraluminal contrast. The main problem with manually-assessed contours is the influence of window-level setting on the visualization of

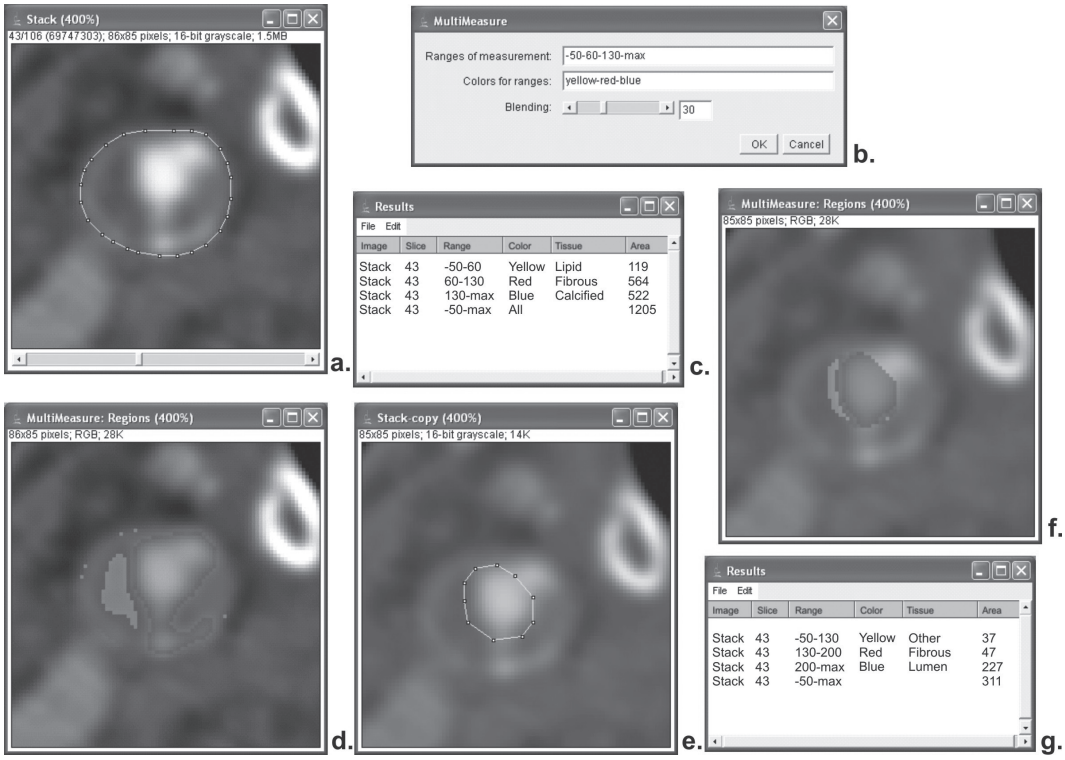

Figure 10. Semi-automatic assessment of plaque component areas in MDCT images. This software allows an observer to draw a region of interest (ROI) (=vessel outline) (A). After the input of specific ranges of Hounsfield values (HV) (B), which should represent specific plaque components, it assesses the amount of pixels within each range of HV (C). Each range of HV is given a different color and an MDCT-based plaque morphology image is produced (D). To differentiate lumen from the atherosclerotic plaque and from calcified tissue, a second ROI is drawn (E). A second morphology image is produced (F), and the number of lumen pixels are calculated (G). The exact number of fibrous and calcified pixels can now be determined. Fibrous = fibrous measurement-1 (60 to 130 HU) plus fibrous measurement-2 (130 to 200 HU); calcified = calcified measurement-1 (>130 HU) minus lumen measurement-2 (>200 HU) minus fibrous measurement-2 (130-200 HU). (A full color version of this illustration can be found in the color section)

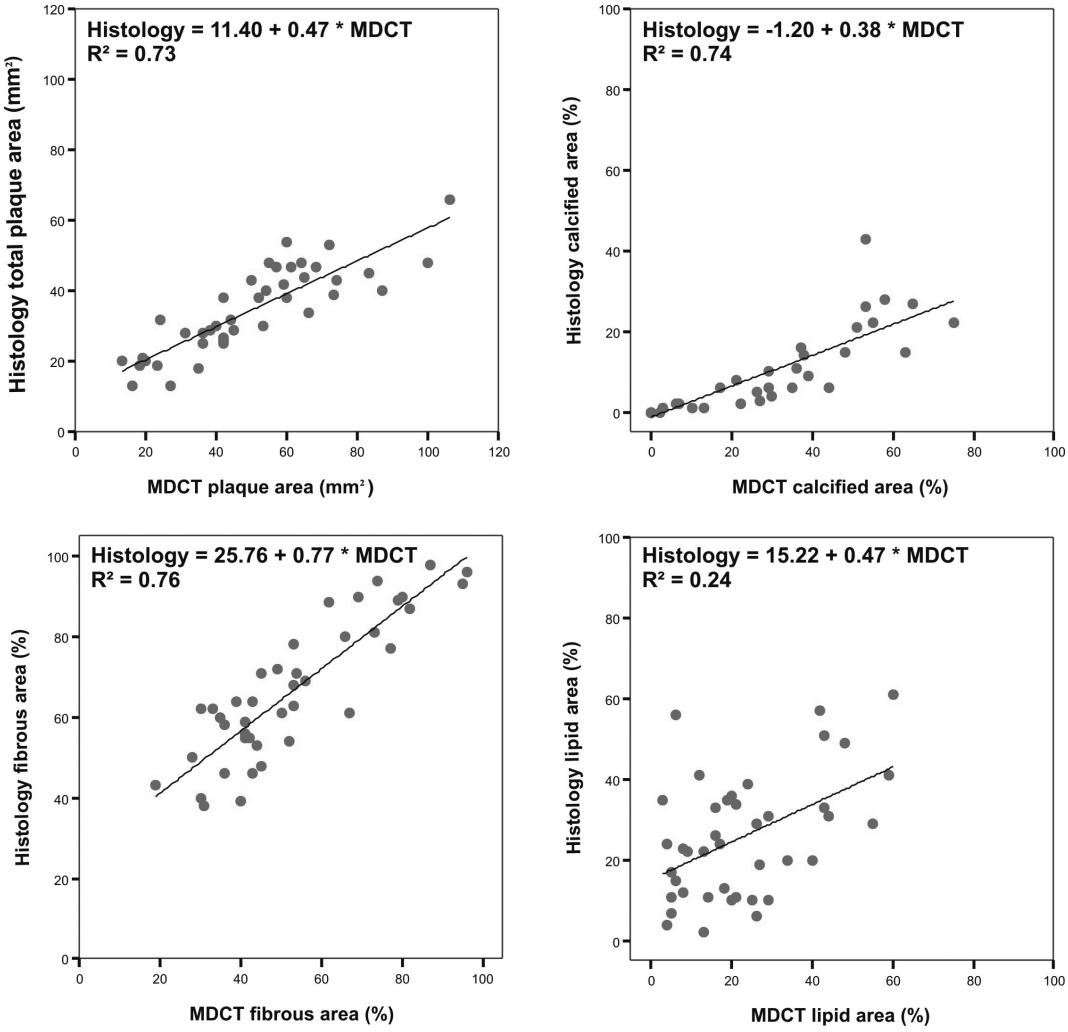

Figure 11. Linear regression analysis of plaque area and plaque component areas in MDCT images and histologic sections.

the boundaries between lumen and plaque, and between vessel wall and surrounding tissues. Validation of plaque area measurements with histology are hampered by the effect of histologic preparation on the tissue dimensions. Shrinkage of 20-25% of the plaque area is normally encountered during fixation. An ex vivo and a subsequent in vivo study on carotid atherosclerotic plaques revealed a strong correlation between MSCT and histology for the assessment of plaque area (r^2 = 0.81 and 0.73, respectively).[21,32] In addition, the interobserver variability of plaque area measurements with MSCT was very low with a coefficient of variation of 10%.[32]

Two coronary in vivo studies compared the plaque volume assessed with MSCT and IVUS.

One study found a strong correlation (r = 0.8) and an underestimation of the coronary plaque volume assessed with MSCT compared to IVUS.[37] The other study found a moderate correlation (r = 0.55) and an overestimation of coronary plaque area assessed with MSCT compared to IVUS.[38]

Plaque component quantification

The difference in density values between the major plaque components (lipid tissue, fibrous tissue and calcifications) is of great interest because this allows the plaque components to be quantified (Fig.10). An in vivo validation study, in which MSCT images of carotid arteries were compared with histologic sections from the endarterectomy specimens, compared the areas of the major plaque components (Fig. 11). As expected, MSCT overestimated the size of the calcifications but the correlation was good. In addition, the correlation for fibrous tissue was good, but was poor for lipid (r^2 = 0.74 and 0.24, respectively). An exploratory analysis revealed that the correlation between lipid areas on histologic sections and in MSCT images improved with a decreasing amount of calcifications in the plaque (r^2 is 0.81 for non-calcified plaques).[32] Therefore, MSCT is capable of quantifying calcifications and fibrous tissue in atherosclerotic carotid plaque in good correlation with histology, and lipid can be adequately quantified in mildly calcified plaques.

The interobserver variability of area measurements of the different plaque components was low, with a coefficient of variation of 8%, 11% and 20% for calcified regions, fibrous regions and lipid regions, respectively.[32]

Clinical applications

Risk prediction

The severity of stenosis in the carotid artery is a well-known predictor of cerebral infarction and is currently used as the main parameter in deciding whether the patient is advised to undergo carotid endarterectomy or stent placement. Plaque morphology is considered an additional independent predictor of cerebral infarction: plaques consisting of a necrotic lipid core covered by a thin fibrous cap (the unstable or vulnerable plaque) are prone to rupture[39-41], leading to thrombo-embolic release of particles to the brain. CT of the plaque in the carotid bifurcation may provide clinicians with these additional independent predictors of (recurrent) stroke which may in the future compete with the severity of stenosis in treatment decisions.

Whether the presence of certain plaque features is a good reason for surgical intervention has to be demonstrated in larger prospective studies, which will determine the significance of CT-assessed plaque features for stroke risk. Such studies will prove whether the concept of vulnerable plaque is applicable to carotid atherosclerosis. Even then, a randomised controlled trial will have to be performed to prove that surgical intervention is beneficial in patients with CT-assessed vulnerable plaques in the carotid artery. Which CT-assessed plaque features will be candidates for an improved risk assessment? To this end, a large prospective study is being conducted in which 800 patients with cerebrovascular symptoms undergo a CTA of the carotid arteries, and CT-derived parameters of the plaque

will be related to future cerebrovascular events.

Lumen surface morphology

Several DSA studies have demonstrated that plaque ulcerations of a symptomatic carotid stenosis is a strong independent predictor of stroke.[42, 43] Angiographic ulceration is associated with plaque rupture, intraplaque hemorrhage, a large lipid core and less fibrous tissue, all features of unstable vulnerable plaques.[26] MSCT can assess luminal surface morphology with the same or better accuracy than DSA.

Lipid

Pathological studies have demonstrated that plaques with a high lipid volume are prone to rupture; additionally, the lipid content is highly thrombogenic after disruption.[44, 45] Other studies have shown no significant difference in plaque morphology, with respect to lipid, between symptomatic and asymptomatic plaques. Duplex ultrasonography studies confirmed the hypothesis about the risk of lipid, by demonstrating that echolucent plaques which are supposed to correspond with lipid-rich plaques are associated with a higher risk for future ischemic cerebrovascular events.[46] These studies failed, however, in quantifying lipid or other plaque components. The important role of lipid is also strengthened by the success of lipid-lowering therapy in preventing acute atherosclerotic-related events. This success could be explained by the reduction of the lipid content of vulnerable plaques.[47]

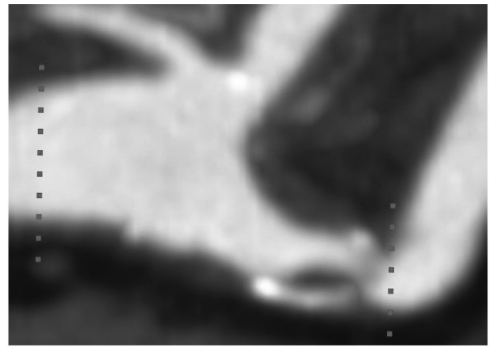

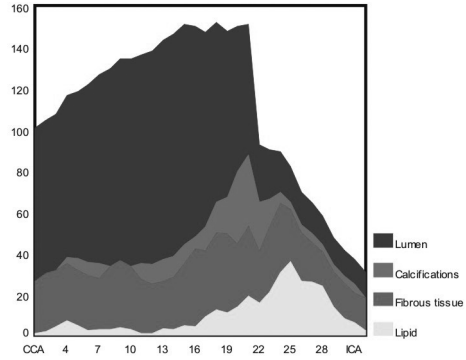

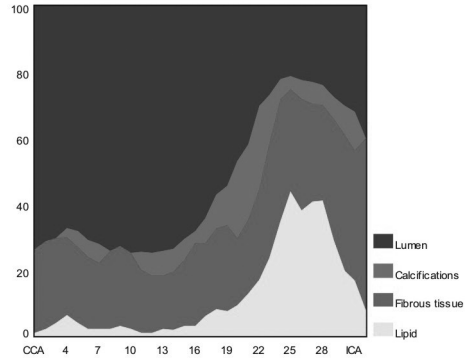

Tissue	mm²	%	%
Lumen	2062	51	
Calcified	257	8	9
Fibrous	860	28	60
Lipid	328	14	31

Figure 12. Sagittal MDCT image of the carotid bifurcation with an atheroscleric plaque (A). Absolute (B) and relative (C) area measurements of lumen, fibrous tissue, lipid tissue and calcifications in consecutive MDCT images. The x-axis represent the numbers of consecutive MDCT images. Volume measurements of the different plaque components (D).

Calcifications

Coronary calcification is an independent predictor of coronary heart disease and stroke.[48], 49 Measures of carotid atherosclerosis, like intima-media thickness measured with b-mode ultrasound, are independent predictors of stroke.[50] Whether carotid calcification assessed with MSCT is an independent predictor of stroke is currently under investigation in a large population-based study which includes over 2,500 subjects. Calcifications are one of the components of the atherosclerotic plaque and are related to the amount of plaque. Nevertheless, atherosclerotic plaque may almost totally consist of non-calcified components and these plaques are missed on non-contrast CT scans.

With CTA the total amount of plaque can be assessed and, subsequently, the relative contribution of calcium to the plaque. The calcified plaque area percentage in carotid atherosclerosis assessed with CT is two-fold greater in asymptomatic versus symptomatic plaques.[51] This was not confirmed in a study in which microscopic plaque morphology from symptomatic and asymptomatic patients was compared.[52] Another CT study demonstrated that calcified plaques (defined as plaques with a median density greater than 130 HU) were 21 times less likely to be symptomatic than non-calcified plaques.[53] In other words, the relative amount of non-calcified plaque components may be related to an increased risk of being symptomatic.

Plaque volume

In the early phase of atherosclerosis preservation of a patent lumen is achieved by outward remodelling of the vessel wall. Therefore, significant atherosclerotic plaque is already present before moderate to severe luminal compromise is detected on DSA.

Since CT enables the visualization of the atherosclerotic plaque and the process of vascular remodeling, it can detect changes in atherosclerotic plaque volume which would have stayed unrecognized by luminal measurements only. The question arises whether the amount of plaque will be a better predictor of neurologic events than the severity of stenosis.

Natural history of atherosclerosis and pharmacological intervention

From manual or semi-automated measurements of plaque area in consecutive CT images in which vessel thickening is present, it is possible to calculate the plaque volume and relative contribution of each plaque component (Fig. 12). In addition, the spatial distribution of the plaque components can be depicted. These measures can be used in follow-up studies in which disease progression is evaluated. Moreover, they can be used as surrogate endpoints in clinical studies in which the effect of pharmacological intervention is studied.

References

1. Caplan LR. Diagnosis and treatment of ischemic stroke. Jama. 1991;266:2413-2418
2. Beneficial effect of carotid endarterectomy in symptomatic patients with high-grade carotid stenosis. North american symptomatic carotid endarterectomy trial collaborators. N Engl J Med. 1991;325:445-453
3. Randomised trial of endarterectomy for recently symptomatic carotid stenosis: Final results of the mrc european carotid surgery trial (ecst). Lancet. 1998;351:1379-1387
4. Naghavi M, Libby P, Falk E, Casscells SW, Litovsky S, Rumberger J, Badimon JJ, Stefanadis C, Moreno P, Pasterkamp G, Fayad Z, Stone PH, Waxman S, Raggi P, Madjid M, Zarrabi A, Burke A, Yuan C, Fitzgerald PJ, Siscovick DS, de Korte CL, Aikawa M, Juhani Airaksinen KE, Assmann G, Becker CR, Chesebro JH, Farb A, Galis ZS, Jackson C, Jang IK, Koenig W, Lodder RA, March K, Demirovic J, Navab M, Priori SG, Rekhter MD, Bahr R, Grundy SM, Mehran R, Colombo A, Boerwinkle E, Ballantyne C, Insull W, Jr., Schwartz RS, Vogel R, Serruys PW, Hansson GK, Faxon DP, Kaul S, Drexler H, Greenland P, Muller JE, Virmani R, Ridker PM, Zipes DP, Shah PK, Willerson JT. From vulnerable plaque to vulnerable patient: A call for new definitions and risk assessment strategies: Part i. Circulation. 2003;108:1664-1672
5. Koelemay MJ, Nederkoorn PJ, Reitsma JB, Majoie CB. Systematic review of computed tomographic angiography for assessment of carotid artery disease. Stroke. 2004;35:2306-2312
6. Heinz ER, Pizer SM, Fuchs H, Fram EK, Burger P, Drayer BP, Osborne DR. Examination of the extracranial carotid bifurcation by thin-section dynamic ct: Direct visualization of intimal atheroma in man (part 1). AJNR Am J Neuroradiol. 1984;5:355-359
7. Cumming MJ, Morrow IM. Carotid artery stenosis: A prospective comparison of ct angiography and conventional angiography. AJR Am J Roentgenol. 1994;163:517-523
8. Link J, Brossmann J, Grabener M, Mueller-Huelsbeck S, Steffens JC, Brinkmann G, Heller M. Spiral ct angiography and selective digital subtraction angiography of internal carotid artery stenosis. AJNR Am J Neuroradiol. 1996;17:89-94
9. Randoux B, Marro B, Koskas F, Duyme M, Sahel M, Zouaoui A, Marsault C. Carotid artery stenosis: Prospective comparison of ct, three-dimensional gadolinium-enhanced mr, and conventional angiography. Radiology. 2001;220:179-185
10. Agatston AS, Janowitz WR, Hildner FJ, Zusmer NR, Viamonte M, Jr., Detrano R. Quantification of coronary artery calcium using ultrafast computed tomography. J Am Coll Cardiol. 1990;15:827-832
11. Arad Y, Spadaro LA, Roth M, Scordo J, Goodman K, Sherman S, Lledo A, Lerner G, Guerci AD. Correlations between vascular calcification and atherosclerosis: A comparative electron beam ct study of the coronary and carotid arteries. J Comput Assist Tomogr. 1998;22:207-211

12. Estes JM, Quist WC, Lo Gerfo FW, Costello P. Noninvasive characterization of plaque morphology using helical computed tomography. J Cardiovasc Surg (Torino). 1998;39:527-534
13. Oliver TB, Lammie GA, Wright AR, Wardlaw J, Patel SG, Peek R, Ruckley CV, Collie DA. Atherosclerotic plaque at the carotid bifurcation: Ct angiographic appearance with histopathologic correlation. AJNR Am J Neuroradiol. 1999;20:897-901
14. Walker LJ, Ismail A, McMeekin W, Lambert D, Mendelow AD, Birchall D. Computed tomography angiography for the evaluation of carotid atherosclerotic plaque: Correlation with histopathology of endarterectomy specimens. Stroke. 2002;33:977-981
15. Schroeder S, Flohr T, Kopp AF, Meisner C, Kuettner A, Herdeg C, Baumbach A, Ohnesorge B. Accuracy of density measurements within plaques located in artificial coronary arteries by x-ray multislice ct: Results of a phantom study. J Comput Assist Tomogr. 2001;25:900-906
16. Hoffmann U, Kwait DC, Handwerker J, Chan R, Lamuraglia G, Brady TJ. Vascular calcification in ex vivo carotid specimens: Precision and accuracy of measurements with multi-detector row ct. Radiology. 2003;229:375-381
17. Nikolaou K, Becker CR, Muders M, Babaryka G, Scheidler J, Flohr T, Loehrs U, Reiser MF, Fayad ZA. Multidetector-row computed tomography and magnetic resonance imaging of atherosclerotic lesions in human ex vivo coronary arteries. Atherosclerosis. 2004;174:243-252
18. Cademartiri F, van der Lugt A, Luccichenti G, Pavone P, Krestin GP. Parameters affecting bolus geometry in cta: A review. J Comput Assist Tomogr. 2002;26:598-607
19. Cademartiri F, Mollet NR, Runza G, Bruining N, Hamers R, Somers P, Knaapen M, Verheye S, Midiri M, Krestin GP, de Feyter PJ. Influence of intracoronary attenuation on coronary plaque measurements using multislice computed tomography: Observations in an ex vivo model of coronary computed tomography angiography. Eur Radiol. 2005;15:1426-1431
20. Kalender WA. Computed tomography: Fundementals, system technology, image quality, applications. Publicis MCD Verlag. 2000
21. de Weert TT, Ouhlous M, Zondervan PE, Hendriks JM, Dippel DW, van Sambeek MR, van der Lugt A. In vitro characterization of atherosclerotic carotid plaque with multidetector computed tomography and histopathological correlation. Eur Radiol. 2005;15:1906-1914
22. Cademartiri F, Runza G, Mollet NR, Luccichenti G, Belgrano M, Somers P, Knaapen M, Verheye S, Bruining N, Hamers R, Midiri M, De Feyter PJ, Krestin GP. Influence of increasing convolution kernel filtering on plaque imaging with multislice ct using an ex-vivo model of coronary angiography influenza dei filtri di convoluzione sulla misurazione dei valori di attenuazione della placca durante angiografia coronarica mediante tc multistrato. Radiol Med (Torino). 2005;110:234-240
23. de Monye C, Cademartiri F, de Weert TT, Siepman DA, Dippel DW, van Der Lugt A. Sixteen-detector row ct angiography of carotid arteries: Comparison of different volumes of contrast material with and without a bolus chaser. Radiology. 2005;237:555-562

24. de Monye C, de Weert TT, Zaalberg W, Cademartiri F, Siepman DA, Dippel DW, van Der Lugt A. Optimization of ct angiography of the carotid artery with a 16-multidetector-row ct scanner: Craniocaudal scan direction reduces contrast material-related perivenous artifacts. AJR Am J Roentgenol. accepted
25. Streifler JY, Eliasziw M, Fox AJ, Benavente OR, Hachinski VC, Ferguson GG, Barnett HJ. Angiographic detection of carotid plaque ulceration. Comparison with surgical observations in a multicenter study. North american symptomatic carotid endarterectomy trial. Stroke. 1994;25:1130-1132
26. Lovett JK, Gallagher PJ, Hands LJ, Walton J, Rothwell PM. Histological correlates of carotid plaque surface morphology on lumen contrast imaging. Circulation. 2004;110:2190-2197
27. Allison MA, Criqui MH, Wright CM. Patterns and risk factors for systemic calcified atherosclerosis. Arterioscler Thromb Vasc Biol. 2004;24:331-336
28. Hong C, Bae KT, Pilgram TK. Coronary artery calcium: Accuracy and reproducibility of measurements with multi-detector row ct--assessment of effects of different thresholds and quantification methods. Radiology. 2003;227:795-801
29. Stary HC, Chandler AB, Glagov S, Guyton JR, Insull W, Jr., Rosenfeld ME, Schaffer SA, Schwartz CJ, Wagner WD, Wissler RW. A definition of initial, fatty streak, and intermediate lesions of atherosclerosis. A report from the committee on vascular lesions of the council on arteriosclerosis, american heart association. Circulation. 1994;89:2462-2478
30. Stary HC, Chandler AB, Dinsmore RE, Fuster V, Glagov S, Insull W, Jr., Rosenfeld ME, Schwartz CJ, Wagner WD, Wissler RW. A definition of advanced types of atherosclerotic lesions and a histological classification of atherosclerosis. A report from the committee on vascular lesions of the council on arteriosclerosis, american heart association. Circulation. 1995;92:1355-1374
31. Stary HC. Natural history and histological classification of atherosclerotic lesions: An update. Arterioscler Thromb Vasc Biol. 2000;20:1177-1178
32. de Weert TT, Ouhlous M, Meijering E, Zondervan PE, Hendriks JM, van Sambeek MR, Dippel DW, van der Lugt A. In vivo characterization and quantification of atherosclerotic carotid plaque components with multidetector computed tomography and histopathological correlation. submitted
33. Becker CR, Nikolaou K, Muders M, Babaryka G, Crispin A, Schoepf UJ, Loehrs U, Reiser MF. Ex vivo coronary atherosclerotic plaque characterization with multi-detector-row ct. Eur Radiol. 2003;13:2094-2098
34. Schroeder S, Kuettner A, Leitritz M, Janzen J, Kopp AF, Herdeg C, Heuschmid M, Burgstahler C, Baumbach A, Wehrmann M, Claussen CD. Reliability of differentiating human coronary plaque morphology using contrast-enhanced multislice spiral computed tomography: A comparison with histology. J Comput Assist Tomogr. 2004;28:449-454

35. Leber AW, Knez A, Becker A, Becker C, von Ziegler F, Nikolaou K, Rist C, Reiser M, White C, Steinbeck G, Boekstegers P. Accuracy of multidetector spiral computed tomography in identifying and differentiating the composition of coronary atherosclerotic plaques: A comparative study with intracoronary ultrasound. J Am Coll Cardiol. 2004;43:1241-1247
36. Schroeder S, Kopp AF, Baumbach A, Meisner C, Kuettner A, Georg C, Ohnesorge B, Herdeg C, Claussen CD, Karsch KR. Noninvasive detection and evaluation of atherosclerotic coronary plaques with multislice computed tomography. J Am Coll Cardiol. 2001;37:1430-1435
37. Achenbach S, Moselewski F, Ropers D, Ferencik M, Hoffmann U, MacNeill B, Pohle K, Baum U, Anders K, Jang IK, Daniel WG, Brady TJ. Detection of calcified and noncalcified coronary atherosclerotic plaque by contrast-enhanced, submillimeter multidetector spiral computed tomography: A segment-based comparison with intravascular ultrasound. Circulation. 2004;109:14-17
38. Moselewski F, Ropers D, Pohle K, Hoffmann U, Ferencik M, Chan RC, Cury RC, Abbara S, Jang IK, Brady TJ, Daniel WG, Achenbach S. Comparison of measurement of cross-sectional coronary atherosclerotic plaque and vessel areas by 16-slice multidetector computed tomography versus intravascular ultrasound. Am J Cardiol. 2004;94:1294-1297
39. Fuster V, Badimon L, Badimon JJ, Chesebro JH. The pathogenesis of coronary artery disease and the acute coronary syndromes (1). N Engl J Med. 1992;326:242-250
40. Fuster V, Badimon L, Badimon JJ, Chesebro JH. The pathogenesis of coronary artery disease and the acute coronary syndromes (2). N Engl J Med. 1992;326:310-318
41. Virmani R, Burke AP, Farb A, Kolodgie FD. Pathology of the unstable plaque. Prog Cardiovasc Dis. 2002;44:349-356
42. Eliasziw M, Streifler JY, Fox AJ, Hachinski VC, Ferguson GG, Barnett HJ. Significance of plaque ulceration in symptomatic patients with high-grade carotid stenosis. North american symptomatic carotid endarterectomy trial. Stroke. 1994;25:304-308
43. Rothwell PM, Gibson R, Warlow CP. Interrelation between plaque surface morphology and degree of stenosis on carotid angiograms and the risk of ischemic stroke in patients with symptomatic carotid stenosis. On behalf of the european carotid surgery trialists' collaborative group. Stroke. 2000;31:615-621
44. Davies MJ, Woolf N, Rowles P, Richardson PD. Lipid and cellular constituents of unstable human aortic plaques. Basic Res Cardiol. 1994;89 Suppl 1:33-39
45. Seeger JM, Barratt E, Lawson GA, Klingman N. The relationship between carotid plaque composition, plaque morphology, and neurologic symptoms. J Surg Res. 1995;58:330-336
46. Polak JF, Shemanski L, O'Leary DH, Lefkowitz D, Price TR, Savage PJ, Brant WE, Reid C. Hypoechoic plaque at us of the carotid artery: An independent risk factor for incident stroke in adults aged 65 years or older. Cardiovascular health study. Radiology. 1998;208:649-654

47. Zhao XQ, Yuan C, Hatsukami TS, Frechette EH, Kang XJ, Maravilla KR, Brown BG. Effects of prolonged intensive lipid-lowering therapy on the characteristics of carotid atherosclerotic plaques in vivo by mri: A case-control study. Arterioscler Thromb Vasc Biol. 2001;21:1623-1629
48. Vliegenthart R, Oudkerk M, Hofman A, Oei HH, van Dijck W, van Rooij FJ, Witteman JC. Coronary calcification improves cardiovascular risk prediction in the elderly. Circulation. 2005;112:572-577
49. Vliegenthart R, Hollander M, Breteler MM, van der Kuip DA, Hofman A, Oudkerk M, Witteman JC. Stroke is associated with coronary calcification as detected by electron-beam ct: The rotterdam coronary calcification study. Stroke. 2002;33:462-465
50. Hollander M, Bots ML, Del Sol AI, Koudstaal PJ, Witteman JC, Grobbee DE, Hofman A, Breteler MM. Carotid plaques increase the risk of stroke and subtypes of cerebral infarction in asymptomatic elderly: The rotterdam study. Circulation. 2002;105:2872-2877
51. Shaalan WE, Cheng H, Gewertz B, McKinsey JF, Schwartz LB, Katz D, Cao D, Desai T, Glagov S, Bassiouny HS. Degree of carotid plaque calcification in relation to symptomatic outcome and plaque inflammation. J Vasc Surg. 2004;40:262-269
52. Fisher M, Paganini-Hill A, Martin A, Cosgrove M, Toole JF, Barnett HJ, Norris J. Carotid plaque pathology: Thrombosis, ulceration, and stroke pathogenesis. Stroke. 2005;36:253-257
53. Nandalur KR, Baskurt E, Hagspiel KD, Phillips CD, Kramer CM. Calcified carotid atherosclerotic plaque is associated less with ischemic symptoms than is noncalcified plaque on mdct. AJR Am J Roentgenol. 2005;184:295-298

PART 3

Clinical Studies

7 INTRACRANIAL INTERNAL CAROTID ARTERY CALCIFICATIONS: ASSOCIATION WITH VASCULAR RISK FACTORS AND ISCHEMIC CEREBROVASCULAR DISEASE

Thomas T de Weert • Hamit Cakir • Sietske Rozie • Sander Cretier • Erik Meijering • Diederik WJ Dippel • Aad van der Lugt

American Journal of Neuroradiology 2008; Oct 8 [Epub ahead of print]

Intracranial internal carotid artery calcifications: Association with vascular risk factors and ischemic cerebrovascular disease

Abstract

Objective

We assessed the association between intracranial internal carotid artery calcifications and cardiovascular risk factors in patients with ischemic cerebrovascular disease, and the association between calcifications and the presence of ischemic cerebrovascular disease.

Materials and Methods

Patients undergoing MDCT angiography of the carotid arteries for assessment of stenosis degree were included in the study. A semi-automatic custom-made system to quantify calcifications was developed. The associations between the volume of calcifications and cardiovascular risk factors and type of ischemic cerebrovascular symptomatology were assessed with logistic regression.

Results

MDCT angiography was performed in 406 patients (age 62±14 years; 242 men). Men had a significantly higher calcification volume (66mm^3) than women (33mm^3). Calcification volume was positively associated with age in both men and women. Smoking, hypercholesterolemia and history of cardiac disease were independently related to the presence of calcifications. History of cardiac disease and ischemic cerebrovascular disease were independently related to the volume of calcification. No association was found between calcifications and the presence or type of ischemic cerebrovascular disease in the vascular territory of the intracranial internal carotid artery.

Conclusions

Calcifications were associated with higher age and male gender. The presence and volume of calcifications were independently associated with cardiovascular risk factors. Calcifications were not related to presence or type of ischemic cerebrovascular disease.

Introduction

Coronary artery calcification, visualized with electron beam or multidetector computed tomography (MDCT) and assessed with the Agatston score, has been the most frequently imaged atherosclerotic plaque feature. Coronary artery calcification reflects the total plaque burden[1], is associated with cardiovascular risk factors[2-5], and is an independent risk factor for future ischemic cardiac and cerebral events[2,6,7]. Although atherosclerotic calcifications in the intracranial internal carotid arteries are very frequent, their association with cardiovascular risk factors and their predictive value for ischemic cerebrovascular events has not been studied extensively.

The Agatston score is calculated as the product of the area of a calcified lesion, defined as the number of voxels with an attenuation value ≥130 Hounsfield units (HU), and the size of one voxel, and a factor assigned according to the maximum attenuation value of the lesion[2]. This score can be calculated semi-automatically when the atherosclerotic calcifications are surrounded by soft tissue, as in the coronary arteries and at the carotid bifurcation. However, the Agatston score cannot be applied semi-automatically to calcifications in the intracranial internal carotid artery, because the close relationship between calcifications in the arterial wall and the bony structures of the skull base prohibits an easy segmentation of the calcifications based on HU. Consequently, previous studies made use of a qualitative grading system[8-12]. Although Taoka et al. have used commercially available software to assess the Agatston score of intracranial calcifications, they had to eliminate the contamination of bone density on wide-windowed CT images[13]. We developed custom-made software for quantification of intracranial calcifications.

The purpose of this study was to evaluate the reproducibility of a semi-automatic system for quantification of intracranial internal carotid artery calcifications, to assess the association between these calcifications and cardiovascular risk factors in patients with ischemic cerebrovascular disease, and to assess the association between calcifications and the presence and type of ischemic cerebrovascular disease.

Materials and Methods

Study population

Consecutive patients from the neurology department's rapid TIA service and stroke unit, with ischemic cerebrovascular symptoms, underwent a full neurological examination and recording of their medical history. Patients that were selected for MDCT angiography (MDCTA) of the carotid arteries for assessment of possible carotid artery stenosis were included in this study. Normally, all patients got a MDCTA, except those with a major stroke as judged by the treating physician, because they lack a clinical indication for extensive evaluation of the carotid arteries. All scanning was part of a research protocol that was approved by the Institutional Review Board and for which patients had given written informed consent.

Scanning and image reconstruction

Scanning was performed on a 16-slice MDCT scanner (Siemens, Sensation 16, Erlangen, Germany) with a standardized optimized contrast-enhanced protocol (120 kVp, 180 mAs, collimation 16 x 0.75 mm, table feed 12 mm/rotation, pitch 1)[14]. The MDCTA scan range reached from the ascending aorta to the intracranial circulation (2 cm above the sella turcica). All patients received 80 ml contrast material (Iodixanol 320 mg/ml, Visipaque, Amersham Health, Little Chalfont, UK), followed by 40 ml saline bolus chaser, both with an injection rate of 4 ml/sec. Synchronization between the passage of contrast material and data acquisition was achieved by real time bolus tracking at the level of the ascending aorta.

Image reconstructions were made with field of view 100 mm, matrix size 512 x 512 (real in-plane resolution 0.6 x 0.6 mm), slice thickness 1.0 mm, increment 0.6 mm and with an intermediate reconstruction algorithm[15].

Analysis of intracranial internal carotid artery calcifications

A trained reader (H.C.), who was blinded to the clinical data of the patients, performed the quantification of the calcifications in both intracranial internal carotid arteries. A second trained reader (T.T.d.W.) evaluated independently 100 patients to assess interobserver variability. The intracranial internal carotid artery comprised the horizontal segment of the petrous internal carotid artery to the top of the internal carotid artery (Figure 1).

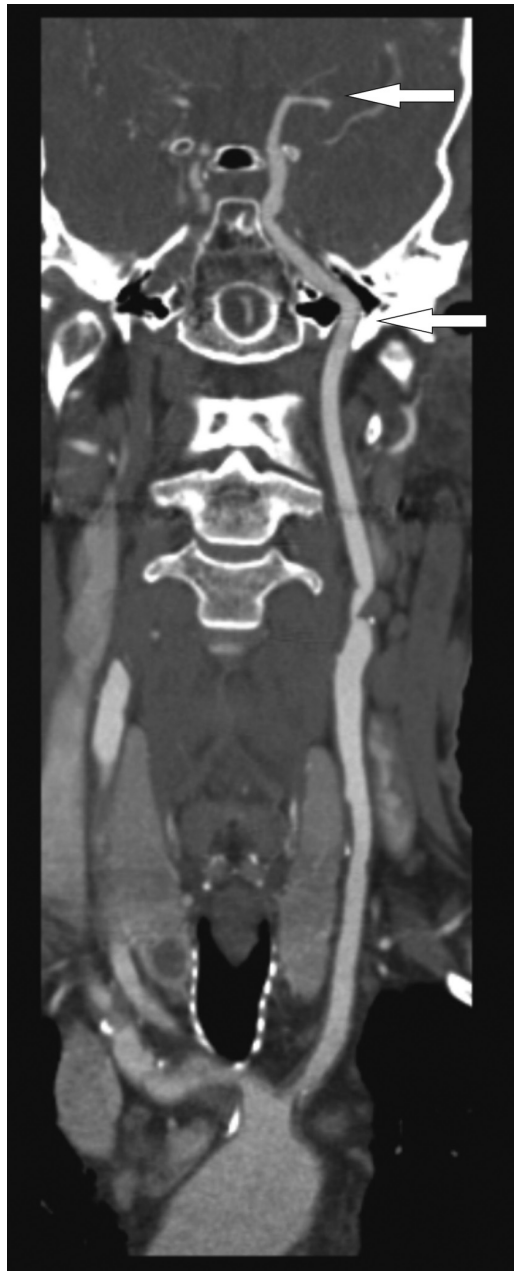

Figure 1. A curved planar reformat image from the aortic arch up to the top of the internal carotid artery. The arrows indicate the part of the internal carotid artery at which calcifications were segmented on axial slices. This part comprises the horizontal segment of the petrous internal carotid artery, to the top of the carotid artery.

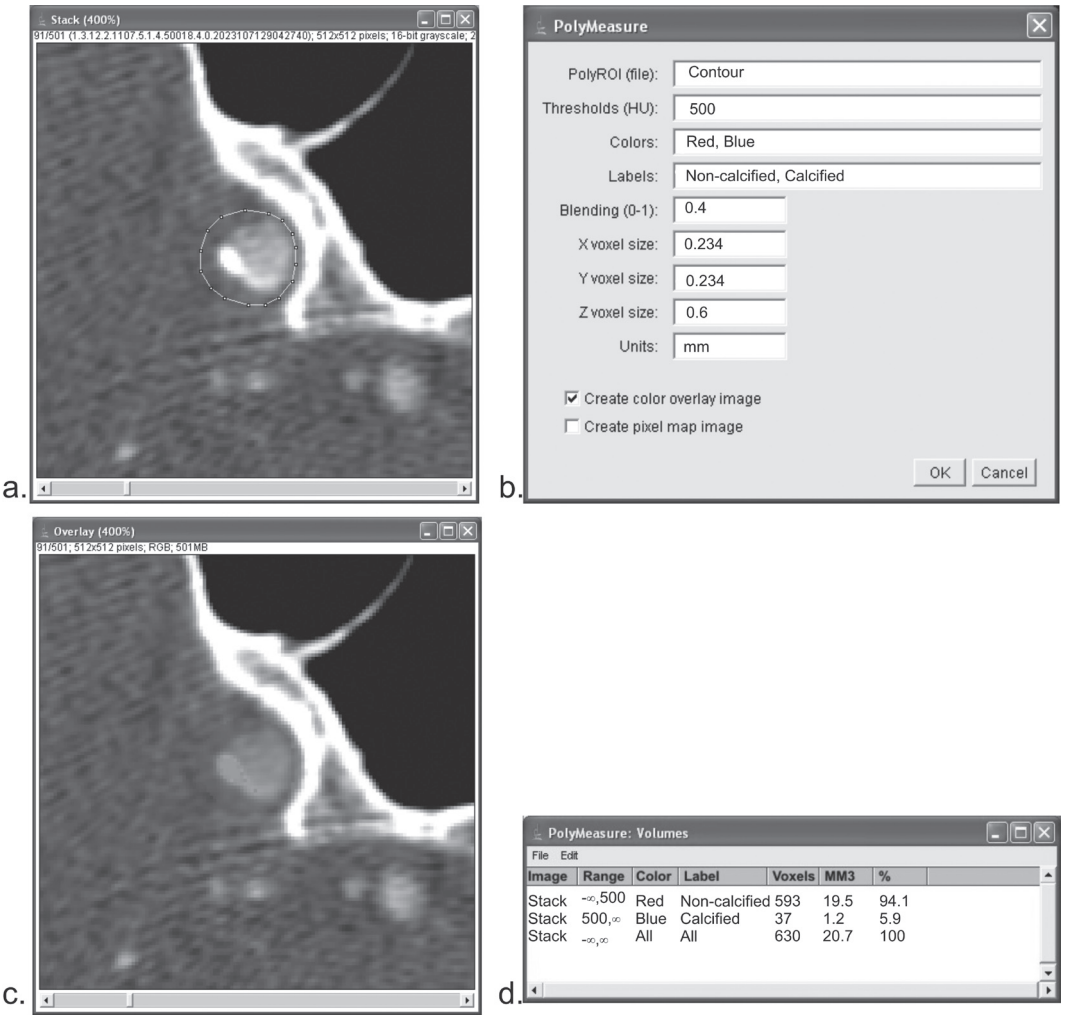

Figure 2. (a.) Regions of interest (ROI) are drawn on axial images that show calcifications. Care is taken to include the whole calcification and not to include any other high density structures (e.g. skull base). Because a minimum attenuation of 500 HU is defined for the presence of calcifications, lumen can be included in this ROI, because lumen will not reach such a high level of attenuation. All ROIs of one patient are saved within one file. (b.) The polymeasure software uses the contour file, the 500 HU threshold and the voxel dimensions (0.234 x 0.234 x 0.6 mm), to create a color overlay image, and a statistics table. (c.) The color overlay image shows which pixels within the ROI are above the pre-defined 500 HU threshold (blue) and which are below this threshold (red). (d.) The statistics table presents the amount of calcium pixels and the calcium volume (mm^3). (A full color version of this illustration can be found in the color section)

The volume of calcifications was measured with the custom-made 'Polymeasure' plug-in for the freely available software ImageJ (Rasband, National Institute of Mental Health, Bethesda, USA). This plug-in made it possible for an observer to draw polygonal regions of interest (ROI) in consecutive axial MDCTA images and to automatically calculate the total number of pixels above a predefined HU value within the ROI (Figure 2). The threshold value for calcification was set at 500 HU, which is above the normally used value of 130 HU for

the Agatston score[2]. This threshold was chosen to enable an automatic differentiation between contrast material in the lumen, which was <500 HU[14], and calcifications in the vessel wall. In case a calcification was close to the skull base, care was taken to delineate the calcification and to include it in the ROI (Figure 3). The volume of calcifications was calculated by multiplying the number of pixels above the threshold (500 HU), the pixel size and the increment.

(including present) or never smokers. Hypertension was defined as a mean systolic blood pressure over 140 mmHg and/or mean diastolic blood pressure over 90 mmHg during 2 episodes of at least 15 minutes of continuous non-invasive blood pressure measurement, or treatment with antihypertensive medication (i.e. ACE-inhibitors, calcium antagonists, beta-blockers and diuretics). Hypercholesterolemia was defined as fasting cholesterol over 5.0 mmol/l, or on treatment with cholesterol-

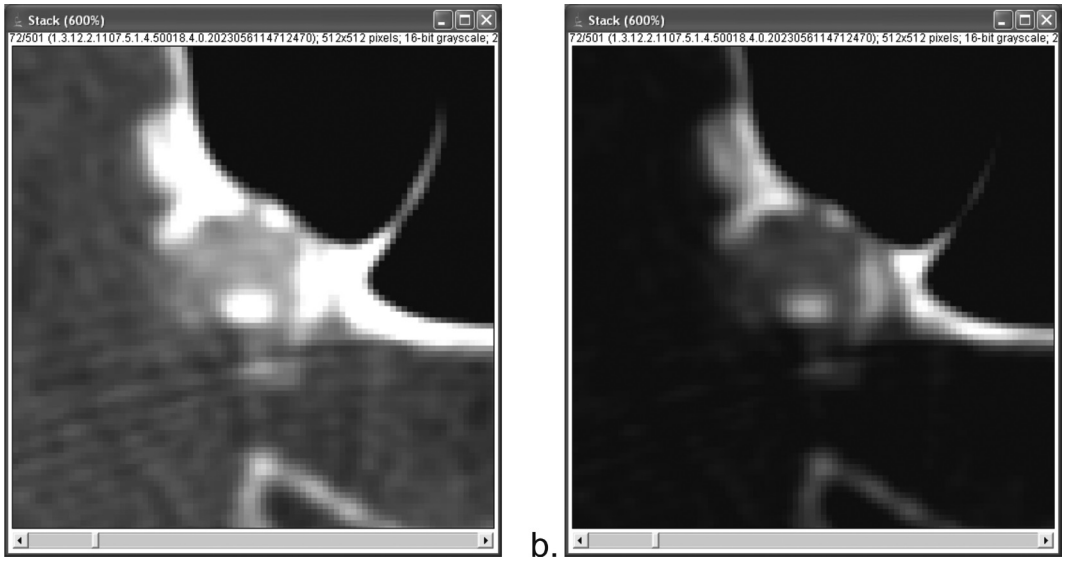

Figure 3. (a.) Where calcifications merge with the skull base, it is hard to define the delineation. (b.) Changing the window-level setting can then be of help, but observers might still disagree about the exact position of the delineation line. However, the low observer variability assessed in the present study shows that such disagreement only minimally influences total quantification results. Furthermore, it should be noted that the merging of calcifications and skull base prohibits, up to now, fully automated quantification.

Cardiovascular risk factors

Clinical measures and information on risk factors and medication were obtained at admission to the hospital, or in cases were measurements at this time point can be biased (e.g. blood pressure at admission) they were derived from clinical history or obtained at discharge. Subjects were categorized as ever

lowering drugs. Diabetes was defined as fasting serum glucose levels over 7.9 mmol/l, nonfasting serum glucose levels over 11.0 mmol/l, or use of antidiabetic medication. Information on history of cardiovascular disease (defined as a clinical diagnosis of a history of myocardial infarction, atrial fibrillation, angina pectoris, chronic heart failure, or coronary ar-

tery bypass grafting) and a history of ischemic cerebrovascular disease (defined as a clinical diagnosis of amaurosis fugax, TIA, or ischemic stroke) was collected.

Symptoms

Amaurosis fugax was defined as a sudden loss of vision of presumed vascular origin and confined to one eye. TIA was defined as a sudden focal neurological deficit that was presumed to be of vascular origin and was confined to an area of the brain perfused by a specific artery and that was resolved within 24 hours. In addition, no relevant infarct (one that explains the deficit) was visible on the CT scan. An ischemic stroke was defined as a sudden focal neurologic deficit which lasted more than 24 hours or which was accompanied by a relevant infarct on the CT scan.

Statistics

Data are presented as mean ± standard deviation. Baseline characteristics between men and woman were evaluated for differences. Interobserver differences in volume measurements were presented with an intraclass correlation coefficient, a coefficient of variation (defined by the standard deviation of the paired difference divided by the mean of the absolute value), and a Bland-Altman plot. Differences between categorical data and continuous data were analysed with Chi-squared test and Mann-Whitney test or Student's t-test, respectively. Spearman's correlation coefficient was

Table 1. Baseline characteristics of the study population.

	Patients 406	Men 242 (60%)	Women 164 (40%)	P-value
Age (mean ± SD; years)	62 ± 14	62 ± 13	62 ± 14	0.57
Symptomatic artery				
Carotid	351 (86%)	212 (88%)	139 (85%)	0.41
Vertebrobasilar	55 (14%)	30 (12%)	25 (15%)	
Cerebrovascular symptoms				
Amaurosis fugax	84 (21%)	50 (21%)	34 (21%)	0.99
Transient ischemic attack	122 (30%)	72 (30%)	50 (30%)	0.87
Minor stroke	200 (49%)	120 (50%)	80 (49%)	0.87
Risk factors				
Smoking	197 (49%)	136 (56%)	61 (37%)	<0.01
Hypertension	290 (71%)	177 (73%)	113 (69%)	0.35
Diabetes	61 (15%)	38 (16%)	23 (14%)	0.64
Hypercholesterolemia	319 (79%)	177 (73%)	142 (87%)	<0.01
History of cardiac disease	107 (26%)	73 (30%)	34 (21%)	0.03
History of cerebrovascular disease	105 (26%)	70 (29%)	35 (21%)	0.09
Calcifications				
Presence	263 (65%)	171 (71%)	92 (56%)	<0.01
Volume (mm^3)	53 ± 114	66 ± 124	33 ± 49	<0.01

used to analyze the association between age and calcifications for men and women. Logistic regression was used to evaluate the association between cardiovascular risk factors and calcifications. The presence of calcifications (left and right summated) was compared with the absence of calcifications and the highest quartile of calcification was compared to the lower 3 quartiles. Firstly, the regression analysis was adjusted only for age and gender. Secondly, additional adjustments were made for all risk factors.

The volume of intracranial calcifications in the left and right, and symptomatic and asymptomatic internal carotid artery were compared with a paired t-test. The association between the volume of intracranial calcifications in the symptomatic internal carotid artery and the type of cerebral vascular disease was assessed with logistic regression analysis with adjustment for age, gender and cardiovascular risk factors.

The intraclass correlation coefficient for the assessment of intracranial calcifications was excellent (0.99), and the coefficient of variation for the inter-observer differences was very low (7%). Absolute differences between observers were low and did not depend on the size of the calcifications (Figure 4).

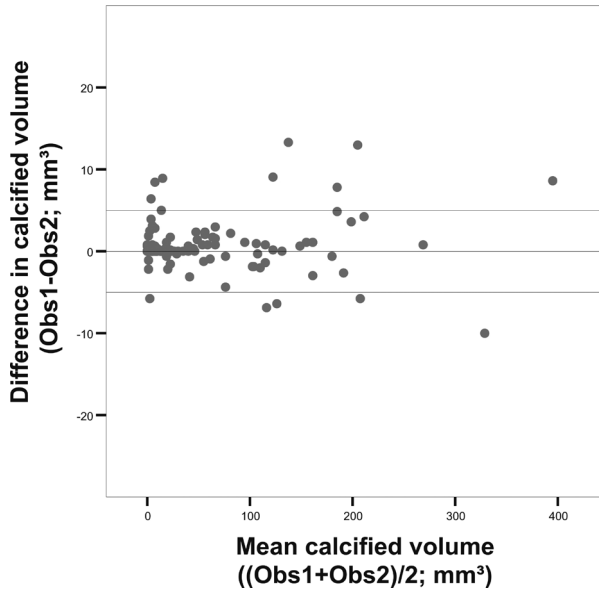

Figure 4. Bland-Altman plots of calcium volume assessed by two observers. The horizontal lines express the mean difference, and the mean difference ± 2 standard deviations.

Results

A total of 406 patients with amaurosis fugax, TIA or minor ischemic stroke were analyzed. Patient characteristics are shown in Table 1. There were no significant differences between men and women in age, symptomatic artery and ischemic cerebrovascular symptoms. However, men were more often smokers, and had more often experienced cardiac disease; women had more often experienced hypercholesterolemia.

Intracranial internal carotid artery calcifications were more frequent in men than in women (71% and 56%, respectively; p=0.003), and they were larger in men (66 ± 124 mm^3 and 33 ± 91 mm^3, respectively; p<0.001). Figure 5 shows the association between age and calcifications for both men and women with a Spearman's rho of 0.548 (p<0.001) for men and 0.501 (p<0.001) for women, and 0.531 (p<0.001) for men and women together.

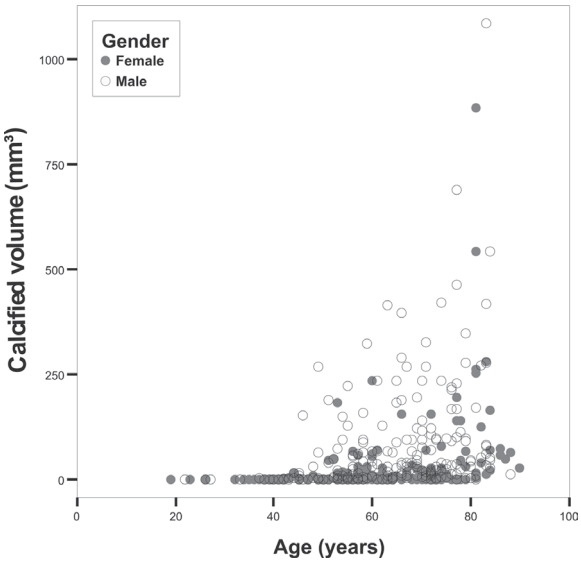

Figure 5. Scatterplot of calcium volume versus age for men and women separately. Correlation coefficient for men is 0.548 (p<0.001) and for women 0.501 (p<0.001).

Table 2 presents the age and gender adjusted and multivariate adjusted odds ratios for the associations between cardiovascular risk factors and intracranial calcium volume. Smoking, hypercholesterolemia, and history of cardiac disease, were independently associated with the presence of intracranial internal carotid artery calcifications. History of cardiac disease and history of ischemic cerebrovascular disease were independently associated with the highest quartile of intracranial calcium volume.

There was no significant difference between the intracranial calcium volumes of the left and right carotid ar-

Table 2. The association between risk factors and presence of calcifications in the intracranial internal carotid artery. (A) Presence of calcifications versus absence and (B) upper quartile versus lower 3 quartiles.

A CI = Confidence interval	**Odds ratios adjusted for age and sex**		**Odds ratios adjusted for age, sex and all risk factors**	
Variable	**Odds ratio (95% CI)**	**P-value**	**Odds ratio (95% CI)**	**P-value**
Smoking (ever)	1.7 (1.0-2.8)	0.04	1.9 (1.1-3.3)	0.01
Hypertension	1.8 (1.1-3.1)	0.03	1.6 (0.9-2.8)	0.11
Hypercholesterolemia	2.0 (1.1-3.8)	0.02	1.9 (1.0-3.7)	0.04
Diabetes	1.7 (0.8-3.4)	0.15	1.6 (0.8-3.4)	0.21
History of cardiac disease	2.3 (1.3-4.2)	<0.01	2.1 (1.1-4.0)	0.02
History of cerebrovascular disease	1.2 (0.7-2.0)	0.59	1.0 (0.6-1.9)	0.93

B	**Odds ratios adjusted for age and sex**		**Odds ratios adjusted for age, sex and all risk factors**	
Variable	**Odds ratio (95% CI)**	**P-value**	**Odds ratio (95% CI)**	**P-value**
Smoking (ever)	1.5 (0.9-2.5)	0.14	1.4 (0.8-2.4)	0.20
Hypertension	1.2 (0.6-2.1)	0.63	1.0 (0.5-1.8)	0.90
Hypercholesterolemia	1.7 (0.9-3.3)	0.11	1.7 (0.9-3.4)	0.13
Diabetes	1.4 (0.7-2.6)	0.33	1.3 (0.7-2.6)	0.44
History of cardiac disease	2.2 (1.3-3.7)	<0.01	2.0 (1.2-3.5)	0.01
History of cerebrovascular disease	2.0 (1.2-3.4)	0.01	1.9 (1.1-3.3)	0.03

Table 3. Calcium volumes (mean ± standard deviation) in the left and right internal carotid arteries, the symptomatic and asymptomatic internal carotid artery, and in the symptomatic artery of patients with amaurosis fugax, transient ischemic attack and minor ischemic stroke.

	N	Calcifications (mm^3)
Left internal carotid artery	406	26 ± 60
Right internal carotid artery	406	26 ± 57
Symptomatic internal carotid artery	351	28 ± 64
Asymptomatic internal carotid artery	351	28 ± 59
Vertebrobasilar symptoms	2 x 55	16 ± 31
Amaurosis fugax	84	20 ± 48
Transient ischemic attack (TIA)	97	23 ± 55
Minor ischemic stroke	170	34 ± 74

tery (p=0.97). Table 3 provides the intracranial calcium volume for the symptomatic and contralateral asymptomatic internal carotid artery and the intracranial calcium volume in the symptomatic internal carotid artery of patients with amaurosis fugax, TIA and minor ischemic stroke. No significant differences were found in intracranial calcium volumes at the symptomatic and asymptomatic side (p=0.73). In a logistic regression analysis adjusted for age, sex and all risk factors, intracranial calcifications were not related to the type of symptoms (amaurosis fugax versus TIA or minor stroke).

Discussion

This study shows that a dedicated custom-made software tool can reproducibly quantify intracranial internal carotid artery calcifications. Furthermore, it shows that the presence of intracranial calcifications is associated with smoking, hypercholesterolemia and history of cardiac disease, and that the severity of calcifications is related to history of cardiac disease and history of ischemic cerebrovascular disease.

No difference was found in the volume of intracranial calcifications between the symptomatic and asymptomatic internal carotid artery, and in the volume of intracranial calcifications in the symptomatic artery between patients with amaurosis fugax and patients with TIA or minor stroke.

Previous studies[8-12] had a binary or a qualitative (5-point scale) grading system for classification of intracranial calcifications, probably because quantification difficulties arose due to the close relationship between calcifications and the bony structures of the skull. Taoka et al.[13] were able to use commercially available software for quantification of intracranial calcifications but they had to eliminate the contamination of bone density on wide-windowed CT images. We dealt with this problem

by developing a custom-made software tool which allowed manual segmentation of intracranial calcifications without contamination of the bony skull, and assessed the volume of calcifications instead of the Agatston score. Because this quantification method was HU based, the manual outline of the border between calcifications and the skull was the only time-consuming part. However, this border was in most cases clearly visible, enabling the segmentation per patient to be done relatively quickly (<15 min). Observer differences were caused by the differences in the manual outline of the border between calcifications and skull. The very low observer variability indicates that observers do recognize the same hyperdense areas as possible calcifications, and that their manual outlines between calcifications and skull are very similar.

Our study in patients with ischemic cerebrovascular symptoms and a mean age of 73 years revealed a prevalence of intracranial internal carotid artery calcifications of 65%. Age, gender, smoking, hypercholesterolemia, history of cardiac disease and history of ischemic cerebrovascular disease were independently related to the presence or volume of intracranial internal carotid artery calcifications. Associations between cardiovascular risk factors and intracranial calcifications have been studied in patients referred for brain CT[10-12]. One study had a prevalence of 36% in a group of patients with a mean age of 51 years[11], while the second study found a prevalence of 67% in a group of patients with a mean age of 63 years[10]. Both studies confirmed the association between age and calcifications, an association which was also found in coronary artery studies[2].

The present study found a higher prevalence and volume of calcifications in men, a finding which is in agreement with studies on coronary arteries[16,17] and carotid bifurcations[17]. One study found an independent association between gender and intracranial internal carotid artery calcifications[11] while another study did not find this association[10].

In the present study, we found that smoking and hypercholesterolemia are independently associated with the presence of intracranial calcifications. Other studies showed independent associations of smoking with coronary, aortic arch, carotid bifurcation calcification[4,5,18,19] and intracranial internal carotid artery calcifications[11]. Hoff et al.[5] found in a large study among asymptomatic individuals an independent association of hypercholesterolemia with coronary calcification in both men and women. However, a study by Allison et al.[3] examining risk factors for coronary, proximal aorta and carotid calcification, found no independent associations with hypercholesterolemia. An independent association between hypertension and coronary calcification[3-5,18], aortic arch calcification[18] and carotid bifurcation calcification[3], has been described, however the present study did not find an association between hypertension and the presence of intracranial carotid calcifications. Neither did we find an association between the presence of calcifications and diabetes, as is known from coronary literature.[6] A possible explanation for the absence of such associations, could be the fact that we are dealing

with a fundamentally different pathophysiology. In the intracranial arteries atherosclerotic calcifications normally develop within the vessel wall, with little non-calcified atherosclerotic components and little luminal compromise, while in the coronary arteries the calcified parts in the plaque are accompanied by extensive non-calcified components and considerable luminal narrowing.

Internal carotid artery calcifications might be an indicator of arterial stenosis[13,20]. Stenosis in the intracranial internal carotid artery carries an increased risk of stroke[21,22]. Therefore we compared the volume of calcification in the symptomatic and asymptomatic internal carotid artery; however, no difference in intracranial calcium volume was found between the symptomatic and asymptomatic side. This is in agreement with Babiarz et al. who found no differences in the scores ipsilateral and contralateral to the stroke[8,9]. In addition, in two cross-sectional studies[8,9] they found that intracranial internal carotid artery calcification was not independently related to the extent of white matter lesions or the presence of stroke. In a follow-up study of 72 patients, Taoka et al.[13] did not find a association between the intracranial internal carotid artery calcification score and the later occurrence of stroke. Therefore, they concluded that intracranial calcifications should not be considered as the cause of an ischemic event by being a source of embolism or thrombosis, but as a marker of systemic atherosclerotic disease, which is closely related to stroke.

A limitation of the present study was that it is still labor-intensive to draw a ROI on each image that shows an intracranial internal carotid artery calcification; therefore, a tool should be developed which locates the calcification and quantifies it automatically. A second limitation is the lack of a gold standard. The accuracy of MDCTA-based assessment of the presence and volume of intracranial internal carotid artery calcifications could therefore not be established. However, the ability to accurately determine and quantify calcifications has been proven in other vascular beds[2,23]. In addition,, it can be addressed as a limitation, that the calcium volume in the intracranial contralateral carotid artery of patients with ischemic cerebrovascular symptoms has been used in the analysis as the asymptomatic volume, instead of the calcium volume in intracranial carotid artery of completely asymptomatic patients. Finally, it is a limitation of our study that we could not, due to ethical reasons, include patients with severe stroke because especially their data will contain relevant information on who is at risk of developing a severe stroke.

This study showed that with custom-made software quantitative evaluation is reproducible. Therefore, follow-up studies should explore the association between the presence and volume of intracranial internal carotid artery calcifications and (recurrent) ischemic cerebrovascular events. Furthermore, these studies should assess the additional value of this measure over commonly used parameters in the prediction of ischemic cerebrovascular events, as well as its value as a marker of systemic atherosclerotic disease.

In conclusion, our study has shown that intracranial internal carotid artery calcifications

can reproducibly be quantified with a dedicated custom-made software tool, and that age, gender, smoking, hypercholesterolemia, history of cardiac disease and history of ischemic cerebrovascular disease are independently related to the presence or volume of arterial calcification. Furthermore, it is shown that the degree of calcifications does not differ between the symptomatic and contralateral asymptomatic artery, and that calcifications are not related to presence or type of ischemic cerebrovascular disease.

References

1. Rumberger JA, Simons DB, Fitzpatrick LA, et al. Coronary artery calcium area by electron-beam computed tomography and coronary atherosclerotic plaque area. A histopathologic correlative study. Circulation. 1995;92:2157-62.
2. Agatston AS, Janowitz WR, Hildner FJ, et al. Quantification of coronary artery calcium using ultrafast computed tomography. J Am Coll Cardiol. 1990;15:827-32.
3. Allison MA, Criqui MH, Wright CM. Patterns and risk factors for systemic calcified atherosclerosis. Arterioscler Thromb Vasc Biol. 2004;24:331-6.
4. Allison MA, Wright CM. Age and gender are the strongest clinical correlates of prevalent coronary calcification (R1). Int J Cardiol. 2005;98:325-30.
5. Hoff JA, Daviglus ML, Chomka EV, et al. Conventional coronary artery disease risk factors and coronary artery calcium detected by electron beam tomography in 30,908 healthy individuals. Ann Epidemiol. 2003;13:163-9.
6. Arad Y, Goodman KJ, Roth M, et al. Coronary calcification, coronary disease risk factors, C-reactive protein, and atherosclerotic cardiovascular disease events: the St. Francis Heart Study. J Am Coll Cardiol. 2005;46:158-65.
7. Vliegenthart R, Hollander M, Breteler MM, et al. Stroke is associated with coronary calcification as detected by electron-beam CT: the Rotterdam Coronary Calcification Study. Stroke. 2002;33:462-5.
8. Babiarz LS, Yousem DM, Wasserman BA, et al. Cavernous carotid artery calcification and white matter ischemia. AJNR Am J Neuroradiol. 2003;24:872-7.
9. Babiarz LS, Yousem DM, Bilker W, et al. Middle cerebral artery infarction: relationship of cavernous carotid artery calcification. AJNR Am J Neuroradiol. 2005;26:1505-11.
10. Chen XY, Lam WW, Ng HK, et al. The frequency and determinants of calcification in intracranial arteries in Chinese patients who underwent computed tomography examinations. Cerebrovasc Dis. 2006;21:91-7.
11. Ptak T, Hunter GH, Avakian R, et al. Clinical significance of cavernous carotid calcifications encountered on head computed tomography scans performed on patients seen in the emergency department. J Comput Assist Tomogr. 2003;27:505-9.

12. Sohn YH, Cheon HY, Jeon P, et al. Clinical implication of cerebral artery calcification on brain CT. Cerebrovasc Dis. 2004;18:332-7.
13. Taoka T, Iwasaki S, Nakagawa H, et al. Evaluation of arteriosclerotic changes in the intracranial carotid artery using the calcium score obtained on plain cranial computed tomography scan: Correlation with angiographic changes and clinical outcome. J Comput Assist Tomogr. 2006;30:624-8.
14. de Monye C, Cademartiri F, de Weert TT, et al. Sixteen-detector row CT angiography of carotid arteries: comparison of different volumes of contrast material with and without a bolus chaser. Radiology. 2005;237:555-62.
15. de Weert TT, Ouhlous M, Zondervan PE, et al. In vitro characterization of atherosclerotic carotid plaque with multidetector computed tomography and histopathological correlation. Eur Radiol. 2005;15:1906-14.
16. Janowitz WR, Agatston AS, Kaplan G, et al. Differences in prevalence and extent of coronary artery calcium detected by ultrafast computed tomography in asymptomatic men and women. Am J Cardiol. 1993;72:247-54.
17. Odink AE, van der Lugt A, Hofman A, et al. Association between calcification in the coronary arteries, aortic arch and carotid arteries: The Rotterdam study. Atherosclerosis. 2006.
18. Iribarren C, Sidney S, Sternfeld B, et al. Calcification of the aortic arch: risk factors and association with coronary heart disease, stroke, and peripheral vascular disease. Jama. 2000;283:2810-5.
19. Reilly MP, Wolfe ML, Localio AR, et al. Coronary artery calcification and cardiovascular risk factors: impact of the analytic approach. Atherosclerosis. 2004;173:69-78.
20. Woodcock RJ, Jr., Goldstein JH, Kallmes DF, et al. Angiographic correlation of CT calcification in the carotid siphon. AJNR Am J Neuroradiol. 1999;20:495-9.
21. Craig DR, Meguro K, Watridge C, et al. Intracranial internal carotid artery stenosis. Stroke. 1982;13:825-8.
22. Marzewski DJ, Furlan AJ, St Louis P, et al. Intracranial internal carotid artery stenosis: longterm prognosis. Stroke. 1982;13:821-4.
23. de Weert TT, Ouhlous M, Meijering E, et al. In vivo characterization and quantification of atherosclerotic carotid plaque components with multidetector computed tomography and histopathological correlation. Arterioscler Thromb Vasc Biol. 2006;26:2366-72.

8

ATHEROSCLEROTIC PLAQUE SURFACE MORPHOLOGY IN THE CAROTID BIFURCATION ASSESSED WITH MULTIDETECTOR COMPUTED TOMOGRAPHY ANGIOGRAPHY

Thomas T de Weert • Sander Cretier • Harald C Groen • P Homburg •
Hamit Cakir • Jolanda J Wentzel • Diederik WJ Dippel • Aad van der Lugt

Accepted for publication in Stroke

Atherosclerotic plaque surface morphology in the carotid bifurcation assessed with multidetector computed tomography angiography

Abstract

Objective

Complicated (irregular or ulcerated) carotid plaques have proven to be independent predictors of stroke. We analyzed the frequency and location of plaque irregularities in a large cohort of patients with ischemic cerebrovascular disease, and the relation with severity of stenosis, cardiovascular risk factors and symptomatology.

Materials and Methods

Multidetector computed tomography angiography (MDCTA) images from 406 patients were evaluated. Plaque surface morphology was classified as smooth, irregular or ulcerated. The location of the ulceration was defined as proximal or distal to the point of maximum stenosis.

Results

Atherosclerotic plaques with an open lumen were present in 448 carotid arteries, these plaque were classified as: smooth: 276(62%), irregular: 99(22%) and ulcerated: 73(16%). Sixty-two(69%) of the ulcerations were located proximal to the point of maximum luminal stenosis. Complicated plaques were significantly ($p<0.001$) more common in carotid arteries with stenosis >30%, than in those with stenosis <30%. There is an association between complicated plaques and hypercholesterolemia (OR 3.0) and a trend towards an association with smoking (OR 1.9). Complicated plaques are more often present in the symptomatic carotid artery than in the contralateral asymptomatic carotid artery, however this is fully attributed to a significantly higher degree of stenosis in the symptomatic arteries.

Conclusions

MDCTA allows the classification of atherosclerotic carotid plaque surface. Complicated plaques are frequent in atherosclerotic carotid disease, especially with higher stenosis degree. Ulcerations are mostly located in the proximal part of the atherosclerotic plaque. Hypercholesterolemia and smoking are related with the presence of complicated plaques.

Introduction

Cerebral infarction is one of the most important causes of death and the greatest cause of disability in the western world. About 20%-30% of the infarcts can be related to carotid artery stenosis[1,2]. The severity of stenosis is an important predictor of (recurrent) ischemic cerebrovascular events and is used in therapeutic decision-making: patients with symptomatic or asymptomatic carotid stenosis above a certain degree are considered candidates for carotid intervention, such as carotid endarterectomy or stent placement.

Besides the severity of stenosis, plaque ulceration on intra-arterial contrast angiography is a strong independent predictor of stroke[3,4]. It is current opinion that atherosclerotic plaque rupture plays an important role in acute events, like transient ischemic accidents (TIA) and stroke[5]. Rupture-prone plaques have specific morphological features: the most frequently seen vulnerable plaque type has a large lipid-rich core with a thin fibrous cap[5] and has proved to be an independent predictor of ischemic cerebrovascular events[6,7]. With microscopic evaluation of the plaque it became clear that angiographic ulceration and irregularities were strongly associated with the presence of plaque rupture, plaque hemorrhage, a large lipid core size and less fibrous tissue, i.e. features that are all closely related with the concept of a vulnerable plaque[8]. Plaque ulceration has been more frequently observed proximal to the point of maximum luminal stenosis[9], which is exposed to higher wall shear stress[10].

The accuracy of digital subtraction angiography (DSA) in the detection of ulceration, with surgical observations as reference, has been reported to be low (sensitivity 46% and specificity 74%)[11]. The first reports on the accuracy of computed tomography angiography (CTA) compared with DSA in the assessment of plaque ulcers were disappointing, but this might be explained by the rather thick slice thickness used with single section computed tomography (CT)[12]. A later report demonstrated that CTA was superior to DSA in the detection of plaque irregularities and ulcerations[13]. Walker and colleagues evaluated 165 CTA studies, compared them with endarterectomy specimens, and reported a sensitivity of 60% and a specificity of 74%[14]. A recent multi-detector CTA (MDCTA) study reported an even higher sensitivity and specificity for the detection of ulcerations (94% and 99%, respectively)[15].

The purpose of this study was to assess atherosclerotic plaque surface morphology in the carotid arteries with MDCTA in a large consecutive cohort of patients with ischemic cerebrovascular disease. Plaque surface morphology was related to severity of stenosis, cardiovascular risk factors, and type of ischemic cerebrovascular symptoms.

Materials and Methods

Study population

Consecutive patients (n=406) with ischemic cerebrovascular disease including amaurosis fugax or focal cerebral ischemia (TIA and minor ischemic stroke) were prospectively

studied. Patients were enrolled from the neurology department's specialized TIA/stroke outpatient clinic or neurology ward. Patients underwent neurological examination on admission. Medical history was recorded from all patients. All patients underwent multidetector CT (MDCT) of the brain and MDCTA of the carotid arteries. In all patients MDCTA has been performed as part of a research protocol that was approved by the Institutional Review Board and all patients had given written informed consent. The inclusion period ranged from November 2002 to January 2005.

Scanning and image reconstruction

Scanning was performed on a 16-slice MDCT scanner (Siemens, Sensation 16, Erlangen, Germany) with a standardized optimized contrast-enhanced protocol (120 kVp, 180 mAs, collimation 16 x 0.75 mm, pitch 1)[16,17]. The MDCTA scan range reached from the ascending aorta to the intracranial circulation (2 cm above the sella turcica). All patients received 80 ml contrast material (Iodixanol 320 mg/ml, Visipaque, Amersham Health, Little Chalfont, UK), followed by 40 ml saline bolus chaser, both with an injection rate of 4 ml/sec. Synchronization between the passage of contrast material and data acquisition was achieved by real time bolus tracking at the level of the ascending aorta. The trigger threshold was set at an increase in attenuation of 75 Hounsfield Units (HU) above baseline attenuation (≈ 150 HU in absolute HU value).

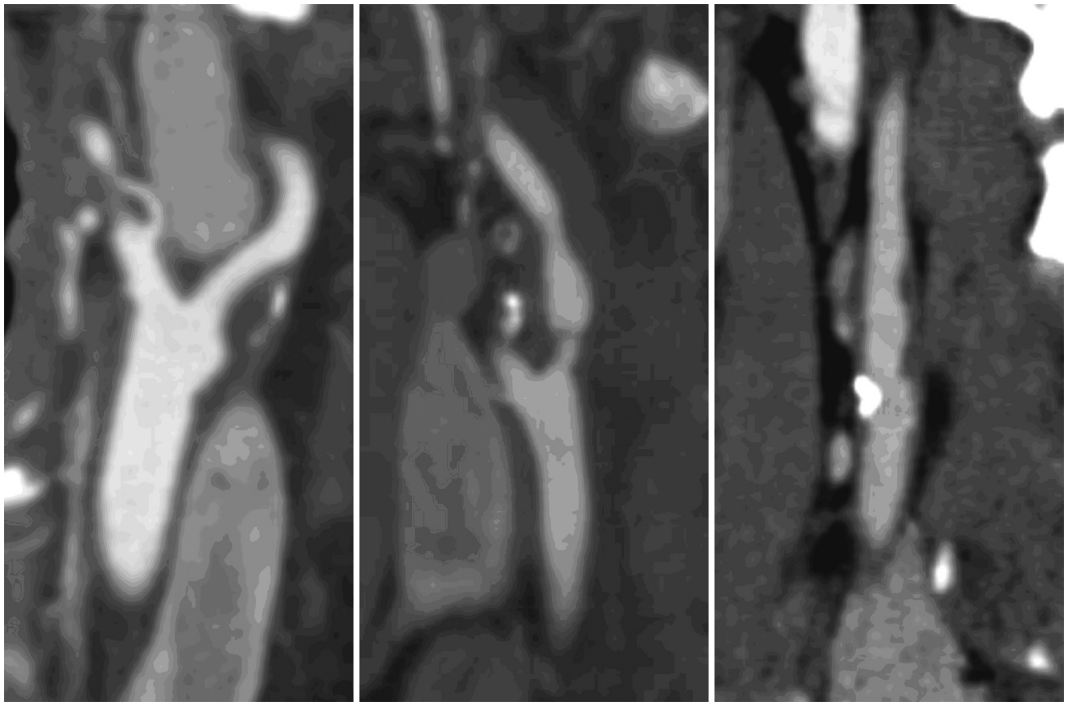

Figure 1. Multiplanar reformat images (1 mm thick). (a.) Smooth atherosclerotic carotid plaque surface. (b and c.) Irregular plaque surface.

Image reconstructions were made with field of view 100 mm, matrix size 512 x 512 (real in-plane resolution 0.6 x 0.6 mm), slice thickness 1.0 mm, increment 0.6 mm and with an intermediate reconstruction algorithm[18].

Analysis of the atherosclerotic plaque

The MDCTA images were sent to a stand-alone workstation (Leonardo – Siemens Medical Solutions, Forchheim, Germany) with dedicated 3D analysis software. On the workstation both carotid bifurcations were evaluated with multiplanar reformatting (MPR) software. With this software oblique planes can be adjusted in order to evaluate the carotid bifurcation in multiple reformations in the short axis and long axes with respect to the carotid artery.

Firstly, the presence of an atherosclerotic plaque was evaluated. The criterion used for the presence of an atherosclerotic lesion was: the presence of a calcification and/or thickening of the vessel wall. If a plaque was visible, the surface of the plaque was evaluated and classified as ulcerated, irregular or smooth (Figure 1, Figure 2). Plaques were classified as ulcerated if extension of contrast material was present beyond the vascular lumen into the surrounding plaque. Ulcerated plaques were categorized according to the shape of the ulcer as type 1 to 4 (Figure 2), as previously described by Lovett et al[8]. Type 1 is an ulcer that points out perpendicular to the lumen; type 2 has a narrow neck, and points out proximally and distally; type 3 has an ulcer neck proximally and points out distally, and type 4 has an ulcer neck distally and points out proximally. The location of the ulcer was defined as proximal or distal to the point of maximum luminal stenosis. Plaques were classified as irregular if pre- or post-stenotic dilatation was

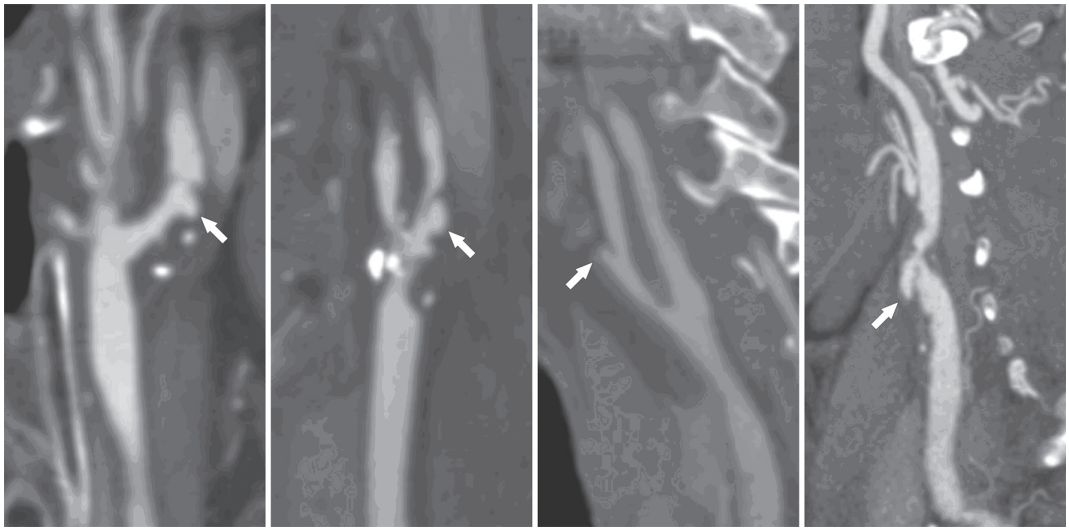

Figure 2. Multiplanar reformat images (1 mm thick) with (a.) a Type 1, (b.) a Type 2, (c.) a Type 3, and (d.) a Type 4 atherosclerotic carotid plaque ulceration.

present and/or if the plaque surface morphology showed irregularities without any sign of ulceration. If the plaque was not ulcerated or irregular, it was classified as smooth. To calculate interobserver reproducibility a second observer reassessed 100 consecutive MDCTA scans.

Severity of stenosis

The severity of stenosis on CTA was measured according to the North American Symptomatic Carotid Endarterectomy Trial (NASCET)[19] criteria. Oblique MPR images, parallel to the central lumen line were used for measurements. The severity of stenosis was defined as the remaining lumen at the site of stenosis as percentage of the normal lumen distal to the stenosis, and categorized into 0-29%, 30-49%, 50-69%, 70-99% and 100%.

Cardiovascular risk factors

Clinical measures and information on risk factors and medication were obtained at admission to the hospital. Subjects were categorized as current, past and never smokers. Hypertension was defined as systolic blood pressure over 140 mmHg and/or diastolic blood pressure over 90 mmHg during two episodes of at least 15 minutes of continuous non-invasive blood pressure measurement or treatment with antihypertensive medication. Blood pressure lowering drugs comprised ACE inhibitors, calcium antagonists, beta-blockers and diuretics.

Hypercholesterolemia was defined as fasting cholesterol over 5.0 mmol/l, or on treatment with cholesterol-lowering drugs. Diabetes was defined as fasting serum glucose levels over 7.9 mmol/l, nonfasting serum glucose levels over 11.0 mmol/l, or use of antidiabetic medication.

Information on previous cardiovascular disease (myocardial infarction, atrial fibrillation, angina pectoris, chronic heart failure, coronary artery bypass grafting) and previous ischemic cerebrovascular disease (TIA or ischemic stroke other than the event for which the patient was currently evaluated) was collected.
Symptoms

Amaurosis fugax was defined as a sudden, focal neurological deficit that was presumed to be of vascular origin and confined to the eye. TIA was defined as a sudden, focal neurological deficit that was presumed to be of vascular origin and was confined to an area of the brain perfused by a specific artery and that lasted less than 24 hours. In addition, no relevant infarct (one that explains the deficit) should be seen on the CT scan. An ischemic stroke was defined as a sudden focal neurologic deficit which lasted more than 24 hours or which was accompanied by a relevant infarct on the CT scan.

Statistics

Data are presented as mean ± standard deviation. Analysis was performed for complicated (irregular or ulcerated) plaques. Reliability of assessment of plaque surface morphology was measured using the kappa statistics. Differences between categorical data and continuous data were analysed with a Chi-squared test and a Mann-Whitney test or Student's t-test, respectively. In an exploratory analysis we evaluated the association

between the presence of complicated plaque and possible determinants (severity of stenosis and cardiovascular risk factors (smoking, hypertension, hypercholesterolemia, diabetes, previous cardiovascular disease, previous ischemic cerebrovascular disease)). All determinants were included in a multiple logistic regression model to assess their association with complicated plaque independently from other determinants. No stepwise procedures were used. The associations were expressed as odds ratios with 95% confidence intervals, which implies we used P<0.05 as the value for statistical significance. The same analysis was repeated for ulcerated plaques only. Finally, in the patients with symptoms in territory of the carotid arteries the association between the presence of complicated plaque and symptomatic side was evaluated with a logistic regression model after adjustment for severity of stenosis. All calculations were made with SPSS 14.0 for Windows.

Results

The MDCTA images and medical histories of 406 patients were evaluated. Two patients were excluded because of poor image quality due to dental artifacts. General patient characteristics are shown in Table 1. With respect to age, the symptomatic artery, and ischemic cerebrovascular disease, there were no significant differences between men and women. However, men were more frequently smokers and had more frequently experienced previous cardiac disease, while women had more frequently hypercholesterolemia.

Table 1. Baseline characteristics of the study population.

	Patients 404	Men 242 (60%)	Women 162 (40%)	p-value
Age (mean ± SD; years)	62 ± 14	62 ± 13	62 ± 14	0.57
Symptomatic artery				
Carotid	350 (87%)	212 (88%)	138 (85%)	0.48
Vertebrobasilar	54 (13%)	30 (12%)	24 (15%)	
Cerebrovascular symptoms				
Amaurosis fugax	83 (21%)	50 (21%)	33 (20%)	0.94
Transient ischemic attack	122 (30%)	72 (30%)	50 (31%)	0.81
Minor stroke	199 (49%)	120 (50%)	79 (49%)	0.87
Risk factors				
Smoking	195 (48%)	136 (56%)	59 (36%)	<0.01
Hypertension	288 (71%)	177 (73%)	111 (69%)	0.31
Diabetes	61 (15%)	38 (16%)	23 (14%)	0.68
Hypercholesterolemia	317 (78%)	177 (73%)	140 (86%)	<0.01
Previous cardiac disease	107 (26%)	73 (30%)	34 (21%)	0.04
Previous cerebrovascular disease	105 (26%)	70 (29%)	35 (21%)	0.10

Table 2. Plaque surface morphology characteristics of 448 atherosclerotic carotid arteries with number, type (Type 1-4) and location of plaque ulceration.

Carotid arteries with atherosclerosis	
Smooth surface	276 (62%)
Irregular surface	99 (22%)
Ulcerated surface	73 (16%)
Number of ulcerations per carotid artery	
1	61 (84%)
2	8 (11%)
3	3 (4%)
4	1 (1%)
Type of ulceration	
1	43 (48%)
2	12 (13%)
3	24 (27%)
4	11 (12%)
Location of ulceration	
Proximal	62 (69%)
Distal	28 (31%)

In 142 patients (35%) both carotid arteries were free of atherosclerosis, in 68 patients (17%) presence of atherosclerosis was determined in one of the carotid arteries, in 190 patients (47%) both carotid arteries showed atherosclerosis, in 21 patients at least one of the carotid arteries was occluded. Overall, from the 808 studied arteries, 337 (42%) were normal without atherosclerotic plaque, 448 (55%) were diseased, and 23 (3%) were occluded. Table 2 shows the plaque surface morphology characteristics of the remaining 448 (55%) carotid arteries with atherosclerotic plaque. We found 90 ulcers in 73 carotid arteries of 61 patients. Both carotid arteries were ulcerated in 12 patients, and some patients had multiple (up to 4) ulcerations in the same carotid artery. The prevalence of ulceration among the patients with at least one atherosclerotic carotid artery (n=258) was 24%. Most of the ulcerations (69%) were located proximal to the point of maximum stenosis, and ulcer type 1 and ulcer type 3 were most frequently observed. An irregular plaque was demonstrated in 22% of the carotid arteries with atherosclerotic disease. The two observers agreed on the presence of complicated plaque in 93% of the cases (kappa =0.84; 95%CI = 0.70-0.97), on the presence of ulcerated plaque in all cases (kappa = 1; 95%CI =0.86-1.00), on the location of plaque

Table 3. Cross-table with the degree of stenosis according to the NASCET criteria compared with plaque surface morphology of 448 atherosclerotic carotid arteries. The presence of irregular and ulcerated plaques is significantly different between the lowest degree of stenosis (0-29%) and the higher degrees of stenosis (30-99%) (p-value for both <0.001).

	Number of carotids	**Smooth**	**Irregular**	**Ulcerated**
0% - 29%	346	265 (77%)	49 (14%)	32 (9%)
30% - 49%	48	8 (17%)	23 (48%)	17 (35%)
50% - 69%	29	1 (3%)	13 (45%)	15 (52%)
70% - 99%	25	2 (8%)	14 (56%)	9 (36%)
Total	448	276	99	73

Table 4. (a.) The multivariable adjusted odds ratios for associations between the complicated carotid plaques and cardiovascular risk factors for all patients with atherosclerosis (n=258). (b.) The multivariable adjusted odds ratios for associations between the ulcerated carotid plaques and cardiovascular risk factors for all patients with atherosclerosis (n=258). In both analyses the most severe stenosis per patient and the most severe plaque surface morphology per patient was used.

a.	**Complicated plaque**	
Variable	Odds ratio (95% CI)	P-value
Age (per increasing decade)	1.1 (0.8-1.5)	0.50
Gender	1.1 (0.5-2.3)	0.88
Previous cerebrovascular disease	1.8 (0.9-3.7)	0.12
Previous cardiac disease	0.8 (0.4-1.7)	0.55
Hypertension	0.9 (0.4-2.3)	0.87
Hypercholesterolemia	3.0 (1.0-8.9)	<0.05
Diabetes	0.6 (0.2-1.9)	0.43
Smoking	1.9 (0.9-4.1)	0.09
Degree of stenosis (per 10% increase)	2.3 (1.9-2.9)	<0.001

b.	**Ulcerated plaque**	
Variable	Odds ratio (95% CI)	P-value
Age (per increasing decade)	1.0 (0.7-1.4)	0.92
Gender	1.2 (0.6-2.6)	0.61
Previous cerebrovascular disease	1.0 (0.5-2.0)	0.94
Previous cardiac disease	0.8 (0.4-1.6)	0.52
Hypertension	0.9 (0.4-2.2)	0.27
Hypercholesterolemia	0.9 (0.4-2.2)	0.89
Diabetes	0.5 (0.2-1.4)	0.21
Smoking	1.6 (0.8-3.3)	0.23
Degree of stenosis (per 10% increase)	1.5 (1.4-1.8)	<0.001

ulceration in 96% of the cases (kappa =0.91; 95% = 0.54-1.00) and on the types of plaque ulceration in 98-100% of the cases (kappa = 0.98-1.00; 95%CI = 0.89-1.00).

Table 3 shows a cross-table with the degree of stenosis compared with the plaque surface morphology. It can be observed that ulcerated and irregular plaques are significantly (p<0.001) more common, and smooth plaques less common among carotid arteries with a higher degree of stenosis (30-99%). There were not enough ulcerated plaques to determine significant differences in the distribution of ulcer type among the different degrees of stenosis.

The odds ratio for the association between complicated plaques and severity of stenosis (per 10% increase) adjusted for age and gender is 2.3 (95%CI 1.9-2.9). The odds ratio for the association between ulcerated plaques

Table 5. Plaque surface morphology in symptomatic and asymptomatic carotid arteries stratified for cerebrovascular symptoms.

	Cerebrovascular symptoms		
	Total	**Amaurosis fugax**	**TIA / Minor stroke**
Symptomatic carotid artery (Ipsilateral)	350	83	267
Atherosclerotic plaque (%)	193 (55%)	39 (47%)	154 (58%)
Complicated plaque (%)	89 (25%)	14 (17%)	75 (28%)
Asymptomatic carotid artery (Contralateral)	458	83	267
Atherosclerotic plaque (%)	255 (56%)	41 (49%)	155 (58%)
Complicated plaque (%)	83 (18%)	14 (17%)	54 (20%)

For patients with vertebrobasilar symptoms both carotidarteries were considerd asymptomatic. Symptomatic vs. asymptomatic complicated plaque for all patients: p = 0.01; Symptomatic vs. asymptomatic complicated plaque surface for patients with TIA or minor stroke: p =0.03.

and severity of stenosis (per 10% increase) adjusted for age and gender is 1.5 (95%CI 1.3-1.7).

The multivariable adjusted odds ratios for the association between cardiovascular risk factors and complicated plaque in one of the carotid arteries with at least atherosclerotic disease in one of the carotid arteries (n=258) are shown in Table 4. A significant association was found with hypercholesterolemia (OR 3.0, 95%CI 1.0-8.9), and a trend towards an association with smoking (OR 1.9, 95%CI 0.9-4.1).

The multivariable analysis for the association between cardiovascular risk factors and plaque ulceration in one of the carotid arteries showed no significant association between cardiovascular risk factors and plaque ulceration.

Table 5 shows that atherosclerotic plaques were present in both symptomatic and asymptomatic carotid arteries (55% vs 56%). Symptomatic carotid arteries more often harbored complicated plaques than asymptomatic carotid arteries (25% vs 18%, p=0.01, respectively). However, multivariable analysis showed that this can be attributed to the significantly higher degree of stenosis present in symptomatic arteries compared to asymptomatic arteries (p <0.01).

Complicated plaques were less often observed among patients with amaurosis fugax (17%) compared to patients with focal cerebral ischemia (28%); moreover, in the patients with amourosis fugax symptomatic arteries were not more often complicated than asymptomatic arteries (17% vs 17%), as opposed to patients with focal cerebral ischemia (28% vs 20%; p=0.03). Nonetheless, also in patients with focal cerebral ischemia the difference in incidence of complicated plaques was attributable to the significantly higher stenosis degree present in symptomatic arteries.

Discussion

This study demonstrates that MDCTA can assess atherosclerotic carotid plaque surface morphology, with differentiation between smooth, irregular and ulcerated surfaces. It shows that the majority of ulcerations are located proximally to the maximum stenosis, and that ulcerated and irregular plaques are more frequently encountered with a higher degree of stenosis. Of all cardiovascular risk factors, hypercholesterolemia was associated with complicated plaque while smoking showed a trend towards an association with complicated plaque.

Finally, it was shown that complicated plaque is more common in the symptomatic artery of patients with cerebrovascular symptomatology than in the asymptomatic artery, however this can be ascribed to the significantly higher stenosis degree present in symptomatic arteries compared to asymptomatic arteries.

The present study found ulceration in 11% of the symptomatic carotid artery, and in 40% of the carotid arteries with a moderate to severe degree of stenosis (30-99%). Although, the proportion of ulcerated plaques in high grade stenosis is not significantly different from the proportion in the group with 50-69% stenosis our results are suggestive for the fact that there might be a real discrepancy, for which we can think of two possible explanations: 1) With severe stenosis calcifications are larger, which hampers identification of ulcerations with MDCTA. 2) The risk of rupture might differ with plaque composition. Plaques with a moderate stenosis degree have a larger proportion of lipid, while plaque with severe stenosis are more calcified.

Based on the DSA data of the ECST study Lovett et al.[9] reported a prevalence of ulceration of 14% in 3007 symptomatic carotid arteries in patients with atrial fibrillation, TIA or minor stroke patients, and a prevalence of 18% for symptomatic carotid arteries with a stenosis >30%. In the NASCET study ulcerations were found in 35% of symptomatic carotid arteries with a stenosis >70%[3]. In the present study, complicated plaque was present in 89% of the carotid arteries with stenosis >30%, which exceeds the reported frequency (63%) of carotid plaque surface abnormality detected with DSA[4]. The discrepancy in the frequencies of ulceration with MDCTA and DSA can be explained by the higher sensitivity of MDCTA in the detection of ulcerations[13]: MDCTA has a reported sensitivity of 60-94%[14,15], whereas DSA has a sensitivity of 46%-69%[4,11]. The lower sensitivity for DSA might be a result of the limited viewing directions (usually two). Besides MDCTA and DSA, MRA has been used for the assessment of atherosclerotic carotid plaque surface morphology. One study made a comparison between these techniques (n=22, number of carotids studied 44) and concluded that luminal surface irregularities were most frequently seen at CTA, and that with CTA and MRA more ulcerations were detected than with DSA[13]. Saba et al.[15] have recently showed that ultrasound has a high specificity (93%), but a low sensitivity (38%) for the detection of carotid ulceration, which is in concordance with previous studies[20,21]. The low sensitivity can be ascribed, in part, to the fact that acoustic shadowing

from calcifications obscures the presence of ulcerations.

A recent histological study[22] of symptomatic carotid endarterectomy specimens from 526 consecutive patients with a stenosis degree of 75-90% found ulceration in 58% of the specimens. The discrepancy in the frequencies of ulceration between MDCTA and histology in patients with a severe degree of stenosis can be explained by the higher resolution of histology which enables the detection of small ulcerations, the higher volume of calcifications in severe stenosis, which hampers accurate detection of small ulcerations by MDCTA. In addition, thrombus formation on the location of a rupture may fill the ruptured site, which will lead to non-visualization with MDCTA.

Lovett et al.[8] characterized ulcerations as type 1 to 4, and determined that type 1 and type 3 are the most frequent type of rupture; the present study confirms these findings. However, the categorization of ulcers is only important when their occurrence can be related to different clinical behavior; this has not yet been demonstrated.

Ulcerations were most frequently seen at the proximal site of the maximum stenosis. The ECST data revealed the same distribution of ulcer location in the carotid artery (71% at the proximal site) as in the present study[9]. An intracoronary ultrasound study found that 69% of the ulcerated ruptured plaques (80%) were proximal to the minimal lumen site[23]. The proximal site as predilection site for ulceration is in concordance with shear stress theories. It is thought that high shear stress on the plaque surface (due to the lumen narrowing) weakens the cap through numerous signaling pathways[10]. Indeed, in a recent case report Groen et al.[24] showed in a serial MRI study that the ulceration was located at the high shear stress region. Shear stress may therefore play an important role in the rupture of plaques.

The present study showed that plaque ulceration is not only present in high-grade stenosis, but can also occur in hemodynamically insignificant stenosis. A similar observation was made on the ECST data[4]. Most of the patients with an ischemic stroke did not have a severe stenosis, despite the accumulation of a substantial amount of atherosclerotic plaque in the carotid bifurcation. Detection of plaque ulceration thereby provides a clue to the underlying pathophysiology of the previously occurring ischemic stroke: rupture of the plaque may have been accompanied by thrombus formation and embolisation of plaque material or thrombus into the intracranial circulation. In addition, detection of plaque ulceration indicates that a patient has an increased risk of a new ipsilateral ischemic stroke[4]. Whether surgical or endovascular intervention in symptomatic patients without a significant stenosis but with a plaque ulceration is justified remains to be demonstrated in larger prospective studies. Ideally, these studies should use the non-invasive imaging tools that are currently available.

In the present study hypercholesterolemia is positively and significantly associated with the presence of complicated plaques, while smoking, had a positive (but not significant) association with the presence of complicated

plaques. Previous studies with univariate analysis revealed associations between irregular plaques and gender[3], age[4], carotid stenosis[4], hypercholesterolemia[4] and previous myocardial infarction[4]. Since irregular plaques are related to the severity of stenosis, multivariable analysis with adjustment for the severity of stenosis is necessary to demonstrate whether certain cardiovascular risk factors are independently related to the presence of irregular plaques.

The association with hypercholesterolemia might be explained by the atherogenic effect of lipoprotein(a) in the presence of high plasma LDL-C levels, which increases lipid deposition in atherosclerotic plaque[25,26], making the plaque probably more vulnerable for rupture. Cigarette smoking is considered to influence inflammation and hemostasis in such a way that plaque inflammation and thrombogenicity increases, with cap degradation, plaque rupture and subsequent thrombus formation as a possible result[27].

In the present study, ulcerated and irregular plaques are significantly more common in the ipsilateral symptomatic carotid artery than in the asymptomatic carotid artery, which is in line with the findings of Sitzer et al.[28], who concluded that plaque ulceration is more common in carotid endarterectomy specimens from symptomatic arteries, than from asymptomatic arteries. However, multivariate analysis showed that this difference does not remain significant when severity of stenosis was added to the model. This indicates that besides local factors like plaque composition or shear stress, also systemic factors are important in the occurrence of plaque rupture. A reasoning that is supported by the findings of Rothwell et al.[29], who reported that patients with irregular plaque in the symptomatic carotid artery were more likely to have irregular plaques in the contralateral artery, and by a study from Fisher et al.[30] which concluded that plaque ulceration was more common in symptomatic patients than in asymptomatic patients, but that the prevalence of ulceration in the ipsilateral and contralateral carotid artery in symptomatic patients was the same.

Although, the recent paper by Saba et al.[15] showed that MDCTA is an excellent technique to evaluate carotid ulceration, we realize that it is a limitation of our study that we do not have a gold standard (e.g. histologic specimens). Unfortunately, correlation with histological results is troublesome, because only patients with a severe stenosis (NASCET >70% stenosis) are eligible for intervention, which in our hospital includes stenting in approximately 50% of the cases. Therefore, it is not possible to obtain histology from a vast majority of patients.

A second limitation of our study is its cross-sectional design. The evaluation of the causal association between severity of stenosis and complicated plaques, between cardiovascular risk factors and complicated plaques, and between complicated plaques and ischemic cerebrovascular disease requires a prospective design in which the atherosclerotic plaque is evaluated serially to detect changes in plaque surface morphology.

Conclusion

This study shows that MDCTA can classify atherosclerotic carotid plaque surface morphology. Furthermore, it shows that the presence of a complicated plaque surface in an atherosclerotic plaque is strongly related with the severity of stenosis, and that the site of ulceration is mostly proximal to the most stenotic site. In addition, it is shown that hypercholesterolemia and probably smoking are related with the presence of complicated plaques.

References

1. Caplan LR. Diagnosis and treatment of ischemic stroke. Jama. 1991;266:2413-2418
2. Warlow C, Sudlow C, Dennis M, Wardlaw J, Sandercock P. Stroke. Lancet. 2003;362:1211-1224
3. Eliasziw M, Streifler JY, Fox AJ, Hachinski VC, Ferguson GG, Barnett HJ. Significance of plaque ulceration in symptomatic patients with high-grade carotid stenosis. North American Symptomatic Carotid Endarterectomy Trial. Stroke. 1994;25:304-308
4. Rothwell PM, Gibson R, Warlow CP. Interrelation between plaque surface morphology and degree of stenosis on carotid angiograms and the risk of ischemic stroke in patients with symptomatic carotid stenosis. On behalf of the European Carotid Surgery Trialists' Collaborative Group. Stroke. 2000;31:615-621
5. Naghavi M, Libby P, Falk E, Casscells SW, Litovsky S, Rumberger J, Badimon JJ, Stefanadis C, Moreno P, Pasterkamp G, Fayad Z, Stone PH, Waxman S, Raggi P, Madjid M, Zarrabi A, Burke A, Yuan C, Fitzgerald PJ, Siscovick DS, de Korte CL, Aikawa M, Juhani Airaksinen KE, Assmann G, Becker CR, Chesebro JH, Farb A, Galis ZS, Jackson C, Jang IK, Koenig W, Lodder RA, March K, Demirovic J, Navab M, Priori SG, Rekhter MD, Bahr R, Grundy SM, Mehran R, Colombo A, Boerwinkle E, Ballantyne C, Insull W, Jr., Schwartz RS, Vogel R, Serruys PW, Hansson GK, Faxon DP, Kaul S, Drexler H, Greenland P, Muller JE, Virmani R, Ridker PM, Zipes DP, Shah PK, Willerson JT. From vulnerable plaque to vulnerable patient: a call for new definitions and risk assessment strategies: Part I. Circulation. 2003;108:1664-1672
6. Polak JF, Shemanski L, O'Leary DH, Lefkowitz D, Price TR, Savage PJ, Brant WE, Reid C. Hypoechoic plaque at US of the carotid artery: an independent risk factor for incident stroke in adults aged 65 years or older. Cardiovascular Health Study. Radiology. 1998;208:649-654
7. Takaya N, Yuan C, Chu B, Saam T, Underhill H, Cai J, Tran N, Polissar NL, Isaac C, Ferguson MS, Garden GA, Cramer SC, Maravilla KR, Hashimoto B, Hatsukami TS. Association between carotid plaque characteristics and subsequent ischemic cerebrovascular events: a prospective assessment with MRI--initial results. Stroke. 2006;37:818-823
8. Lovett JK, Gallagher PJ, Hands LJ, Walton J, Rothwell PM. Histological correlates of carotid plaque surface morphology on lumen contrast imaging. Circulation. 2004;110:2190-2197

9. Lovett JK, Rothwell PM. Site of carotid plaque ulceration in relation to direction of blood flow: an angiographic and pathological study. Cerebrovasc Dis. 2003;16:369-375
10. Slager CJ, Wentzel JJ, Gijsen FJ, Thury A, van der Wal AC, Schaar JA, Serruys PW. The role of shear stress in the destabilization of vulnerable plaques and related therapeutic implications. Nat Clin Pract Cardiovasc Med. 2005;2:456-464
11. Streifler JY, Eliasziw M, Fox AJ, Benavente OR, Hachinski VC, Ferguson GG, Barnett HJ. Angiographic detection of carotid plaque ulceration. Comparison with surgical observations in a multicenter study. North American Symptomatic Carotid Endarterectomy Trial. Stroke. 1994;25:1130-1132
12. Oliver TB, Lammie GA, Wright AR, Wardlaw J, Patel SG, Peek R, Ruckley CV, Collie DA. Atherosclerotic plaque at the carotid bifurcation: CT angiographic appearance with histopathologic correlation. AJNR Am J Neuroradiol. 1999;20:897-901
13. Randoux B, Marro B, Koskas F, Duyme M, Sahel M, Zouaoui A, Marsault C. Carotid artery stenosis: prospective comparison of CT, three-dimensional gadolinium-enhanced MR, and conventional angiography. Radiology. 2001;220:179-185
14. Walker LJ, Ismail A, McMeekin W, Lambert D, Mendelow AD, Birchall D. Computed tomography angiography for the evaluation of carotid atherosclerotic plaque: correlation with histopathology of endarterectomy specimens. Stroke. 2002;33:977-981
15. Saba L, Caddeo G, Sanfilippo R, Montisci R, Mallarini G. Efficacy and sensitivity of axial scans and different reconstruction methods in the study of the ulcerated carotid plaque using multidetector-row CT angiography: comparison with surgical results. AJNR Am J Neuroradiol. 2007;28:716-723
16. de Monye C, Cademartiri F, de Weert TT, Siepman DA, Dippel DW, van Der Lugt A. Sixteen-detector row CT angiography of carotid arteries: comparison of different volumes of contrast material with and without a bolus chaser. Radiology. 2005;237:555-562
17. de Monye C, de Weert TT, Zaalberg W, Cademartiri F, Siepman DA, Dippel DW, van der Lugt A. Optimization of CT angiography of the carotid artery with a 16-MDCT scanner: craniocaudal scan direction reduces contrast material-related perivenous artifacts. AJR Am J Roentgenol. 2006;186:1737-1745
18. de Weert TT, Ouhlous M, Zondervan PE, Hendriks JM, Dippel DW, van Sambeek MR, van der Lugt A. In vitro characterization of atherosclerotic carotid plaque with multidetector computed tomography and histopathological correlation. Eur Radiol. 2005;15:1906-1914
19. Rothwell PM, Gibson RJ, Slattery J, Warlow CP. Prognostic value and reproducibility of measurements of carotid stenosis. A comparison of three methods on 1001 angiograms. European Carotid Surgery Trialists' Collaborative Group. Stroke. 1994;25:2440-2444
20. Bluth EI, McVay LV, 3rd, Merritt CR, Sullivan MA. The identification of ulcerative plaque with high resolution duplex carotid scanning. J Ultrasound Med. 1988;7:73-76

21. Lammie GA, Wardlaw J, Allan P, Ruckley CV, Peek R, Signorini DF. What pathological components indicate carotid atheroma activity and can these be identified reliably using ultrasound? Eur J Ultrasound. 2000;11:77-86
22. Redgrave JN, Lovett JK, Gallagher PJ, Rothwell PM. Histological assessment of 526 symptomatic carotid plaques in relation to the nature and timing of ischemic symptoms: the Oxford plaque study. Circulation. 2006;113:2320-2328
23. Fujii K, Kobayashi Y, Mintz GS, Takebayashi H, Dangas G, Moussa I, Mehran R, Lansky AJ, Kreps E, Collins M, Colombo A, Stone GW, Leon MB, Moses JW. Intravascular ultrasound assessment of ulcerated ruptured plaques: a comparison of culprit and nonculprit lesions of patients with acute coronary syndromes and lesions in patients without acute coronary syndromes. Circulation. 2003;108:2473-2478
24. Groen HC, Gijsen FJ, van der Lugt A, Ferguson MS, Hatsukami TS, van der Steen AF, Yuan C, Wentzel JJ. Plaque rupture in the carotid artery is localized at the high shear stress region: a case report. Stroke. 2007;38:2379-2381
25. Baldassarre D, Tremoli E, Franceschini G, Michelagnoli S, Sirtori CR. Plasma lipoprotein(a) is an independent factor associated with carotid wall thickening in severely but not moderately hypercholesterolemic patients. Stroke. 1996;27:1044-1049
26. Rath M, Niendorf A, Reblin T, Dietel M, Krebber HJ, Beisiegel U. Detection and quantification of lipoprotein(a) in the arterial wall of 107 coronary bypass patients. Arteriosclerosis. 1989;9:579-592
27. MacCallum PK. Markers of hemostasis and systemic inflammation in heart disease and atherosclerosis in smokers. Proc Am Thorac Soc. 2005;2:34-43
28. Sitzer M, Muller W, Siebler M, Hort W, Kniemeyer HW, Jancke L, Steinmetz H. Plaque ulceration and lumen thrombus are the main sources of cerebral microemboli in high-grade internal carotid artery stenosis. Stroke. 1995;26:1231-1233
29. Rothwell PM, Villagra R, Gibson R, Donders RC, Warlow CP. Evidence of a chronic systemic cause of instability of atherosclerotic plaques. Lancet. 2000;355:19-24
30. Fisher M, Paganini-Hill A, Martin A, Cosgrove M, Toole JF, Barnett HJ, Norris J. Carotid plaque pathology: thrombosis, ulceration, and stroke pathogenesis. Stroke. 2005;36:253-257

9

VOLUME AND COMPOSITION OF THE SYMPTOMATIC ATHEROSCLEROTIC CAROTID PLAQUE ON MDCTA AND THE RELATIONSHIP WITH SEVERITY OF STENOSIS AND RISK FACTORS

Sietske Rozie • Thomas T de Weert • Cécile de Monyé •
Philip J Homburg • Hervé L Tanghe • Diederik WJ Dippel • Aad van der Lugt

Recommended for publication in European Radiology

Volume and composition of the symptomatic atherosclerotic carotid plaque on MDCTA and the relationship with severity of stenosis and risk factors

Abstract

Objective

Luminal stenosis as a parameter of carotid artery disease does not necessarily reflect the amount of atherosclerosis. Therefore, we assessed the volume and composition of carotid plaque, and related these to the severity of stenosis and to the presence of risk factors.

Materials and Methods

Hundred patients (61 male; mean age 61 ± 15.3 years, range 19-88 years) with TIA or minor ischemic stroke underwent MDCT angiography. We measured plaque volume (PV) manually. The contribution of different plaque components to the PV was measured with ranges of HU-values (calcification >130 HU, fibrous tissue 60-130 HU, lipid core <60 HU).

Results

Fifty-seven patients had symptomatic carotid plaque and the mean PV was 773 ± 685 mm3. The mean proportion of the lipid, fibrous and calcified plaque component was 18 % ± 12 %, 68 % ± 14 % and 13% ± 11%, respectively. Severity of stenosis and PV were correlated (R = 0.66). Age and smoking were independently related to PV (odds ratio 3.1 per 10 years; 95% CI 1.7-5.6 and 4.9; 95% CI 1.2-19.3). Patients with hypercholesterolemia had significantly less lipid and more calcium in their plaques than patients without hypercholesterolemia (12% versus 26.0% and 9.9% versus 2.0%, respectively). Other risk factors were not significantly related to PV or plaque composition.

Conclusions

PV was moderately related to severity of stenosis. PV was associated with age and smoking and plaque composition was associated with hypercholesterolemia. PV and plaque composition might play a role in the assessment of stroke risk.

Introduction

Accumulation of atherosclerotic plaque causes luminal stenosis in the carotid bifurcation. Stenosis is an important risk factor for (recurrent) stroke and is used to decide which patients could benefit from carotid intervention like endarterectomy and or stent placement. However, most symptomatic patients have only mildly stenotic lesions whereas most patients with severe carotid stenosis are asymptomatic. This demonstrates that other plaque features besides the degree of stenosis play a role in an acute ischemic event and may help in the assessment of stroke risk.

Accumulation of atherosclerotic plaque in the carotid artery may lead to positive remodelling in which the artery enlarges to preserve the luminal area[1]. In addition, a certain amount of atherosclerosis should be present in the carotid bulb before it will cause stenosis. Thus, plaque volume (PV) is usually underestimated by the degree of stenosis.

Rupture of an atherosclerotic plaque, which leads to embolisation of thrombus or plaque material to the intracranial arteries, is considered as an important underlying event of cerebrovascular symptoms. It is current opinion that plaque vulnerability to rupture is related to the composition of the plaque. Therefore, volume of the plaque and the its components (lipid, fibrous tissue, and calcifications) may be parameters, which may help in a better risk prediction and selection of patients who could benefit from surgical or endovascular intervention.

CTA has established itself as an accurate modality to assess the presence of atherosclerotic disease and to grade the severity of stenosis. In addition, MDCTA has the ability to identify the different components (lipid, fibrous tissue and calcifications) of the atherosclerotic plaque and to quantify PV and volume of different components[2-5] In this cross-sectional study, we measured the volume of the atherosclerotic plaque and the proportion of the different plaque components in symptomatic carotid arteries with MDCTA. We analyzed the relationship of these volumes with severity of stenosis and risk factors for atherosclerosis. We hypothesized 1) that severity of stenosis was not closely related to PV and 2) that risk factors are more related to PV than to severity of stenosis.

Materials and Methods

Subjects

We studied 107 consecutive patients with cerebrovascular symptoms (amaurosis fugax, retinal infarct, hemispheric transient ischemic attack, or stroke) in the territory of the carotid artery. Seven patients were excluded from this study because their symptomatic carotid artery was occluded. The study was approved by the Institutional Review Board; all patients had given written informed consent.

Scan protocol and image reconstruction

Scanning of the carotid arteries was performed on a 16-slice MDCT scanner (Siemens, Sensation 16, Erlangen, Germany) with a standardized optimized contrast-enhanced proto-

col (120 kVp, 180 mAs, collimation 16 x 0.75 mm, table feed 12mm/rotation, pitch 1)[6].
Image reconstructions were made with a 12 mm field of view, a matrix size of 512 x 512, a slice thickness of 1.0 mm, an increment 0.6 mm and with an intermediate reconstruction algorithm.

Volume of plaque and its components

We measured plaque and plaque-component volumes with a polymeasure plug-in[5] for the freely available software package ImageJ (Rasband, National Institute of Mental Health, Bethesda, USA).

This plug-in made it possible to draw ROI over the outer vessel wall contour in consecutive axial MDCTA images and to automatically calculate the total number of pixels and the number of pixels of different HV ranges within these ROI. Different HV ranges represent different plaque components (Figure 1).

The cut-point between calcifications and fibrous tissue was set at 130 HU. The cut-point between fibrous tissue and lipid was set at 60 HU as assessed in previous studies[2]. We adjusted the cut-point between atherosclerotic plaque and lumen for each patient on the basis of the full-width-half-maximum principle (mean lumen attenuation plus mean fibrous tissue attenuation (≈ 88 HU) divided by two). The pixels around the lumen, with a HV between 130 HU and the adjusted cut-off value, were considered to be fibrous tissue.

To assess the border between lumen and atherosclerotic plaque it was necessary to draw a second ROI in each image. Normally, the lumen area was then automatically differentiated from atherosclerotic plaque on the basis of the adjusted cut-off value. But in those plaques in which calcifications bordered the lumen and the two structures merged with each other, lumen area and calcifications had to be separated by manual drawing.

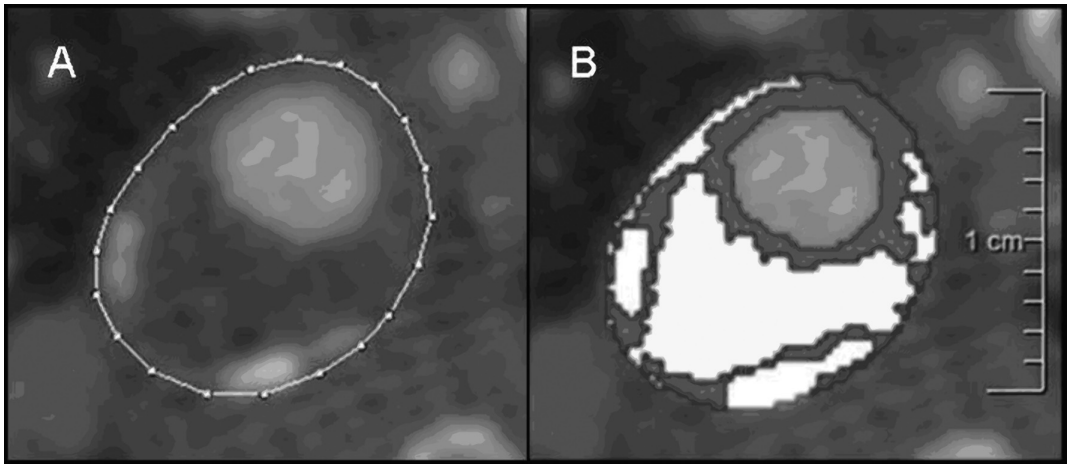

Figure 1. Semi-automatic assessment of plaque component areas in MDCT images. Axial MDCT image of an atherosclerotic carotid plaque; the region of interest is drawn on the outer vessel wall (A). Ranges of Hounsfield values represent 3 different plaque components Yellow = lipid core (<60 HU), red = fibrous tissue (60 to 130 HU), and white = calcification (>130 HU) (B). (A full color version of this illustration can be found in the color section)

The volume of the atherosclerotic plaque and its components was calculated by multiplying the calculated number of pixels, the pixel size and the increment. Two observers (S.R; T.T.d.W.) performed the volume measurements. The proportion of plaque components was calculated as the ratio of volume of the component to the total plaque volume multiplied by 100. The length of the plaque was calculated by multiplying the number of slices which contained plaque with the increment (0.6 mm).

We evaluated the reproducibility of the volume measurements in 56 patients. The averaged interclass correlation coefficient was 0.88 for PV, 0.97 for % calcification, 0.90 for % fibrous tissue and 0.76 for % lipid tissue[5].

Severity of stenosis

One observer (C.d.M.) measured the severity of stenosis according to the NASCET criteria on MPR images parallel to the central lumen line. Severe stenoses with a collapsed distal internal carotid artery were classified as 99%. Negative stenosis grades were considered as a stenosis grade of 0%. We categorized the severity of stenosis into five categories (0%, 1-29%, 30-49%, 50-69% and 70-99%).

Cardiovascular risk factors

We obtained clinical measures and information on risk factors and medication during the patient's visit at the outpatient clinic. Subjects were categorized as currently, ever, or never smoking. Hypertension was defined as systolic blood pressure over 140 and/or diastolic blood pressure over 90 mmHg during 2 episodes of at least 15 minutes of continuous non-invasive blood pressure measurement and/or treatment with antihypertensive medication. Blood-pressure-lowering drugs comprised ACE-inhibitors, calcium- antagonists, beta-blockers, and diuretics.

Hypercholesterolemia was defined as fasting cholesterol over 5.0 mmol/l, and/or use of cholesterol-lowering drugs. Diabetes was defined as fasting serum glucose levels over 7.9 mmol/l, nonfasting serum glucose levels over 11.0 mmol/l, or use of antidiabetic medication.

Information was collected on previous cardiovascular events and conditions (myocardial infarction, atrial fibrillation, angina pectoris, chronic heart failure, coronary artery bypass grafting) and previous cerebrovascular events (ischemic stroke or TIA).

Statistical analysis

Data are presented as mean ± SD. Spearmen's correlation coefficients (Rs) were calculated to analyse the relation between 1) severity of stenosis and PV, 2) the proportion of plaque components and PV and 3) age and PV.

Logistic regression was used to determine the associations between cardiovascular risk factors and PV or stenosis. The highest quartile of volume or stenosis was compared to the lower 3 quartiles. Firstly, age and gender were entered into the model. Secondly, all cardiovascular risk factors were added. To analyze the association of cardiovascular risk factors with plaque composition, we used linear regression, adjusting for age, sex, PV and all risk factors. Because the distribution of the proportion of plaque components was skewed,

we made a natural log-transformation (ln). To calculate the mean ln proportion of plaque components for the presence of significant cardiovascular risk factors, we used analysis of covariance (ANCOVA), adjusting for age, sex, PV and all other risk factors. SPSS 11.0 for Windows (SPSS, Inc, Chicago, Illinois) was used for data analysis.

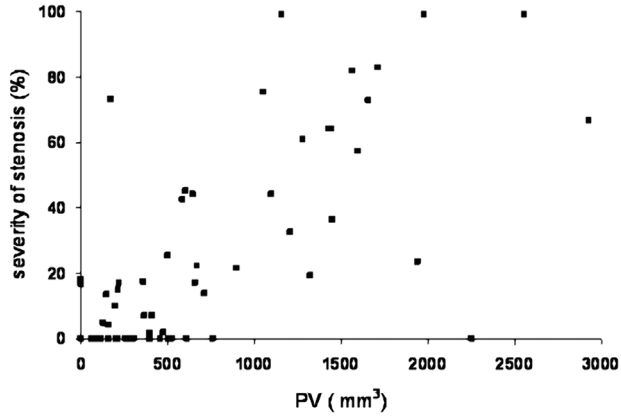

Figure 2. The relation between luminal stenosis and PV.
Scatter plots showing the relation between severity of stenosis (%) and total PV (mm^3) in 57 patients.

Results

Baseline characteristics

The baseline clinical characteristics are presented in table 1. Fifty-seven of 100 patients had atherosclerotic plaque in the symptomatic carotid artery. The length of the 57 symptomatic atherosclerotic plaques was 20.9 ± 13.5 mm (range 3.6–70.2 mm). PV of the 57 atherosclerotic plaques was 773 ± 685 mm3. Fibrous tissue and lipid were present in all plaques. Calcifications were present in 54 of the 57 plaques. The contribution of the lipid, fibrous and calcified plaque component was 18 ± 12 %, 68 ± 14 % and 13 ± 11%, respectively.

Table 1. Demographic and clinical characteristics in patients with cerebrovascular symptoms (n = 100).

Characteristic	
Age (yrs)*	61±15
Male sex (%)	61
Symptoms	
Amaurosis fugax, retinal infarct (%)	27
Transient ischemic attack (%)	19
Ischemic stroke (%)	54
Hypertension (%)	70
Hypercholesterolemia (%)	73
Diabetes Mellitus (%)	11
Smoking: current or past (%)	53
Previous cardiac disease (%)	18
Previous cerebrovascular disease (%)	24

* Mean and standard deviation.

Plaque volume and severity of stenosis

Table 2 shows the volume of the plaque and the contribution of the plaque components for the different grades of stenosis. In 20 out of 61 patients with a stenosis grade of 0%, atherosclerotic plaque was present (PV = 411±472 mm3). In 18 of the 20 patients with a stenosis grade of 1-29% plaque was present with a PV of 543±464 mm3. The correlation between PV and severity of stenosis in the group of patients who had an atherosclerotic plaque (n=57) was moderate with an Rs of 0.66 ($p<0.0001$) (Figure 2 and 3).

Table 2. Severity of stenosis, number of patients with a certain degree of stenosis, number of patients with atherosclerotic plaque and plaque volume (PV) characteristics in the patients with atherosclerotic plaque.

Stenosis(%)	n	n(PV>0)	PV(mm3)*	Calcium(%)*	Lipid(%)*	Fibrous(%)*
0	61	20	411±472	10±8	13±11	76±9
1-29	20	18	543±464	13±13	16±9	70±12
30-49	6	6	930±367	14±10	23±13	63±14
50-69	5	5	1734±675	24±13	26±8	50±7
70-99	8	8	1480±708	14±11	30±13	55±17
Total	100	57	773±685	13±11	18±12	68±14

* Mean and standard deviation.

Plaque volume and plaque composition

Figure 4 shows the relationship between the contribution of calcium, fibrous tissue, and lipid and total PV in the 57 patients with atherosclerotic plaque. With increasing PV, the contribution of fibrous tissue decreased (Rs = -0.83, p<0.001) and the contribution of lipid increased (Rs = 0.62, p<0.001). With an increase in PV the contribution of calcium increased slightly (Rs = 0.42, p=0.001).

Risk factors

There was a moderate relationship between age and PV for both men and women (Rs = 0.493, p=0.001 and Rs = 0.484, p<0.001 respectively). Table 3 shows the age and gender-adjusted odds ratios (ORs) and the multivariable adjusted ORs for associations between cardiovascular risk factors and 1) atherosclerotic carotid PV and 2) severity of stenosis (upper quartile versus lower 3 quartiles). Smoking was independently related to PV (OR 4.9, 95%CI 1.2-19.3) and to severity of stenosis (OR 4.6, 95%CI 1.2-18.1).

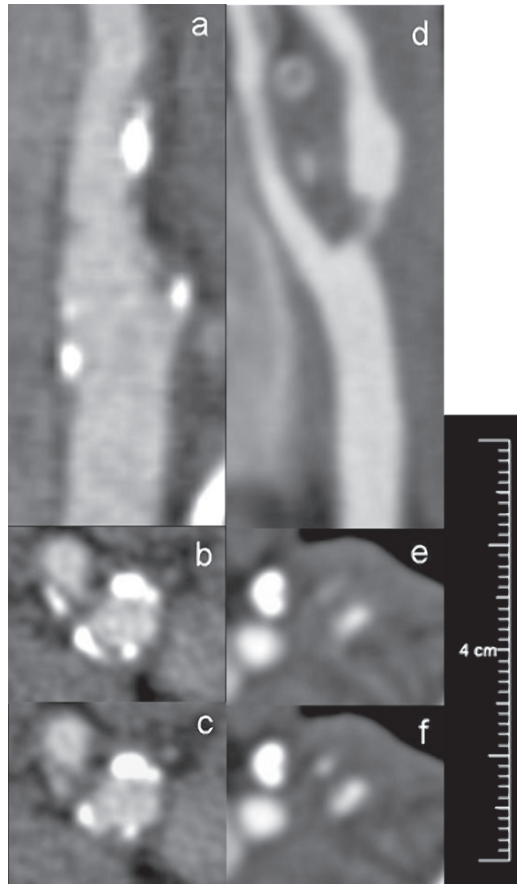

Figure 3. CT angiograms of the carotid bifurcation with lesion Sagittal (A,D) and axial (B,C, E,F) images of atherosclerotic plaques in the carotid bifurcation The left panels showed an extensive calcified atherosclerotic plaque (PV=1318 mm3) without severe stenosis (20%). The right panels revealed a focal lesion at origin of internal carotid artery with moderate amount of atherosclerosis (PV=169 mm3) but a severe stenosis (73%).

Table 3. Relation between risk factors and atherosclerotic plaque volume or severity of stenosis in the symptomatic carotid artery (n=100).

Variable	OR† (95% CI)* adjusted for age and gender	OR (95% CI) adjusted for all risk factors
Plaque volume		
Age (per 10 years)	2.3(1.4-3.6)	3.1(1.7-5.6)
Gender (male versus female)	2.0(0.7-6.3)	1.7(0.5-5.5)
Hypertension (yes versus no)	1.7(0.5-5.9)	2.3(0.6-8.7)
Hypercholesterolemia (yes versus no)	0.9(0.3-3.0)	0.8(0.2-3.0)
Diabetes mellitus (yes versus no)	0.4(0.1-2.3)	0.5(0.1-4.0)
Smoking (ever versus never)	3.9(1.1-13.2)	4.9(1.2-19.3)
Previous cardiac disease (yes versus no)	1.8(0.5-6.3)	2.5(0.6-9.6)
Previous cerebrovascular disease (yes versus no)	1.3(0.4-4.2)	1.0(0.3-3.6)
Severity of stenosis		
Age (per 10 years)	2.0(1.3-3.0)	2.9(1.6-5.4)
Gender (man versus female)	2.0(0.7-6.1)	1.9(0.6-6.2)
Hypertension (yes versus no)	1.7(0.5-5.6)	1.7(0.5-6.0)
Hypercholesterolemia (yes versus no)	1.8(0.5-5.9)	2.5(0.6-10.7)
Diabetes mellitus (yes versus no)	0.4(0.1-2.3)	0.5(0.1-4.1)
Smoking (ever versus never)	4.4(1.3-14.8)	4.6(1.2-18.1)
Previous cardiac disease (yes versus no)	0.9(0.8-7.7)	0.8(0.2-3.3)
Previous cerebrovascular disease (yes versus no)	2.5(0.8-7.7)	2.4(0.7-8.4)

*CI=confidence interval. †OR=odds ratio

Table 4. Cardiovascular risk factors and the ln proportion calcium, lipid and fibrous tissue in patients with atherosclerotic plaque (n=57)

Variable	**Ln calcium**	**Ln lipid**	**Ln fibrous**
Age (per 10 years)	0.21(-0.12;0.54)	-0.09(-0.23;0.05)	-0.02(-0.05;0.02)
Gender (male versus female)	0.03(-0.7;0.8)	0.15(-0.17;0.46)	-0.02(-0.10;0.06)
Plaque volume mm3 (per SD)	0.46(0.07;0.85)	0.39(0.23;0.55)	-0.18(-0.22;-0.14)
Hypertension (yes versus no)	-0.38(-1.21;0.45)	0.17(-0.18;0.51)	-0.04(-0.13;0.04)
Hypercholesterolemia (yes versus no)	1.61(0.70;2.53)	-0.76(-1.14;-0.38)	0.03(-0.06;0.13)
Smoking (ever versus never)	0.52(-0.28;1.33)	0.10(-0.26;0.42)	-0.07(-0.15;0.01)
Diabetes mellitus (yes versus no)	-0.20(-1.53;1.13)	0.23(-0.32;0.78)	-0.04(-0.18;0.10
Previous cardiac disease (yes versus no)	0.84(-0.00;1.69)	-0.30(-0.65;0.05)	0.02(-0.07;0.11)
Previous cerebrovascular disease (yes versus no)	-0.44(-1.26;0.38)	0.17(-0.17;0.51)	0.04(-0.04;0.13)

Values are adjusted mean differences (95%CI) in a natural log-transformation (ln) of the proportion of plaque component. The linear regression analysis was adjusted for age, gender, plaque volume, and all cardiovascular risk factors.

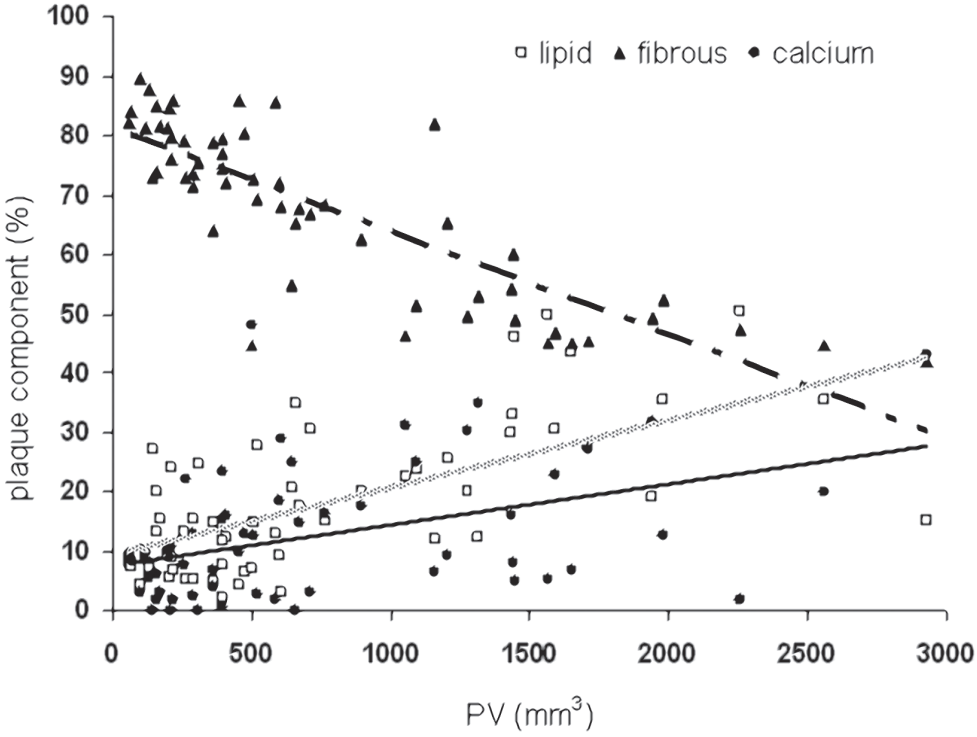

Figure 4. The relation between PV and plaque components.
Scatter plot demonstrates the relation between the contribution of the different components of the plaque and total plaque volume in 57 patients.

Table 4 shows the associations between cardiovascular risk factors and the contribution of the different plaque components in the patients with atherosclerotic plaque (n=57). Patients with hypercholesterolemia had a significantly higher contribution of calcium and a significantly lower contribution of lipid in the atherosclerotic plaque. The mean proportion of calcium in the plaque of patients with and without hypercholesterolemia was 9.9% and 2.0%, respectively. The ln mean difference was 1.61 (95%CI 0.70-2.53). The mean proportion of lipid in the plaque of patients with and without hypercholesterolemia was 12.2% and 26.0%, respectively. The ln mean difference was -0.76 (95%CI -1.14 - -0.38).

Discussion

In this study, we quantified and characterized atherosclerotic carotid plaque with MDCTA and examined the relation between PV and the severity of luminal stenosis. In conformity with our hypothesis, the relation between the severity of luminal stenosis and PV was not

strong. Smoking was associated with both PV and severity of stenosis. Our hypothesis that cardiovascular risk factors were more strongly associated with PV than severity of stenosis was not supported in this study. We demonstrated that an increasing PV is associated with a change in plaque composition: the proportion of calcium and lipid increased and the proportion of fibrous tissue decreased. Finally, hypercholesterolemia was independently related to plaque composition.

Plaque volume and stenosis

Assessment of the severity of atherosclerosis in the carotid artery has long been based on the evaluation of luminal compromise caused by the accumulation of atherosclerotic plaque. The main reason for this approach was the availability of (digital subtraction) angiography and the absence of an optimal cross-sectional imaging tool for quantification of the amount of atherosclerotic plaque. The results of the NASCET and ECST trial established the severity of luminal stenosis as an important parameter in risk prediction and decision-making.

There are several reasons why severity of stenosis is not a good reflection of the amount of atherosclerotic disease. Firstly, extensive atherosclerotic disease can be present without stenosis of the lumen and vice versa, stenosis can be caused by a focal accumulation of a small amount of atherosclerotic plaque (Figure 3). Secondly, the configuration of a normal carotid bulbus and bifurcation allows the accumulation of extensive atherosclerotic plaque before a luminal stenosis become visible on angiography. Thirdly, vessel remodelling plays an additional role since the discrepancy between the atherosclerotic plaque load and angiographic appearance of the lumen is also present in other vessel beds. A recent MRI study shows that luminal stenosis provides an incomplete picture of atherosclerotic progression and regression and that expansive remodelling occurs specifically in the earlier stage of atherosclerosis development in carotid arteries[7].

Multiple studies with intracoronary ultrasound have demonstrated that atherosclerotic disease is present in angiographically normal coronary segments[8, 9]. This phenomenon could be demonstrated also in coronary arteries with MDCTA.

It is well known that atherosclerosis with low-grade stenosis in the carotid bifurcation may result in cerebrovascular events[10]. In the present study, a relatively large proportion of the patients with cerebrovascular symptoms had atherosclerotic plaque with no luminal narrowing measured according to the NASCET criteria. Since PV is a better descriptor of the severity of atherosclerotic disease than degree of stenosis and CT and MRI allows nowadays the quantification of atherosclerotic plaque we advocate to evaluate the role of PV as an additional parameter in the assessment of stroke risk and finally in treatment decision making.

Plaque volume and composition

The composition of the atherosclerotic plaque changes during the progression of atherosclerotic disease and this plays an important role in the development of a vulnerable plaque. Until now most data on the temporal change of the composition of the atherosclerotic plaque is based on cross-sectional studies in which vessel specimens obtained during autopsy or operation (carotid endarterectomy) were evaluated. Atherosclerotic plaques were classified based on their composition and that classification was considered to reflect the temporal natural history of atherosclerotic disease[11]. Such studies have provided tremendous information on the process of atherosclerotic disease and the occurrence of clinical events. However, much more can be expected from serial evaluation of an atherosclerotic plaque with clinical imaging tools because this will truly provide insight in the natural history of atherosclerotic plaque and in the causal association of changes in plaque composition and clinical events. With regard to the natural history, the present cross-sectional imaging study shows that plaque composition changes with increasing PV. According to the AHA-criteria, which describe that advanced atherosclerotic lesions in the carotid artery contain more lipid and more calcium, we found an increase of the proportion lipid and calcification with increasing PV. It will be of interest to confirm with serial MDCTA these temporal changes in PV and composition. One other cross-sectional imaging study has also demonstrated that plaque composition in the carotid artery changed with an increase in plaque content: a study on the relation between IMT and quantity of carotid calcification concludes that these two features were strongly associated[12]. MRI studies of the carotid artery were mostly performed on severely diseased arteries and reports on this relation between plaque size and plaque composition are not available yet.

Plaque volume and cardiovascular risk factors

The relation between cardiovascular risk factors and the severity of atherosclerotic disease is difficult to evaluate and most studies have correlated cardiovascular risk factors to indirect instead of direct measures of atherosclerotic plaque burden[13]. Several large population-based studies have demonstrated independent associations between cardiovascular risk factors like smoking, hypertension, hypercholesterolemia and diabetes and US measured IMT in the carotid artery[14], severity of stenosis in the carotid artery[15], carotid calcification[16], coronary stenosis[13], and coronary calcification[13].

In our study, smoking was independently related to severity of stenosis and PV. Other risk factors did not reach a statistically significant association due to the limited number of studied patients. Severity of stenosis as an indirect parameter of atherosclerotic plaque burden has its limitations. It reflects luminal narrowing and not the true amount of atherosclerotic disease. Two recent studies demonstrated that the relation between severity of stenosis and cardiovascular risk factors was less strong than the relation between IVUS-assessed atherosclerotic plaque burden and cardiovascular risk factors was[17, 18]. Nicholls et al. concluded that probably different mechanisms drive stenosis development and atheroma accumulation[17].

In the present study, we hypothesized that the risk factors were more related to PV than to severity of stenosis. Probably due to the smaller number of patients in comparison to the coronary studies, we did not find a difference in the relation with risk factors.

Plaque composition and cardiovascular risk factors

Besides the association between cardiovascular risk factors and PV, it might be that the risk factors are also associated with plaque composition. Plaque composition is considered as an important feature of the so-called vulnerable plaque. Histological studies that examined carotid endarterectomy specimens have shown that the composition of the plaque is influenced by cardiovascular risk factors: hypercholesterolemia and hyperfibrinogenemia were correlated with plaques rich in foam cells[19, 20].

To our knowledge, this is the first study, which describes the relationship between the proportions of three different carotid plaque components measured with MDCTA, and risk factors for atherosclerosis. We found that hypercholesterolemia was independently associated with the proportion of lipid and calcium in the plaque. In contrast to the histological studies, we found that patients with hypercholesterolemia had a smaller proportion lipid and larger proportion calcium in their symptomatic plaques. This might be explained by the large proportion of patients on lipid lowering drugs. IVUS studies in coronary arteries have revealed that statins reduce the lipid content of atherosclerotic plaques[21]. MRI studies on the carotid plaque have shown that prolonged lipid lowering drug therapy is associated with markedly decreased lipid content[22].

Limitations

The first limitation of this study is the relatively small number of patients on whom we performed our analysis. We expect that analysis of a larger number of patients will provide more evidence for the associations we investigated. A second limitation is the cross-sectional design of this study. Longitudinal studies are necessary to prove the value of PV as a parameter for risk stratification.

Despite these limitations, the conclusion of our study might have some clinical implications. Firstly, the quantity of atherosclerotic plaque, expressed as plaque volumes, was not closely associated with the severity of stenosis, which implicates that PV might be an important additional parameter in the analysis of atherosclerosis in the carotid artery. Secondly, PV and plaque composition are related to each other and to risk factors for atherosclerosis. Non-invasive imaging of these plaque parameters will increase the understanding of the natural history of atherosclerotic disease in humans.

References

1. Glagov S, Weisenberg E, Zarins CK, Stankunavicius R, Kolettis GJ. Compensatory enlargement of human atherosclerotic coronary arteries. N Engl J Med 1987;316:1371-1375
2. de Weert TT, Ouhlous M, Meijering E, et al. In vivo characterization and quantification of atherosclerotic carotid plaque components with multidetector computed tomography and histopathological correlation. Arterioscler Thromb Vasc Biol 2006;26:2366-2372
3. Nandalur KR, Hardie AD, Raghavan P, Schipper MJ, Baskurt E, Kramer CM. Composition of the stable carotid plaque: insights from a multidetector computed tomography study of plaque volume. Stroke 2007;38:935-940
4. Wintermark M, Jawadi SS, Rapp JH, et al. High-resolution CT imaging of carotid artery atherosclerotic plaques. AJNR Am J Neuroradiol 2008;29:875-882
5. de Weert TT, de Monye C, Meijering E, et al. Assessment of atherosclerotic carotid plaque volume with multidetector computed tomography angiography. Int J Cardiovasc Imaging 2008
6. de Monye C, Cademartiri F, de Weert TT, Siepman DA, Dippel DW, van Der Lugt A. Sixteen-detector row CT angiography of carotid arteries: comparison of different volumes of contrast material with and without a bolus chaser. Radiology 2005;237:555-562
7. Saam T, Yuan C, Chu B, et al. Predictors of carotid atherosclerotic plaque progression as measured by noninvasive magnetic resonance imaging. Atherosclerosis 2006
8. Mintz GS, Painter JA, Pichard AD, et al. Atherosclerosis in angiographically "normal" coronary artery reference segments: an intravascular ultrasound study with clinical correlations. J Am Coll Cardiol 1995;25:1479-1485
9. Hausmann D, Johnson JA, Sudhir K, et al. Angiographically silent atherosclerosis detected by intravascular ultrasound in patients with familial hypercholesterolemia and familial combined hyperlipidemia: correlation with high density lipoproteins. J Am Coll Cardiol 1996;27:1562-1570
10. Wasserman BA, Wityk RJ, Trout HH, 3rd, Virmani R. Low-grade carotid stenosis: looking beyond the lumen with MRI. Stroke 2005;36:2504-2513
11. Stary HC, Chandler AB, Dinsmore RE, et al. A definition of advanced types of atherosclerotic lesions and a histological classification of atherosclerosis. A report from the Committee on Vascular Lesions of the Council on Arteriosclerosis, American Heart Association. Arterioscler Thromb Vasc Biol 1995;15:1512-1531
12. Allison MA, Tiefenbrun J, Langer RD, Wright CM. Atherosclerotic calcification and intimal medial thickness of the carotid arteries. Int J Cardiol 2005;103:98-104
13. Schmermund A, Baumgart D, Gorge G, et al. Measuring the effect of risk factors on coronary atherosclerosis: coronary calcium score versus angiographic disease severity. J Am Coll Cardiol 1998;31:1267-1273

14. Bots ML, Hofman A, De Jong PT, Grobbee DE. Common carotid intima-media thickness as an indicator of atherosclerosis at other sites of the carotid artery. The Rotterdam Study. Ann Epidemiol 1996;6:147-153
15. Mast H, Thompson JL, Lin IF, et al. Cigarette smoking as a determinant of high-grade carotid artery stenosis in Hispanic, black, and white patients with stroke or transient ischemic attack. Stroke 1998;29:908-912
16. Allison MA, Criqui MH, Wright CM. Patterns and risk factors for systemic calcified atherosclerosis. Arterioscler Thromb Vasc Biol 2004;24:331-336
17. Nicholls SJ, Tuzcu EM, Crowe T, et al. Relationship between cardiovascular risk factors and atherosclerotic disease burden measured by intravascular ultrasound. J Am Coll Cardiol 2006;47:1967-1975
18. Kahlon JP, Torey J, Nordstrom CK, et al. The impact of coronary artery disease risk factors on intravascular ultrasound-derived morphologic indices of human coronaries. Echocardiography 2006;23:308-311
19. Spagnoli LG, Mauriello A, Palmieri G, Santeusanio G, Amante A, Taurino M. Relationships between risk factors and morphological patterns of human carotid atherosclerotic plaques. A multivariate discriminant analysis. Atherosclerosis 1994;108:39-60
20. Mauriello A, Sangiorgi G, Palmieri G, et al. Hyperfibrinogenemia is associated with specific histocytological composition and complications of atherosclerotic carotid plaques in patients affected by transient ischemic attacks. Circulation 2000;101:744-750
21. Kawasaki M, Sano K, Okubo M, et al. Volumetric quantitative analysis of tissue characteristics of coronary plaques after statin therapy using three-dimensional integrated backscatter intravascular ultrasound. J Am Coll Cardiol 2005;45:1946-1953
22. Zhao XQ, Yuan C, Hatsukami TS, et al. Effects of prolonged intensive lipid-lowering therapy on the characteristics of carotid atherosclerotic plaques in vivo by MRI: a case-control study. Arterioscler Thromb Vasc Biol 2001;21:1623-1629

SUMMARY AND CONCLUSIONS

This thesis evaluates the role of MDCT angiography in 1) the depiction of atherosclerotic disease and subsequent luminal stenosis in the arteries that supplies the brain with blood, and 2) the assessment of atherosclerotic plaque features that have been related to plaque vulnerability.

The studies can be subdivided in three main categories: 1) optimization of data acquisition protocol, 2) validation studies, including assessment of the accuracy of MDCTA in comparison to histology and interobserver studies, and 3) clinical cross-sectional studies.

Part 1: Optimization of contrast, scanning and reconstruction protocol

Optimization of contrast material injection protocol with a saline bolus chaser was evaluated in **Chapter 1**. Contrast material is expensive and potentially nephrotoxic. The use of a saline bolus chaser after contrast material administration can potentially decrease the use of contrast material. This study revealed that the addition of a 40 ml bolus chaser to 80 ml contrast material results in a significantly higher enhancement in the supra-aortic arteries. The peak enhancement was near the carotid bifurcation. However, decreasing the volume of contrast material from 80 ml to 60 ml, when using a bolus chaser, results in significantly lower vessel enhancement. The study also revealed that vessel enhancement was inversely correlated with body weight. Therefore, 60 ml contrast media with 40 ml saline chaser was sufficient for optimal vessel attenuation in patients weighing less than 75 kg.

Scan direction in CTA is normally based on the direction of the blood flow. With a caudocranial scan direction the presence of undiluted contrast material in the subclavian vein, brachiocephalic vein and/or superior caval vein frequently produces perivenous artifacts, which can obscure adjacent structures and hamper adequate vessel imaging.

The work in **Chapter 2** shows that a change in scan direction from caudocranial to craniocaudal reduced the number of perivenous artifacts and that, although arterial enhancement slightly decreased, a better evaluation of the ascending aorta and origo of the supraaortic arteries was possible.

Blooming artifacts of calcifications on CT images result in a larger appearance of the calcifications, which hampers an accurate characterization of the non-calcified part of the plaque and quantification of plaque components. An optimal voltage and CT image reconstruction algorithm setting might reduce this hampering effect. In **Chapter 3** we show that increasing the tube energy, reduces the size of the calcifications. Furthermore, we demonstrated that smooth and sharp reconstructed images resulted in less interpretability due to averaging of contrast differences and edge-enhancement artefacts, respectively, and that intermediate algorithms showed good interpretability.

Based on these studies, we recommend to use 120 kVp and a medium sharp reconstruction algorithm for atherosclerotic plaque imaging.

Part 2: Validation studies

MDCT angiography has the potential to characterize and quantify plaque components in carotid endarterectomy specimens. To validate this technique, we performed an in vitro and in vivo study. In the first study we matched MDCTA images of 15 endarterectomy specimens with corresponding histologic sections, and measured the Hounsfield unit value (HV) of pure lipid regions and pure fibrous regions. A receiver-operating-characteristic curve revealed 60 HU as the optimal cut-off point to differentiate between lipid and fibrous tissue (**Chapter 3**).

Subsequently we matched in vivo MDCTA images of 15 significant atherosclerotic lesions with corresponding histologic sections. We determined the HV of pure lipid regions and pure fibrous regions. Again, 60 HU emerged as the optimal cut-off point to differentiate between lipid and fibrous tissue. Re-analysis of the in vivo MDCTA images, in which all hypodense regions with a HV <30 or <60 HU were detected based on thresholding, revealed that the positive predictive value of a hypodense region in the plaque with a density value <30 HU for a lipid-rich region was 97%, while the positive predictive value of a hypodense region with a density value between 30 and 60 HU was 23% (**Chapter 4**).

Besides the detection of specific plaque components MDCTA enables to quantify the plaque volume, and the absolute and relative contribution of specific plaque components to the total plaque volume. With freely available software and custom-made plug-ins we were able to semi-automatically assess plaque and plaque component areas in the MDCT images. The in vitro study revealed strong correlations between MDCTA and histology area measurements for total plaque area, calcified area and lipid area (R^2=0.81, R^2=0.83 and R^2=68, respectively) and a poor correlation for fibrous tissue area measurements (R^2=0.26) (**Chapter 3**). Our in vivo study showed strong correlations for total plaque area, calcified area and fibrous area (R^2=0.73, R^2=0.74, and R^2=0.76, respectively) and a poor correlation for lipid area (R^2=0.24). However, when we performed an exploratory analysis by evaluating the lipid area measurements in severely and mildly calcified plaques the correlation between lipid areas improved for the mildly calcified plaques, while it remained poor for the severely calcified plaques (**Chapter 4**).

Because plaque and plaque component area measurements are performed semi-automatically with a custom-made software tool, we performed an interobserver variability study. The in vivo MDCTA area measurements of two observers showed significant differences ($p<0.05$) for the assessment of total plaque area, fibrous tissue area and lipid core area. The lumen area and calcified area were assessed with no significant difference ($p>0.05$). The interobserver coefficients of variation for the absolute measurement of lumen, plaque, calcified, fibrous tissue and lipid core areas were: 4%, 19%, 16%, 21% and 40%, respectively, and the interobserver coefficients of variation for the relative measurement (%) of calcified, fibrous tissue and lipid core areas were: 26%, 10% and 20%, respectively (**Chapter 4**).

After this validation, the software tool was updated to allow analysis of consecutive MDCTA images in order to measure plaque volume and plaque component volume. An interobserver study revealed that the interclass correlation coefficient (ICC) was excellent for all volume measurements (ICC>0.80), except for the lipid core volume measurements, for which it was good (ICC=0.76 (range 0.54-0.87)). The coefficient of variation between observers for plaque volume ranged from 17 to 24%, for calcified volume it ranged from 13 to 33%, for fibrous tissue volume from 18 to 24%, for lipid core volume from 37 to 47%, and for lumen volume from 3 to 10%. The coefficient of variation between observers for the assessment of calcified volume percentage ranged from 15 to 26%, for fibrous volume percentage from 10 to 15%, and for lipid core volume percentage from 21 to 30% (**Chapter 5**).

The same software tool was used to assess the volume of intracranial calcifications and was also validated by an observer variability analysis. We showed that the ICC between two observers for the assessment of intracranial calcifications was excellent (ICC = 0.99), and that the coefficient of variation for the interobserver differences was very low (< 7%). Furthermore, it was shown that the absolute differences between observers did not depend on the size of the calcifications (**Chapter 7**).

Finally, the observer variability in the assessment of plaque surface morphology was analysed. Two observers agreed on the presence of ulcerated plaque in all cases (kappa = 1; 95%CI =0.86-1.00), on the presence of irregular plaque in 93% of the cases (kappa =0.84; 95%CI = 0.70-0.97), and on the location of plaque ulceration in 96% of the cases (kappa =0.91; 95% = 0.54-1.00) (**Chapter 8**).

Part 3: Clinical studies

The first clinical study (**Chapter 7**) revealed that intracranial internal carotid artery calcifications were very frequent in patients with cerebrovascular symptoms. Men more frequently had intracranial calcifications than women (71% and 56%, respectively) and the volumes were larger in men (66 ± 124 mm^3 vs. 33 ± 91 mm^3, respectively). Presence and size of the calcifications were associated with higher age. The presence or volume of calcifications was independently associated with smoking, hypercholesterol-emia, history of cardiac disease, and history of ischemic cerebrovascular disease.

Furthermore, we showed that the degree of calcifications does not differ between the symptomatic and contralateral asymptomatic artery. Intracranial calcifications were not related to the type of symptoms (amaurosis fugax versus TIA or minor stroke).

.

Our second clinical study (**Chapter 8**) showed that MDCTA can differentiate and classify ulcerated, irregular and smooth plaques. The presence of ulcerated plaques in the carotid artery was strongly related with the severity of stenosis. Ulcerated plaques were significantly ($p<0.001$) more common in carotid arteries with stenosis >30%, than in those with stenosis <30% (40% versus 9%, respectively; $p=0.001$). The ulceration was mostly located proximal to the site with the severest stenosis. This finding supports the hypothesis that shear stress

plays a crucial role in the development of vulnerable plaque and plaque rupture.

Hypercholesterolemia and probably smoking were independently related to the presence of complicated plaques (ulcerated and/or irregular).

Symptomatic carotid arteries more often showed a complicated plaque surface than asymptomatic carotid arteries (25% vs 18%, respectively), however this is fully attributed to a significantly higher degree of stenosis in the symptomatic arteries. A complicated plaque was less often observed among patients with amaurosis fugax (17%) compared to patients with focal cerebral ischemia (28%).

In our third clinical study (**Chapter 9**) we measured the volume of the atherosclerotic plaque and the proportion of the different plaque components in symptomatic carotid arteries with MDCTA. We showed that plaque volume was moderately related to severity of stenosis, and that plaque volume was associated with age and smoking. In addition, it appeared that hypercholesterolemia was positively associated with a larger volume of calcifications, and with a smaller volume of lipid.

Conclusions

From the first part of this thesis we can conclude that an optimal protocol for MDCT angiography of the supra-aortic arteries incorporates the use of 80 ml contrast material and a 40 ml saline bolus chaser, a craniocaudal scan direction, and in respect to atherosclerotic carotid plaque imaging a tube current of 120 kVp and an intermediate reconstruction algorithm.

The second part of this thesis allows to conclude that MDCTA is capable of characterizing and quantifying plaque and plaque component areas in good correlation with histology. However, lipid core can only be adequately quantified in mildly calcified plaques, and in vivo assessment of atherosclerotic plaque and plaque component volumes is feasible with a moderate reproducibility. In addition we can conclude that, with MDCT angiography, intracranial carotid artery calcifications can reproducibly be quantified and that carotid plaque surface morphology can be assessed with a high reproducibility.

In the third part of this thesis we evaluated the characteristics of possible MDCTA-assessed plaque parameters (the volume of intracranial calcifications, carotid plaque morphology, and carotid plaque volume and plaque component volumes). Associations were found with several cardiovascular risk factors. Some plaque parameters were related to the presence and type of cerebrovascular symptomatology.

We conclude that atherosclerotic plaque parameters can be imaged adequately with MDCTA. These parameters seem to have a possible additional value, besides the degree of stenosis, as a marker of atherosclerotic disease and as predictor of (recurrent) ischemic cerebrovascular events.

Direction of further research

MDCTA emerges as an efficient means to image vulnerable atherosclerotic plaque parameters. Furthermore, we hypothesize that MDCTA-assessed vulnerable plaque parameters are at least equally important as luminal stenosis for the development of acute neurovascular events. Therefore, follow-up studies are planned that will explore the association between these vulnerable plaque parameters and (recurrent) ischemic cerebrovascular events.

In addition, the required prospective design of these studies allows assessment of changes in serially imaged vulnerable plaque parameter characteristics, which might further clarify the natural course of atherosclerotic disease in the carotid arteries (Figure 1.). This follow-up allows to evaluate the role of shear stress in the

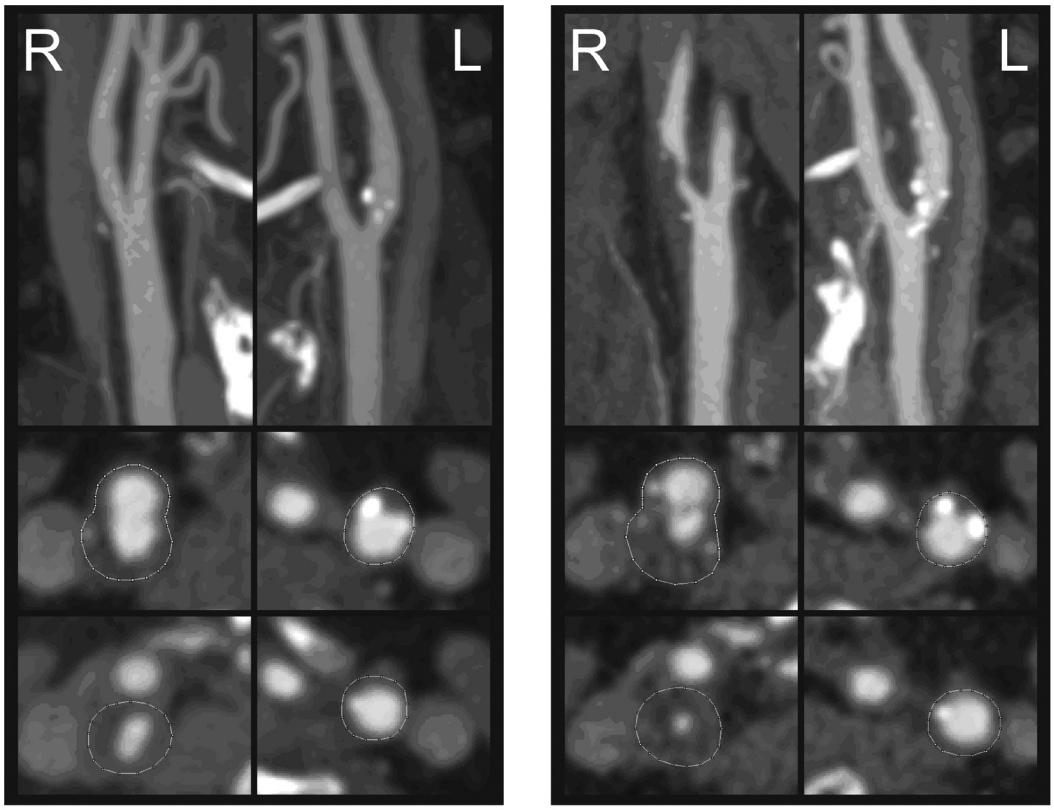

Stenosis(%)	Plaque (mm³)	Lipid (mm³)	Fibrous (mm³)	Calcified (mm³)
R 60→90	+201	+211	-19	+9
L 30→30	+206	+41	+31	+35

Figure 1. Serial imaging by MDCT angiography of a bilateral atherosclerotic carotid bifurcation allows the detection of changes in stenosis degree, plaque volume and plaque component volume.

development of plaque rupture. Shear stress is most frequently found at the upstream part of a plaque. However, little is known about the influence of shear stress on plaque progression, change in plaque composition and plaque surface morphology (rupture). MDCTA-based 3D lumen geometry assessment allows the calculation of hemodynamic parameters such as local shear stress. Serial MDCTA will reveal the temporal changes in shear stress, plaque volume and composition, as well as the prevalence and incidence of plaque rupture.

Specific research questions we plan to address are: a) What is the prevalence of atherosclerotic disease (plaque volume, composition, rupture and shear stress) in patients with TIA or minor ischemic stroke? b) What is the natural course of atherosclerotic disease in the carotid artery? c) Can a change in plaque volume, plaque composition and plaque rupture be predicted based on risk factor profiles, current plaque status and shear stress? and d) What is the predictive value of atherosclerotic plaque features (at baseline and after changes) for risk of recurrent ipsilateral stroke?

Elucidating the relation between atherosclerotic plaque morphology and composition and risk of stroke will lead to improved insight in the pathophysiology of ischemic stroke, to treatment decisions based on the assessment of plaque features, and to new treatment strategies focused on the morphology and components of the atherosclerotic plaque.

SAMENVATTING EN CONCLUSIES

Dit proefschrift evalueert het gebruik van MDCT angiografie (MDCTA) voor 1) het afbeelden van atherosclerose en bijbehorende bloedvat vernauwing in de bloedvaten die de hersenen van bloed voorzien, en 2) het afbeelden van atherosclerotische plaque kenmerken die gerelateerd zijn aan een instabiele plaque formatie.

De gedane onderzoeken kunnen als volgt worden verdeeld: Deel 1) onderzoeken met betrekking tot optimalisatie van het data acquisitie protocol, Deel 2) validatie onderzoeken, waaronder evaluatie van de accuratesse van MDCTA in vergelijk met histologie, en interoberserver onderzoeken, en Deel 3) klinische cross-sectionele onderzoeken.

Deel 1: Optimalisatie van contrast, scan en reconstructie protocol

Het optimaliseren van het contrastmiddel protocol door het inspuiten van een zoutoplossing direct na het beëindigen van het inspuiten van contrastmiddel (het zogenoemde bolus chaser principe) wordt beschreven in **Hoofdstuk 1**. Contrastmiddelen zijn kostbaar en potentieel nefrotoxisch. Het gebruik van een bolus chaser kan het gebruik van contrastmiddel doen laten afnemen. Dit onderzoek laat zien dat het toedienen van 40 ml zoutoplossing na het gebruik van 80 ml contrastmiddel leidt tot een significant hogere aankleuring van de supra aortale arteriën, waarbij de hoogste aankleuring wordt bereikt ter hoogte van de carotis bifurcatie. Desalniettemin, leidt het verminderen van het volume aan contrastmiddel van 80 ml naar 60 ml, bij het gebruik van een bolus chaser toch tot een significant lagere vaat aankleuring. Dit onderzoek laat bovendien zien dat vaat aankleuring omgekeerd evenredig is gecorreleerd aan lichaamsgewicht. Daarom, wordt er als aanbeveling gesteld dat 60 ml contrastmiddel gevolgd door injectie van 40 ml zoutoplossing leidt tot een optimale vaat aankleuring in patiënten die minder dan 75 kg wegen.

De scan richting bij CTA is normaal gebaseerd op de richting van de bloedstroom. Met een scan in caudocraniale (van voeten naar hoofd) richting komt het veelvuldig voor dat ongemengd contrastmiddel voor periveneuze artefacten zorgt in de vena subclavia, vena brachiocephalica en/of in de vena cava superior, waardoor de beoordeling van aanliggende structuren en ook adequate vaatbeoordeling kan worden gehinderd. Het onderzoek beschreven in **Hoofdstuk 2** laat zien dat een wijziging in scan richting van caudocraniaal naar craniocaudaal het optreden van periveneuze artefact vorming verminderd, en ofschoon de arteriële aankleuring iets afneemt, er een betere beoordeling mogelijk is van de aorta ascendens en de origo van de supra aortale vaten.

Blooming artefacten van verkalkingen op CT beelden zorgen voor een grotere dan reële afbeelding van die verkalkingen, hetgeen een belemmerend effect heeft op accurate karakterisatie van het niet gecalcificeerde deel van de atherosclerotische plaque en op de kwantificatie van plaque componenten. Een optimale instelling van voltage en reconstructie filter zou dit belemmerende effect mogelijk kunnen reduceren. In **Hoofdstuk 3** laten we zien dat bij het verhogen van het voltage het afgebeelde volume van verkalkingen vermin-

derd. Bovendien laten we zien dat 'smooth' en 'sharp' reconstructie filters leiden tot verminderde interpreteerbaarheid ten gevolge van middeling van contrast verschillen en het ontstaan van edge-enhancement artefacten, respectievelijk, en dat de 'intermediate' reconstructie filters goed interpreteerbaar zijn. Gebaseerd op dit onderzoek adviseren we het gebruik van 120 kVp en een 'intermediate' reconstructie filter voor beeldvorming van atherosclerotische plaque.

Deel 2: Validatie studies

MDCTA kan mogelijk atherosclerotische plaque en plaque componenten karakteriseren en kwantificeren. Om deze techniek te valideren hebben we een in vitro en een in vivo studie uitgevoerd. In de eerste studie hebben we MDCTA beelden van 15 endarterectomie specimens gematched met de overeenkomende histologische coupes, waarna we de Hounsfield unit (HU) waarde van puur vet weefsel en puur fibreus weefsel hebben gemeten. Een 'receiver-operating-characteristic curve ' (ROC curve) liet zien dat 60 HU het optimale afkappunt is om te differentiëren tussen vet en fibreus weefsel (**Hoofdstuk 3**).

Vervolgens hebben we in vivo MDCTA beelden van 15 significant atherosclerotische leasies gematched met corresponderende histologische coupes, en werd de HU waarde van puur vet weefsel en puur fibreus weefsel vastgesteld. Wederom bleek 60 HU het optimale afkappunt te zijn om te differentiëren tussen vet en fibreus weefsel. Een tweede analyse op de in vivo MDCTA beelden, waarin alle hypodense zones met een HU waarde van <30 HU en <60 HU werden bepaald door middel van thresholding, liet zien dat de positief predictieve waarde van een hypodense zone in een atherosclerotische plaque met een densiteit van <30 HU voor de aanwezigheid van vet weefsel 97% bedroeg, terwijl de positief predictieve waarde van een zone met een densiteit van tussen de 30 en 60 HU 23% bedroeg (**Hoofdstuk 4**).

Naast de detectie van specifieke plaque componenten maakt MDCTA het mogelijk om het plaque oppervlak en de relatieve bijdrage van specifieke plaque componenten ten opzichte van het totale plaque oppervlak te kwantificeren.

Met vrij verkrijgbare software en custom-made plug-ins waren wij in staat om semi-automatisch in MDCTA beelden oppervlakten van plaque en plaque componenten te berekenen. Onze in vitro studie liet een sterke correlatie zien tussen MDCTA gebaseerde en histologie gebaseerde metingen van het totale plaque oppervlak, het verkalkte oppervlak en het vet oppervlak (R^2=0.81, R^2=0.83 en R^2=68, respectievelijk), en een zwakke correlatie voor het meten van het fibreuze oppervlak (R^2=0.26) (**Hoofdstuk 3**). Onze in vivo studie liet een sterke correlatie zien voor het totale plaque oppervlak, het verkalkte oppervlak en het fibreuze oppervlak (R^2=0.73, R^2=0.74, en R^2=0.76, respectievelijk) , en een zwakke correlatie voor het vet oppervlak (R^2=0.24). Maar, bij het verrichten van verdere analyse, waarbij we keken naar de correlatie van het vet oppervlak in ernstig, en mild verkalkte plaques, bleek de correlatie voor mild verkalkte plaques significant beter te worden, terwijl de

correlatie voor ernstig verkalkte plaques zwak bleef (**Hoofdstuk 4**).

Omdat plaque en plaque componenten metingen semi-automatisch worden uitgevoerd met een custom-made software tool hebben we een interobserver variabiliteits studie uitgevoerd. De in vivo MDCTA oppervlakte metingen van 2 observers lieten significante verschillen ($p<0.05$) zien ten aanzien van het meten van het totale plaque oppervlak, het fibreuze oppervlak, en het vet oppervlak. Metingen van het lumen oppervlak en het verkalkte oppervlak toonden geen significante verschillen ($p>0.05$) tussen observers. De 'interobserver coefficients of variation' voor de absolute meting van lumen, plaque, verkalkt, fibreus en vet oppervlak bedroegen: 4%, 19%, 16%, 21% en 40%, respectievelijk, en de 'interobserver coefficients of variation' voor de relatieve meting (%) van verkalkt, fibreus en vet oppervlak bedroegen: 26%, 10% en 20%, respectievelijk (**Hoofdstuk 4**).

Na deze validatie werd onze software tool geüpdatet zodat analyse van opeenvolgende MDCTA beelden en dus het meten van plaque volume en plaque component volume mogelijk werd gemaakt. Een interobserver studie tussen drie observers liet zien dat de 'interclass correlation coefficient (ICC)' exellent was voor alle volume metingen (ICC>0.80), behalve voor de vet volume metingen, die was goed (ICC=0.76 (range 0.54-0.87)). De 'interobserver coefficient of variation' varieerde voor plaque volume tussen 17-24%, voor verkalkt volume tussen 13-33%, voor fibreus volume tussen 18-24%, voor vet volume tussen 37-47%, en voor lumen volume tussen 3-10%. De 'interobserver coefficient of variation' varieerde voor het percentage verkalkt volume tussen 15-26%, fibreus volume tussen 10-15% en voor vet volume tussen 21-30% (**Hoofdstuk 5**). Dezelfde software werd gebruikt om het volume van intracraniële verkalkingen te meten, en werd wederom gevalideerd middels een observer variabiliteits analyse. We lieten zien dat de ICC tussen twee observers voor het meten van intracraniële kalk volumes excellent is (ICC=0.99), en dat de 'coefficient of variation' voor interobserver verschillen zeer laag is (<7%). Bovendien, werd aangetoond dat de absolute verschillen tussen observers niet afhankelijk waren van de grootte van de verkalkingen (**Hoofdstuk 7**).

Als laatste werd de observer variabiliteit bepaald bij het beoordelen van plaque oppervlakte morfologie. Twee observers waren het in alle gevallen eens over de aanwezigheid van ulceraties (kappa = 1; 95%CI =0.86-1.00), over de aanwezigheid van irregulaire plaques in 93% van de gevallen (kappa =0.84; 95%CI = 0.70-0.97), en over de locatie van een plaque ulceratie in 96% van de gevallen (kappa =0.91; 95% = 0.54-1.00) (**Hoofdstuk 8**).

Deel 3: Klinische studies

De eerste klinische studie (**Hoofdstuk 7**) liet zien dat intracraniële carotis interna verkalkingen vaak voorkomen bij patiënten met cerebrovasculaire symptomen. Mannen vaker intracraniële verkalkingen hebben dan vrouwen (71% en 56%, respectievelijk) en dat het volume van de verkalkingen groter is bij mannen (66 ± 124 mm^3 vs. 33 ± 91 mm^3, respectievelijk). Aanwezigheid en grootte van de verkalkingen bleek geassocieerd te zijn

met een hogere leeftijd. De aanwezigheid en grootte van verkalkingen was onafhankelijk geassocieerd met roken, hypercholesterol, cardiale voorgeschiedenis, en ischemische cerebrovasculaire voorgeschiedenis. Hiernaast lieten we zien dat de mate van verkalking niet verschilt tussen de symptomatische en contralaterale asymptomatische arterie, en dat intracraniële verkalkingen niet geassocieerd zijn met het type klachten (amaurosis fugax vs TIA or minor stroke).

Onze tweede klinische studie (**Hoofdstuk 8**) liet zien dat MDCTA gladde, irregulaire en geulcereerde plaque oppervlakken kan differentiëren en classificeren. De aanwezigheid van geulcereerde plaques in de arterie carotis was sterk geassocieerd met de mate van stenosis. Geulcereerde plaques werden significant vaker aangetroffen in carotiden met een stenose graad van >30%, dan in carotiden met een stenose graad van <30% (40% versus 9%, respectievelijk; p=0.001). Ulceraties waren meestal proximaal van de meest ernstige stenose gelegen. Deze bevinding ondersteunt de theorie dat 'shear stress' (wrijvingsspanning) een cruciale rol speelt bij het ontstaan van ruptuur gevoelige plaques en uiteindelijke plaque ruptuur. Hypercholesterol en waarschijnlijk ook roken zijn onafhankelijk geassocieerd met de aanwezigheid van plaque ulceratie of irregulariteit. Symptomatische arteriën carotis hadden vaker een plaque oppervlak irregulariteit of ulceratie dan asymptomatishe arteriën carotis (25% vs 18%, respectievelijk).

Een irregulair of geulcereerd plaque oppervlak werd minder vaak gezien onder patiënten met amourosis fugax (17%) dan onder mensen met focale cerebrale ischemie (28%). Symptomatische arteriën waren niet significant vaker irregulair of geulcereerd dan asymptomatische arterien carotis als er werd gecorrigeerd voor stenose graad.

In onze derde klinische studie (**Hoofdstuk 9**) hebben we in MDCTA beelden in de symptomatische arterien carotis het volume van de atherosclerotische plaque en de proportie van de verschillende plaque componenten gemeten. We lieten zien dat het plaque volume matig geassocieerd was met de ernst van de stenose, en dat plaque volume geassocieerd was met leeftijd en roken. Bijkomend bleek dat hypercholesterol positief geassocieerd was met een groter volume aan kalk en een kleiner volume aan vet.

Conclusies

Uit het eerste deel van deze thesis kunnen we concluderen dat een optimaal protocol voor MDCT angiografie van de supra-aortale arteriën gebruik maakt van 80 ml contrastmiddel gevolgd door injectie van 40 ml zoutoplossing , een craniocaudale scan richting, en met het oog op atherosclerotische carotis plaque afbeelding een buis voltage van 120 kVp en een 'intermediate' reconstructie filter.

Het tweede deel van deze thesis staat de conclusie toe dat MDCTA plaque en plaque componenten kan differentiëren en kwantificeren in een goede correlatie met histologie. Echter, vet gebieden binnen de plaque kunnen alleen adequaat gekwantificeerd worden in mild gecalcificeerde plaques. Hiernaast, concluderen we dat in vivo volume metingen van plaque en plaque componenten mogelijk zijn met

een redelijke reproduceerbaarheid, en dat met MDCTA intracraniële arterie carotis verkalkingen reproduceerbaar kunnen worden gekwantificeerd en dat het plaque oppervlak in atherosclerotische arterien carotis beoordeeld kan worden met een excellente reproduceerbaarheid.

In het derde deel van deze thesis hebben we de karakteristieken van mogelijke MDCTA-gebaseerde plaque parameters (het volume van intracraniële kalk, plaque oppervlak morfologie, plaque volume en plaque componenten volumes) geëvalueerd. Er werden correlaties gevonden met verschillende cardiovasculaire risicofactoren. Enkele plaque parameters bleken gecorreleerd aan de aanwezigheid van het optreden en het type van cerebrovasculaire symptomatologie.

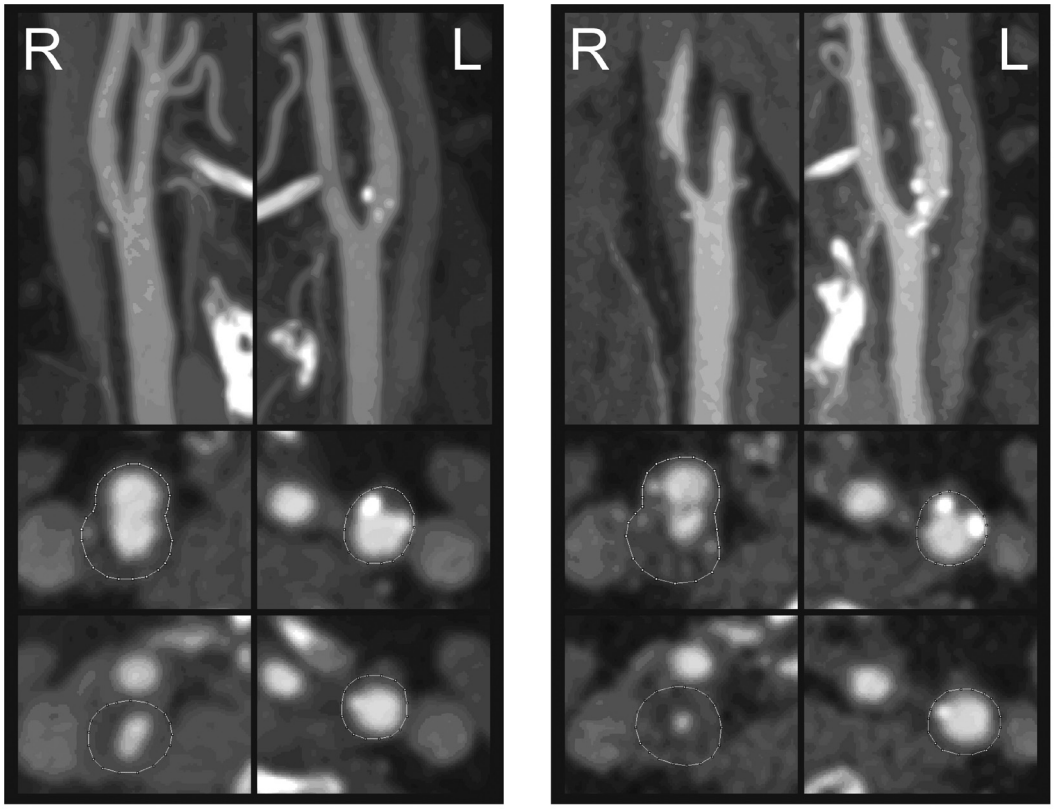

Stenosis(%)	Plaque (mm³)	Lipid (mm³)	Fibrous (mm³)	Calcified (mm³)
R 60→90	+201	+211	-19	+9
L 30→30	+206	+41	+31	+35

Figuur 1. Seriële beeldvorming middels MDCT angiografie van een beiderzijds atherosclerotische arterie carotis bifurcatie, maakt het mogelijk om veranderingen waar te nemen in stenose graad, plaque volume en plaque componenten volumina.

Wij concluderen dat atherosclerotische plaque parameters adequaat kunnen worden afgebeeld met MDCTA. Deze parameters lijken mogelijk een additionele waarde te hebben, naast de mate van stenose, als marker van atherosclerotische ziekte en bij het voorspellen van het risico op een (recidief) ischemisch cerebrovasculair event.

Richting van toekomstig onderzoek

MDCTA ontwikkelt zich als een doeltreffende manier om atherosclerotische plaque parameters af te beelden. Daarnaast, verwachten wij dat MDCTA-gebaseerde plaque parameters minstens even belangrijk blijken te zijn als lumen vernauwing tijdens de ontwikkeling van cerebrovasculaire events. Daarom staan er follow-up studies in de planning, die de correlatie moeten onderzoeken tussen deze MDCTA gebaseerde atherosclerotische plaque parameters en (hernieuwd) optredende ischemische cerebrovasculaire events.

Daarnaast, biedt de noodzakelijke prospectieve opzet van deze studies de mogelijkheid om seriële veranderingen in plaque parameter karakteristieken op te merken, welke mogelijk meer inzicht zouden kunnen verschaffen in het natuurlijk beloop van atherosclerose in de arteriën carotis (zie Figuur 1.).
Tenslotte biedt deze follow-up setting de mogelijkheid om de rol van shear stress bij het ontstaan van plaque ruptuur te onderzoeken. Hogere shear stress waarden worden gewoonlijk proximaal van de ernstigste stenose gevonden. Echter, er is maar weinig bekend van de invloed van shear stress op plaque progressie, verandering in plaque compositie en oppervlak morfologie (ruptuur). MDCTA-gebaseerde 3d lumen geometrie beoordeling maakt het mogelijk om hemodynamische parameters zoals lokale shear stress te berekenen.

Seriële MDCTA kan daardoor de temporele veranderingen aantonen in shear stress, plaque volume en compositie, evenals de prevalentie en incidentie van plaque ruptuur.

Specifieke onderzoeksvragen betreffen: a) Wat is de prevalentie van atherosclerose (plaque volume, compositie, ruptuur en shear stress) in patiënten met TIA of minor ischemic stroke?, b) Wat is het natuurlijk beloop van atherosclerose in de arterie carotis?, c) Kunnen veranderingen in plaque volume, plaque compositie en plaque ruptuur voorspelt worden op basis van risicofactor profiel, huidige plaque status en shear stress?, d) Wat is de predictieve waarde van atherosclerotische plaque kenmerken (bij de uitgangswaarden en na veranderingen) voor het optreden van (hernieuwde) ipsilaterale cerebrovasculaire ischemie?

Verder inzicht in de relatie tussen atherosclerotische plaque morfologie en compositie en het risico op cerebrovasculaire ischemie zal lijden tot een verbeterd inzicht in de pathofysiologie, verbeterde behandeling gebaseerd op de aanwezigheid van specifieke plaque kenmerken, en mogelijk tot nieuwe behandelingsopties welke zich dan zouden moeten richten op de morfologie en componenten van de atherosclerotische plaque.

APPENDIX

Dankwoord

Met nu voor het eerst voor mij op mijn bureau de nog provisorische bundeling van de artikelen die samen dit proefschrift vormen, huist er bij mij een paradoxaal gevoel.
Allereerst, is er het uiterst trotse gevoel dat deze bundeling MIJN proefschrift betreft!, een gevoel dat ik mij genoegzaam laat aanleunen en savoureer. Even zozeer, en vandaar het paradoxale gevoel, realiseer ik me dat ik MIJN proefschrift te danken heb aan de inzichten, samenwerking, betrokkenheid en steun van velen en dat het evengoed ONS proefschrift is dat er hier voor mij op mijn bureau ligt.
Een ieder die zich herkent in deze ONS wil ik van harte danken voor zijn bijdrage!
Enkele personen wil ik met name noemen omdat zij een proportioneel grote bijdrage hebben geleverd aan MIJN, ONS proefschrift.

Prof. dr. PMT Pattynama, mijn promotor, bedank ik voor zijn begeleiding en de grote mate van vrijheid die hij mijn co-promotoren en mij gaf.
Dr. Aad van der Lugt, mijn co-promotor van het eerste uur, bedank ik omdat zonder diens visie en ambities dit proefschrift nooit tot stand had kunnen komen, maar meer nog om zijn betrokken en enthousiaste begeleiding, zijn open vizier voor mijn ideeën, en de buitengewoon plezierige samenwerking.
Dr. Diederik WJ Dippel, mijn tweede copromotor wil ik bedanken voor zijn toegankelijke brede kennis en zijn heldere oordeel, waarmee hij naast alle neurologische dilemma's ook vele statistische vraagstukken oploste en hij onmisbaar werd voor deze onderzoekslijn.
Aad en Diederik jullie samenwerking is daadkrachtig en inspirerend, en daardoor uiterst vruchtbaar. Dankzij jullie kon ik waar nodig direct op adequate professionele hulp rekenen van andere specialismen, waarvoor ik de direct betrokkenen van deze specialismen hartelijk dank: Dr. M van Sambeek en J Hendriks (Vaatchirurgie), dr. P Zondervan (Pathologie), dr. H van Beusekom (Cardiologie), dr. J Wentzel en H Groen (Biomedical Engineering), en Prof. dr. W Niessen, dr. E Meijering, dr. T van Walsum, dr. R Manniesing, en D Vukadinovic (Biomedical Imaging Group Rotterdam).
Prof. dr. H van Urk, prof. dr. PWJC Serruys en prof. dr. JCM Witteman wil ik bedanken voor hun bereidheid in de kleine commissie zitting te nemen en voor de inhoudelijke beoordeling van dit proefschrift. De overige leden van de promotiecommissie wil ik bedanken voor hun bereidheid zitting te nemen in de grote commissie.
Prof. dr. GP Krestin, wil ik bedanken voor alle mogelijkheden en voor de steun die hij promovendi biedt om hun onderzoeken uit te voeren, te presenteren en te publiceren.
Mijn paranimfen Guus Beljaars en Mohamed Ouhlous bedank ik omdat ze me tot steun willen zijn tijdens mijn verdediging, maar meer nog omdat ze me tot steun zijn geweest tijdens mijn studie en/of mijn promotie periode in woord, daad en vriendschap.
Hervé Tanghe wil ik bedanken voor het bouwen, onderhouden en bewaken van onze waardevolle en groeiende database.

Ton Everaers bedank ik voor zijn expertise om van simpele Word files en aangeleverde figuren en tabellen zo'n prachtig boekje te vervaardigen, en niet te vergeten voor de prachtige omslag.
Speciale vermelding en dank voor hun directe betrokkenheid bij, hun inzet voor, en hun gezelligheid naast mijn onderzoeken verdienen Ronald Booy, Hamit Cakir, Sander Cretier, Harald Groen, Philip Homburg, Erik Meijering, Cécile de Monyé, Sietske Rozie, en Evert van Velzen.
De co-auteurs bedank ik voor hun bijdragen aan en hun waardevolle commentaar op de artikelen gebundeld in dit proefschrift.
Oude en nieuwe collegae 'van de 23-ste', en van kamer Hs-223 (Monique Bernsen, Maka Kekelidze, Marc Kock, Adriaan Moelker, Edwin Oei, Rody Ouwendijk, Anda Preda, Teun Rijsdijk, Caroline Schraa-Tam, Sandra van Tiel, Dirk Verver, Marion van Vliet, Mika Vogel, Piotr Wielopolski, Alexandra Wils, Karin ten Wolde, en Andries Zwamborn) bedank ik voor de onontbeerlijke prettige dagelijkse afleiding. Het was goed toeven met jullie!
De medewerkers van het Research Office, het Trial bureau en het secretariaat Radiologie bedank ik voor hun altijd onmisbare hulp.
De radiologen en arts-assistenten Radiologie van het Erasmus MC dank ik voor hun betrokkenheid bij het afronden van mijn proefschrift.
Vrienden dank voor jullie interesse, medeleven, en begrip.
Lieve familie en schoonfamilie, te nuchter zijn jullie voor de vele lofuitingen die ik jullie oprecht kan toedichten, ik beperk me daarom tot één: Jullie zijn mij en wat mij het allerliefste is, Debora, Olivier en Fieke tot onvolprezen steun, diepe dank!
Debora, je verdient wat je zelf hebt voorgesteld, een dankwoord dat enkel bestaat uit: 1000x dank Debora! Maar, verrassing, er zijn ook anderen die ik moet bedanken, dus ter compensatie naast mijn diepe dank, ook mijn bekentenis dat het me zonder jou nooit was gelukt, luf u!

Publications

Articles

- Rozie S, **de Weert TT**, de Monyé C, Homburg PJ, Tanghe HLJ, Dippel DWJ, van der Lugt A.
  Atherosclerotic plaque volume and composition in symptomatic carotid arteries assessed with multidetector CT: Relationship with severity of stenosis and cardiovascular riskfactors.
  European Radiology. Recommended for publication
- **de Weert TT**, Cretier S, Groen HC, Homburg P, Cakir H, Wentzel JJ, Dippel DWJ, van der Lugt A.
  Atherosclerotic plaque surface morphology in the carotid bifurcation assessed with multidetector computed tomography angiography.
  Stroke. Accepted for publication
- **de Weert TT**, Cakir H, Rozie S, Cretier S, Meijering E, Dippel DWJ, van der Lugt A.
  Intracranial internal carotid artery calcifications: Association with vascular risk factors and ischemic cerebrovascular disease.
  American Journal of Neuroradiology 2008; Oct 8 [Epub ahead of print]
- **de Weert TT**, de Monyé C, Meijering E, Booij R, Niessen WJ, Dippel DWJ, van der Lugt A.
  Assessment of atherosclerotic carotid plaque volume with multidetector computed tomography angiography.
  International Journal of Cardiovascular Imaging 2008; 24: 751-9
- Ouhlous M, Moelker A, Flick HJ, Wielopolski PA, **de Weert TT**, Pattynama PM, van der Lugt A.
  Quadrature coil design for high-resolution carotid artery imaging scores better than a dual phased-array coil design with the same volume coverage.
  Journal of Magnetic Resonance Imaging 2007; 25: 1079-84.
- van Velsen EF, Niessen WJ, **de Weert TT**, de Monyé C, van der Lugt A, Meijering E, Stokking R.
  Evaluation of an improved technique for lumen path definition and lumen segmentation of atherosclerotic vessels in CT angiography.
  European Radiology 2007; 17: 1738-45.
- **de Weert TT**, Ouhlous M, Meijering E, Zondervan PE, Hendriks JM, van Sambeek MRHM, Dippel DWJ, van der Lugt A.
  In vivo characterization and quantification of atherosclerotic carotid plaque components with multidetector computed tomography and histopathological correlation.
  Arteriosclerosis, Thrombosis and Vascular Biology 2006; 26: 2366-72.

- de Monye C, **de Weert TT**, Zaalberg W, Cademartiri F, Siepman DA, Dippel DWJ, van der Lugt A.
  Optimization of CT angiography of the carotid artery with a 16-multidetector-row CT scanner: Craniocaudal scan direction reduces contrast material-related perivenous artifacts.
  American Journal of Roentgenology 2006;186: 1737-45.
- de Monye C, Cademartiri F, **de Weert TT**, Siepman DA, Dippel DWJ, van der Lugt A.
  Sixteen-detector row CT angiography of carotid arteries: Comparison of different volumes of contrast material with and without a bolus chaser.
  Radiology 2005; 237: 555-62.
- Ouhlous M, Flach HZ, **de Weert TT**, Hendriks JM, van Sambeek MRHM, Dippel DWJ, Pattynama PM, van der Lugt A.
  Carotid plaque composition and cerebral infarction: MR imaging study.
  American Journal of Neuroradiology 2005; 26: 1044-9.
- **de Weert TT**, Ouhlous M, Zondervan PE, Hendriks JM, Dippel DWJ, van Sambeek MRHM, van der Lugt A.
  In vitro characterization of atherosclerotic carotid plaque with multidetector computed tomography and histopathological correlation.
  European Radiology 2005; 15: 1906-14.
- Leiner T, **de Weert TT**, Nijenhuis RJ, Vasbinder GB, Kessels AG, Ho KY, van Engelshoven JM.
  Need for background suppression in contrast-enhanced peripheral magnetic resonance angiography.
  Journal of Magnetic Resonance Imaging 2001; 14: 724-33.

Abstracts

- **de Weert TT**, Cretier S, Rozie S, Groen H, Wentzel J, Dippel DWJ, van der Lugt A. Carotid plaque ulceration assessed with multidetector computed tomography angiography.
  Presented at the Congress of Radiology, Mar 7-11, 2008; Vienna, Austria. Published in *Eur Radiol* 2008; 18(suppl. 1) .
- **de Weert TT**, Cakir H, Rozie S, Cretier S, Meijering E, Dippel DWJ, van der Lugt A. Intracranial internal carotid artery calcifications: association with vascular risk factors and cerebrovascular symptomatology.
  Presented at the Congress of Radiology, Mar 7-11, 2008; Vienna, Austria. Published in *Eur Radiol* 2008; 18(suppl. 1) .
- **de Weert TT**, Cretier S, Rozie S, Groen H, Wentzel J, Dippel DWJ, van der Lugt A. Frequency and location of plaque rupture in carotid arteries assessed with multidetector computed tomography angiography.
  Presented at the 2nd Symposium on Biomechanics in Cardiovascular Disease: Shear Stress in Vascular Biology, Apr 19-20, 2007; Rotterdam, the Netherlands.

- **de Weert TT**, Vukadinovic D, de Monye C, van Walsum T, Niesen WJ, van der Lugt A. Atherosclerotic carotid plaque quantification with multidetector computed tomography angiography.
  Presented at the European Congress of Radiology, Mar 9-13, 2007; Vienna, Austria. Published in *Eur Radiol* 2007; 17(s1):506.
- **de Weert TT**, Rozie S, Meijering E, Dippel DWJ, van der Lugt A.
  Is there a relationship between carotid calcifications and atherosclerotic carotid plaque volume?
  Presented at the 92nd Annual Meeting of the Radiological Society of North America; Nov 26 - Dec 1, 2006; Chicago, USA. Published in *Radiology* 2006; 458.
- **de Weert TT**, Ouhlous M, Zondervan PE, van Sambeek MRHM, Dippel DWJ, van der Lugt A.
  Atherosclerotic carotid plaque imaging with multidetector computed tomography angiography.
  Presented at the 92nd Annual Meeting of the Radiological Society of North America; Nov 26 - Dec 1, 2006; Chicago, USA. Published in *Radiology* 2006; 880.
- **de Weert TT**, Cretier S, Cakir H, Meijering E, Dippel DWJ, van der Lugt A.
  Serial assessment of atherosclerotic carotid plaque volume and plaque component volumes with multidetector computed tomography angiography.
  Presented at the 11th Annual Meeting of the Radiological Society of the Netherlands; Nov 17, 2006; Kaatsheuvel, The Netherlands. Published in *Memorad* 2006; 11; 3.
- **de Weert TT**, Ouhlous M, Meijering E, Zondervan PE, van Sambeek MRHM, van der Lugt A
  In vivo characterisation and quantification of atherosclerotic carotid plaque with 16-slice MDCT and histopathololological correlation.
  Presented at the European Congress of Radiology, Mar 3-7, 2006; Vienna, Austria. Published in *European Radiology* 2006; 16(S1): 152.
- **de Weert TT**, Ouhlous M, Meijering E, Zondervan PE, van Sambeek MRHM, van der Lugt A
  In vivo characterisation and quantification of atherosclerotic carotid plaque with 16-slice MDCT and histopathololological correlation.
  Presented at the 10th Annual Meeting of the Radiological Society of the Netherlands; Sep 29-30, 2005; Noordwijkerhout, The Netherlands. Published in *Memorad* 2005; 10; 3.
- **de Weert TT**, Ouhlous M, Zondervan PE, Hendriks JM, van Sambeek MRHM, van der Lugt A.
  Quantification of lipid in atherosclerotic plaque with multidetector CT: Ex vivo validation with histopathological correlation.
  Presented at the 90th Annual Meeting of the Radiological Society of North America; Nov 28 - Dec 3, 2004; Chicago, USA. Published in *Radiology* 2004; 233(s): 214.

- **de Weert TT**, Ouhlous M, Zondervan PE, Hendriks JM, van Sambeek MRHM, van der Lugt A.
  Characterization of atherosclerotic plaque with multidetector CT: Correlation of endarterectomy specimens with histopathology.
  Presented at the European Congress of Radiology, Mar 5-9, 2004; Vienna, Austria. Published in *European Radiology* 2004; 14(S): 178.
- **de Weert TT**, Ouhlous M, Zondervan PE, Hendriks JM, van Sambeek MRHM, van der Lugt A.
  Characterization of atherosclerotic plaque with multidetector CT: Correlation of endarterectomy specimens with histopathology.
  Presented at the 89th Annual Meeting of the Radiological Society of North America; Nov 30 - Dec 5, 2003; Chicago, USA. Published in *Radiology* 2003: 229(s): 245.
- **de Weert TT**, Ouhlous M, Zondervan PE, Hendriks JM, van Sambeek MRHM, van der Lugt A. [Characterization of atherosclerotic plaque with MDCT.]
  Presented at the Dutch Vascular Meeting, Apr 10-11, 2003; Noordwijkerhout, The Netherlands.

Book chapter

- **de Weert TT**, Ouhlous M, van Sambeek MRHM, van der Lugt A.
  CT of the plaque.
  In: J. Gillard; M. Graves; T. Hatsukami; C. Yuan (Eds). *Imaging carotid disease*.
  Cambridge: Cambridge University Press, 2006.

Award

- **Certificate of Merit** from the Radiological Society of North America, Dec 2006.
  de Weert TT, Ouhlous M, Zondervan PE, van Sambeek MRHM, Dippel DWJ, van der Lugt A. Atherosclerotic carotid plaque imaging with multidetector computed tomography angiography. Presented at the 92nd Annual Meeting of the Radiological Society of North America; Nov 26 - Dec 1, 2006; Chicago, USA. Published in *Radiology* 2006; 880.

PhD Portfolio

Summary of PhD training and teaching activities

Name PhD student - Thomas T de Weert
Erasmus MC Department - Radiology
Research School - COEUR
PhD period - 2002[7]-2009[2]
Promotor - Prof dr PMT Pattynama
Supervisors - Dr A van der Lugt & dr DWJ Dippel

1. PhD training

General academic skills

- Biomedical English writing and communication, NIHES, Rotterdam, NL, 2003[6-11]

Research skills

- Classical Methods for Data-analysis, NIHES, Rotterdam, NL, 2004[9-10]
- Methodologie betreffende patiëntgebonden onderzoek en voorbereiding van subsidieaanvragen, CPO, 2004[1]

In-depth courses

- School of MRI, Basic course, ESMRMB, CH, 2002[9]
- Pathophysiology of ischemic heart disease, COEUR training modules, Rotterdam, 2003[10]
- Vascular medicine, COEUR training modules, Rotterdam, 2003[10]
- Atherosclerosis Research, COEUR training modules, Rotterdam, 2004[3]
- Cardiovascular imaging and diagnostics, COEUR training modules, Rotterdam, 2004[3-4]
- Design of cardiovascular trials, COEUR training modules, Rotterdam, 2004[4]
- Abdominal aortic aneurysm, COEUR training modules, Rotterdam, 2005[3]

Presentations

- Carotid plaque characterization with MDCT, COEUR Research Seminar, 2005[4]
- Numeral abstracts have been presented at National and International congresses (see for first author presentations abstract list on page 195)

Award

- Certificate of Merit from the Radiological Society of North America, 2006[12].

National and international conferences

Visited and presented at the European Congress of Radiology in 2004, 2006, 2007 and 2008, the Annual Meeting of the Radiological Society of North America in 2003, 2004 and 2006, the Annual Meeting of the Radiological Society of the Netherlands in 2005, 2006, 2007 and 2008 , the Dutch Vascular Meeting in 2003, and the Symposium on Biomechanics in Cardiovascular Disease: Shear Stress in Vascular Biology in 2007.

2. Teaching activities

- Tutor of first year medical students, Erasmus University, Rotterdam, 2003-2004
- Supervising fourth year medical students during their Research projects:
  - Quantification of intracranial calcifications with MDCT angiography
  - Assessment of atherosclerotic carotid plaque surface morphology

Curriculum Vitae

Thomas de Weert was born on July 1, 1973 in Nijmegen, The Netherlands. He was granted his MD in 1998 at the University of Maastricht and completed his final board certification in 2000. Thomas first became interested in Radiology during a student research project in cardiovascular imaging under supervision of dr. Tim Leiner, department of Radiology, at the University Hospital Maastricht. This research project resulted in his first authorship. Although this first authorship made a research career very tempting, he decided to obtain more clinical expertise and experience first. During residencies in Internal Medicine and Cardiology at the Reinier de Graaf Hospital in Delft, he took part in the exciting world of intensive care, ER-reanimation, and cardiac defibrillation. However, when in July 2002, the opportunity arose to start full time cardiovascular research at the Erasmus MC University Hospital, Rotterdam, The Netherlands, he took it. Thomas decided to follow his heart and started his PhD research under the supervision of prof. dr. PMT Pattynama (department of Radiology; head of the department, prof. dr. GP Krestin) and direct tutelage of dr. Aad van der Lugt (department of Radiology) and dr. Diederik WJ Dippel (department of Neurology). The results of this research are presented in this thesis. Since December 2006 Thomas is enrolled in the Radiology training at Erasmus MC Rotterdam.

COLOR SECTION

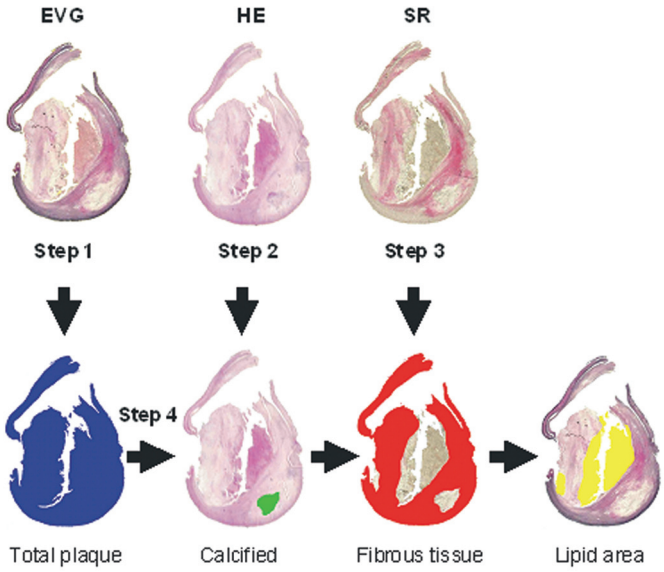

Chapter 3, page 60
Figure 2. Assessment in histologic sections of plaque component areas with a microscopy image analysis system (Clemex vision 3.5). Step 1, total plaque area was determined with a color threshold (any color = plaque). Step 2, calcified areas were manually drawn. Step 3, fibrous tissue was determined automatically with color threshold (red = collagen) and manually (tunica media). Step 4, remaining tissue was considered to be lipid.

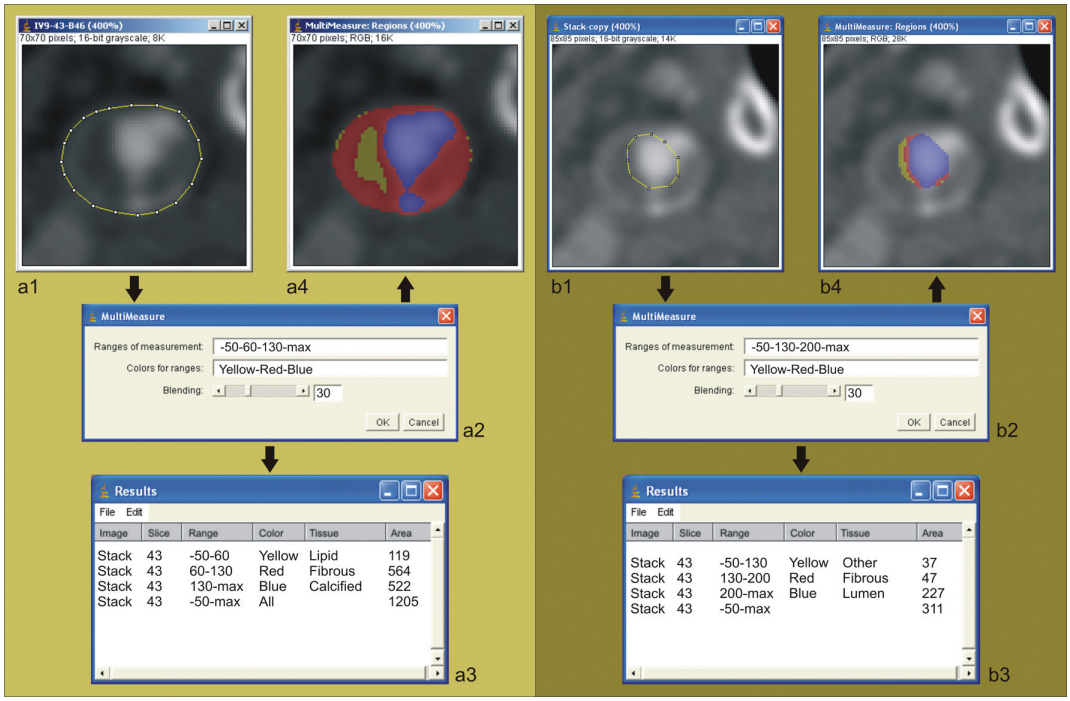

Chapter 4, page 77

Figure 1. Semi-automatic assessment of plaque component areas in MDCT images with the ImageJ plug-in 'MultiMeasure'. (a1.) This plug-in allows an observer to draw a region of interest (ROI) (=vessel outline). (a2.) After the input of specific ranges of Hounsfield values (HV), which should represent specific plaque components, the amount of pixels (a3.) within each range of HV is assessed. (a4.) Each range of HV is given a different colour and a MDCT-based plaque morphology image is produced. (b1.) To differentiate lumen from the atherosclerotic plaque and from calcified tissue, a second ROI is drawn. (b2.) After the input of specific ranges of HV, which should differentiate lumen and fibrous tissue located at the border of the lumen, the amount of pixels (b3.) within each range of HV is assessed. (b4.) Each range of HV is given a different colour and a second MDCT-based plaque morphology image is produced. The number of lumen pixels has now been calculated (b3). The exact number of fibrous and calcified pixels can now be determined (fibrous = fibrous measurement a (60 to 130 HU) plus fibrous measurement b (130 to 200HU); calcified = calcified measurement a (>130 HU) minus lumen measurement b (>200HU) minus fibrous measurement b (130-200HU)).

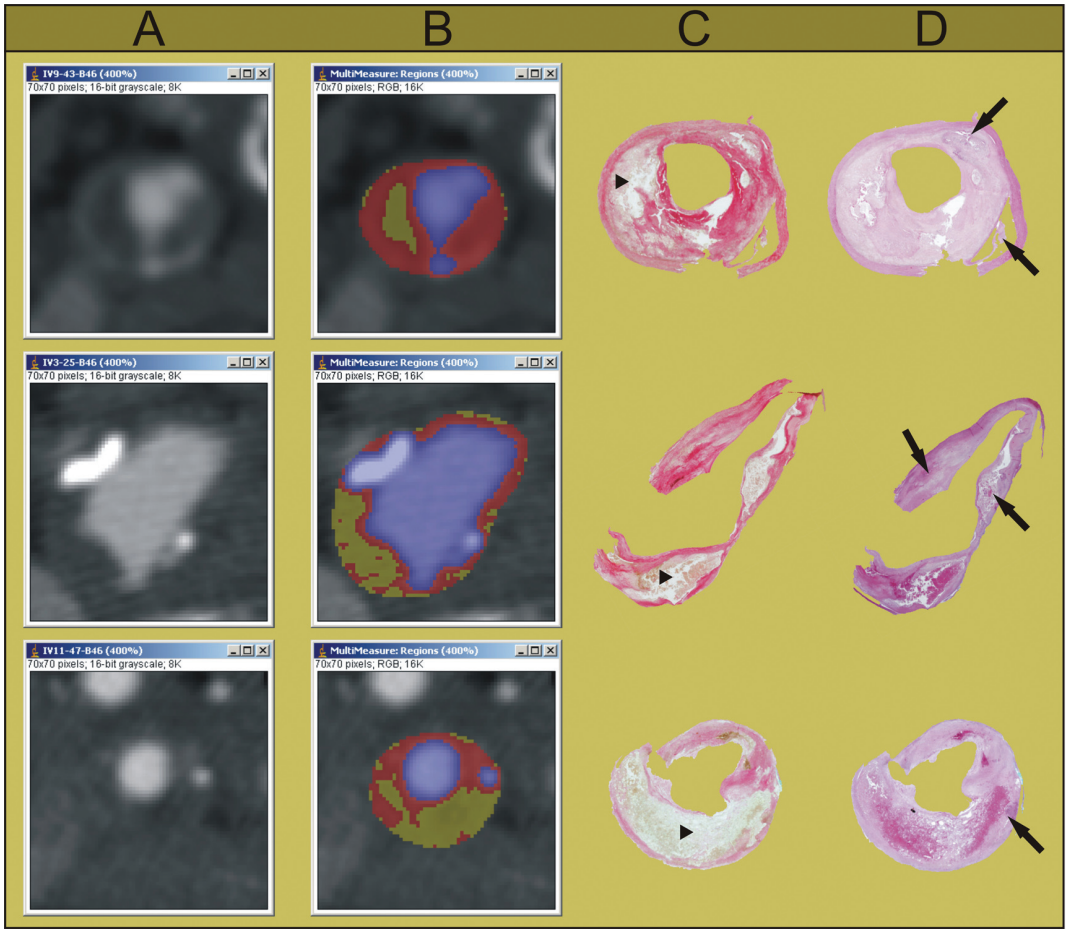

Chapter 4, Page 83

Figure 5. Column A: three axial MDCT images of the carotid artery with atherosclerotic plaque. Column B: MDCT plaque morphology images based on differences in Hounsfield Units. Column C and D: Corresponding histological sections with Sirius Red (SR) and haematoxylin eosin (HE) staining, respectively). The blue regions in the MDCT morphology images correspond well with the lumen and calcifications (arrow) on HE stained histological sections. The red regions in the MDCT morphology images correspond well with the red collagen-rich regions in the SR stained histological sections. The yellow regions in the MDCT morphology images correspond well with lipid core (i.e. lipid, haemorrhage and necrotic debris) (arrowhead) regions on histology (the non-red regions on the SR stained sections that are not calcified areas on the HE stained sections).

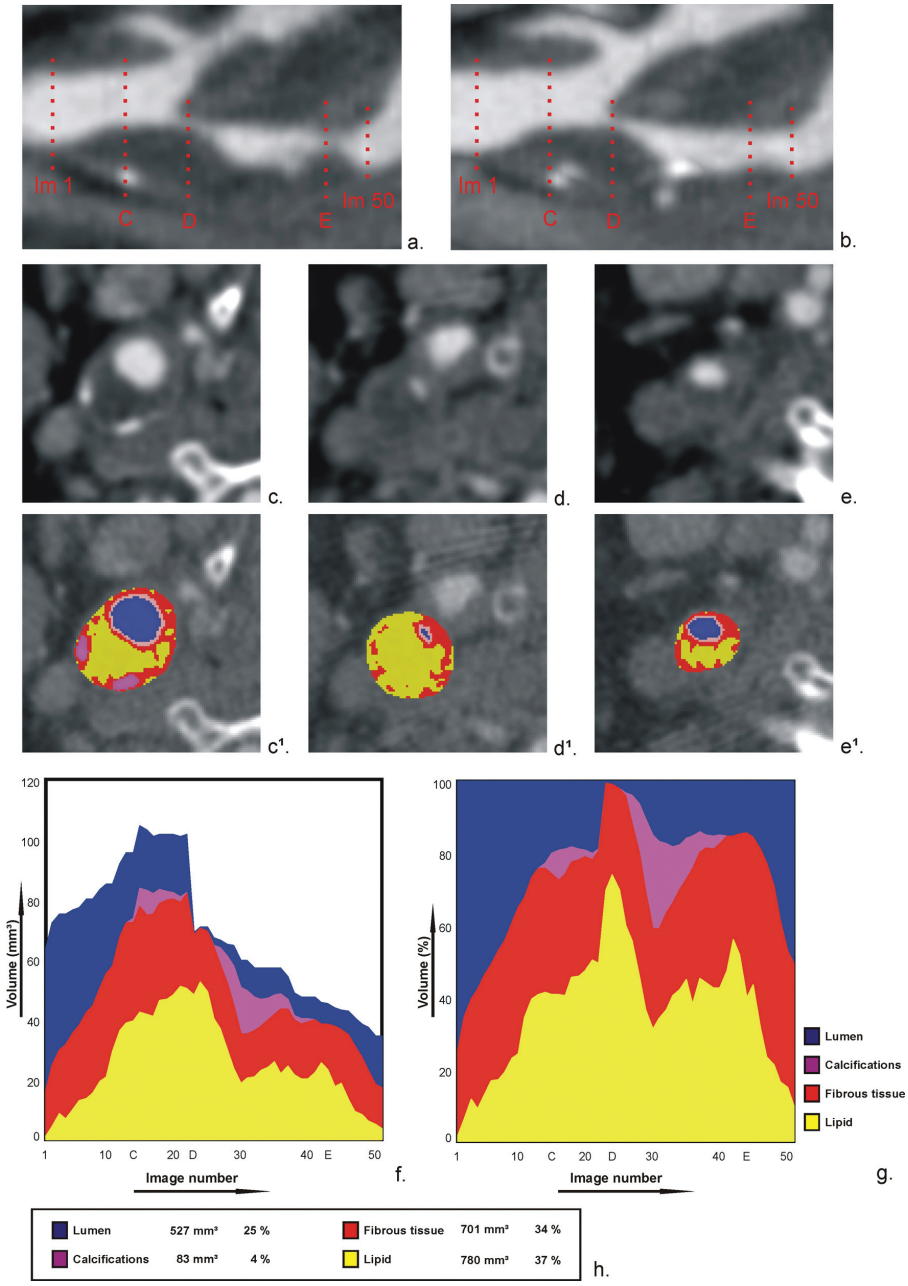

Chapter 5, Page 99

Figure 2. One mm multiplanar reformat (a.) and 2 mm maximum intensity projection (b.) in the sagittal plane depicts the carotid bifurcation with an atherosclerotic plaque. The startpoint (Im 1) and endpoint (Im 50) of atherosclerotic plaque volume assessment in this patient, and the position (C, D, E) of the three thin sliced (0.75 mm) axial MDCT images (c., d. and e.) of the internal carotid artery and their associated color overlay images (c'., d'. and e'.) are indicated. A graphical representation of the absolute (f.) and relative (g.) volume measurements of lumen, calcifications, fibrous tissue, and lipid per MDCT image. The x-axis represents the consecutive MDCT images, the y-axis represents the volume. (h.) A table with the total lumen, total calcified, total fibrous tissue and total lipid volume.

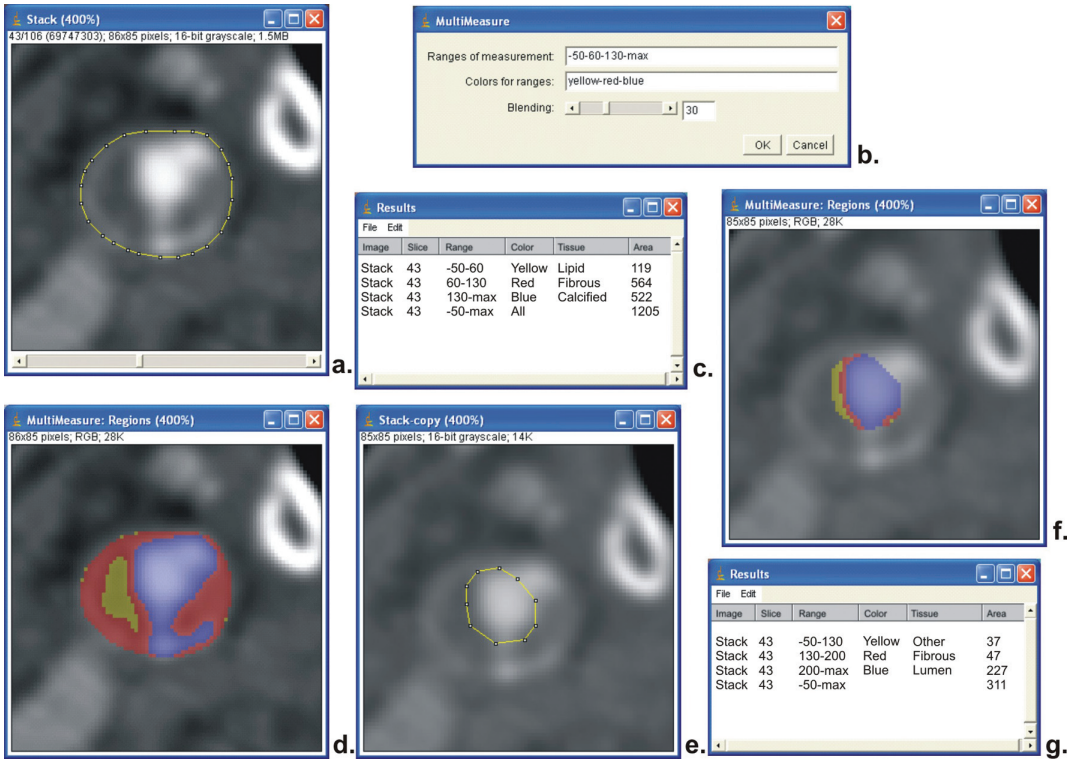

Chapter 6, Page 117

Figure 10. Semi-automatic assessment of plaque component areas in MDCT images. This software allows an observer to draw a region of interest (ROI) (=vessel outline) (A). After the input of specific ranges of Hounsfield values (HV) (B), which should represent specific plaque components, it assesses the amount of pixels within each range of HV (C). Each range of HV is given a different color and an MDCT-based plaque morphology image is produced (D). To differentiate lumen from the atherosclerotic plaque and from calcified tissue, a second ROI is drawn (E). A second morphology image is produced (F), and the number of lumen pixels are calculated (G). The exact number of fibrous and calcified pixels can now be determined. Fibrous = fibrous measurement-1 (60 to 130 HU) plus fibrous measurement-2 (130 to 200 HU); calcified = calcified measurement-1 (>130 HU) minus lumen measurement-2 (>200 HU) minus fibrous measurement-2 (130-200 HU).

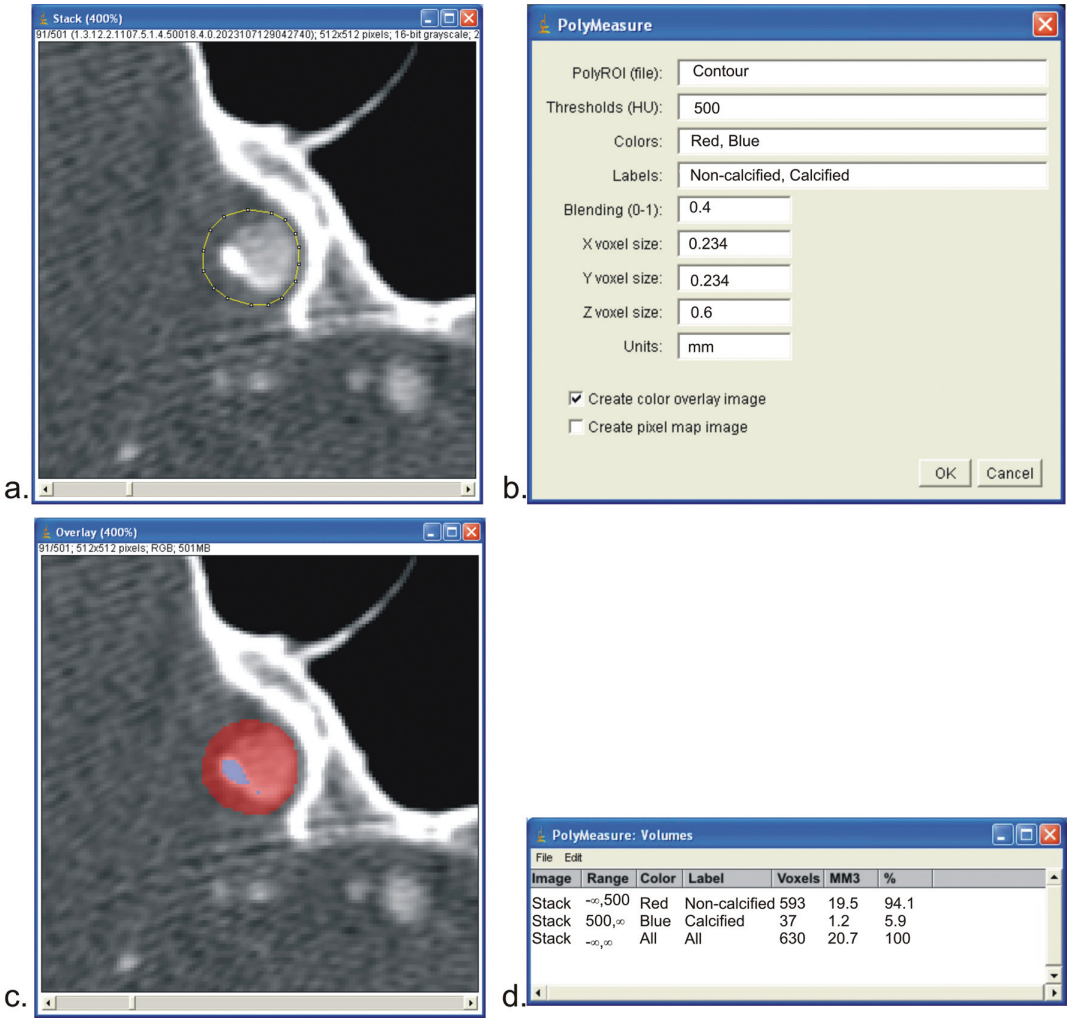

Chapter 7, Page 135

Figure 2. (a.) Regions of interest (ROI) are drawn on axial images that show calcifications. Care is taken to include the whole calcification and not to include any other high density structures (e.g. skull base). Because a minimum attenuation of 500 HU is defined for the presence of calcifications, lumen can be included in this ROI, because lumen will not reach such a high level of attenuation. All ROIs of one patient are saved within one file. (b.) The polymeasure software uses the contour file, the 500 HU threshold and the voxel dimensions (0.234 x 0.234 x 0.6 mm), to create a color overlay image, and a statistics table. (c.) The color overlay image shows which pixels within the ROI are above the pre-defined 500 HU threshold (blue) and which are below this threshold (red). (d.) The statistics table presents the amount of calcium pixels and the calcium volume (mm^3).

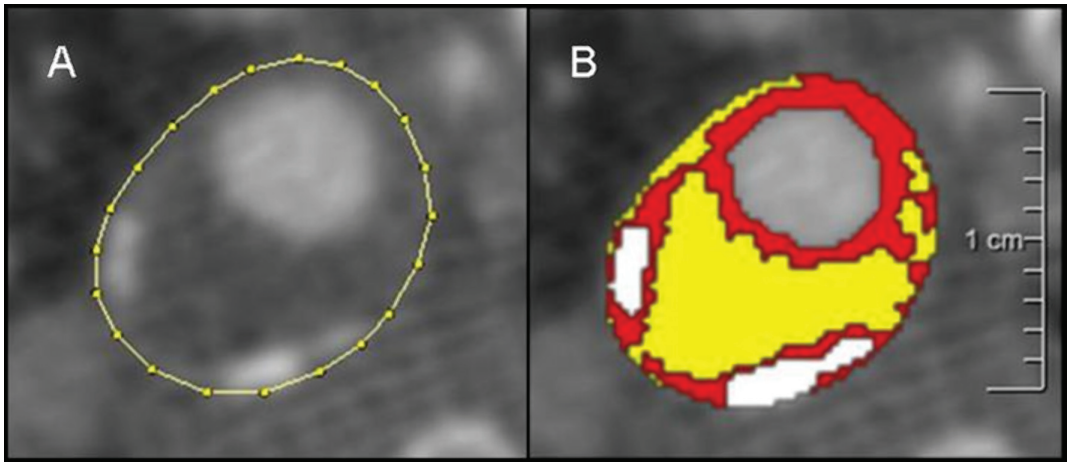

Chapter 9, Page 164

Figure 1. Semi-automatic assessment of plaque component areas in MDCT images. Axial MDCT image of an atherosclerotic carotid plaque; the region of interest is drawn on the outer vessel wall (A). Ranges of Hounsfield values represent 3 different plaque components Yellow = lipid core (<60 HU), red = fibrous tissue (60 to 130 HU), and white = calcification (>130 HU) (B).